Holography, QCD and Regge Theory

Artur Jorge Carvalho Amorim de Sousa
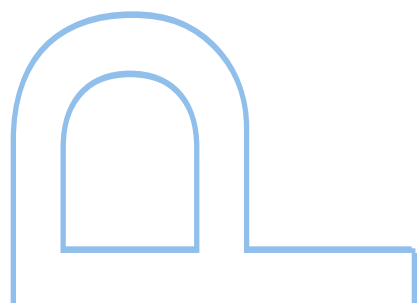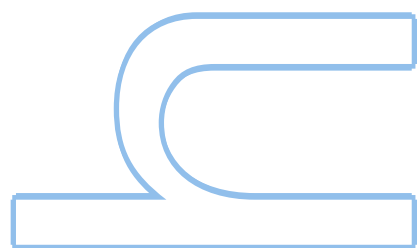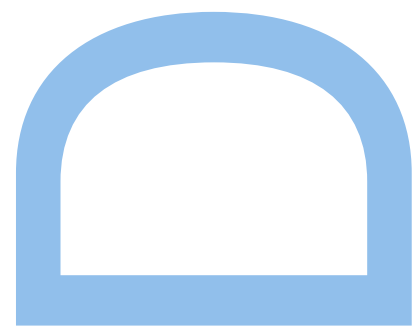Programa Doutoral em Física
Departamento de Física e Astronomia
2021

Orientador
Miguel Sousa da Costa, Faculdade de Ciências, Universidade do Porto

Coorientador
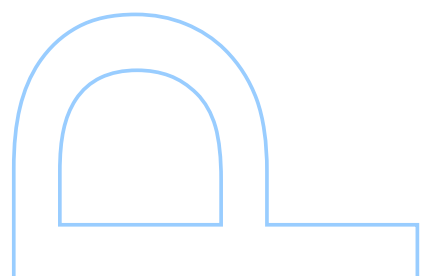Nuno Filipe da Silva Fernandes Castro, Escola de Ciências, Universidade do Minho

To my late grandparents and in-laws, beijinhos.

Acknowledgements

Firstly I would like to thank my supervisor Miguel Costa for giving me the chance of doing a PhD in theoretical physics and for the discussions that allowed to improve my work. This journey not only developed my quantitative skills, but also made me realise that I have the perseverance necessary to achieve my goals. I also want to thank my co-supervisor Nuno Castro for the discussions related to QCD and technical aspects of experimental data. I am fortunate to have friends like João Silva, José Sá and Pedro Leal. Throughout my studies we supported each other and I have learnt a lot from them about physics, mathematics and other topics. I also acknowledge Robert Carcassés Quevedo for being a great partner in the early stages of my PhD and any thanks for Matti Järvinen for his collaboration on my last PhD project.

I am grateful to my wife Serene for all the support and encouragement that she has given me during the hard times, as well to help me see difficulties with the a better perspective. Finally many thanks to my parents and siblings for all the support and happy moments during all these years.

Publication list

This thesis is based in the following publications:

- Non-minimal coupling contribution to DIS at low x in Holographic QCD,
  Phys. Rev. D 98, 026016, arXiv:1804.07778

- $\gamma^*\gamma$ and γ^*p scattering in improved holographic QCD,
  Phys. Rev. D 103, 026007, arXiv:2006.05299

- Deeply Virtual Compton Scattering and the holographic Pomeron,
  Phys. Lett. B, Vol. 819, 2021, 136451, arXiv:2106.09439

- Regge theory in a Holographic dual of QCD in the Veneziano Limit,
  J. High Energ. Phys. 2021, 65 (2021), arXiv:2102.11296

Contents

List of Tables

List of Figures

Abstract

We start to investigate the Pomeron in bottom-up models of AdS/QCD where the conformal symmetry is broken by allowing a non-constant dilaton profile in the dual theory in the bulk. The pomeron is dual to the graviton Regge trajectory and this one is obtained by generalising in a phenomenological way the graviton equation of motion. We extend previous work by considering the addition of data from the longitudinal structure function of the proton F_L and a non-minimal couplings between the higher spin J fields and the spin 1 gauge field dual to the hadronic current. It is shown that a non-minimal coupling improves slightly the description of the proton structure functions F_2 and F_L. Using the optimal values of the free parameters of the model we estimate the gluon PDFs and compare them with the PDF sets of NNPDF31 and CT18 obtaining a fairly good agreement. We test the robustness of these fits by considering global fits that also include the photon structure function F_2^γ and the total cross-section $\sigma\left(\gamma\gamma \to X\right)$. Next, aiming at extending the above model to processes with non-null Mandelstam t, we consider a global fit for Deeply Virtual Compton Scattering (DVCS) total and differential cross-sections. A fit with good quality is found where the parameters of the Pomeron kernel do not vary much. This opens the possibility of including DVCS data in a global fit with other processes. Finally, we consider a bottom-up model of AdS/QCD with non-constant dilaton and tachyon profiles that depend on the numerical values of parameters that enter in the expressions of their potentials. These parameters are fixed by considering the known values of the masses of tensor glueballs and mesons with up and down quark content. After the background is fixed, we propose phenomenological equations of motion for the spin J fields in the Pomeron and meson trajectories that allow to reproduce total cross-sections $\sigma\left(\gamma\gamma \to X\right)$, $\sigma\left(\gamma p \to X\right)$ and $\sigma\left(pp \to X\right)$ data as well the meson spectrum for $J = 2, 3, 4$.

1

Introduction

In the second half of the twentieth century the knowledge about the fundamental constituents of matter increased significantly. The construction of particle colliders with increasingly higher energies allowed us to discover not only new particles, that we now know are made of quarks and leptons, but also another interactions, that we now know to be four in total: gravity, electromagnetic, strong and weak nuclear forces. Around the same time we developed quantum field theories (QFT), that is, theoretical frameworks where quantum mechanical and special relativity principles coexist, for the last three interactions. A quantum field theory of gravity still eludes us today. The vast amount of data collected from the particle colliders was condensed in a single theoretical frame work known as the Standard Model. The Standard Model is a Yang-Mills theory with the gauge group $SU(3) \times SU(2)_L \times U(1)$, where the electromagnetic, strong and weak forces are unified. A central ingredient of it, the Higgs boson, responsible for the spontaneous symmetry breaking mechanism that gives origin to particle masses, was elusive for years until the recent observations of ATLAS and CMS collaborations at CERN verified its existence. This confirms the validity of a physical theory to an extent never seen before.

The conventional technique to extract predictions from a QFT is to look at its field content and interaction terms in order to derive the Feynman rules of the theory. Then we write all the relevant Feynman diagrams up to a given order in the coupling constant in order to compute correlation functions. This is a perturbative computation and it will work as long as it can be expressed in terms of a small parameter. However, in some cases, the kinematical region of interest does not provide such conditions and techniques that go beyond the perturbative procedure are needed. One example of such technique is Regge theory.

In the 1960's there was an effort to explain scattering experiments between strongly interacting particles, although a quantum field theory of these interactions was not available at the time. The solution in those days was to guess the analytic structure of the S-matrix as a function of the Lorentz invariants of the specific process. As an example, for $ab \rightarrow cd$ scattering process the Lorentz invariants are the Mandelstam variables s, t and u. The presence of singularities in the corresponding scattering amplitude is of particular importance since poles in these variables mean bound states or resonances; and threshold energies where new virtual particles could be exchanged correspond to branch points. By looking at the spectrum of the existing particles one can extract information about scattering amplitudes. After decomposing the scattering amplitude in its angular momentum components and doing the analytic continuation to the complex angular momentum plane, Tullio Regge found that poles in this plane can be equivalent to the interchange of an infinite set of particles with the same quantum numbers except for the angular momentum. This set of particles is known as a *Regge trajectory*. This approach had immediate success by explaining the power law dependence of total cross-sections with s observed in higher energy experiments at the Stanford Linear Accelerator (SLAC) in the 60's. In particular, by using the intercept of the straight line obtained by fitting a plot of J vs m^2 of the meson Regge trajectory, one could obtain the same exponent observed in the scattering experiments. At SLAC it was observed that the total cross-sections decayed with s, but in subsequent more powerful colliders at higher center of mass energies a raise in the total cross-sections was observed. It became clear that in the context of Regge theory one needed an additional trajectory with the quantum numbers of the vacuum and with an intercept around 1.08. This additional trajectory became known as the Pomeron and till today the particles it is made of have not been detected experimentally. However, since then the Pomeron has been extremely successful in explaining most of the total cross-section data at high energies [2].

After it was shown that Quantum Chromodynamics (QCD) exhibited asymptotic freedom, researchers started to devote more attention to it. The predictions of QCD were confirmed with great experimental precision till today, establishing it as the quantum field theory of strong interactions. QCD and Regge theory must be compatible, although it is still not clear how to extract in the former the analytic structure of the complex angular momentum. The most serious attempt in this direction is what we call the BFKL pomeron [3–5], where the pomeron appears after resummation of an infinite set of gluon ladder diagrams. One of the deficiencies of this approach is that it leads to a branch cut in the complex angular momentum plane instead of poles. This can be fixed by introducing a momentum cut-off that will yield a discrete set

of poles whose predictions are in good agreement with HERA data for $x < 0.01$ and $Q^2 \leq 100\,\text{GeV}^2$ [6]. Another problem is that next-to-leading order (NLO) contribution to the BFKL kernel is greater then the leading order (LO) one, which demands the difficult task of computing the next-to-next-to-leading (NNLO) order contribution. The last problem is that the Pomeron can be an intrinsically non-perturbative object and then one needs to take into account the Feynman diagrams of all perturbation orders. If this is the case non-perturbative tools will be needed to study the Pomeron in the context of QCD.

The AdS/CFT correspondence [7], or gauge / gravity duality, establishes a dictionary between a quantum field theory in the strong coupling regime with a classical theory of gravity, and has been used to study QCD in the strongly coupled limit. In particular, in [8] it was conjectured that the Pomeron is dual the graviton Regge trajectory of the dual string theory. This fact has been widely explored in the description of QCD processes where Pomeron exchange dominates [1, 9–49]. These include deep inelastic scattering (DIS) , deeply virtual Compton scattering, vector meson production, double diffractive Higgs production, central production of mesons and other inclusive processes. It is now clear that holographic QCD is a valuable tool to model the physics of gluon rich medium, where standard perturbative techniques like the BFKL Pomeron [3–5] breakdown.

Besides total cross-sections, one can also apply Regge theory to DIS. In this case we can compute the total cross-section for the scattering of an off-shell photon with a proton by taking the imaginary part of the amplitude for $\gamma^* p \to \gamma^* p$ at zero momentum transfer. The total cross-section for single Reggeon exchange is given by $\sigma \sim s^{j(0)-1}$. It was found that the intercept $j(0)$ is not universal, but that it had a dependency with Q^2, the virtuality of the off-shell photon. In HERA, it was observed that the intercept rises from 1.1, close to the Pomeron intercept observed in other total cross-section measurements, to 1.4. This suggests the existence of another trajectory with larger intercept that dominates for hard probes (large Q^2). Because of this, one usually talks about the soft and hard pomerons, although their nature and relation is an unsolved problem in QCD. In the BKFL approach the growth of the intercept with Q^2 can be explained after the introduction of a cut-off provided we consider only $Q^2 > 4\,\text{GeV}^2$ [6]. On the other hand, dual models starting from a conformal limit have given better fits to data after introducing a hard-wall cut in AdS space in order to simulate confinement. This is done at no expense of a stricter kinematical region [26]. Also, in [1] it was shown that the soft and hard pomerons are the leading Regge poles of a kernel associated with the graviton Regge trajectory in a 5-d model inspired by string theory. This

favours strongly the study of pomeron physics using the gauge/gravity duality.

The purpose of this thesis is to extend the bottom-up approach to holographic QCD of [1, 32]. The ultimate goal would be to build the Regge theory of Holographic QCD that could explain all the processes dominated by Pomeron exchange. This thesis is organized as follows. In the remaining of this chapter we start by reviewing the basics of the S-matrix and Regge theory. Then we review QCD, the BFKL approach and its relation to the pomeron. Then, we introduce the AdS/CFT duality and the BPST pomeron, as well an overview of the holographic QCD models used in this work. Then the Witten diagram expansion is reviewed.

Chapter 2, which is based on [33], explores the possibility of having different coupling tensor structures between the spin 1 gauge field and the higher spin fields. This work extends the results of [1] by studying the effect of a non-minimal coupling on the description of the proton structure functions F_2 and F_L. Chapter 3 studies the validity of the holographic model presented of chapter 2 in the context of $\gamma^*\gamma$ observables and also includes the total-cross section $\sigma(\gamma p \to X)$ in $\gamma^* p$ processes. We find that it can describe in a satisfactory way a large number of experimental points from different observables. We also explore the qualitative behaviour of the gluon parton distribution functions extracted from the holographic predictions of this model for the proton structure functions F_2 and F_L. The results of this chapter can be found in the article [34]. Chapter 4 is a first attempt to explore this model in processes with Mandelstam $t < 0$. We propose an ansatz for the gravitational couplings as a function of t based on the results of the $O(N)$ vector model in order to fit both cross-section and differential cross-section data of DVCS. Although we can successfully describe this data, to date, we have not found a way of making the model consistent with previous results. Possible solutions to this issue are also briefly discussed in this chapter. In chapter 5 we initiate the study of holographic Regge theory in a background where the backreaction of quarks to the gluon dynamics is included. We will fix the parameters of the background by performing a fit to the meson spectrum in QCD. We then propose the dynamics of the higher spin J fields in the graviton Regge trajectory, dual to the Pomeron trajectory, by using effective field theory inspired by Regge theory of a 5D string theory. This approach will also be applied to the meson trajectory. The dynamics of these fields depends on two free parameters which will be fixed by the soft pomeron intercept and by the masses of the mesons with spins $J = 2, 3, \text{and} 4$. This fixes the intercepts of all Regge trajectories relevant for hadronic scattering. We then check if the resulting holographic intercept is able to describe the experimental data of the total cross-sections of $\gamma\gamma$, γp and pp scattering. Finally we conclude in chapter

6, making a short resume of the results obtained and discussing about possible future new lines of research.

1.1 Quantum Chromodynamics and the Pomeron

1.1.1 S-matrix theory

In the 1960's the physics community has not come up with a QFT of strong interactions. To work around this the S-matrix theory was developed. The idea was to compute scattering amplitudes by assuming plausible postulates. Suppose we have an initial state $|a\rangle_{\text{in}}$ with n particles with momentum $p_1, \cdots, p_n$ that scatter into a final state $|b\rangle_{\text{out}}$ with m particles with momentum $q_1, \cdots, q_m$. The S-matrix element S_{ab} is the overlap between this two states, i.e. $S_{\text{ab}} = {}_{\text{out}}\langle b|a\rangle_{\text{in}}$. The S-matrix has the following properties:

- it is Lorentz invariant;

- it is unitary ;

- it is an analytic function of Lorentz invariants, with only those singularities allowed by unitarity.

An example of the first postulate is given by the scattering process $1 + 2 \rightarrow 3 + 4$ (particle i with 4-momentum p_i), where we can form the Lorentz invariants s, t and u defined by

$$s = (p_1 + p_2)^2 \,, \tag{1.1}$$

$$t = (p_1 - p_3)^2 \,, \tag{1.2}$$

$$u = (p_1 - p_4)^2 \,, \tag{1.3}$$

$$s + t + u = \sum_i m_i^2 \,. \tag{1.4}$$

For this particular process the first postulate says that the scattering amplitude must be a function of only s and t (or any other pair of s, t and u) i.e. $\mathcal{A} = \mathcal{A}(s,t)$.

The second postulate is equivalent to conservation of probability. This means that given an in state the sum of the probabilities of ending in some out state is one. Among the possible out states one that deserves special attention is the forward scattering case,

i.e. no scattering occurs. The S-matrix elements can then be written in terms of the scattering amplitude as

$$S_{ab} = \delta_{ab} + i(2\pi)^4 \delta^4 \left(\sum_a p_a - \sum_b q_b \right) \mathcal{A}_{ab} \tag{1.5}$$

The forward scattering amplitude is central to the optical theorem that we now review. Due to the unitarity of the S matrix the following relationship holds

$$\delta_{ab} = \langle a|SS^\dagger|b \rangle = \sum_c \langle a|S|c \rangle \langle c|S^\dagger|b \rangle \,, \tag{1.6}$$

which after using equation (1.5) implies

$$(-i)(\mathcal{A}_{ba}^* - \mathcal{A}_{ab}) = (2\pi)^4 \sum_c \delta^4(P^c - P^a) \mathcal{A}_{ac} \mathcal{A}_{bc}^* \,. \tag{1.7}$$

For forward scattering the initial and final states are exactly the same and hence

$$2 \operatorname{Im} \mathcal{A}_{aa} = (2\pi)^4 \sum_c \delta^4(P^c - P^a) |\mathcal{A}_{ac}|^2 \,. \tag{1.8}$$

The sum over c is a sum over final states with different particle number, as well as different momentum vectors for each particle in the final state. The implication of equation (1.8) becomes clear when one examines the expression for the cross-section for the process $p_1 + p_2 \rightarrow p_1' + ... + p_n'$

$$\sigma_{12 \rightarrow n} = \frac{1}{4|\vec{p}_1|\sqrt{s}} \int \left(\prod_{i=1}^n \frac{d^3 p_i'}{2E_i(2\pi)^3} \right) (2\pi)^4 \delta^4 \left(\sum_{n=1}^n p_n' - p_1 - p_2 \right) |\mathcal{A}_{2n}|^2 \,, \tag{1.9}$$

with $\mathcal{A}_{2n}$ being the amplitude that two particles with 4-momentum p_1 and p_2 produce n particles with momentum p_1', p_2', ... and p_n'. If we now sum over all the possible n-particle states and use equation (1.8) the total cross-section for two highly relativistic particles is

$$\sigma_{12}^{Tot} = \frac{1}{s} \operatorname{Im} \mathcal{A}_{aa}(s, t = 0) \tag{1.10}$$

where $\sqrt{s}$ is the center-of-mass energy and $\mathcal{A}_{aa}(s, t = 0)$ is the forward scattering amplitude. This constitutes the optical theorem and it will be used throughout this thesis to compute the proton structure functions F_2 and F_L, the photon structure function F_2^γ, as well the total cross-sections for $\gamma\gamma$, γp and pp scattering.

Finally let us discuss the third postulate, which establishes the connection between the spectrum of a theory and scattering amplitudes in the Regge limit. Analyticity

is a manifestation of the causality principle and each kind of singularity that appears in the scattering amplitude has a physical interpretation. For the case of two particle scattering, a bound state between them corresponds to a pole while a physical thresholds give rise to cuts in the complex plane of the scattering amplitude. As an example, for a bound state of mass $m_B = \sqrt{s_B}$ there is a pole in the complex s-plane. On the other hand, the $2 \to n$ process occurs only if the center of mass energy $\sqrt{s}$ is bigger than the sum of the masses of the n particles in the final state. This means that the total cross-section has a non-analytic behaviour and the optical theorem links this non-analyticity to the imaginary part of the scattering amplitude. The imaginary part has to be discontinuous in the real axis, because, if not, according to [50] the scattering amplitude is real between s_B and $s_{Th} = (m_1 + \cdots m_n)^2$ and since it is an analytic function, by the Schwarz reflection principle it must satisfy

$$\mathcal{A}(s^*, 0) = (\mathcal{A}(s, 0))^* , \tag{1.11}$$

i.e. the imaginary part is null on the real axis. Then the scattering amplitude must have a branch cut on the real axis. This branch cut connects the smaller threshold value to infinity and it contains all the other possible threshold values.

Before we review scattering amplitudes in the Regge limit let us comment on the implications of crossing symmetry to the analytic structure of the scattering amplitudes. According to crossing symmetry, provided we reverse the signs of some of the momenta of the particles, the s-channel Feynman diagram of the process $12 \to 34$ also describes the t-channel Feynman diagram of the process $1\bar{3} \to \bar{2}4$ and the u-channel Feynman diagram of the process $1\bar{4} \to 3\bar{2}$. Here bar denotes the corresponding antiparticle. This implies that the analytic structures of $\mathcal{A}_{12 \to 34}(s, t, u)$ and $\mathcal{A}_{1\bar{3} \to \bar{2}4}(t, s, u)$ are the same. In particular poles and branch points in the s plane of the first amplitude are mapped respectively to poles and branch points in the t plane of second amplitude.

1.1.2 Scattering amplitude in the Regge limit

Now that the S-matrix formalism is introduced we can make some predictions. Consider the process $a + b \to c + d$. Its scattering amplitude in the s-channel can be decomposed into its constituent angular momentum components as [51]

$$\mathcal{A}_{ab \to cd}(s, t) = \sum_{J=0}^{+\infty} (2J + 1) a_J(t) P_J(1 + 2s/t) , \tag{1.12}$$

where $P_J(x)$ is a Legendre polynomial of degree J. This sum can be written as a contour integral in the complex angular momentum plane where the contour is the
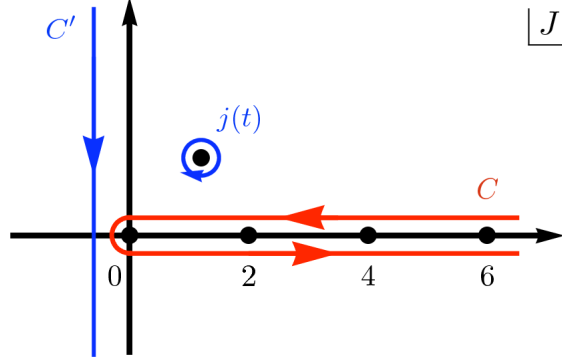
Figure 1.1: Illustration of a Sommerfeld-Watson transform. The original contour C is the red one while the deformed contour is the blue. The points over the real axis represent the integer values of J in the original sum. The point $j(t)$ is one pole picked up in the process of deforming C into C'. In general, these poles in general are not integers and depend on the Mandelstam variable t.

one denominated by C in figure 1.1. This transformation is known as the Sommerfeld-Watson transform

$$\mathcal{A}(s,t) = \frac{1}{2i} \oint_C dJ \frac{2J+1}{\sin \pi J} \sum_{\eta=\pm 1} \frac{\eta + \exp^{-i\pi J}}{2} a^{(\eta)}(J,t) P(J, 1 + 2s/t), \qquad (1.13)$$

where $P(J,x)$ is now the analytic continuation of the Legendre polynomials into the complex plane J. The sum over η inside the integral ensures that this transformation is unique [51].

We are interested in the form of the scattering amplitude in the Regge limit, i.e. $s \gg t$. We then deform the contour C into the contour C' in figure 1.1 defined by the set of complex angular momentum points with the real component equal to $-1/2$. In order to do so we must not forget to encircle all the singularities of $a^{(\eta)}(J,t)$. Considering that the only possible singularities are simple poles, the Residue Theorem implies that the scattering amplitude can be written as

$$\mathcal{A}(s,t) = \frac{1}{2i} \int_{-\frac{1}{2}-i\infty}^{-\frac{1}{2}+i\infty} dJ \left[\frac{2J+1}{\sin \pi J} \sum_{\eta=\pm 1} \frac{\eta + \exp^{-i\pi J}}{2} a^{(\eta)}(J,t) P(J, 1 + 2s/t) \right] +$$

$$+ \sum_{\eta=\pm 1} \sum_{n_\eta} \frac{\eta + \exp^{-i\pi j_{n_\eta}(t)}}{2} \frac{\tilde{\beta}_{n_\eta}^{\eta}(t)}{\sin \pi j_{n_\eta}(t)} P(j_{n_\eta}(t), 1 + 2s/t), \qquad (1.14)$$

9

where $j_{n_\eta}(t)$, known as Regge poles, are the simple poles of $a^{(\eta)}(l, t)$ and their residue values are absorbed in $\tilde{\beta}_{n_\eta}(t)$.

In the Regge limit Legendre polynomials are dominated by the term

$$P_J(1 + 2s/t) \xrightarrow{s \gg |t|} \frac{\Gamma(2J+1)}{\Gamma^2(J+1)}\left(\frac{s}{2t}\right)^J, \tag{1.15}$$

which implies that the contour integral in equation (1.14) vanishes in the limit $s \to +\infty$. If we use the Γ-function identities

$$z\Gamma(z) = \Gamma(z+1), \quad \Gamma(2z) = \frac{\Gamma(a)\Gamma(a+\frac{1}{2})}{2^{1-2z}\sqrt{\pi}}, \quad \frac{\pi}{\sin\pi z} = \Gamma(1-z)\Gamma(z), \tag{1.16}$$

the expression for the scattering amplitude is

$$\mathcal{A}(s,t) = \mathcal{A}^+(s,t) + \mathcal{A}^-(s,t), \tag{1.17}$$

where we have defined two scattering amplitudes, one for positive signature $\mathcal{A}^+$ and another for negative signature $\mathcal{A}^-$:

$$\mathcal{A}^\pm(s,t) = \sum_{n_\pm} \beta_{n_\pm}^\pm(t)\left(\pm 1 + \exp^{-i\pi j_{n_\pm}(t)}\right)\Gamma(-j_{n_\pm}(t))(s/s_0)^{j_{n_\pm}(t)}. \tag{1.18}$$

The Γ-function has simple poles at $\{0, -1, -2, -3, \cdots\}$ and hence the $\Gamma(-j_{n_\pm})$ factor in the above scattering amplitudes has poles for values of t such that $j_{n_\pm}$ is a positive integer. On the other hand the signature factor $1 + e^{-i\pi j_{n_+}(t)}$ is null when j_{n_+} is an odd integer and the signature factor $-1 + e^{-i\pi j_{n_-}(t)}$ vanishes when j_{n_-} is an even integer. This means that $\mathcal{A}^+$ has poles for values of t such that $j_{n_+}(t)$ is even while $\mathcal{A}^-$ has poles for values of t such that $j_{n_-}(t)$ is odd. In [52] it is shown that the amplitudes around these poles have a Breit-Wigner with decay width $\Gamma \propto \operatorname{Im} j_{n_\pm}$ and hence the poles in the amplitudes $\mathcal{A}^\pm$ correspond to the exchange of bound states or resonances in the t-channel with masses $m_R^\pm$ given by

$$\operatorname{Re} j_{n_+}(m_R^{+\,2}) = \sigma^+ \in \{0, 2, 4, \cdots\},$$
$$\operatorname{Re} j_{n_-}(m_R^{-\,2}) = \sigma^- \in \{1, 3, 5, \cdots\}.$$

Another relevant remark is that for the physical $t < 0$ values in the s-channel the positions $j_{n_\pm}(t)$ of the poles and their residues $\beta_{n_\pm}^\pm(t)$ are real, so the phases of the scattering amplitudes $\mathcal{A}^\pm$ comes from the factors $\pm 1 + e^{-i\pi j_{n_\pm}(t)}$ [52].

Of all the Regge poles j_{n_η} that contribute to the scattering amplitude the one that dominates in the limit $s \to \infty$ is the one with largest real part:

$$\mathcal{A}(s,t) \propto s^{j(t)} \tag{1.19}$$

Equation (1.10) then states that the total cross-section for the scattering of two particles a and b is given by

$$\sigma^{\text{Tot.}} \propto s^{j(0)-1} \, , \tag{1.20}$$

where the numerical value of $j(0)$ is commonly known as the intercept. To understand the implication of this result, let us assume that there is only one resonance with spin J being exchanged. Then only one partial wave in equation (1.12) contributes

$$\mathcal{A}(s,t) = (2J+1)a_J(t) \, P_J(1 + 2s/t) \sim f(t)s^J \, . \tag{1.21}$$

Using the optical theorem, we conclude that $\sigma^{\text{Tot.}} \sim s^{J-1}$ at large s. Thus, for a scalar particle the total cross-section would decrease as s^{-1}. For the exchange of a spin-1 meson, such as the ρ meson, the total cross-section is independent of s while with the exchange of a spin-2 meson, like the f_2 tensor meson, the total cross-section should increase linearly. However, what we observe in figure 1.2 is that for large enough s the total cross-section starts to decrease as $s^{-0.5}$ and then it increases much more slowly as if it were due to f_2 exchange. The only way to reconcile the particle exchange picture is to assume that all the mesons are members of a family of particles of increasing spin and mass and that all the members of this family are exchanged. Then their joint contributions reproduce the observed energy dependence of the total cross-section. Today we call these families of particles Regge trajectories, and what equation (1.20) means is that the joint contribution of exchange of all the particles of a Regge trajectory is equivalent to the exchange of a single pseudo-particle called *Reggeon* with spin $j(0)$.

1.1.3   The (soft) pomeron

In this subsection we will use the formalism of Regge trajectories introduced above to make predictions about the s dependence of total cross-sections between hadronic particles. Later we will introduce the (soft) pomeron as a solution to explain the large s dependence of the total cross-sections in figure 1.2.

If we use well-established meson states to make a plot of their spin j against the square of their mass we obtain figure 1.3. This kind of plot is known as a Chew-Frautschi plot. In it we have displayed four Regge trajectories: $\{\rho(770), \rho_3(1690), \cdots\}$, $\{\omega(780), \omega_3(1670), \cdots\}$, $\{f_2(1270), f_4(2050), \cdots\}$ and $\{a_2(1320), a_4(2040), \cdots\}$. The first pair has odd signature while the second has even. Each pair has also a isospin zero and isospin one trajectories. Striking features are that all these four trajectories
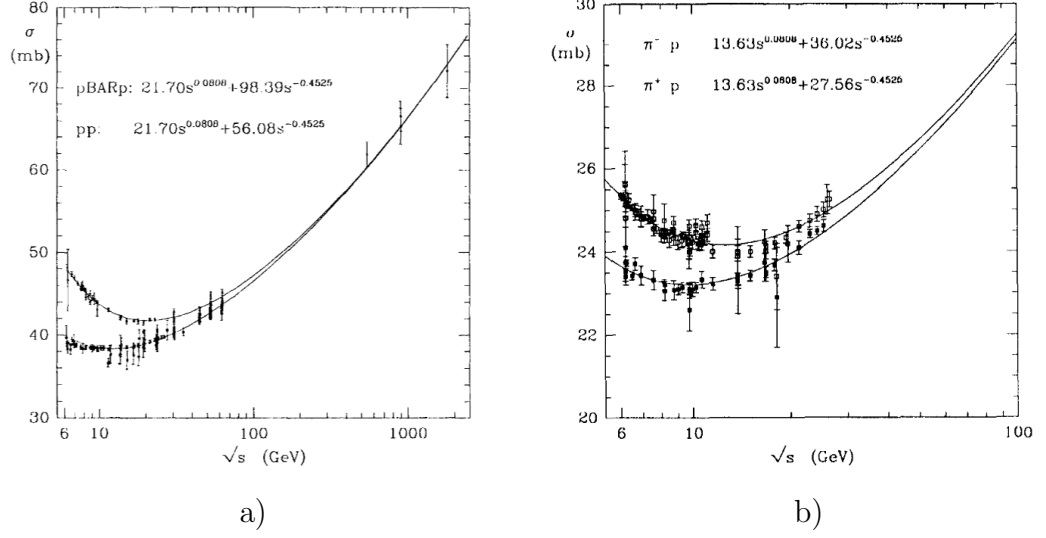
Figure 1.2: a) Data for $p - p$ and $p - \bar{p}$ total cross-sections and b) for $\pi^+ - p$ and $\pi^- - p$ scattering. Figure extracted from [51].
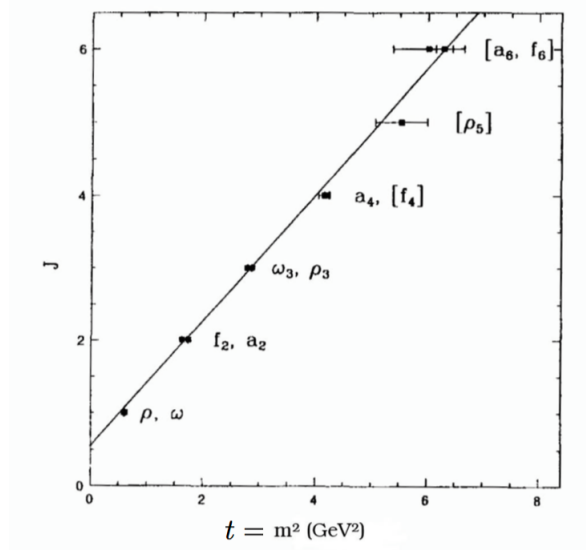
Figure 1.3: Spins of low lying mesons against square mass. This linear Regge trajectory is known as the ρ-trajectory. Figure extracted from [51].

are linear to a very good approximation and that they are nearly degenerate. The straight line $j(t)$ that fits best the points of figure 1.3 is

$$j(t) = j_0 + \alpha' t, \quad j_0 = 0.55, \quad \alpha' = 0.86. \quad (1.22)$$

According to the discussion of the last section, in any process where the meson trajectories are exchanged we expect the total cross-section to decay as $s^{j_0-1} = s^{-0.45}$.

As an example, in the process

$$\pi^- + p \rightarrow \pi^0 + n \,, \tag{1.23}$$

the mesons of isospin 1 with even parity are exchanged and one can see in figure 1.2 that for $\sqrt{s} < 10\,\text{GeV}$ the total cross-section diminishes as predicted by Regge theory. We can also see in the same figure that this behaviour is quite universal for other scattering processes involving hadrons. The examination of total cross-section data only probes the assumption of the linearity of Regge trajectories at $t = 0$. If we extrapolate equation (1.22) to the $t < 0$ region, Regge theory predicts that the differential cross-section for a linear trajectory is given by

$$\frac{d\sigma}{dt} \propto s^{(2j_0 + 2\alpha' t - 2)} \,. \tag{1.24}$$

By analysing pion charge exchange scattering data, Barnes et. al [53] have shown that a linear approximation of the meson Regge trajectories gives a very good fit to data over a wide range of pion energies, as show in figure 1.4.
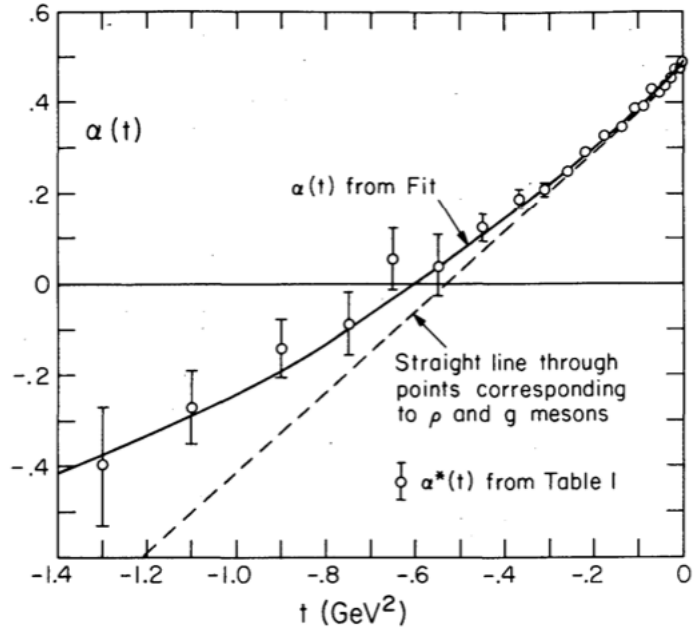
Figure 1.4: $j(t)$ obtained from $\pi^- p \rightarrow \pi^0 n$ data for pion energies between 20.8 and 199.3 GeV. Figure extracted from [53].

As more energetic particle colliders were built, it was realised that at some point the total cross-section started to increase slowly with s as observed in figure 1.2. In the context of Regge theory this can only be explained if another trajectory is
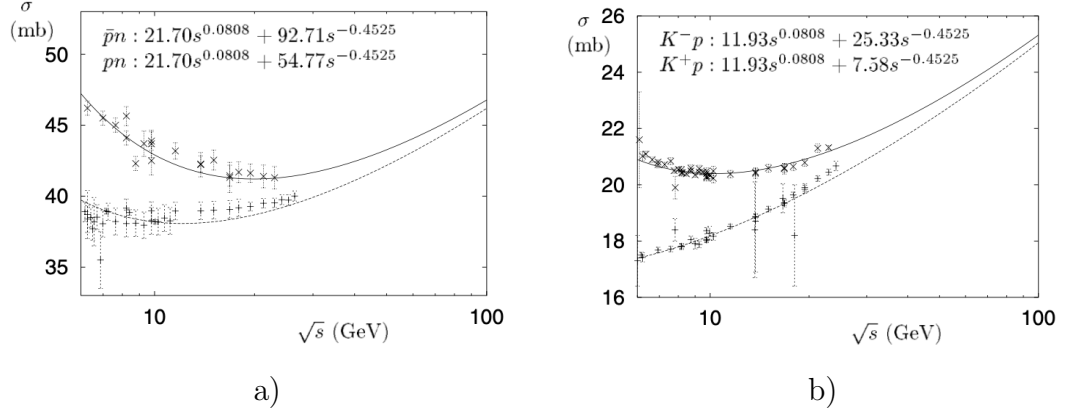
Figure 1.5: a) Data for pn and $\bar{p}n$ total cross-sections and b) for $K^+ - p$ and $K^- - p$ scattering. Figure extracted from [52].
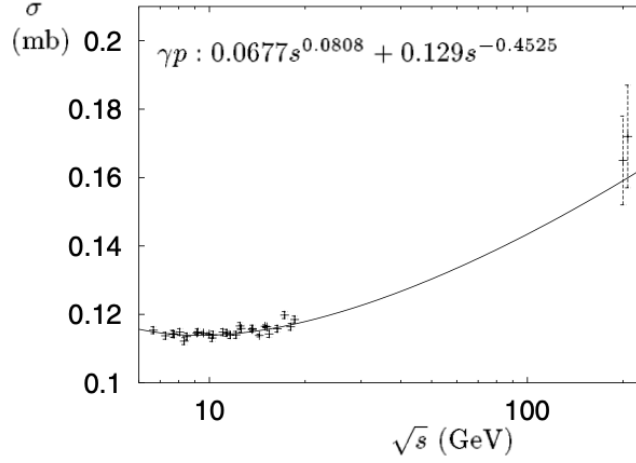
Figure 1.6: Data for γp total cross-sections. Figure extracted from [52].

being exchanged and this trajectory has to have an intercept slightly greater than one. Assuming that such trajectory exists, the particles belonging to it must have the quantum numbers of the vacuum (i.e. isospin zero and even under the operation of charge conjugation) since, has shown by Foldy and Peirls, exchange of such particles guarantees that the total cross-section is a non-decreasing function. This additional trajectory is known today as the (soft) Pomeron in honour of Isaak Pomeranchuk who proposed its existence. The pomeron intercept and Regge slope are determined experimentally to be, respectively, 1.08 and $0.25\,\mathrm{GeV}^{-2}$.

In figures 1.2, 1.5 and 1.6 we can see that the formula $\sigma = a\,s^{-0.45} + b\,s^{0.08}$, motivated by Regge theory with Pomeron and meson exchange, can describe successfully a wide range of scattering processes between strongly interacting particles. The parameters a

and b are determined by fits to data and their values are related to how the scattering particles couple to the Pomeron and meson trajectories. Since the particles in the Pomeron trajectory carry the quantum numbers of the vacuum their coupling with particles and corresponding anti-particles should be the same. Hence, cross sections for processes where we exchange the particle for its anti-particle should have the same value of b and their difference should vanish for $s \to \infty$. This seems to be the case for all the cross-section data in figures 1.2 and 1.5.

Despite the success of the idea of pomeron exchange, until today nobody has found experimentally particles that are members of this trajectory. This is due to the fact that particles with the quantum numbers of the vacuum are difficult to detect experimentally. Theoretically we expect that this trajectory must be composed of glueballs which should emerge in QCD as bound states of gluons. These particles have not been directly observed but there are some experimental candidates. For the pomeron trajectory we expect a spin two particle with mass around 1.9 GeV. In 1994 the WA91 collaboration at CERN announced evidence for a possible glueball with this mass [54] and vector, pseudo-vector or tensor glueball candidates with a mass of about 3.02 GeV/c have been found by the BaBar experiment [55]. A discussion about scalar glueball candidates can be found in [56]. Another problem, is the observation in DIS data (which we will discuss in more detail in the next section), that the structure function $F_2\left(x, Q^2\right)$, related to the total cross-section of $\gamma^* p$ scattering, rises faster than $x^{-0.08}$ as $x \to 0$ for fixed higher values of the photon virtuality Q^2. Here the Mandelstam variable s is related to the Bjorken x and Q^2 through

$$s = \frac{Q^2(1-x)}{x} \, . \tag{1.25}$$

For large Q^2 fixed it is found that F_2 rises as $x^{-0.4}$ when $x \to 0$. We will show in the next section how this is expected in the context of the BFKL pomeron resulting from the leading contributions from perturbative QCD in the low x regime. How this BFKL pomeron is related to the pomeron discussed previously continues to be an open question today.

1.1.4 Quantum Chromodynamics and the Pomeron

In the 1970's a quantum field theory of strong interactions based on local gauge symmetry was formulated [57–59]. Each strongly interacting particle (e.g. proton) is made of six flavours of quarks: up, down, charm, strange, top and bottom. Each of these quarks can be found in three different colour states that are called Red, Blue

and Green. The local gauge symmetry of this theory is $SU(3)$ and the elements of this group act only on the colour degrees of freedom. Quarks interact with each other by exchanging their colour states. This theory of strong interactions is known as Quantum Chromodynamics (QCD).

The lagrangian of this theory is

$$\mathcal{L}_{QCD} = -\frac{1}{4}F^a_{\mu\nu}F^{\mu\nu a} + \sum_q \bar{q}(i\gamma^\mu D_\mu - m_q)q\,. \tag{1.26}$$

Here q are the six different quark fields with mass m_q, γ^μ are the Dirac gamma matrices, $F^a_{\mu\nu}$ the gluon field strength tensor and D_μ is the covariant derivative of the quarks. The gluon strength tensor can be written in terms of the gluon fields A^a_μ, with $a = 1, \cdots, 8$, as

$$F^a_{\mu\nu} = \partial_\mu A^a_\nu - \partial_\nu A^a_\mu - g_s f_{abc}A^b_\mu A^c_\nu\,, \tag{1.27}$$

where g_s is the strong coupling constant and f_{abc} the structure constants of the Lie algebra of the Lie group $SU(3)$. The covariant derivative action on the quark fields is

$$D_\mu q = \partial_\mu q + ig_s A^a_\mu t_a\,, \tag{1.28}$$

where t_a are the Gell-Mann matrices and correspond to the fundamental representation of the infinitesimal generators of $SU(3)$.

From the lagrangian 1.26 we can extract the Feynman Rules for QCD using the path integral formalism. The propagator of the quarks is the usual Dirac propagator since each quark has spin 1/2:

$$\frac{\delta_{ij}}{\not{p} - m + i\epsilon}\,. \tag{1.29}$$

To obtain the gluon propagator one needs to define a gauge because without it one can not invert the equation of motion of the free gluon in order to compute the propagator [60]. In order to do that a gauge fixing term

$$\mathcal{L}_{fix} = -\frac{1}{2\lambda}(\partial^\mu A^a_\mu)^2 \tag{1.30}$$

is added to the QCD langrangian. After we invert the modified equation of motion the gluon propagator in momentum space is

$$-\delta_{ab}\left[\frac{g_{\mu\nu}}{p^2 + i\epsilon} - (1-\lambda)\frac{p_\mu p_\nu}{(p^2 + i\epsilon)^2}\right]\,. \tag{1.31}$$

If we were working on an Abelian gauge theory the problem of the gluon propagator would be finished. The field $\chi^a = \partial \cdot A^a$ is a non-physical degree of freedom since it represents the longitudinal component of the gluon field and gluons are massless. Its QCD equation of motion is

$$\partial^2 \chi^a + g f^{abc} A^{b\mu} \partial_\mu \chi^c = 0 \,, \tag{1.32}$$

and it implies mixing between the non-physical with the physical (transverse) degrees of freedom and hence they contribute to gluon loops. To avoid that, new non-physical degrees of freedom η^a called ghosts are introduced in order to cancel the contributions of χ^a. These new fields, known as Fadeev-Popov ghosts, are complex scalar fields which obey Fermi-Dirac statistics. Their dynamics is described by the lagrangian

$$\mathcal{L}_{ghosts} = \partial_\mu \eta^{a\dagger} (\partial^\mu \eta^a + g f^{abc} A^{b,\mu} \eta^c) \,. \tag{1.33}$$

The interactions between quarks and gluons are determined by the three kinds of QCD vertices : a vertex with two quarks and a gluon, three-gluon vertices and four-gluon vertices. The first vertex can be obtained from the covariant term, while the last two come from the term of the gluon strength tensor. The mathematical expression for each vertex can be obtained by the use of functional derivatives. Their expressions can be found in many QCD textbooks such as [60, 61].

With the Feynman rules of QCD we can now compute a physical observable R in a perturbation series by summing all the possible diagrams contributing to it

$$R = \sum_n c_n \alpha_S^n \,, \quad \alpha_S = g_s^2/4\pi \,. \tag{1.34}$$

In this perturbation series expansion there are Feynman diagrams with loops that lead to divergent integrals present in the definition of c_n in equation (1.34). This unphysical behaviour can be solved by absorbing the divergences in redefinitions in the lagrangian parameters such as α_S. By doing this, besides the energy scale Q of the process involved, one introduces a new scale, the renormalization scale μ. To see how this works, consider the case of vacuum polarization ($e^- e^+$ pairs) in Quantum Electrodynamics. The relevant Feynman diagrams are shown in figure 1.7. The diagram with one loop gives rise to a divergent integral. To avoid it, we introduce a cut-off Λ that when we take to infinity we recover the original integral. That isolates the divergent behaviour of the integral and allows us to write an effective fine structure constant as

$$\alpha(Q^2) = \alpha_0 \left[1 + \frac{\alpha_0}{3\pi} \log \frac{Q^2}{\Lambda^2} + \left(\frac{\alpha_0}{3\pi} \log \frac{Q^2}{\Lambda^2} \right)^2 + ... \right] = \frac{\alpha_0}{1 - \frac{\alpha_0}{3\pi} \log \frac{Q^2}{\Lambda^2}} \,, \tag{1.35}$$
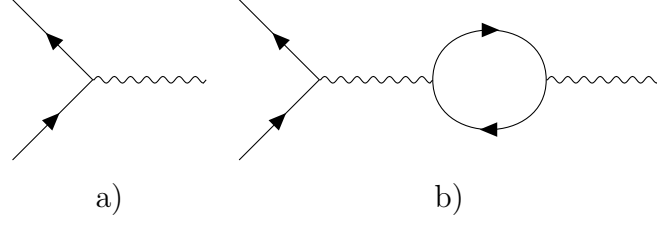
Figure 1.7: Feynman diagrams for vacuum polarization in QED.

with $\alpha_0 = e_0^2/4\pi$ where e_0 is the so called electron bare electric charge. We now introduce a renormalization scale μ such that

$$\alpha(\mu^2) = \frac{\alpha_0}{1 - \frac{\alpha_0}{3\pi}\log\frac{\mu^2}{\Lambda^2}} \tag{1.36}$$

whose experimental value is known. This value can be fixed as Λ goes to infinity by tuning α_0. Moreover we can eliminate α_0 and Λ from equation 1.35 and we get

$$\alpha(Q^2) = \frac{\alpha(\mu^2)}{1 - \frac{\alpha(\mu^2)}{3\pi}\log\frac{Q^2}{\mu^2}} \, . \tag{1.37}$$

In QCD at NLO α_S has a similar expression:

$$\alpha_S(Q^2) = \frac{\alpha_S(\mu^2)}{1 + \frac{33-2n_f}{12\pi}\alpha_S(\mu^2)\log(Q^2/\mu^2)} \tag{1.38}$$

where n_f is the number of active quark flavours (number of quarks with $m_q < Q$). Experimentally we know that there are only 6 quarks. Then, contrary to QED, one expects that α_S decreases as Q increases implying that at high energies quarks interact weakly. This phenomena is known as asymptotically freedom and explains why although the quarks are confined inside the proton they can be treated as free particles in DIS processes between an electron and a proton.

Deep Inelastic Scattering, QCD and the Pomeron

We will know discuss one of the most powerful tests of QCD which is the breaking of Bjorken scaling (defined below) in DIS lepton-hadron processes. This will allow us to introduce some kinematic variables used in diffractive processes, as well as explain how pomeron behaviour is predicted from QCD. We will present the most relevant ideas, more detailed calculations can be found in [61, 62].

In figure 1.8 is shown a deep inelastic e-p scattering process. As an electron with momentum k approaches the proton with momentum P it emits a virtual photon with
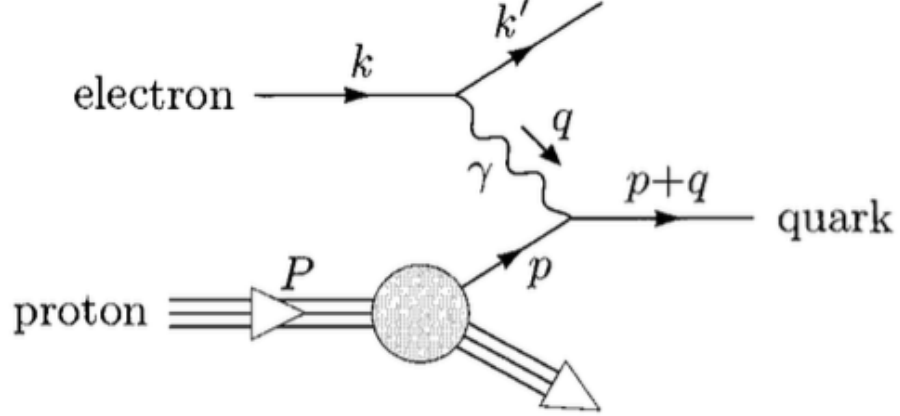
Figure 1.8: Kinematics of deep inelastic electron scattering in the parton model. Extracted from [62].

momentum q. The electron is then scattered with momentum k' while the photon strikes one of the loosely bound quarks inside the proton with momentum p. The strucked quark then interacts with the other quarks of the proton producing jets of hadrons collinear with the direction of the strucked quark.

The averaged amplitude for scattering of unpolarized electrons with a quark q can be computed in QED:

$$\frac{1}{4}\sum_{\text{spins}}|\mathcal{M}|^2 = \frac{8e^4 e_q^2}{\hat{t}^2}\left(\frac{\hat{s}^2 + (\hat{s}+\hat{t})^2}{4}\right), \tag{1.39}$$

which gives the differential cross-section

$$\frac{d\sigma}{d\hat{t}} = \frac{2\pi\alpha^2 e_q^2}{\hat{s}^2}\left(\frac{\hat{s}^2 + (\hat{s}+\hat{t})^2}{4}\right), \tag{1.40}$$

where $\hat{s}$ and $\hat{t}$ are the Mandelstam variables for the electron-quark process, α is the fine-structure constant and e_q is the quark charge in units of the proton charge. Experimentally we do not measure $\hat{s}$ and $\hat{t}$ because we do not have a way to know the momentum of the quark before the scattering. The only variables that are controlled or measured are the initial momentums of the proton and electron and the final momentum of the electron. $\hat{t}$ is related to a variable Q^2 by

$$\hat{t} = -Q^2 = q^2 = (k - k')^2, \tag{1.41}$$

where q is the momentum carried by the virtual photon. To relate $\hat{s}$ with other experimental variables we need to consider the process in the electron-proton center of mass frame. Because of asymptotic freedom, the quarks interact weakly with each other and hence their transverse momentum is negligible. Then we can make the approximation that the strucked quark has a longitudinal fraction x of the proton momentum, i.e. $p = xP$. Then

$$\hat{s} = (p + k)^2 = p^2 + k^2 + 2p \cdot k \approx 2p \cdot k = 2xP \cdot k = xs \tag{1.42}$$

where it is assumed that the mass of the quark and of the electron are small compared with the energy scale of the process. After scattering, the momentum of the quark is $p + q$, so

$$0 \approx (p + q)^2 \approx 2p \cdot q + q^2 = 2xP \cdot q - Q^2 \implies x = \frac{Q^2}{2P \cdot q} \tag{1.43}$$

where x is the famous Bjorken x and is completely determined by experiment. We can introduce a function $f_i(x)$ for the quark flavour i as the probability that inside the proton there is a quark q with flavour i with a fraction of the proton momentum between x and $x + dx$. Then the differential cross-section for DIS is

$$\frac{d^2\sigma}{dx dQ^2} = \frac{2\pi\alpha^2}{Q^4} \left[1 + (1 - y)^2\right] \sum_i f_i(x) e_i^2 , \quad y = \frac{Q^2}{xs} , \tag{1.44}$$

where f_i is called the parton distribution function (PDF) for the quark flavour i and e_i is the charge of the quark with flavour i. Note that if we divide the last equation by the factor

$$\frac{1 + (1 - y)^2}{Q^4} , \tag{1.45}$$

we obtain a quantity that only depends on x, a phenomena known as Bjorken scaling. The remaining quantity depends solely on the quark PDFs and hence this result means that the structure of the proton looks the same to an electromagnetic probe no matter how hard the proton is hit by it.

To gain further insight, let us compare equation (1.44) with a general formula for inelastic lepton-hadron scattering. In general the differential cross-section for DIS can be written as the contraction between a leptonic tensor $L^{\mu\nu}$ with a hadronic tensor $W_{\mu\nu}$ as

$$\frac{d^2\sigma}{dx dQ^2} = \frac{2\pi y\alpha}{Q^4} L^{\mu\nu} W_{\mu\nu} . \tag{1.46}$$

The expression for $L^{\mu\nu}$ can be obtained after computing the square of the modulus of the scattering amplitude and summed over all spin states. After such procedure it is given by

$$L^{\mu\nu} = 2\left(k'^\mu k^\nu + k'^\nu k^\mu - g^{\mu\nu}\left(k' \cdot k - m^2\right)\right) , \tag{1.47}$$

where m is the mass of the lepton. The hadronic tensor describes the interaction between the incoming lepton with the hadron and can be written as

$$W_{\mu\nu} = \frac{1}{4\pi} \int dx e^{iq\cdot x} \langle P| \left[J_\mu^\dagger\left(x\right), J_\nu\left(0\right)\right] |P\rangle . \tag{1.48}$$

Lorentz, gauge and time reversal invariance as well parity conservation constraint the general form of $W_{\mu\nu}$. For unpolarized lepton beams

$$W_{\mu\nu} = \left(-\eta_{\mu\nu} + \frac{q_\mu q_\nu}{q^2}\right) F_1\left(x, Q^2\right) + \left(p_\mu - \frac{p\cdot q}{q^2}q_\mu\right)\left(p_\nu - \frac{p\cdot q}{q^2}q_\nu\right)\frac{F_2\left(x, Q^2\right)}{p\cdot q} , \tag{1.49}$$

where $F_1(x, Q^2)$ and $F_2(x, Q^2)$ are the hadron structure functions and they gather all the information about the interior of the probed hadron. Another useful quantity is the longitudinal structure function $F_L = F_2 - 2xF_1$. In terms of F_2 and F_L the differential cross-section for DIS can be written as

$$\frac{d^2\sigma}{dxdQ^2} = \frac{2\pi\alpha^2}{xQ^4}\left[\left(1 + \left(1 - y\right)^2\right)F_2\left(x, Q^2\right) - y^2 F_L\left(x, Q^2\right)\right] . \tag{1.50}$$

Comparing equation (1.50) with (1.44) one concludes that

$$F_2\left(x, Q^2\right) = \sum_i e_i^2 f_i\left(x\right) , \quad F_L\left(x, Q^2\right) = 0 \tag{1.51}$$

The above relations mean that Bjorken scaling is equivalent to $F_2\left(x, Q^2\right)$ being a function that depends only on x and that the Callan-Gross relationship $F_2 = 2xF_1$ is a consequence of the fact that the quarks inside the hadron are particles with spin $-\frac{1}{2}$ [63].

In figure 1.9 we have a plot of $F_2(x, Q^2)$ as a function of Q^2 for different values of x. For $0.1 \lesssim x < 1$ it is evident that Bjorken scaling holds but for smaller values of x F_2 increases with Q^2 as predicted by NLO QCD. This implies that in fact the quark PDFs have a Q^2 dependence and that the structure of the proton depends on the resolution scale Q of the probe. Until today no one has been able to derive the quark PDFs from first principles in QCD. Instead, one assumes an ansatz for these functions at some scale Q_0^2 and evolve them to a scale Q^2 where we desire to make predictions. By comparing these predictions with data one can improve our initial ansatz. To obtain the set of equations that govern PDF evolution one considers the
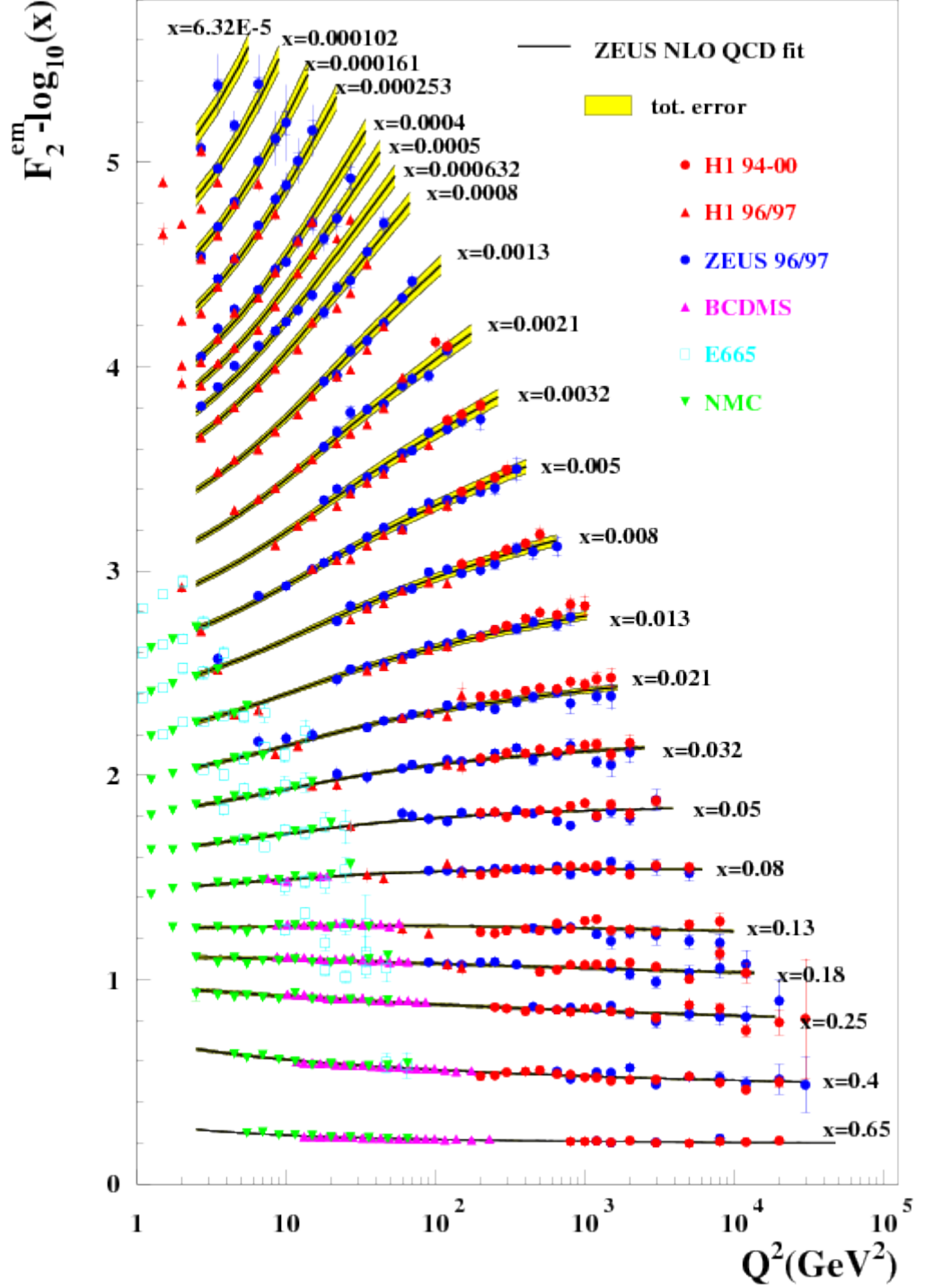
Figure 1.9: Plot of $F_2(x, Q^2)$ as a function of Q^2 for different values of x from the ZEUS experiment at HERA for electron-proton scattering. For $0.1 \lesssim x \lesssim 1$ one finds the predicted Bjorken scaling while for very small x one finds scaling violations. These scaling violations are predicted by NLO QCD after fixing the PDFs at low Q^2 and then applying the DGLAP evolution equations. Figure extracted from [64].

22
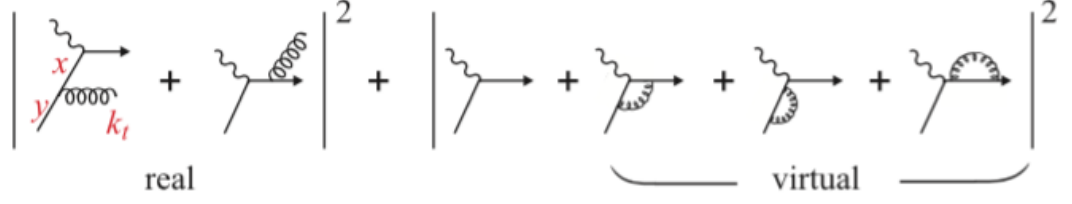
Figure 1.10: Feynman diagrams for deep inelastic scattering at NLO QCD. The first diagram in the second modulus squared is responsible for the zeroth-order term in expansion of F_2 as a power series in α_S. The diagrams in the first modulus plus the interference term of the zeroth order diagram with the virtual diagrams contribute for $O(\alpha_S)$ corrections to F_2. Figure extracted from [65].

scattering process of the quark with the lepton at NLO in QCD. Consider the Feynman diagrams presented in figure 1.10. The first diagram of the second modulus squared is the zeroth order contribution to F_2 as a power series expansion in α_S. The diagrams in the first modulus squared, as well as the virtual diagrams in the second modulus squared, will contribute to corrections of order α_S to the structure functions. After considering the contribution of these diagrams we find that the dependence of the PDFs of the quarks and gluons inside the proton are given by the following set of differential equations [65], [61] :

$$\frac{\partial}{\partial \log \mu^2} \begin{pmatrix} q_i(x,\mu^2) \\ g(x,\mu^2) \end{pmatrix} = \frac{\alpha_S(\mu^2)}{2\pi} \sum_j \int_x^1 \frac{d\zeta}{\zeta} \times \tag{1.52}$$

$$\times \begin{pmatrix} P_{q_i q_j}(\frac{x}{\zeta}, \alpha_S(\mu^2)) & P_{q_i g}(\frac{x}{\zeta}, \alpha_S(\mu^2)) \\ P_{g q_j}(\frac{x}{\zeta}, \alpha_S(\mu^2)) & P_{gg}(\frac{x}{\zeta}, \alpha_S(\mu^2)) \end{pmatrix} \begin{pmatrix} q_j(\zeta,\mu^2) \\ g(\zeta,\mu^2) \end{pmatrix},$$

where the functions $P_{q_i q_j}$, $P_{q_i g}$, $P_{g q_i}$ and P_{gg} are known as splitting functions and can be computed as a power series in α_S using perturbation theory. These coupled equations are known as the Dokshkitzer-Gribov-Lipatov-Altarelli-Parisi (DGLAP) equations. The dependence of the structure functions on Q^2 is analogous to the running couplings constant. The study of the PDFs is an active field of research, with different collaborations employing different methods in their determination. In chapter 3 we will use a NLO relation between F_2 and F_L to extract the gluon PDF from our holographic computation of these structure functions. Then we compare the qualitative dependence of our gluon PDFs with x with the PDFs by the CT18 and NNPDF collaborations. An example of the form of the PDFs can be seen in figure 1.11. As expected at $x \sim 1$ the valence quarks of the proton dominate its parton content, but for low x the proton is essentially made of a sea of gluons.
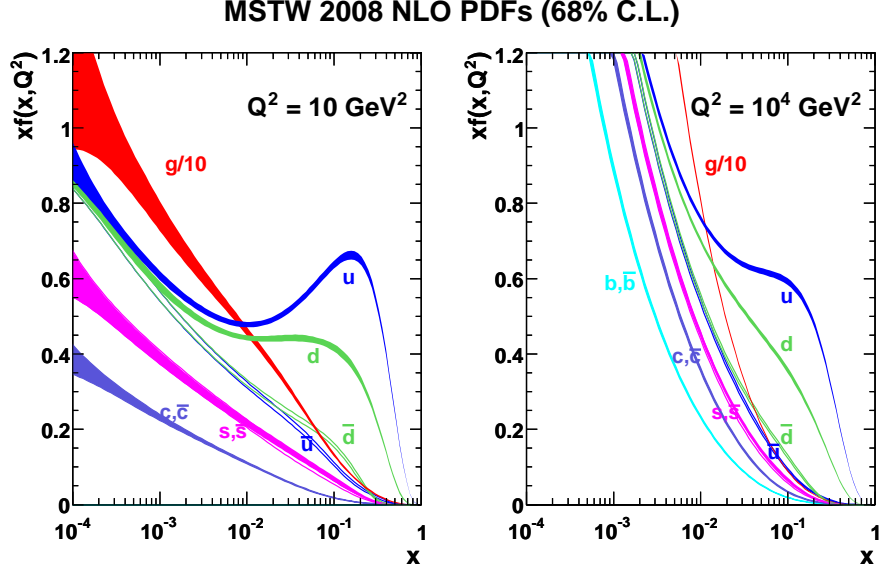
Figure 1.11: Parton distribution functions of the gluon, up, down, strange, charm quarks as well the corresponding quarks. In the left we have the PDFs at $Q^2 = 10\,\text{GeV}^2$ while on the right we have the PDFs at $Q^2 = 10^4\,\text{GeV}^2$. These PDFs are described in [66].

The structure functions are related to the cross-sections $\sigma_{\gamma^*p}^T$ and $\sigma_{\gamma^*p}^L$ of γ^*p scattering [67] for an incoming off-shell photon with transverse and longitudinal polarizations, respectively. For low x they are related by

$$F_2 = \frac{Q^2}{4\pi^2\alpha}\left(\sigma_{\gamma^*p}^T + \sigma_{\gamma^*p}^L\right) = \frac{Q^2}{4\pi^2\alpha}\sigma_{\gamma^*p}\,, \tag{1.53}$$

$$F_L = \frac{Q^2}{4\pi^2\alpha}\sigma_{\gamma^*p}^L\,. \tag{1.54}$$

As we have seen in section 1.1.3, using the concepts of the pomeron and meson Regge trajectory exchange one is able to describe the energy dependence of hadronic total cross-sections, including the case of γp scattering. In [2] Donnachie and Landshoff showed that this same model could be extended to γ^*p scattering by analysing data of σ_{γ^*p} (or equivalently F_2) with $Q^2 \leq 10\,\text{GeV}^2$. Their prediction for F_2 is

$$F_2\left(x, Q^2\right) = Ax^{1-\alpha_P(0)}\left(\frac{Q^2}{Q^2+a}\right)^{\alpha_P(0)} + Bx^{1-\alpha_R(0)}\left(\frac{Q^2}{Q^2+b}\right)^{\alpha_R(0)} \tag{1.55}$$

where $\alpha_P(0)$ and $\alpha_R(0)$ are, respectively, the intercepts of the pomeron and meson trajectories. The parameters A, a, B and b are related to the numerical values that appear in figure 1.6 in the limit $Q^2 \to 0$. Since $\alpha_P(0) = 1.08$ and $\alpha_R(0) = 0.55$, it

is clear from this formula that for $x \to 0$ one expects $F_2 \sim x^{-0.08}$ for any Q^2. The effective power of F_2 as a function of Q^2 at low x is given in figure 1.12 where the data points were obtained by $H1$ and $ZEUS$ collaborations at HERA. The plot shows
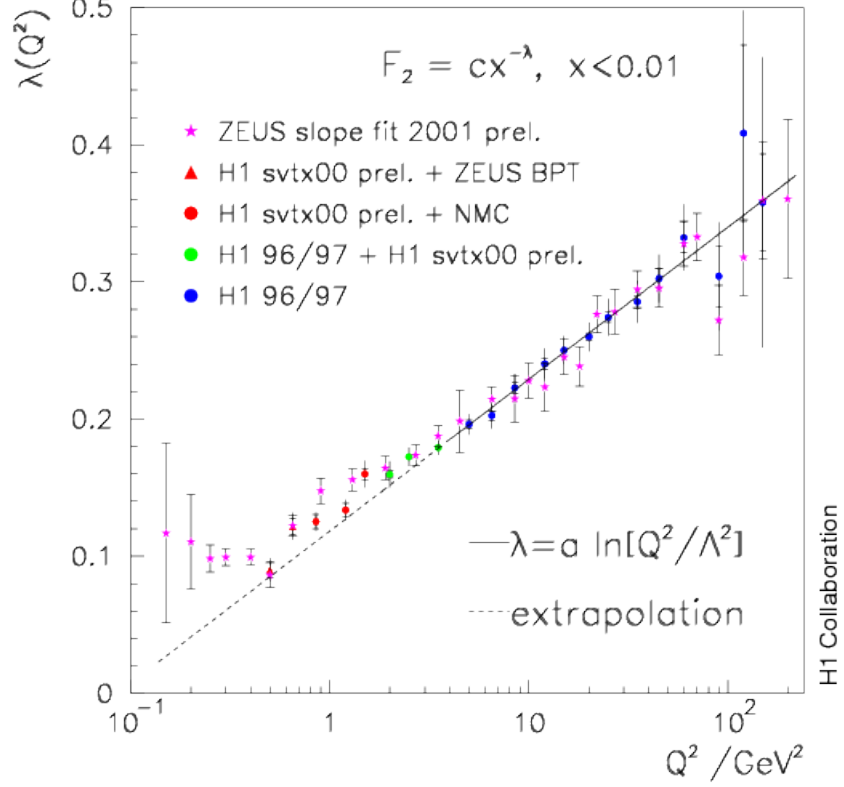
Figure 1.12: Effective power of F_2 at low x as a function of Q^2. Here $\lambda(Q^2) = j(0) - 1$. Figure extracted from [68].

that for low Q^2 the data are compatible with the soft Pomeron observed at hadronic soft processes with an intercept of 1.08. But that for large values of Q^2 the effective intercept increases up to $0.3 - 0.4$ for $Q^2 \approx 100\,\mathrm{GeV}^2$. This value of the intercept is precisely what is expected from the BFKL pomeron which we will review later. This motivated Donnachie and Landshoff to introduce a 'hard' Pomeron component in their Regge ansatz for F_2

$$F_2\left(x, Q^2\right) = f_0(Q^2)x^{-\epsilon_0} + f_1(Q^2)x^{-\epsilon_1} + f_2(Q^2)x^{-\epsilon_2}\,, \qquad (1.56)$$

$$f_0(Q^2) = A_0 \left(Q^2\right)^{1+\epsilon_0} \left(1 + \frac{Q^2}{Q_0^2}\right)^{-1-\epsilon_0/2}\,, \qquad (1.57)$$

$$f_i(Q^2) = A_i \left(Q^2\right)^{1+\epsilon_i} \left(1 + \frac{Q^2}{Q_i^2}\right)^{-1-\epsilon_i}\,, \quad i = 1, 2\,. \qquad (1.58)$$

Here ϵ_1 and ϵ_2 are 0.08 and -0.4525 respectively and were fixed by the hadronic total cross-sections. $1+\epsilon_0$ is the 'hard' Pomeron intercept and takes the value of 1.4372 after

fits to data. In [69, 70] Donnachie and Landshoff showed how this three component model could account for F_2 data with $x < 0.07$, the charm structure function F_2^c and $\sigma\left(\gamma p \to J/\psi\, p\right)$. From their fits to data they have found that the intercept of the hard pomeron is 1.4372.

BFKL pomeron
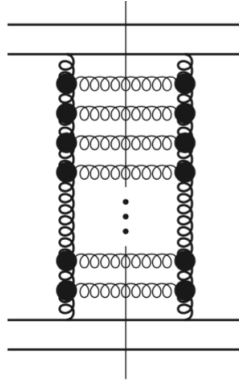
Figure 1.13: Representation of the BFKL evolution as a ladder diagram with effective Lipatov vertices (large solid circles) and "reggeized" gluons (bold corkscrew lines). Figure extracted from [71].

One of the drawbacks of Regge theory is that it does not predict key elements such as the Pomeron intercept. It is still not known how to derive such quantities from QCD. One seminal attempt to derive Regge behaviour from QCD was made by Balitsky, Fadin, Kuraev and Lipatov (BFKL). The BFKL approach is a procedure to sum the contributions of multiple gluon emission at small Bjorken x. In this kinematical regime, the proton, or any other hadron, becomes a dense medium of gluons. Also, for hard probes diagrams of order $[\alpha_s \ln(1/x)]^n$ are also important and should be included, resulting in the leading logarithm approximation.

The BFKL analysis starts by considering the scattering amplitude of two quarks through colour singlet exchange. The relevant diagrams are of the ladder type (see figure 1.13) whose vertical lines are "reggeized" gluons with couplings to gluon rungs given by the effective Fadin-Lipatov Γ vertex. The reggeized gluon is an effective particle that the two quarks exchange whose propagator produces the same amplitude as if we were summing all the diagrams of order $[\alpha_s \ln(1/x)]^n$ (while neglecting diagrams of order $\alpha_s[\alpha_s \ln(1/x)]^n$ and above) that involve exchange of several gluons. This process is shown in figure 1.14. The effective vertex is obtained in an analogous
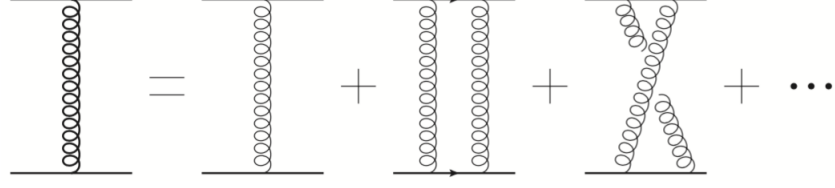
Figure 1.14: Reggeized gluon (bold corkscrew line) represented as the sum of all leading $\ln 1/x$ corrections to the single-gluon exchange amplitude for $qq \to qq$ scattering. Figure extracted from [71]
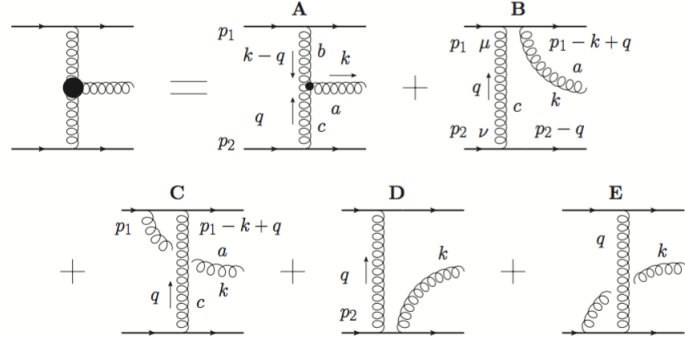
Figure 1.15: The effective real-gluon emission vertex (the Lipatov vertex), defined as the sum of all gluon emission diagrams. The triple gluon vertex is denoted by the smaller solid circle while the Lipatov vertex is shown by the larger solid circle. Figure extracted from [71].

way by considering the gluon emission process $qq \to qqg$, as show in figure 1.15.

BFKL found and solved an integral equation for the reggeized gluon four-point function which is essentially figure 1.13 without the external quark lines. We will not show a derivation of such equation, limiting ourselves to just present it and review its consequences. The BFKL amplitude $f\left(\omega, \vec{k}_1, \vec{k}_2, \vec{q}\right)$ satisfies the following equation for $t = 0$ [3, 4, 72]

$$\omega f\left(\omega, \vec{k}_1, \vec{k}_2, \vec{q}\right) = \delta^2\left(\vec{k}_1 - \vec{k}_2\right) + K_0 \otimes f\left(\omega, \vec{k}_1, \vec{k}_2, \vec{q}\right), \qquad (1.59)$$

where K_0 is the leading order (LO) BFKL kernel and its convolution with f is given

by

$$
K_0 \otimes f\left(\omega, \vec{k}_1, \vec{k}_2, \vec{q}\right) = \frac{\bar{\alpha}_s}{\pi} \int \frac{d^2 k'}{\left(\vec{k}_1 - \vec{k}'\right)^2}
$$

$$
\left[f\left(\omega, \vec{k}', \vec{k}_2, 0\right) - \frac{\vec{k}_1^2}{\vec{k}'^2 + \left(\vec{k}_1 - \vec{k}'\right)^2} f\left(\omega, \vec{k}_1, \vec{k}_2, 0\right) \right] , \qquad (1.60)
$$

where $\bar{\alpha}_s = 3\alpha_s/\pi$ and in the LO BFKL it is at a fixed scale. The solution of this equation is found after computing the eigenvalues and eigenfunctions of K_0 and is given by

$$
f\left(\omega, \vec{k}_1, \vec{k}_2, 0\right) = \sum_i \frac{\phi_i(\vec{k}_1)\phi_i(\vec{k}_2)}{\omega - \lambda_i} , \qquad (1.61)
$$

where

$$
K_0 \otimes \phi_i(\vec{k}) = \lambda_i \phi_i(\vec{k}) . \qquad (1.62)
$$

The sum over i in the above equation is in fact a sum over an integer n from zero to infinity and an integral over a continuous variable ν. The eigenfunctions are given by

$$
\phi_\nu^n = \frac{1}{\pi\sqrt{2}} \left(k^2\right)^{-1/2+i\nu} e^{in\theta} . \qquad (1.63)
$$

The LO BKFL amplitude takes then the form

$$
f\left(\omega, \vec{k}_1, \vec{k}_2, 0\right) = \sum_{n=0}^{\infty} \int_{-\infty}^{+\infty} \frac{d\nu}{2\pi^2 k_1 k_2} \left(\frac{k_1^2}{k_2^2}\right)^{i\nu} \frac{e^{in(\theta_1 - \theta_2)}}{\omega - \bar{\alpha}_s \chi_n(\nu)} , \qquad (1.64)
$$

where

$$
\chi_n(\nu) = 2\psi(1) - \psi\left(\frac{1 + |n|}{2} + i\nu\right) - \psi\left(\frac{1 + |n|}{2} - i\nu\right) , \qquad (1.65)
$$

with $\psi(z)$ defined as the derivative of the logarithm of the Γ-function. Among all the terms in the sum, the one that dominates is $n = 0$. Further progress can be made by rewriting the integral in equation (1.64) in a Mellin integral in γ-space, with $\gamma = \frac{1}{2} + i\nu$

$$
f\left(\omega, \vec{k}_1, \vec{k}_2, 0\right) = \frac{1}{\pi k_1^2} \int_{\frac{1}{2}-i\infty}^{\frac{1}{2}+i\infty} \frac{d\gamma}{2\pi i} \left(\frac{k_1^2}{k_2^2}\right)^{\gamma} \frac{1}{\omega - \bar{\alpha}_s \chi_0(\gamma)} . \qquad (1.66)
$$

The forward colour singlet quark scattering amplitude can be written in terms of the BFKL amplitude as

$$
\frac{A(s,0)}{s} = 4i\alpha_s^2 G_0 \int \frac{d^2 k_1 d^2 k_2}{k_1^2 k_2^2} F\left(s, \vec{k}_1, \vec{k}_2\right) , \qquad (1.67)
$$

where

$$F\left(s, \vec{k}_1, \vec{k}_2\right) = \int \frac{d\omega}{2\pi i} \left(\frac{s}{\vec{k}^2}\right)^\omega f\left(\omega, \vec{k}_1, \vec{k}_2, 0\right) , \tag{1.68}$$

and the ω contour is parallel to the imaginary axis and is to the right of all singularities in the ω plane. We can now deform the ω contour to catch the singularity at $\omega = \bar{\alpha}_s \chi_0(\gamma)$. For large values of s, the integrand in the γ plane is dominated by $\left(s/\vec{k}^2\right)^{\bar{\alpha}_s\chi_0(\gamma)}$ and is highly peaked at $\gamma = 1/2$. Performing a saddle approximation yields

$$F\left(s, \vec{k}_1, \vec{k}_2\right) = \frac{1}{\pi k_1 k_2} \frac{(s/k^2)^{\bar{\alpha}_s\chi(1/2)}}{\sqrt{2\pi\bar{\alpha}_s\chi''(1/2)\log(s/k^2)}} . \tag{1.69}$$

From this result and equation (1.67) one can see that the total cross-section for quark-quark scattering rises as $\omega_0 = \bar{\alpha}_s\chi(1/2) \approx 0.32$ if one takes α_s to be 0.120. For the case of $\gamma^* p$ scattering the total cross-section given by BFKL is

$$\sigma_{\gamma^* p}(s, Q^2) = \frac{1}{(2\pi)^4} \sum_{\lambda=T,L} \int \frac{d^2k_1 d^2k_2}{k_1^2 k_2^2} \Phi_{\gamma,\lambda}\left(\vec{k}_1\right) \Phi_p\left(\vec{k}_2\right) F\left(s, \vec{k}_1, \vec{k}_2\right) , \tag{1.70}$$

where λ is the polarization state of the off-shell photon and $\Phi_{\gamma,\lambda}$, Φ_p are the γ^* and proton impact factors that relate these particles to their quark content. The factor Φ_γ can be calculated by analysing $\gamma^* \to q\bar{q}$, but the associated proton object is non-perturbative in general. Nevertheless one can see that the BFKL total cross-section for $\gamma^* p$ goes like $s^{0.32}$. This value of the BFKL pomeron intercept is larger than the value found at hadron-hadron data. However, it is very close to what Donnachie and Landshoff have found. It is for this reason that the BFKL result received so much attention by the community.

Despite the above results, the BFKL approach has its forthcomings. One of them is that since it is a perturbative approach it will fail to understand the non-perturbative effects related to the Pomeron. In particular, it is still not known how to relate the BFKL pomeron with the soft pomeron. Another problem with this approach is that it is assumed that the strong coupling constant α_s does not run much with the energy scales of the process, which is not true for processes like DIS. Also, a very important issue is that it was shown that the NLO contribution to the scattering amplitude was larger than the LO contribution. This demands the computation of the NNLO computation, which is a formidable task, to check if it is possible to use this technique to make predictions.

Saturation and the BK equation

The DGLAP gluon PDF is related to equation (1.69) and to the proton factor Φ_p through

$$xg(x, Q^2) = \frac{1}{\pi} \int_0^{Q^2} \frac{d^2k}{k^2} \Theta(Q^2 - \vec{k}^2) F_g(x, \vec{k}) \,, \tag{1.71}$$

$$F_g(x, \vec{k}) = \frac{1}{2\pi^3} \int \frac{d^2k'}{k'^2} \Phi_p(\vec{k'}) k^2 F(x, \vec{k}, \vec{k'}) \,, \tag{1.72}$$

where we have used the relation $x \approx Q^2/s$. Although a computation of xg demands knowledge of the proton factor, we can already see from the above equation that BFKL predicts that for very low x (or equivalently for high s) $xg(x, Q^2) \sim x^{-\omega_0}/\sqrt{\log(1/x)}$. It is generally believed that at some point the growth of the gluon density must be tamed in order to satisfy the Froissart bound. The Froissart bound states that the total cross-section of any hadron-hadron scattering process can not grow faster then $\frac{\pi}{m_\pi^2}(\log s)^2$. Although this has not been observed in data, it is believed that it holds since it is derived assuming that the S matrix is unitary and that the strong interaction has a finite range of order $1/m_\pi$ [73, 74]. This scale is of non-perturbative nature and hence the Froissart bound includes both the perturbative and non-perturbative properties of QCD. In order to restore unitarity it is believed that at high energies gluon recombination occurs although the link between them is not understood. By adding Feynman diagrams that are responsible for gluon recombination, Gribov, Levin and Ryskin [72] derived a nonlinear evolution equation for the gluon PDF in the double leading logarithmic approximation (DLLA $\log(1/x) \log Q^2 \gg 1$). Taking into account both gluon production and recombination the evolution equation for the gluon PDF is

$$Q^2 \frac{\partial^2 xg(x, Q^2)}{\partial \log(1/x) \partial Q^2} = \frac{\alpha_s N_c}{\pi} xg(x, Q^2) - \frac{4\alpha_s^2 N_c}{3 C_F R^2 Q^2} \left[xg(x, Q^2) \right]^2 \,. \tag{1.73}$$

The first term in equation (1.73) is what we get from DGLAP equations in the double logarithmic approximation, while the second, nonlinear term is accountable for gluon recombination. Note that the recombination term is inversely proportional to the hadron area $\sim R^2$ and the scale Q^2 at which the gluon density is probed. This makes sense since a bigger area means that it takes more gluons to fill up the hadron. On the other hand the typical gluon size $r \sim 1/Q$ and hence for bigger Q^2 we will need more gluons for saturation to occur.

In the regime of saturation, the BFKL equation is not valid anymore and one needs to include the recombination of gluons. Balitsky and Kovchegov [75,76] derived independently an integro-differential equation with a quadratic term like (1.73) that encodes

parton recombination. The BK equation was derived by Balitsky by considering the operator product expansion for high energy scattering in QCD. With this procedure he derived a hierarchy of coupled equations for correlators of Wilson lines which reduce to a single one in the limit of large number of colours N_c. The same equation was derived by Kovchegov by considering the dipole formulation of high energy scattering.

The dipole formalism works as follows. Consider the process $\gamma^* p$ in the proton's rest frame. The off-shell photon with momentum q, such that $Q^2 = -q^2$, can fluctuate into a $q\bar{q}$ pair. The quark carries a fraction z of q and the pair will scatter coherently with the proton through the strong interaction. Throughout this interaction it is assumed that the transverse size of the pair r remains constant. Also, the interaction time is assumed to be much smaller then the splitting time of the γ^* into a $q\bar{q}$ pair. The initial scattering process is then reduced to a dipole-proton interaction. On the other hand, each quark in the dipole can also emit a gluon which in the limit of large N_c can be represented by a quark-antiquark pair. Thus, in this limit, the emission of one gluon by the quarks is equivalent to the splitting of the original dipole into two dipoles. This can be generalised to an arbitrary number of gluons n where one will have $n + 1$ dipoles.

If we consider only the contribution from the single scattering of one dipole on the target, one obtains a linear evolution equation for the dipole-target amplitude

$$\frac{d\mathcal{N}(\vec{b}_{01}, \vec{x}_{01}, Y)}{dY} = \bar{\alpha}_s \int \frac{d^2 x_2 x_{01}^2}{x_{20}^2 x_{12}^2} \left[\mathcal{N}(\vec{b}_{01} + \frac{\vec{x}_{12}}{2}, \vec{x}_{20}, Y) + \mathcal{N}(\vec{b}_{01} - \frac{\vec{x}_{20}}{2}, \vec{x}_{12}, Y) \right. \tag{1.74}$$
$$\left. - \mathcal{N}(\vec{b}_{01}, \vec{x}_{01}, Y) \right],$$

where $Y = \log(1/x)$ is the rapidity, $b_{ij} = (\vec{x}_i + \vec{x}_j)/2$ and $x_{ij} = \vec{x}_i - \vec{x}_j$. This equation is the dipole version of BFKL in the transverse coordinate space and has been derived in [77]. On the other hand, if we consider multiple incoherent dipole scatterings, one obtains the BK equation

$$\frac{d\mathcal{N}(\vec{b}_{01}, \vec{x}_{01}, Y)}{dY} = \bar{\alpha}_s \int \frac{d^2 x_2 x_{01}^2}{x_{20}^2 x_{12}^2} \left[\mathcal{N}(\vec{b}_{01} + \frac{\vec{x}_{12}}{2}, \vec{x}_{20}, Y) + \mathcal{N}(\vec{b}_{01} - \frac{\vec{x}_{20}}{2}, \vec{x}_{12}, Y) \right. \tag{1.75}$$
$$\left. - \mathcal{N}(\vec{b}_{01}, \vec{x}_{01}, Y) - \mathcal{N}(\vec{b}_{01} + \frac{\vec{x}_{12}}{2}, \vec{x}_{20}, Y) \mathcal{N}(\vec{b}_{01} - \frac{\vec{x}_{20}}{2}, \vec{x}_{12}, Y) \right],$$

which has a nonlinear term for the evolution of the amplitude. The nonlinear term encodes the gluon recombination and for large Y will lead to saturation.

To solve this equation one needs to provide an initial condition that is a non-perturbative object and has to be modelled. Despite this, the solutions of the BK equation

turned out to express geometric scaling phenomena observed in lepton-proton and lepton-nucleus data [78]. Moreover, its solutions also preserve locally unitarity in the transverse configuration space. Until today the BK equation is the best established phenomenological method to include non-linear effects due to the dense gluon medium.

The Colour Glass Condensate

We end our review on the relation between Pomeron physics and QCD by mentioning briefly another approach to study partonic systems at small x called the Colour Glass Condensate (CGC) [79]. The CGC is an effective field theory description of saturated gluons in the Regge limit. In it we have two kinds of degrees of freedom that are separated into fast frozen colour sources ρ_a and slow dynamical gauge fields A_a^μ. Denoting the separation scale by Λ^+, gluons with longitudinal momentum $k^+ > \Lambda^+$ (fast gluons) are frozen by Lorentz time dilatation. This generates a random colour charge density ρ_a that changes with each event. The probability of a particular distribution ρ_a is given by a gauge invariant distribution $W_{\Lambda^+}[\rho]$ provided by the CGC. On the other hand, we have slow gluons with longitudinal momentum $k^+ < \Lambda^+$ which are described by dynamical gauge fields A_a^μ in QCD. The independence of the physical observable with respect to the scale that separates fast and slow degrees of freedom is secured by the Jalilian-Marian-Iancu-McLerran-Weigert-Leonid-Kovner (JIMWLK) renormalization group equation. This JIMWLK evolution is the same hierarchy of coupled evolution equations that Balitsky used to derive the BK equation. In fact, the BK equation is the mean field approximation of JIMWLK evolution, valid at large N_c. This JIMWLK formalism also provides a functional equation that describes the evolution of $W_{\Lambda^+}[\rho]$ with Λ^+

$$\frac{\partial W_{\Lambda^+}[\rho]}{\partial \log(\Lambda^+)} = -\mathcal{H}\left[\rho, \frac{\delta}{\delta\rho}\right] W_{\Lambda^+}[\rho], \qquad (1.76)$$

where $\mathcal{H}$ is the JIMWLK Hamiltonian.

In figure 1.16 it is shown the qualitative phase diagram of QCD evolution. As show in it and discussed above, the evolution of the PDFs to higher Q^2 values is governed by the DGLAP equations while the PDF evolution for small x is given by the BFKL. This BFKL evolution will only be valid up to the point where saturation effects become important. The point at which these effects are important depends on the scale Q that we are operating on and for this reason we have the straight line in the figure. Above this line the hadron is saturated and it is in these conditions that the CGC formalism is expected to work.
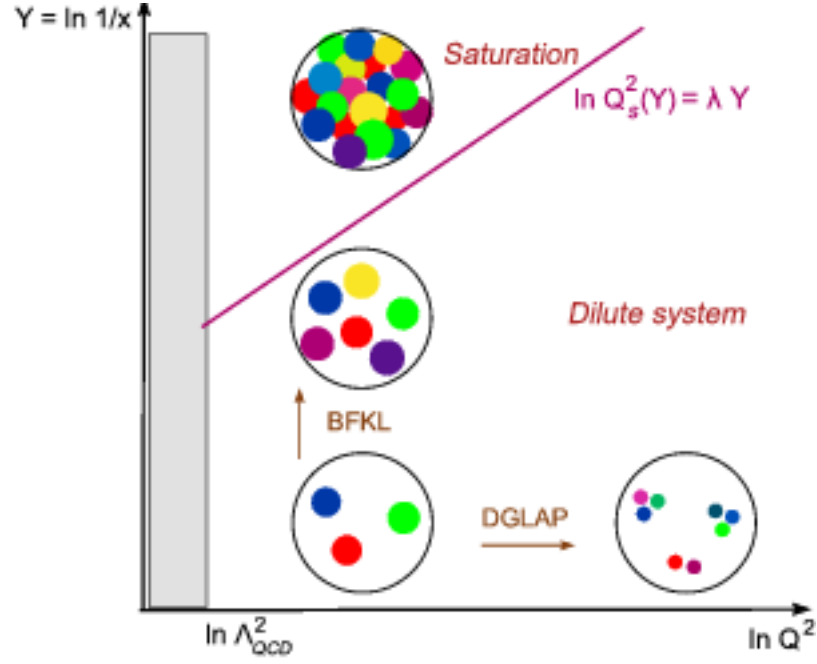
Figure 1.16: Phase diagram of QCD evolution. The small coloured circles represent the partons inside the hadrons. Figure extracted from [79].

The CGC and its derived models have provided a successful phenomenological description of hadron-hadron and lepton-hadron collisions at high energy. They have also provided a semi-quantitative framework that described a large variety of processes at RHIC and HERA. This approach works better provided that the occupancy number of gluons $n \sim 1/\alpha_s$ is large. Then high energies are necessary in order to have a small coupling constant and this why it is believed that the LHC can provide a good test of this theory. However and understanding of QCD soft processes has not been achieved in this framework, although there are attempts to map CGC degrees of freedom to the language of Pomerons.

1.2 Gauge/Gravity duality and the Pomeron

The discovery of the AdS/CFT duality by J. Maldacena [7] gave us a new tool to study QFTs in the strongly coupled regime. This conjecture states that a theory of gravity in AdS_{d+1} is dual to a Conformal Field Theory (CFT) in the boundary of this space. An important result that pre-dates the AdS/CFT correspondence was obtained previously by 't Hooft while studying the relationship between string theory and the generalization of QCD to any number of colours N, i.e. $SU(N)$ Yang-Mills

theories. 't Hooft considered the limit of $N \to \infty$ and showed that the perturbative expansion in Feynman diagrams in these QFTs resembles the genus expansion in string theory. An example of this duality was also given by Maldacena by proposing that type IIB superstring theory on $AdS_5 \times S^5$ is dual to $\mathcal{N} = 4$ Super Yang-Mills theory (SYM) on $3 + 1$ dimensions. A non-supersymmetric example of this duality was also proposed by Klebanov and Polyakov [80] by conjecturing that the $O(N)$ vector model and Vasiliev's higher spin gauge theories are dual to each other.

Soon after the paper of Maldacena, Gubser, Klebanov, Polyakov [81] and Witten [82] showed how to relate correlation functions of operators in $\mathcal{N} = 4$ SYM with the supergravity action, how the conformal dimension of the operators are related to particle masses in supergravity and how AdS black holes thermodynamics are related to a phase transition in $\mathcal{N} = 4$ SYM in the large N limit. The duality can be stated as

$$ Z_{QFT}[J(x)]_{\partial\mathcal{M}} = Z_{gravity}[\phi(X)]_{\mathcal{M}}, \qquad \phi(X \to \partial\mathcal{M}) = J(x), \qquad (1.77) $$

where $\partial\mathcal{M}$ is the boundary of the manifold $\mathcal{M}$ where the theory of gravity is defined. The quantum field theory lives on $\partial\mathcal{M}$ and $J(x)$ is the source of some operator $\mathcal{O}$ of the QFT dual to some field $\phi(X)$ in $\mathcal{M}$. Although it is quite remarkable that two different theories are related to each other, what makes the duality useful is the fact that it maps a strongly coupled QFT, which we do not know how to solve with Feynman diagrams, to a weakly coupled theory of gravity, which we do know how to solve. In the particular example of $\mathcal{N} = 4$ and type IIB strings in $AdS_5 \times S_5$, the relation between the gauge theory coupling constant and the string theory coupling constant is

$$ \frac{L^4}{l_s^4} = g_{YM}^2 N = \lambda, \qquad (1.78) $$

where λ is the t'Hooft coupling and L is the AdS radius. When the 't Hooft coupling is large, $L/l_s \gg 1$ which means that we are in the limit of weakly coupled gravity.

So far the examples found for the duality involve quantum field theories that are not like QCD, since it is not supersymmetric or conformal at all energy scales. Although the gravity dual of QCD is not known, we can still use the AdS/CFT correspondence by studying it in certain limits and learn how to construct a gravity dual close to QCD. This has allowed to understand how to include flavour degrees of freedom (quarks), spontaneous chiral symmetry breaking or the understanding of the quark-gluon plasma. In the next subsections we will give more details about the gauge/gravity duality and discuss the concept of the Witten diagram. We also quickly review some bottom-up approaches of Holographic QCD since these will serve as basis for the work presented in this thesis.

1.2.1 An example of the duality

The AdS/CFT correspondence, or gauge/gravity duality, is a conjectured relationship between quantum theories of gravity formulated in AdS spaces and conformal field theories. As mentioned before the most useful feature of this duality is that it is a strong-weak duality: we can solve field theory strong coupling problems by solving the corresponding gravitational weak coupling problem on the other side of the duality. This conjecture is also a realisation of the holographic principle which states that the information within a volume of space is encoded on the boundary of that region. This principle emerged after the results of black hole thermodynamics, where it was found that that the number of degrees of freedom in a volume V_d are given by the area A_{d-1} of the boundary ∂V_d of this volume measured in units of the Planck area l_P^{d-1}.

As an example of the correspondence, we describe briefly the case of $\mathcal{N} = 4$ SYM in $3 + 1$ dimensions dual to IIB superstring theory on $AdS_5 \times S^5$. In this concrete example, on the CFT side, $\mathcal{N} = 4$ Super Yang-Mills is a gauge theory with gauge group $SU(N)$ with coupling constant g_{YM}. In the string theory side the string length is $l_s = \sqrt{\alpha'}$, coupling constant g_s, the radius of curvature of $AdS_5 \times S^5$ is L and there are N units of a 5-form $F_{(5)}$ flux on S^5. The relations between the free parameters of these theories are the following :

$$g_{YM}^2 = 4\pi g_s \,, \quad 4\pi g_s N = L^4/\alpha'^2 \,. \tag{1.79}$$

Note that in the first equation we have only the coupling constant g_{YM}, while on the second one has the 't Hooft coupling constant $\lambda = g_{YM}^2 N$.

The conjecture follows from the fact that D-branes in string theory and p-brane solutions from supergravity are the same object. Consider IIB string theory on $9 + 1$ dimensional Minkowski spacetime where a closed string is propagating and where we have N coincident D3-branes. This closed string can interact with these branes by either letting the loop breaking in two open strings with ends moving on the branes (open string perspective) or by considering this set of branes as a soliton of the theory and hence curving the spacetime where the closed string propagates (closed string perspective).

From the open string perspective the N coincident D3-branes only conserve 16 of the 32 supercharges of IIB superstring theory on the 10-dimensional Minkowski spacetime. We have open strings propagating on the 4-dimensional branes and closed strings on the 10-dimensional flat spacetime. Moreover, we will consider only the low energy scenario where only the massless excitations of the strings are considered. Because the

N branes are coincident the open strings between different branes are massless and the states are valued in the adjoint representation of the gauge group $U(N)$. The action for the string modes is then

$$S = S_{closed} + S_{open} + S_{int} \tag{1.80}$$

where the last term regulates the interaction between the open and closed modes.

In the low energy limit $\alpha' \to 0$, the closed string dynamics is given by type IIB supergravity whose bosonic action is

$$S_{IIB} = \frac{1}{2k^2} \int d^{10}x \left\{ \sqrt{-g} \left[e^{-2\phi} \left(R + 4\partial_M\phi\partial^M\phi - \frac{1}{2}|H|^2 \right) - \right. \right.$$
$$\left. \left. - \frac{1}{2}|F_1|^2 - \frac{1}{2}|\tilde{F}_3|^2 - \frac{1}{4}|\tilde{F}_5|^2 \right] - \frac{1}{2}A_4 \wedge H_3 \wedge F_3 \right\} \tag{1.81}$$

with $2k^2 = (2\pi)^7\alpha'^4 g_s^2$. The above action has the following field content: the spacetime metric g_{MN}; the dilaton field ϕ; the field strength tensor H_{MNR} of the antisymmetric field B_{MN}; a scalar A_0 with $F_1 = dA_0$; a 2-index antisymmetric field A_{MN} with field strength $F_{MNR} = 3\partial_{[M}A_{NR]}$; and a 4-index antisymmetric tensor field A_{MNRS} with modified field strength $\tilde{F}_5$, which is self-dual

$$\tilde{F}_{\mu_1\cdots\mu_5} = \frac{1}{5!}\epsilon_{A_1\cdots A_5}{}^{A_6\cdots A_{10}}\tilde{F}_{A_6\cdots A_{10}} . \tag{1.82}$$

In the action (1.81) $\tilde{F}_3$ and $\tilde{F}_5$ are given by

$$\tilde{F}_3 = F_3 - A_0 \wedge H_3 \,,$$
$$\tilde{F}_5 = F_5 - \frac{1}{2}A_2 \wedge H_3 + \frac{1}{2}B \wedge F_3 \,. \tag{1.83}$$

If we now expand the metric as $g = \eta + kh$ the action becomes

$$S_{closed} = -\frac{1}{2} \int d^{10}x \partial_M h \partial^M h + \mathcal{O}(k) \,, \tag{1.84}$$

where the $\mathcal{O}(k)$ terms consist of field strength tensors as well fermionic fields. Since k is proportional to α', S_{closed} reduces to the free supergravity action in 10-dimensional Minkowski spacetime in the limit $\alpha' \to 0$.

Since we have N coincident D3-branes we will have six scalar fields ϕ^{ia} and and a gauge field A_μ^a defined on the worldvolume in the adjoint representation a of the $U(N)$ gauge group. Because the gauge field is massless we have a total of eight on-shell bosonic degrees of freedom. By supersymmetry we should have eight fermionic degrees of freedom. Since in 4-dimensional on-shell fermion has two degrees of freedom

this means that in order to complete the supersymmetric multiplet we need to have 4 fermionic fields ψ^{Ia}, $I = 1, \cdots, 4$ in the adjoint representation of $U(N)$. Thus the total field content matches the one of $\mathcal{N} = 4$ SYM in four dimensions. A single D3-brane is described by a Dirac-Born-Infeld (DBI) plus Wess-Zumino (WZ) action. This action includes the interaction with the closed string sector. If we take into account that we have N coincident D3-branes so that we have to take traces over the gauge group to obtain a gauge invariant action, as well use the corresponding covariant derivatives, after we expand the DBI term we find that the action around flat space for the bosonic open string sector is

$$S_{open} = -\frac{1}{2\pi g_s} \int d^4x \, \mathrm{Tr}\Big[\frac{1}{4}F_{\mu\nu}F^{\mu\nu} + \frac{1}{2}\sum_i D_\mu\phi^i D^\mu\phi^i - \sum_{i,j}[\phi^i, \phi^j]^2 + \mathcal{O}(\alpha')\Big] \quad (1.85)$$

where $F_{\mu\nu} = \partial_\mu A_\nu - \partial_\nu A_\mu + i[A_\mu, A_\nu]$, the covariant derivative $D_\mu = \partial_\mu \cdot + i[A_\mu, \cdot]$ with $\phi^i = \phi^{ia}T_a$ and $A_\mu = A_\mu^a T_a$. If we take the limit $\alpha' \to 0$ and make the identification $4\pi g_s = g_{YM}^2$ we get precisely the bosonic part of $\mathcal{N} = 4$ SYM. On the other hand, the interaction term action S_{int} has terms proportional to α' and vanishes when $\alpha' \to 0$.

To sum up, in the open string perspective we have two theories that are completely decoupled in the low energy limit $\alpha' \to 0$: $N = 4$ SYM in the D3-branes and free supergravity in the bulk.

In the closed string perspective we substitute the D3-branes by the corresponding p-brane supergravity solution. For N coincident branes the IIB supergravity solution for the metric is

$$ds^2 = \frac{1}{\sqrt{H(r)}}\eta_{\mu\nu}dx^\mu dx^\nu + \sqrt{H(r)}[dr^2 + d\Omega_5^2] \quad , \quad H(r) = 1 + \frac{L^4}{r^4}, \quad (1.86)$$

where $\eta_{\mu\nu}$ is the metric of the four dimensional Minkowski spacetime and

$$H(r) = 1 + \frac{L^4}{r^4}, \quad L^4 = 4\pi g_s N\alpha'^2. \quad (1.87)$$

For large values of r relative to L, $H(r) \approx 1$ and the metric is reduced to ten dimensional Minkowski spacetime. On the other hand, in the neighbourhood of $r = 0$, $H(r) \approx L^4/r^4$ and by making the change of variables $z = L^2/r$ we get the metric of $AdS_5 \times S^5$:

$$ds^2 = \frac{L^2}{z^2}(dz^2 + \eta_{\mu\nu}dx^\mu dx^\nu) + L^2 d\Omega_5^2, \quad (1.88)$$

where both spaces have the same radius of curvature. It is then clear that we have two types of closed strings, one that propagates in flat 10 dimensional spacetime and

other that propagates near $r = 0$. When the gauge theory is at strong coupling (i.e. $4\pi g_s N = \lambda \gg 1$ the size of the string is very small compared with the radius of curvature and we are working with very low energies. The closed strings near $r = 0$ are described by type IIB supergravity on $AdS_5 \times S^5$ and the dynamics of the closed string on the asymptotic flat spacetime is given again by type IIB supergravity but on 10 dimensional Minkowski spacetime. Moreover from the perspective of an observer at infinity, these two sectors are also decoupled.

At this point we have two equivalent perspectives each described by two decoupled effective theories. In both perspectives the theory type IIB supergravity on 10-dimensional Minkowski spacetime is present. On the other hand in the open string perspective we have $\mathcal{N} = 4$ SYM theory while on the closed string perspective we have type IIB supergravity on $AdS_5 \times S^5$, which is a low energy limit of type IIB superstring theory on $AdS_5 \times S^5$. By relaxing this low energy limit Maldacena conjectured that $\mathcal{N} = 4$ SYM on 4 dimensional flat spacetime is equivalent to type IIB string theory on $AdS_5 \times S^5$.

With relations 1.79 one can analyze the strong-weak feature of the duality. Consider the weak coupling regime in the string theory side , i.e. $g_s \ll 1$ while the ratio $L/\sqrt{\alpha'}$ is kept constant. This means that $g_{YM} \ll 1$ while $g_{YM}^2 N$ is kept constant which means that $N \to +\infty$. This is the well known 't Hoof limit. Note that since the 't Hooft coupling is fixed λ, then $g_s \propto \frac{1}{N}$ suggesting a map between an $1/N$ expansion in the field theory side with an expansion in the genus of the string genus on the string theory side. This situation is known as the *strong form* of the duality. When the field theory is strongly coupled, i.e. λ is large, the size of the string compared with the radius of curvature L is very small and then the string can be approximated by a point particle. In this limit IIB superstring theory is given by IIB supergravity on $AdS_5 \times S^5$ and the strongly coupled $\mathcal{N} = 4$ SYM is mapped to the weakly curved $AdS_5 \times S^5$.

Of course, the above discussion does not constitute a proof that $\mathcal{N} = 4$ SYM is dual to type IIB superstring theory. However, the discovery of integrability structures of in both $\mathcal{N} = 4$ SYM and semi-classical type IIB strings in $AdS_5 \times S_5$ allowed to confirm its validity. A review of these results can be found in [83].

1.2.2 Correlators and Witten diagrams

In this section we will introduce the Witten diagram expansion. We have seen previously that the gauge/gravity duality states that the partition function of a theory

of gravity (e.g. string theory) defined in an asymptotically AdS space $\mathcal{M}$ is equal to the partition function of a QFT in the boundary $\partial\mathcal{M}$ of this space. Moreover to each boundary field $\mathcal{O}$ there is a bulk field ϕ in $\mathcal{M}$ that satisfies the boundary condition $\phi(X \to \partial\mathcal{M}) = J(x)$, where $J(x)$ is the source of $\mathcal{O}$.

The duality becomes very useful to study strong coupling physics in the large N limit of the QFT because in this regime the path integral in the gravity side is dominated by the classical configuration:

$$Z_{\text{gravity}} \sim e^{iS_{\text{on-shell}}} \,. \tag{1.89}$$

The bulk fields can be expressed in terms of the boundary sources $J(x)$ of the QFT operators. To compute the correlation functions one then needs to take functional derivatives of 1.89 with respect to the sources $J(x)$. The Witten's diagram expansion is a systematic way of computing $\exp(iS_{\text{on-shell}})$.

We will illustrate this procedure by considering the case of a scalar operator $\mathcal{O}$ of a CFT in d dimensions with conformal dimension Δ. From the gauge/gravity duality we know this operator is dual to a bulk scalar field $\phi(X)$ in AdS_{d+1} with bulk mass $m^2 L^2 = \Delta(\Delta - d)$, where L is the AdS space radius. The action for such a scalar field is

$$S_\phi = -\frac{1}{2} \int d^{d+1} X \sqrt{-g} \left(g^{AB} \partial_A \phi \partial_B \phi + m^2 \phi^2 \right) \,. \tag{1.90}$$

The Klein-Gordon equation for a scalar field is then

$$\left(\nabla^2 - m^2 \right) \phi = 0 \,. \tag{1.91}$$

where

$$\nabla^2 \phi = \frac{1}{L^2} \left(z^2 \partial_z^2 - (d-1) z \partial_z + z^2 \eta_{\mu\nu} \partial^\mu \partial^\nu \right) \phi \,, \tag{1.92}$$

for AdS spaces. To make progress it is useful to perform a Fourier decomposition in the Minkowski coordinates x^μ and consider the ansatz $\phi(z, x) = e^{ik \cdot x} \phi_k(z)$. The resulting equation for the modes $\phi_k(z)$ is

$$z^2 \partial_z^2 \phi_k(z) - (d-1) z \partial_z \phi_k(z) - (m^2 L^2 + k^2 z^2) \phi_k(z) = 0 \,, \tag{1.93}$$

where $p^2 = \eta_{\mu\nu} p^\mu p^\nu$. There are two independent solutions to this equation with different asymptotics near the boundary, i.e. $z \to 0$,

$$\phi_k(z) = \begin{cases} z^{\Delta_+} & \text{normalisable} \,, \\ z^{\Delta_-} & \text{non} - \text{normalisable} \,, \end{cases} \tag{1.94}$$

where $\Delta^{\pm}$ are the roots of $\Delta(\Delta - d) = m^2 L^2$, i.e.

$$\Delta^{\pm} = \frac{d}{2} \pm \sqrt{\frac{d^2}{4} + m^2 L^2} \,. \tag{1.95}$$

Near the boundary the scalar field can be expressed in terms of these solutions as

$$\phi(z, x) \sim \phi_{(0)}(x) z^{\Delta^-} + \phi_{(+)}(x) z^{\Delta^+} + \cdots \tag{1.96}$$

By dimensional analysis the normalisable mode is identified with the vacuum expectation value of a dual scalar field operator $\mathcal{O}$ of dimension $\Delta = \Delta^+$, while the non-normalisable mode ϕ_0 as a source of this operator. The bulk field and the boundary source are then related through

$$\phi_{(0)}(x) = \lim_{z \to 0} \phi(z, x) z^{-\Delta^-} \,. \tag{1.97}$$

Now that we know the relationship between the bulk field and a boundary source, we would like to find a solution of equation (1.91) satisfying the boundary condition $\phi(z, x) = \phi_{(0)}(x) z^{d-\Delta}$ for $z \to 0$. The solution to this problem can be obtained by considering an integral kernel K, known as bulk-to-boundary propagator, that will relate the boundary conditions to the bulk field by

$$\phi(z, x) = \int_{\partial \text{AdS}} d^d \bar{x} K(z, x; \bar{x}) \phi_{(0)}(\bar{x}) \,. \tag{1.98}$$

A related problem is the solution of the Klein-Gordon equation with a source $J(x)$. The solution to this problem is to determine first the bulk-to-bulk propagator $G(z, x; \bar{z}, \bar{x})$ that satisfies the equation

$$\left(\nabla^2 - m^2\right) G(z, x; \bar{z}, \bar{x}) = \frac{1}{\sqrt{-g}} \delta^{(d+1)}(X - \bar{X}) \,, \tag{1.99}$$

The convolution of G with the source $J(x)$

$$\phi(X) = \int d^{d+1} \bar{X} \sqrt{-\bar{g}} \, G(X; \bar{X}) J(\bar{X}) \,, \tag{1.100}$$

will then satisfy the equation $\left(\nabla^2 - m^2\right) \phi(X) = J$. The solution to equation (1.99) is

$$G(z, x; \bar{z}, \bar{x}) = \frac{C_\Delta}{2^\Delta (2\Delta - d)} \zeta^\Delta \, {}_2F_1 \left(\frac{\Delta}{2}, \frac{\Delta + 1}{2}; \Delta - \frac{d}{2} + 1; \zeta^2\right) \,, \tag{1.101}$$

with

$$C_\Delta = \frac{\Gamma(\Delta)}{\pi^{d/2} \Gamma(\Delta - \frac{d}{2})} \,,$$

where the quantity ζ is known as chordal distance and can be determined after computing the AdS geodesics between points (z, x) and $(\bar{z}, \bar{x})$:

$$\zeta = \frac{2z\bar{z}}{z^2 + \bar{z}^2 + (x - \bar{x})^2}\,. \tag{1.102}$$

The bulk-to-boundary propagator is related to the bulk-to-bulk propagator in the $\bar{z} \to 0$ limit of the latter. More precisely

$$K(z, x; \bar{x}) = \lim_{\bar{z} \to 0} \frac{2\Delta - d}{\bar{z}^\Delta} G(z, x; \bar{z}, \bar{x}) = C_\Delta \left(\frac{z}{z^2 + (x - y)^2} \right)^\Delta\,. \tag{1.103}$$

We wish to compute the on-shell action of the scalar field and express it in terms of the sources $J(x)$ in order to compute correlation functions. As a first step we can write the action of the scalar field as

$$S_\phi = -\frac{1}{2} \int d^{d+1} X \sqrt{-g}\, \phi \left(-\nabla^2 + m^2 \right) \phi + \frac{1}{2} \int d^{d+1} X \partial_A \left(\sqrt{-g} g^{AB} \phi \partial_B \phi \right)\,, \tag{1.104}$$

where we have used integration by parts. Since we are looking for the on-shell action the first term vanishes and we are only left with second term which can be rewritten as a surface integral

$$S_{\text{on-shell}} = \frac{1}{2} \int_{\mathcal{M}} d^{d+1} X \partial_A \left(\sqrt{-g} g^{AB} \phi \partial_B \phi \right) = \frac{1}{2} \int_{\partial \mathcal{M}} d^d x \sqrt{\gamma}\, \phi n^A \partial_A \phi\,, \tag{1.105}$$

where n^A is a vector normal to $\partial \mathcal{M}$, γ is the induced metric and x the surface coordinates. In AdS the boundary is located at $z = \infty$ and $z = \epsilon$, where $\epsilon \to 0$ was introduced in order to deal with the fact that the metric of AdS diverges for $z = 0$. Moreover, assuming an exponential decay for ϕ at $z \to \infty$ we have

$$S_{\text{on-shell}} = -\frac{1}{2} \int d^d x \sqrt{\gamma_\epsilon}\, \phi n^z \partial_z \phi \Big|_{z=\epsilon}\,, \tag{1.106}$$

where

$$\gamma_\epsilon = \frac{L^2}{\epsilon^2} \eta\,, \quad n^z = -\frac{\epsilon}{L}\,. \tag{1.107}$$

The on-shell action in equation (1.106) diverges as $\epsilon \to 0$. This can be fixed through holographic renormalization by introducing counter-terms to the action [84]. Then, the action we will use to take functional derivatives is the renormalised action given by

$$S_{\text{reg}} = \frac{L^{d-1}}{2} (d - 2\Delta) \frac{\Gamma(\Delta)}{\pi^{d/2} \Gamma(\Delta - \frac{d}{2})} \int d^d x d^d y \frac{\phi_{(0)}(x) \phi_{(0)}(y)}{(x - y)^{2\Delta}} + \cdots\,, \tag{1.108}$$

where the dots represent terms that are finite when taking $\epsilon \to 0$. Taking functional derivatives with respect to the sources $\phi_{(0)}(x)$ one obtains the two-point function

$$\langle \mathcal{O}(x)\mathcal{O}(y) \rangle = L^{d-1}(2\Delta - d)\frac{\Gamma(\Delta)}{\pi^{d/2}\Gamma(\Delta - \frac{d}{2})}\frac{1}{(x-y)^{2\Delta}}\,, \tag{1.109}$$

which is the result we expect from Conformal Field Theory.

The above discussion considered a free scalar field in AdS. We wish now to consider a bulk theory with interactions. Consider three bulk fields with cubic couplings with action $S = S_0 + S_{\text{int}}$ where

$$S_0 = -\frac{1}{2}\int d^{d+1}X\sqrt{-g}(g^{AB}\partial_A\phi_i\partial_B\phi_i + m_{ij}^2\phi_i\phi_j), \quad m_{ij} = m_i\delta_{ij}\,, \tag{1.110}$$

$$S_{\text{int}} = -\int d^{d+1}X\sqrt{-g}\lambda_{ijk}\phi_i\phi_j\phi_k\,, \tag{1.111}$$

where each field ϕ_i satisfies the Klein-Gordon equation with source $\lambda_{ijk}\phi_j\phi_k$

$$(\nabla^2 - m_i^2)\phi_i = -\lambda_{ijk}\phi_j\phi_k\,. \tag{1.112}$$

The solution for the set of equations (1.112) can be found perturbatively in terms of powers of λ_{ijk}

$$\phi_i(z,x) = \int d^d x_1 K_i(z,x;x_1)\phi_{i0}(x_1) + \sum_{j,k}\lambda_{ijk}\int d^{d+1}\bar{X}G_i(z,x;\bar{z},\bar{x})\times$$

$$\times\int d^d x_1 d^d x_2 K_j(\bar{z},\bar{x};x_1)K_k(\bar{z},\bar{x};x_2)\phi_{0j}(x_1)\phi_{0k}(x_2) + \cdots \tag{1.113}$$

In order to compute correlation functions in this theory one proceeds as in the free case and writes the action $S = S_0 + S_{\text{int}}$ in terms of on-shell quantities and boundary sources. In addition to two source terms coming from the free action we will also have terms with three or more source terms due to the interaction term. From S_{int} we get the three source term

$$S_{\text{int.}}^{(3)} = \lambda_{ijk}\int d^d x_1 d^d x_2 d^d x_3\int d^{d+1}X K_i(z,x;x_1)K_j(z,x;x_2)K_k(z,x;x_3)\times$$

$$\times\phi_{0i}(x_1)\phi_{0j}(x_2)\phi_{0k}(x_3)\,. \tag{1.114}$$

From this interaction term it follows that the three point function $\langle\mathcal{O}_i(x_1)\mathcal{O}_j(x_2)\mathcal{O}_k(x_3)\rangle$ is proportional to the integral over all the bulk points X. We note that the interaction part does not contribute to the quadratic term in the sources hence we do not need to worry about renormalization.

In this bulk theory with cubic couplings the computation of the 2-point and 3-point functions can be summarised in the two Witten diagrams of figure 1.17. The value of
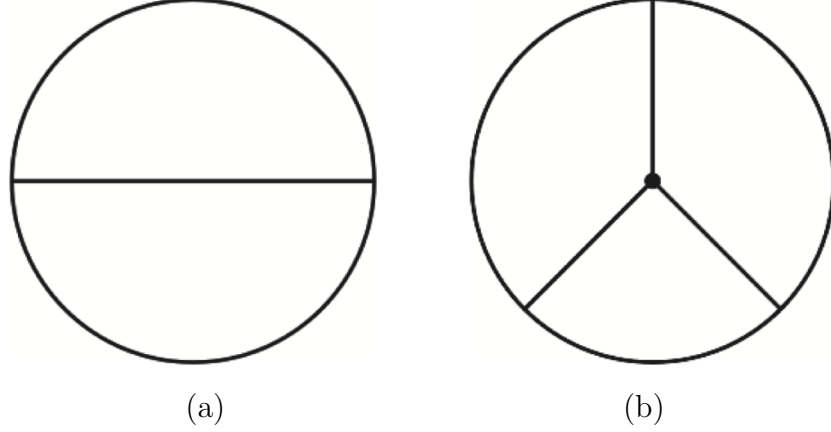
Figure 1.17: Witten diagrams for (a) the 2-point and (b) the 3-point correlation functions for a scalar theory with cubic couplings. Figure extracted from [85].

the correlation functions mentioned above could be extracted from those diagrams if we use the following set of rules:

- The circle represents the AdS space and its boundary is the circumference;

- Points on the circle correspond to operator insertions in the field theory;

- Lines departing from the boundary are mapped to bulk-to-boundary propagators;

- Lines between two bulk points correspond to bulk-to-bulk propagators;

- An interaction point in the bulk X is equivalent to an integral $\int d^{d+1}X\sqrt{-g}$. Later we will have functions of background fields like the dilaton Φ and the tachyon τ. In this case we insert such function in the vertex.

With this new set of rules we can now compute the 4-point function, or any n-point function without the need to write the on-shell action in terms of n source terms through the perturbative expansion (1.113). This is why the Witten diagram expansion is such a powerful computational technique in holography. Later we will use this procedure to compute the scattering amplitudes of processes that are dominated by Pomeron exchange. Before we start to do that we need first to select a holographic model for our QCD vacuum. In the next section we give a brief overview of the models available. Finally we will review the BPST pomeron, since it hints how to model holographically Pomeron exchange.

1.2.3   Overview of AdS/QCD

A big and rapid progress has been made in understanding the gauge/gravity duality in the context of $\mathcal{N} = 4$ SYM and type IIB superstrings on the $AdS_5 \times S_5$ background. As we have seen in the previous section, these two theories are claimed to be dual to each other and there are results that support this conjecture. However the gravity dual of QCD still eludes us. Inspired by the $\mathcal{N} = 4$ SYM case, top-down approaches propose certain configuration of branes in string theory in order to derive the Yang-Mills theory that is defined in the world volume of the branes. Perhaps the most famous model in this approach is the Witten-Sakai-Sugimoto model [86, 87]. This model captures features of low-energy QCD such as confinement, chiral symmetry breaking, mesons, glueballs, baryons, and effects from the axial anomaly. A review of this model can be found in [88].

A more practical approach is the bottom-up one. Here instead of deriving the gravity dual from some string theory, one assumes that it exits and adds fields to the bulk that capture experimental and theoretical features of QCD. The dynamics of these fields can of course be based on principles of effective string field theory. Because QCD is not a conformal field theory, it is necessary that its bulk dual has elements that break conformal symmetry in the boundary theory. The simplest way is to introduce a IR cut-off to the holographic radial variable z and relate it to some QCD scale e.g. the mass of the ρ meson. The metric of this models is the one of a slice of the AdS metric

$$ds^2 = \frac{1}{z^2}\left(dz^2 + \eta_{\mu\nu}dx^\mu dx^\nu\right), \quad 0 < z \leq z_m \,. \tag{1.115}$$

This types of models are known as hard-wall models. This simple model predicts a discrete spectrum for the particles that is linear with the resonance index, i.e. $m_n \sim n$. However it is observed, in particular with mesons, that the correct relationship should be $m_n^2 \sim n$. The desired relationship between m_n and n was obtained by Karch, Katz, Son and Stephanov in [89]. They have considered a string dual of QCD with a dilaton field and five dimensional metric that are, respectively, dual to the lagrangian and the energy momentum-tensor. For the QCD vacuum these fields have the form

$$ds^2 = e^{2A}\left[dz^2 + \eta_{\mu\nu}dx^\mu dx^\nu\right] \,, \quad \Phi = \Phi(z) \,. \tag{1.116}$$

The authors of such model showed that in the IR, i.e. $z \to \infty$, the dilaton Φ and warp factor A should satisfy $\Phi - A \sim z^2$ in order to get a linear spectrum for the ρ mesons. By considering the spectrum of higher spin mesons one finds that A can not grow as z^2 if we wish to have linear Regge trajectories in the spin. Plus, if one adds conformal symmetry in the UV, i.e. $z \to 0$, then $\Phi - A \sim \log z$.

This result motivates the study of 5D Einstein-Dilaton system whose action in the Einstein frame is

$$S_g^E = M^3 N_c^2 \int d^5 x \sqrt{-g} \left(R - \frac{4}{3} g^{MN} \partial_M \Phi \partial_N \Phi + V(\Phi) \right) . \qquad (1.117)$$

Here M is the Planck mass, N_c is the number of colours that we assume is large, g, Φ and V are the 5D metric, the dilaton field and dilaton potential in the Einstein frame, respectively. The 't Hooft coupling of the gauge theory is related to the dilaton, up to a multiplicative constant by

$$\lambda = e^\Phi . \qquad (1.118)$$

This action can be thought of a two-derivative effective action, including a dilaton potential, describing the low-lying excitations of some string theory in the bulk. Using 1.116 as an ansatz the equations of motion of the warp factor A and dilaton profile Φ read as

$$\dot{\Phi}^2 = -\frac{9}{4} \left(\ddot{A} - \dot{A}^2 \right) , \quad \ddot{\Phi} + 3\dot{A}\dot{\Phi} - \frac{3}{8} e^{2A} \partial_\Phi V(\Phi) = 0 . \qquad (1.119)$$

To solve this system of differential equations there are two common approaches. One can start to assume the profile of the dilaton and solve equations (1.119) to obtain the warp factor and the corresponding dilaton potential. For example assuming the dilaton profile $\Phi = \mu^2 z^2$ one gets [90]

$$A(z) = -\log \left(\frac{z}{L} \right) - \log \left({}_0F_1(5/4, \frac{\Phi^2}{9})^2 \right) , \qquad (1.120)$$

$$V(\Phi) = -\frac{12 \, {}_0F_1(1/4, \frac{\Phi^2}{9})^2}{L^2} + \frac{16 \, {}_0F_1(5/4, \frac{\Phi^2}{9})^2 \Phi^2}{3L^2} , \qquad (1.121)$$

where ${}_0F_1(a; z)$ is the hypergeometric function.

On the other hand, one can determine what properties the dilaton potential should satisfy in order for the resulting geometry and dilaton profile to reproduce known features of QCD. This is the approach of the Improved Holographic QCD model proposed in [91,92] and the one we will use as our QCD vacuum in chapters 2, 3 and 4 of this thesis. In this model the dilaton potential is associated to a phenomenological superpotential $W(\Phi)$ through

$$V(\Phi) = e^{-\frac{4}{3}\Phi} \left[\frac{64}{27} W(\Phi)^2 - \frac{4}{3} \left(\frac{dW}{d\Phi} \right)^2 \right] . \qquad (1.122)$$

Among the backgrounds in those works we take the Background I whose superpotential is

$$W = \frac{9}{4L} \left(1 + \frac{2}{3} b_0 \lambda \right)^{\frac{2}{3}} \left[1 + \frac{(2b_0^2 + 3b_1) \log(1 + \lambda^2)}{18a} \right]^{\frac{4a}{3}} , \qquad (1.123)$$

with the numerical values

$$b_0 = 4.2 \,, \quad \frac{b_1}{b_0^2} = \frac{51}{121} \,, \quad a = \frac{3}{16} \,. \tag{1.124}$$

With this choice of background one gets the following features: (i) the β function of the Yang-Mills theory; (ii) existence of a metric singularity at some coordinate value z in order to have confinement as defined by the holographic computation of a rectangular Wilson loop; (iii) existence of a mass gap in the spectrum of the glueballs 0^{++} and 2^{++}; (iv) linear Regge trajectories for the glueballs in the radial quantum number. The value of b_0 was fixed in order to match the mass ratio between the first excited scalar glueball 0^{++*} and the lightest scalar glueball 0^{++} (i.e. $R_{00} = m_{0^{++*}}/m_{0^{++}}$), which is 1.87 according to the lattice results of [93–95]. With all the parameters of the model fixed, the predicted the mass ratio between the lightest tensor glueball 2^{++} and the lowest scalar glueball is 1.40, very close to the reported 1.46.

This model has also been applied to compute QCD quantities at finite temperature like transport coefficients, bulk viscosity, drag force and jet quenching parameters, providing a good phenomenological description of the Quark-Gluon Plasma. A good summary of these results can be found in [96].

Despite its successes, the Improved Holographic QCD model is an incomplete dual model of QCD since it does not include flavour degrees of freedom. Later we will consider a specific model from the family of holographic duals of QCD in the Veneziano limit studied in [97,98]. This class of models is built on top of Improved Holographic QCD by adding space-time filling $D4 - \bar{D}4$ "flavour branes". This system produces an open string tachyon T that generates chiral symmetry breaking and gauge fields A_L and A_R related to the meson sector. The dynamics of the tachyon and gauge fields will be encoded in a Dirac-Born-Infeld (DBI) action of the form

$$S_{DBI} = -\frac{x}{2} M_p^3 N_c^2 \int d^5 X \, \mathbf{Str} \Big[V_f(\lambda, T^\dagger T) \sqrt{det(g_{ab} + k(\lambda)D_{(a}T^\dagger D_{b)}T + w(\lambda)F_{ab}^L)} +$$
$$+ V_f(\lambda, TT^\dagger) \sqrt{det(g_{ab} + k(\lambda)D_{(a}TD_{b)}T^\dagger + w(\lambda)F_{ab}^R)} \Big] \,. \tag{1.125}$$

In chapter 5 we will provide more details about a parameterisation of the potentials V_f, k and w. Our background fields will be computed including the tachyon backreaction and will be fixed by the spectrum of the lowest lying mesons.

1.2.4   BPST Pomeron

Throughout this thesis we model the Pomeron on the gravity side as the graviton's Regge trajectory. In this section we will motivate this statement by summarising the arguments of Brower, Polchinski, Strassler and Tan (BPST) [8]. This work started the application of the gauge/gravity duality to the study of scattering processes where Pomeron exchange dominates. The work by BPST also suggested that the observed soft and hard pomerons manifest themselves at different values of the 't Hooft coupling.

In the limit of a very small 't Hooft coupling g^2N with N large, after applying BFKL methods, a Pomeron object can be extracted from a conformal field theory with kernel

$$\mathcal{K}(p_\perp, p'_\perp, s) \approx \frac{s^{j_0}}{\sqrt{4\pi\mathcal{D}\log s}} e^{-(\log p'_\perp - \log p_\perp)^2/4\mathcal{D}\log s} , \qquad (1.126)$$

where

$$j_0 = 1 + \frac{4\log 2}{\pi}\alpha N , \quad \mathcal{D} = \frac{7\zeta(3)}{2\pi}\alpha N . \qquad (1.127)$$

Here we keep up with the definitions of BPST. The object $\mathcal{K}$ can be derived from equation (1.68) as follows: multiply it by $(2\pi)^2 s k_1 k_2$ and use the definition (1.64) of the BFKL amplitude. Keep only the dominant $n = 0$ term, perform the change of variables $\omega \to j - 1$ and $\nu \to 2\nu$ and define $\hat{j}(\nu) = 1 + \bar{\alpha}_s \chi_0(\nu/2)$ as the position of the pole in the j plane. If we expand $\hat{j}$ quadratically and pick the pole we are left with a gaussian integral whose evaluation yields equations (1.126) and (1.127).

The Pomeron kernel $\mathcal{K}$ is a power of s times a diffusion kernel in the variable $\log p_\perp$, with diffusion time $\tau \sim \log s$. On the other hand, consider a scattering amplitude in the Regge regime $\mathcal{A} \sim s^{\alpha(t)}$. For small t, the Regge trajectory in flat-space string theory is linear, with $\alpha(t) = \alpha_0 + \alpha' t$. Consider now the scattering of particles along the x^1 axis with momentum transfer k^μ in the $x^2 - x^3$ plane, i.e. $t = -k_\perp^2$. If we now compute the Fourier transform of such scattering amplitude we get

$$\int d^{d-2}k_\perp e^{i\vec{k}_\perp \cdot \vec{x}_\perp} s^{\alpha(t)} = s_0^\alpha \int d^{d-2}k_\perp e^{i\vec{k}_\perp \cdot \vec{x}_\perp} e^{-\alpha' k_\perp^2 \log s} = \frac{s^{\alpha_0} e^{-x_\perp^2/4\alpha'\log s}}{(4\pi\alpha'\log s)^{(d-2)/2}} . \qquad (1.128)$$

It is quite remarkable the similarity between these two kernels since in one case we are in a regime far from confinement (as in the BFKL case) while in the other we are within confinement. This motivated BPST to use the gauge/gravity duality to understand this relationship, concluding later that the Pomeron of the gauge theory is dual to the graviton Regge trajectory of the gravity theory. In this section we briefly review this result that is central for this thesis.

Their argument starts with considering the $2 \rightarrow 2$ scattering of bosonic string tachyon states in flat-space string theory. At tree level in string theory, the scattering amplitude for this process is the Virasoro-Shapiro amplitude

$$\mathcal{A} = \int d^2w |w|^{-4-\alpha't/2}|1-w|^{-4-\alpha's/2} \, . \tag{1.129}$$

The integrand of the above equation has a saddle point for

$$w = \frac{4 + t\alpha'}{8 + s\alpha' + t\alpha'} \, . \tag{1.130}$$

For large s and t with $s \gg t$ this saddle point is of order s^{-1}, i.e. in the large s limit the integration region around $w = t/(s+t) \rightarrow 0$ in the world-sheet complex plane w contributes the most to the integral. In this limit

$$|1-w|^{-4-\frac{\alpha'}{2}s} \approx \left(1 + \left(2 + \frac{s\alpha'}{4}\right)w\right)\left(1 + \left(2 + \frac{s\alpha'}{4}\right)\bar{w}\right) \approx e^{\frac{s\alpha'}{4}(w+\bar{w})} \tag{1.131}$$

and the Virasoro-Shapiro amplitude becomes

$$\mathcal{A} \sim \int d^2w |w|^{-4-\alpha't/2} e^{\frac{s\alpha'}{4}(w+\bar{w})} = 2\pi \frac{\Gamma(-1-\frac{\alpha'}{4}t)}{\Gamma(2+\frac{\alpha'}{4}t)}(e^{-i\pi/2}\alpha's/4)^{2+\alpha't/2} \, , \tag{1.132}$$

where the change of variable $w = x + iy$ and Γ-function identities were used to compute the integral over the whole complex w plane. As we have seen previously in this chapter, this functional form is expected from Regge theory.

The Shapiro-Virasoro amplitude can be obtained through the four-point function of the tachyon vertex operators inserted on 4 points of the Riemann sphere. Because of Mobius symmetry the position of three of these operators are fixed at 0, 1 and ∞ so that

$$\mathcal{A}(s,t) = \int d^2w \langle e^{ip_1 \cdot X(w,\bar{w})} e^{ip_2 \cdot X(0)} e^{ip_3 \cdot X(1)} e^{ip_4 \cdot X(\infty)} \rangle \tag{1.133}$$

As we have seen above the vertex operators $e^{ip_1 \cdot X(w,\bar{w})}$ and $e^{ip_2 \cdot X(0)}$ are very close to each other in the Regge limit. Hence, it is expected that Regge regime can also be extracted from the Operator Product Expansion (OPE) of these vertex operators. Because in the Regge limit $sw \sim 1$, contractions involving $p_1 \cdot (w\partial + \bar{w}\bar{\partial})X(0)$, which generate a factor of s, also need to be included. The OPE of these operators is then

$$e^{ip_1 \cdot X(w,\bar{w})} e^{ip_2 \cdot X(0)} \sim |w|^{-4-\frac{\alpha'}{2}t} e^{ik \cdot X(0) + p_1 \cdot (w\partial + \bar{w}\bar{\partial})X(0)} + \cdots \tag{1.134}$$

and introducing it in the expectation value above yields

$$\langle e^{ip_1 \cdot X(w,\bar{w})} e^{ip_2 \cdot X(0)} e^{ip_3 \cdot X(1)} e^{ip_4 \cdot X(\infty)} \rangle \sim \tag{1.135}$$

$$|w|^{-4-\frac{\alpha'}{2}t} \langle e^{ik \cdot X(0) + p_1 \cdot (w\partial + \bar{w}\bar{\partial})X(0)} e^{ip_3 \cdot X(1)} e^{ip_4 \cdot X(\infty)} \rangle \, .$$

The expectation value is the exponential term that appears in the integrand of equation (1.132) and hence we recover the same result.

One can isolate the Pomeron contribution to the scattering amplitude by performing the integration over the complex w plane before inserting the OPE in the expectation value,

$$\int d^2w \, e^{ip_1 \cdot X(w,\bar{w})} e^{ip_2 \cdot X(0)} \sim \Pi(\alpha't) e^{ik \cdot X(0)} \left[p_1 \cdot \partial X(0) \, p_1 \cdot \bar{\partial} X(0) \right]^{1+\alpha't/4}, \qquad (1.136)$$

where the right-hand side is the Pomeron vertex operator. The above integral was evaluated using the same techniques as in (1.132) after using the OPE (1.134). Inserting the Pomeron vertex operator into the expectation values gives the Regge behaviour of the amplitude.

To study the general case, BPST consider string states that are grouped into two arbitrary sets of vertex operators. One set is $\mathcal{W}_R$, which consists of l_R vertex operators and their $l_R - 2$ world-sheet integrations, while $\mathcal{W}_L$ is a set of l_L vertex operators and their $l_L - 2$ world-sheet integrations. The scattering amplitude involving these states is considered when $\mathcal{W}_L$ and $\mathcal{W}_R$ differ by a large boost in the $\pm$ plane, so that that $\mathcal{W}_R$ has a large $+$ component while $\mathcal{W}_R$ has a large $-$ component, justifying the subscripts R and L. As in the tachyonic case the momentum exchanged k is orthogonal to the $\pm$ plane. To write the amplitude in a general way we also need to introduce the worldsheet evolution operators w^{L_0-2} and $\bar{w}^{\bar{L}_0-2}$ between these sets of operators, where L_0 and $\bar{L}_0$ are the right-moving and left-moving Virasoro operators, respectively. In fact these operators are already present in the OPE (1.134) since

$$|w|^{-4-\frac{\alpha'}{2}t} e^{ik \cdot X(0) + p_1 \cdot (w\partial + \bar{w}\bar{\partial})X(0)} = w^{L_0-2} \bar{w}^{\bar{L}_0-2} e^{ik \cdot X(0) + ip_1 \cdot (w\partial + \bar{w}\bar{\partial})X(0)}. \qquad (1.137)$$

The scattering amplitude for these set of states is then

$$\mathcal{A}_{\mathcal{W}_L \mathcal{W}_R} = \int d^2w \left\langle \mathcal{W}_R w^{L_0-2} \bar{w}^{\bar{L}_0-2} \mathcal{W}_L \right\rangle. \qquad (1.138)$$

We proceed by inserting a complete set of string states between the operators w^{L_0-2} and $\bar{w}^{\bar{L}_0-2}$ and keep only the dominant ones in the Regge limit, i.e. $ws \sim 1$. The states that survive are those of the form $(\alpha^n_{-1} \bar{\alpha}^m_{-1})|0\rangle$ with $n, m = 1, 2, \cdots$, which are the ones in the graviton Regge trajectory. At this point the scattering amplitude takes the form

$$\mathcal{A}_{\mathcal{W}_L \mathcal{W}_R} \sim \sum_{m,n=0}^{\infty} \int d^2w \frac{2^{m+n} w^{m-2-\alpha't/4} \bar{w}^{n-2-\alpha't/4}}{\alpha'^{m+n} m! n!} \times \qquad (1.139)$$

$$\times \left\langle \mathcal{W}_R e^{ik \cdot X} \left(\partial X^- \right)^m \left(\bar{\partial} X^- \right)^n \right\rangle \left\langle e^{-ik \cdot X} \left(\partial X^+ \right)^m \left(\bar{\partial} X^+ \right)^n \mathcal{W}_L \right\rangle.$$

49

These states can be reorganised in the arguments of an exponential which after acting with $\int d^2w|w|^{-4-\alpha't/2}$ yields

$$\mathcal{A}_{\mathcal{W}_L\mathcal{W}_R} \sim \Pi(\alpha't)(s/s_0)^{2+\alpha't/2}\times \tag{1.140}$$
$$\left\langle \mathcal{W}_{R0}e^{ik\cdot X}\left(2\partial X^-\bar\partial X^-/\alpha'\right)^{1+\alpha't/4}\right\rangle \left\langle e^{-ik\cdot X}\left(2\partial X^+\bar\partial X^+\alpha'\right)^{1+\alpha't/4}\mathcal{W}_{L0}\right\rangle ,$$

where the states $\mathcal{W}_{L/R}$ were boosted back to their rest frames.

The above general scattering amplitude for string states can be understood as the convolution of the external string states with the Pomeron propagator $\Pi(\alpha't)(s/s_0)^{2+\alpha't/2}$ times couplings between the string states with the Pomeron vertex operator

$$\mathcal{V}_P^\pm = \left(2\partial X^\pm\bar\partial X^\pm/\alpha'\right)^{1+\alpha't/4}e^{\mp ik\cdot X} . \tag{1.141}$$

As we will see in later chapters, this structure of the scattering amplitude is present in all the processes dominated by Pomeron exchange that we will consider in this thesis.

Finally let us look at the bosonic string in a curved space-time case with metric

$$ds^2 = e^{2A(y)}\eta_{\mu\nu}dx^\mu dx^\nu + ds_\perp^2 . \tag{1.142}$$

In general the string solutions for this background are not known, although they might be the relevant ones for QCD. In this kind of background the string wavefunctions are of the form $e^{ip\cdot x}\psi(y)$. These wavefunctions can be promoted to operators by substituting x and y by worldsheet fields X and Y, yielding a vertex operator $e^{ip\cdot X}\psi(Y)$. One can then proceed as in the flat-space case and consider the OPE

$$e^{ip_1X(w,\bar w)}\psi_1(Y(w,\bar w))e^{ip_2X(0)}\psi_2(Y(0)) \sim \tag{1.143}$$
$$w^{L_0-2}\bar w^{\bar L_0-2}e^{ik\cdot X(0)+ip_1\cdot(w\partial+\bar w\bar\partial)}\psi_1(Y(w,\bar w))\psi_2(Y(0)) .$$

To include terms of order up to $(\log s)/\sqrt{\lambda} \sim |\log w|/\sqrt{\lambda}$ one needs to terms of order $1/\sqrt{\lambda}$ in the world-sheet dimension L_0. The next steps follow the same logic as the flat-space case and the following formula for the scattering amplitude in the background (1.142) is derived

$$\mathcal{A} \sim \int d^6y\sqrt{G_\perp}e^{2A(y)}\psi_3(y)\psi_4(y)\Pi(\alpha'\Delta_2)(\alpha's)^{2+\alpha'\Delta_2/2}e^{2A(y)}\psi_1(y)\psi_2(y) , \tag{1.144}$$

where Δ_2 is an operator that depends on Mandelstam t. The major difference between the above expression for the amplitude and the flat-space case is the promotion of the Mandelstam t to this operator. For forward scattering, and for coordinates such that $AdS_5 \times W$ can be written as

$$ds^2 = \frac{r_0^2}{R^2}e^{2u}\eta_{\mu\nu}dx^\mu dx^\nu + R^2du^2 + ds_W^2 , \tag{1.145}$$

the Δ_2 operator is

$$\alpha' \Delta_2 = \frac{1}{\sqrt{\lambda}} (\partial_u^2 - 4) + \alpha' \nabla_W^2 \,. \tag{1.146}$$

For simplicity , consider that the wavefunctions ψ do not depend on W. Then the s dependence of the amplitude is associated to a diffusion operator through

$$s^{2 + (\partial_u^2 - 4)/2\sqrt{\lambda}} \tag{1.147}$$

The corresponding Schrodinger problem is

$$[-\partial_u^2 + 4]\psi = E\psi \,, \tag{1.148}$$

with eigenvalues $E = 4 + \nu^2$ where $\nu \in \mathbb{R}$. This implies that the operator in the exponent of s has eigenvalues

$$j = j_0 - \mathcal{D}\nu^2 \,, \tag{1.149}$$

with

$$j_0 = 2 - \frac{2}{\lambda} \,, \quad \mathcal{D} = \frac{1}{2\sqrt{\lambda}} \,. \tag{1.150}$$

The implications of this result is that there is a branch cut in the j plane that ends at j_0. This is precisely what happens for the BFKL case using perturbative methods and j_0 can be identified as the BFKL exponent in the strong coupling limit.

Another derivation of the above results was also presented by BPST by considering the light-cone gauge for a superstring in $AdS_5 \times W$. In this approach the same result is obtained by a semi-classical computation of the Euclidean Polyakov path integral in this gauge. The results obtained need to be generalised to theories with confinement in order to understand QCD. BPST considered the effects of confinement by (i) considering theories that have conformal symmetry in the UV or (ii) a logarithmic running coupling. Using string theory they were able to derive model-independent features of the Pomeron for values of $|t|$ large compared with Λ^2, where Λ has the same order as the confinement scale. In particular, for the hard-wall model Regge trajectories with bound states poles are found for large $t > 0$ but for large $t < 0$ the trajectories disappear under a cut. If a running coupling is introduced this cut breaks up into poles that descend slowly as t decreases. However, for $t \sim \Lambda^2$ the behaviour of the Pomeron kernel becomes model dependent. This is the region of interest for total cross-sections and DIS structure functions. One of the objectives of this thesis is precisely to study holographic Pomeron physics in this region using dual models of QCD that describe as many features of this theory as possible.

2

Non-minimal coupling contribution to DIS at low x in Holographic QCD

Chapter abstract: We consider the effect of including a nonminimal coupling between a $U(1)$ vector gauge field and the graviton Regge trajectory in holographic QCD models. This coupling describes the QCD interaction between the quark bilinear electromagnetic current and the Pomeron. We test this new coupling against the proton structure functions F_2 and F_L data at low Bjorken x and obtain a good fit with a χ^2_{dof} of 1.4 over a very large kinematical range in the photon virtuality $Q^2 < 400\,\mathrm{GeV}^2$ and for $x < 10^{-2}$. The scale of the new dimension full coupling, which arises from integrating higher spin fields, is in the range of $10 - 100$ GeV.

2.1   Introduction

In this chapter we focus on low x DIS, extending the work of [1]. The basic idea is to construct the holographic Regge theory for the glueball exchange associated with the Pomeron trajectory. In DIS the Pomeron couples to the quark bilinear electromagnetic current $J^\mu = \bar{\psi}\gamma^\mu\psi$, which is described holographically by the interaction between a bulk $U(1)$ vector gauge field and the graviton Regge trajectory. Here we shall extend the analysis of [1] by (i) allowing for a nonminimal coupling between this gauge field and the higher spin fields in the graviton Regge trajectory and (ii) adding the longitudinal proton structure function $F_L(x, Q^2)$ data. We will consider HERA measurements of F_2 and F_L available in [99,100], yielding 249 points in the kinematical region with $x < 10^{-2}$ and $Q^2 \le 400\,\mathrm{GeV}^2$ for $F_2(x, Q^2)$, and 64 points with $x < 10^{-2}$ and $Q^2 \le 45\,\mathrm{GeV}^2$ for $F_L(x, Q^2)$. As a result, we manage to improve the quality of the

fit from a chi squared per degree of freedom χ^2_{dof} of 1.70 in [1] to 1.42, without including the non-minimal coupling. The inclusion of a non-minimal coupling improves slightly the χ^2_{dof} to 1.40.

The existence of such non-minimal coupling between the bulk $U(1)$ gauge field and the graviton Regge trajectory is expected. Starting from the UV high energy limit, the OPE expansion of the two currents, $J_\mu(x)J_\nu(y)$, contains two OPE coefficients for each spin J symmetric traceless operator associated with the glueballs on the Pomeron trajectory, $\mathcal{O}_J \sim \text{tr}(F_{\mu\alpha_1}D_{\alpha_2}\cdots D_{\alpha_{J-1}}F_{\alpha_J}{}^\mu)$. Holographically, and for pure AdS space, this amounts to precisely the same counting when coupling a vector gauge field to the graviton, or to the higher spin fields in the gravity Regge trajectory. Thus we shall consider such non-minimal coupling. In fact, since QCD is not a conformal theory, there is actually more freedom in the choice of such couplings in holographic QCD which, as we shall see, are very much model dependent. For concreteness we shall consider one such coupling, which arises in an effective field theory expansion in the dual QCD string tension. First we will summarize the expressions for the DIS structure functions $F_2(x, Q^2)$ and $F_L(x, Q^2)$ in generic AdS/QCD models. We then compute the corresponding non-minimal coupling contribution to these functions. Finally we focus on the specify holographic QCD model of [91, 92, 96], allowing us to put numbers in our expressions that are then tested against available low x DIS data.

2.2 Holographic computation of F_2 and F_L structure functions

The proton structure functions $F_2(x, Q^2)$ and $F_L(x, Q^2)$ are related to the total cross-sections of the inelastic $\gamma^* p \to X$ process. As discussed in the standard literature (see for instance [67]), and reviewed in the introduction in (1.53) and (1.54), defining σ_T and σ_L to be the cross sections for transverse and longitudinal polarizations, we have

$$F_2^p(x, Q^2) = \frac{Q^2}{4\pi^2\alpha}\left[\sigma^T_{\gamma^* p}(s, Q^2) + \sigma^L_{\gamma^* p}(s, Q^2)\right], \tag{2.1}$$

$$F_L^p(x, Q^2) = \frac{Q^2}{4\pi^2\alpha}\,\sigma^L_{\gamma^* p}(s, Q^2), \tag{2.2}$$

where α is the fine structure constant. The structure functions depends on the photon virtuality Q^2 and on the Bjorken $x \ll 1$, which we take to be small. Through the optical theorem, these total cross-section can be related to the imaginary part of the amplitude $\mathcal{A}$ for elastic forward scattering $\gamma^* p \to \gamma^* p$, with the appropriate

polarizations. Thus

$$F_2(x, Q^2) = \frac{Q^2}{4\pi^2\alpha} \frac{1}{s} \left(\text{Im} \, \mathcal{A}^\perp(s, t = 0) + \text{Im} \, \mathcal{A}^\parallel(s, t = 0) \right), \tag{2.3}$$

$$F_L(x, Q^2) = \frac{Q^2}{4\pi^2\alpha} \frac{1}{s} \text{Im} \, \mathcal{A}^\parallel(s, t = 0), \tag{2.4}$$

where s and t are the usual Mandelstam variables (in the low x regime, $s = Q^2/x$) and $\mathcal{A}^\perp$ and $\mathcal{A}^\parallel$ are the scattering amplitudes for the case of a transverse and longitudinal off-shell photon, respectively. We will compute these amplitude using the AdS/QCD prescription as described below.

First let us define our kinematical variables. We use light-cone coordinates $(+, -, \perp)$, with the flat space metric given by $ds^2 = -dx^+ dx^- + dx_\perp^2$, where $x_\perp \in \mathbb{R}^2$ is a vector in impact parameter space. We take for the large s kinematics of $12 \to 34$ scattering the following

$$k_1 = \left(\sqrt{s}, -\frac{Q^2}{\sqrt{s}}, 0 \right), \quad k_3 = -\left(\sqrt{s}, \frac{q_\perp^2 - Q^2}{\sqrt{s}}, q_\perp \right),$$

$$k_2 = \left(\frac{M^2}{\sqrt{s}}, \sqrt{s}, 0 \right), \quad k_4 = -\left(\frac{M^2 + q_\perp^2}{\sqrt{s}}, \sqrt{s}, -q_\perp \right). \tag{2.5}$$

where k_1 and k_3 are respectively the incoming and outgoing photon momenta. The proton target has mass M and incoming and outgoing momenta k_2 and k_4, respectively. For the forward scattering considered in the optical theorem we set $q_\perp = 0$, so that $k_1 = -k_3$, and we take the same polarization for the incoming and outgoing photon. The possible polarization vectors are

$$n^\mu(\lambda) = \begin{cases} (0, 0, \epsilon_\lambda), & \lambda = 1, 2, \\ (\sqrt{s}/Q, Q/\sqrt{s}, 0), & \lambda = 3, \end{cases} \tag{2.6}$$

where ϵ_λ is just the usual transverse polarization vector.

2.2.1 AdS/QCD

We shall compute the above scattering amplitudes using the framework of AdS/QCD. First we present general formulae and then specify to a particular model. As explained in the introduction, we are interested in the Regge limit where the amplitudes are dominated by the exchange of the graviton Regge trajectory, which includes fields of even spin J. We also need to define our holographic external states. The corresponding Witten diagram is shown in Fig. 2.1. The upper part of the diagram, is related to the incoming and outgoing virtual photons, whereas the bottom part to the proton target.

(a)
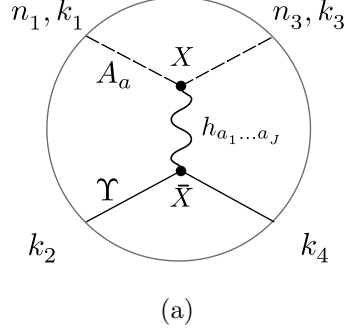
Figure 2.1: Tree level Witten diagram representing spin J exchange in $12 \rightarrow 34$ scattering. The n_1 label denotes the incoming photon polarization while n_3 label the outgoing photon polarization. For forward scattering $n_1 = n_3$. A_a represents the non-normalizable mode of a $U(1)$ gauge field dual to the source of the conserved current $\bar{\psi}\gamma^\mu\psi$ and Υ is a normalizable mode of a bulk scalar field that represents an unpolarised proton. X and $\bar{X}$ represent the bulk points where the external scattering states couple with the spin J fields.

The holographic dual of QCD will have a dilaton field and a five-dimensional metric, which in the vacuum will have the form

$$ds^2 = e^{2A(z)} \left[dz^2 + \eta_{\mu\nu}dx^\mu dx^\nu \right] , \qquad \Phi = \Phi(z) , \qquad (2.7)$$

for some unknown functions $A(z)$ and $\Phi(z)$. The dilaton is dual to the Lagrangian and the metric to the energy-momentum tensor. We shall use greek indices in the boundary, with flat metric $\eta_{\mu\nu}$. We will work with the string frame metric.

In DIS the external photon is a source for the conserved $U(1)$ current $\bar{\psi}\gamma^\mu\psi$, where the quark field ψ is associated to the open string sector. The five dimensional dual of this current is a massless $U(1)$ gauge field A. We shall assume that this field is made out of open strings and that is nonminimally coupled to the metric, with the following action

$$S_A = -\frac{1}{4} \int d^5X \sqrt{-g}\, e^{-\Phi} \left(F_{ab}F^{ab} + \beta R_{abcd}F^{ab}F^{cd} \right) , \qquad (2.8)$$

where $F = dA$ and we use the notation $X^a = (z, x^\alpha)$ for five-dimensional points. The corresponding equation of motion can be easily derived to be

$$\nabla_a \left[e^{-\Phi} \left(F^{ab} + \beta R^{ab}{}_{cd}F^{cd} \right) \right] = 0 . \qquad (2.9)$$

The coupling β has dimensions of length squared. At this order in derivatives of the fields, we could have other couplings to the Riemann tensor, to derivatives of the

dilaton field and also higher derivative terms in the field strength F. As we shall see bellow, we will be mostly interested in the coupling to the graviton in the linearised theory, in which case there are only two possible local couplings. Thus, for our purposes the above action is rather general.

We will fix the gauge of the $U(1)$ bulk field to be $D_a A^a = 0$, which gives $A_z = 0$ and $\partial_\mu A^\mu = 0$. The solution of the equation of motion (2.9) in this gauge is then

$$A_\mu^\lambda(X; k, \lambda) = n_\mu(\lambda) f_k(z) e^{ik \cdot x}, \tag{2.10}$$

where $f_k(z)$ solves the differential equation

$$\left[-Q^2 + e^{\Phi - A} \partial_z \left(e^{A - \Phi} \partial_z \right) + \beta \Delta_\beta \right] f_Q(z) = 0, \tag{2.11}$$

with

$$\Delta_\beta = -2e^{-2A} \left[\left(-\dot{A}\ddot{A} - \dot{\Phi}\ddot{A} + \dddot{A} \right) \partial_z + \ddot{A}\partial_z^2 - \dot{A}^2 Q^2 \right]. \tag{2.12}$$

Notice that here, and in the remainder of this chapter, we shall denote derivatives with respect to z with a dot. The momentum k and the polarization vector $n(\lambda)$ satisfy

$$k^2 = Q^2, \qquad n_z(\lambda) = 0, \qquad k \cdot n(\lambda) = 0, \tag{2.13}$$

where the boundary polarization is given by 5.37. We choose as UV boundary condition $f(0) = 1$ which gives the non-normalizable solution, since the off-shell photon acts as a source for the quark bilinear current $\bar{\psi}\gamma^\mu\psi$. Finally, let us note that, for the computation of the Witten diagram in figure 2.1, it is convenient to compute the field strength of a given mode

$$F_{\mu\nu}(X; k, \lambda) = 2ik_{[\mu}n_{\nu]}(\lambda)f_Q(z)e^{ik \cdot x},$$
$$F_{z\mu}(X; k, \lambda) = n_\mu(\lambda)\dot{f}_Q(z)e^{ik \cdot x}, \tag{2.14}$$

where $Q^2 = k^2$.

For the proton target we consider a scalar field Υ that represents an unpolarized proton described by a normalizable mode of the form

$$\Upsilon(X; p) = \upsilon_m(z) e^{ip \cdot x}, \tag{2.15}$$

where p is the momentum and $m^2 = -p^2$. As explained in detail in [1], the specific details of the function will not be important because it will appear in an integral that can be absorbed in the coupling between the Pomeron and the proton.

2.2.2   Minimal and Non-minimal couplings

To compute the Witten diagram of figure 2.1, we need to consider the interaction between the external scattering states and the spin J fields in the graviton Regge trajectory. Thus, the higher spin field comes from the closed string sector while the external fields come from the open sector.

First we consider the coupling between the $U(1)$ gauge field and the graviton. In Einstein-Maxwell theory, and for *AdS* or flat space, it is well known that there are only two possible cubic couplings between these fields, namely

$$F^{ac}F^b_{\ c}h_{ab}\,, \quad F^{ac}F^{bd}\nabla_c\nabla_d h_{ab}\,, \tag{2.16}$$

where h_{ab} is the metric fluctuation. The present case, however, is less restrictive because we have an additional scalar field and also because space-time is not maximally symmetric. To understand this better, let us linearize the action (2.8) around the background metric, that is, we write $g_{ab} = \bar{g}_{ab} + h_{ab}$. Setting $h = h^a_{\ a} = 0$ we have the cubic couplings

$$\delta S = -\frac{1}{2}\int d^5 X\sqrt{-\bar{g}}\,e^{-\Phi}\Big(F^{ab}F^c_{\ b}h_{ac} + \frac{\beta}{2}h_{ap}\bar{R}^p_{bcd}F^{ab}F^{cd} - \beta F^{ac}F^{bd}\bar{\nabla}_a\bar{\nabla}_b h_{cd}\Big)\,. \tag{2.17}$$

To study the graviton Regge trajectory in the background (2.7) we need to decompose the metric in $SO(1,3)$ irreducible representations. We will be only interested in the graviton TT components $h_{\alpha\beta}$, satisfying $\partial^\alpha h_{\alpha\beta} = 0$ and $h^\alpha_{\ \alpha} = 0$, and we set $h_{z\alpha} = 0 = h_{zz}$. Using that $R_{\alpha\mu\beta\nu} = \dot{A}^2 e^{2A}(\eta_{\alpha\nu}\eta_{\mu\beta} - \eta_{\alpha\beta}\eta_{\mu\nu})$ and $R_{\alpha z\beta z} = -\ddot{A}e^{2A}\eta_{\alpha\beta}$ in the background (2.7), and computing the covariant derivatives, we obtain

$$\delta S = -\frac{1}{2}\int d^5 X\sqrt{-\bar{g}}\,e^{-\Phi}\Big[F^{\alpha\mu}F^\beta_{\ \mu}\big(1 - \beta e^{-2A}\dot{A}\partial_z\big) - \beta F^{\alpha\mu}F^{\beta\nu}\partial_\mu\partial_\nu$$
$$- 2\beta F^{\alpha z}F^{\beta\nu}\big(\partial_z - 2\dot{A}\big)\partial_\nu + F^{\alpha z}F^\beta_{\ z}\Big(1 - \beta e^{-2A}\big(\partial_z^2 - 3\dot{A}\partial_z + 2\dot{A}^2\big)\Big)\Big]h_{\alpha\beta}\,. \tag{2.18}$$

Notice that in the AdS case ($A = -\log z$) these couplings reduce to the two allowed couplings in (2.16). However, in the present case there are more possibilities. For example, other contractions with the Riemann tensor will give different functions multiplying the same tensor structures in the couplings. We may also use derivatives of the scalar field to contract with the field strength. For simplicity, the approach we follow in this chapter will be to focus on the coupling given by the action (2.8). Our aim is to test whether this type of corrections are important in describing DIS using holographic QCD.

Next we wish to generalize the previous coupling to case of the cubic interaction between the gauge field and a symmetric, transverse and traceless spin J field, $h_{a_1\ldots a_J}$.

The Pomeron trajectory includes such higher spin fields of even J. Again there are several possibilities, but we shall focus on the simplest extension of the two couplings to the graviton considered above. The first term is the minimal coupling term, which can be generalized to

$$\kappa_J \int d^5 X \sqrt{-\bar{g}} \, e^{-\Phi} F^{a_1 b} \bar{\nabla}^{a_2} \dots \bar{\nabla}^{a_{J-1}} F^{a_J}_{b} h_{a_1 \dots a_J}. \tag{2.19}$$

The transverse condition of $h_{a_1 \dots a_J}$ guarantees that this term is unique up to dilaton derivatives. For the nonminimal coupling we will write

$$\beta_J \int d^5 X \sqrt{-\bar{g}} e^{-\Phi} \Big(F^{c a_1} \bar{\nabla}^{a_2} \dots \bar{\nabla}^{a_{J-1}} F^{a_J d} \bar{\nabla}_c \bar{\nabla}_d +$$
$$+ \frac{1}{2} F^{a_1 b} \bar{\nabla}^{a_2} \dots \bar{\nabla}^{a_{J-1}} F^{cd} R^{a_J}_{bcd} \Big) h_{a_1 \dots a_J}. \tag{2.20}$$

We remark that in both expressions (2.19) and (2.20) the way we distribute the covariant derivatives acting on the field strength is important. After integrating by parts such a covariant derivative, we are left with an extra term in the derivative of the background dilaton field. However, these terms will have a component of the higher spin field along the z direction, which can be dropped in the case of the Pomeron.

Next we need to decompose the spin J fields in $SO(1,3)$ irreducible representations. In the Regge limit we are only interested in the TT components of these fields, that is in $h_{\alpha_1 \dots \alpha_J}$ with $\partial^\nu h_{\nu \alpha_2 \dots \alpha_J} = 0$ and $h^\nu_{\nu \alpha_3 \dots \alpha_J} = 0$. From now on we will assume these two conditions. Thus for the minimal coupling (2.19) we obtain simply

$$\kappa_J \int d^5 X \sqrt{-\bar{g}} \, e^{-\Phi} \Big(F^{\alpha_1 \mu} \partial^{\alpha_2} \dots \partial^{\alpha_{J-1}} F^{\alpha_J}_{\mu} + F^{\alpha_1 z} \partial^{\alpha_2} \dots \partial^{\alpha_{J-1}} F^{\alpha_J}_{z} \Big) h_{\alpha_1 \dots \alpha_J}. \tag{2.21}$$

For the nonminimal coupling (2.20) we obtain after a cumbersome computation

$$\beta_J \int d^5 X \sqrt{-\bar{g}} e^{-\Phi} \Big[F^{z \alpha_1} \partial^{\alpha_2} \cdots \partial^{\alpha_{J-1}} F^{\alpha_J}_{z} \mathcal{D}^J_{\parallel} + F^{\mu \alpha_1} \partial^{\alpha_2} \cdots \partial^{\alpha_{J-1}} F^{\alpha_J \nu} \times$$
$$\times \big(e^{2A} \mathcal{D}^J_{\perp} \eta_{\mu\nu} + \partial_\mu \partial_\nu \big) + 2 F^{\mu \alpha_1} \partial^{\alpha_2} \cdots \partial^{\alpha_{J-1}} F^{\alpha_J z} \Big(\partial_z - J \dot{A} \Big) \partial_\mu \Big] h_{\alpha_1 \cdots \alpha_J}, \tag{2.22}$$

where

$$\mathcal{D}^J_{\perp} = e^{-2A} \dot{A} \Big(\partial_z - (J-2) \dot{A} \Big),$$
$$\mathcal{D}^J_{\parallel} = e^{-2A} \Big(\partial_z^2 - (2J-1) \dot{A} \partial_z - (J-2) \ddot{A} + J(J-1) \dot{A}^2 \Big). \tag{2.23}$$

For $J = 2$ this coupling reduces to the graviton nonminimal coupling given in (2.18).

For the scalar field Υ we will consider a minimal coupling with spin J closed string fields

$$\bar{\kappa}_J \int d^5 X \sqrt{-\bar{g}} \, e^{-\Phi} \left(\Upsilon \nabla^{a_1} \dots \nabla^{a_J} \Upsilon \right) h_{a_1 \dots a_J}. \tag{2.24}$$

Again, this coupling is unique up to derivatives of the dilaton field that are subleading in the Regge limit. Focusing on the TT part of the spin J field, we are left with the single coupling

$$\bar{\kappa}_J \int d^5 X \sqrt{-\bar{g}}\, e^{-\Phi} \left(\Upsilon \partial^{\alpha_1} \ldots \partial^{\alpha_J} \Upsilon\right) h_{\alpha_1 \ldots \alpha_J}. \tag{2.25}$$

2.2.3 Witten diagrams in Regge limit

The scattering amplitude will have a contribution from the minimal and the non-minimal coupling. The contribution of the minimal coupling to the structure functions F_2 and $2xF_1$ is presented and described in [1]. Here we will just outline the results since the later calculation of the non-minimal coupling contribution to the DIS structure functions is similar.

Using the optical theorem the structure functions can be related to the amplitude for forward Compton scattering

$$A^{FC}(q, P) = i(2\pi)^4 \delta^4 \left(\sum_i k_i\right) \left[n_T^2 \tilde{F}_1(x, Q^2) + \frac{2x}{Q^2} \left(n_T \cdot P\right)^2 \tilde{F}_2(x, Q^2)\right], \tag{2.26}$$

where q is the momentum of the incoming photon, P is the momentum of the incoming hadron and $n_T = n_T(q)$ is the transverse projection of the virtual photon polarization n^μ. The DIS structure functions are extracted from the forward Compton amplitude through

$$F_i(x, Q^2) = 2\pi \operatorname{Im}\tilde{F}_i(x, Q^2), \qquad (i = 1, 2) \tag{2.27}$$

and $F_L = F_2 - 2xF_1$.

Using the ingredients of the sections 2.2.1 and 2.2.2 the minimal coupling contribution to the forward Compton scattering amplitude due to spin J exchange can be computed. Then one sums over the fields with of spin $J = 2, 4, \ldots$ in the graviton Regge trajectory. This sum can be converted into an integral in the complex J-plane through a Sommerfeld-Watson transform.

$$\frac{1}{2} \sum_{J \geq 2} \left(s^J + (-s)^J\right) = -\frac{\pi}{2} \int \frac{dJ}{2\pi i} \frac{s^J + (-s)^J}{\sin \pi J}. \tag{2.28}$$

From the resulting expression and using (2.27) one obtains for the DIS structure functions F_1 and F_2 [1]

$$xF_i(x, Q^2) = 4\pi Q^2 \int dz d\bar{z}\, P_{13}^{(i)}(Q^2, z) P_{24}(P^2, \bar{z}) \operatorname{Im}\left[\chi(s, t = 0, z, \bar{z})\right], \tag{2.29}$$

where

$$P_{13}^{(1)}(Q^2, z) = e^{A(z)-\Phi(z)} f_Q^2 \,, \tag{2.30}$$

$$P_{13}^{(2)}(Q^2, z) = e^{A(z)-\Phi(z)} \left[f_Q^2 + \frac{1}{Q^2}(\partial_z f_Q)^2 \right] \,, \tag{2.31}$$

$$P_{24}(P^2, \bar{z}) = e^{3A(\bar{z})-\Phi(\bar{z})} \Upsilon^2(P^2, \bar{z}) \,, \tag{2.32}$$

and

$$\chi(s, t, z, \bar{z}) = \frac{\pi}{4} \int \frac{dJ}{2\pi i} \frac{S(z, \bar{z})^{J-1} \left(1 + (-1)^J\right) k_J \bar{k}_J}{\sin(\pi J)} \frac{k_J \bar{k}_J}{2^J} G_J(z, \bar{z}, t) \,, \tag{2.33}$$

with $S(z, \bar{z}) = s e^{-A(z)-A(\bar{z})}$. The eikonal phase $\chi(s, t, z, \bar{z})$ results from the component $+ \cdots +, - \cdots -$ of the spin J propagator $\Pi_{a_1 \ldots a_J, b_1 \ldots b_J}\left(X, \bar{X}\right)$, which satisfies the identity

$$\int \frac{dw^+ dw^- d^2 l_\perp}{2} e^{-iq_\perp \cdot l_\perp} \Pi_{+\cdots+,-\cdots-}\left(X, \bar{X}\right) = -\frac{i}{2^J} \left(e^{A+\bar{A}}\right)^{J-1} G_J\left(z, \bar{z}, t\right) \,, \tag{2.34}$$

where $w = x - \bar{x} = (w^+, w^-, l_\perp)$. $G_J(z, \bar{z}, t)$ admits the spectral representation

$$G_J(z, \bar{z}, t) = e^{B(z)+B(\bar{z})} \sum_n \frac{\psi_n(J, z) \psi_n^*(J, \bar{z})}{t_n(J) - t} \,, \tag{2.35}$$

where $\psi_n(J, z)$ are the normalizable modes associated to the spin J fields, that is they describe massive spin J glueballs. The function $B(z)$ depends on the differential equation of the propagator Π, and for the Improved Holographic QCD model considered here $B = \Phi - A/2$.

The next step is to assume that the J-plane integral can be deformed from the poles at even J, to the poles $J = j_n(t)$ defined by $t_n(J) = t$. The scattering domain of negative t contains these poles along the real axis for $J < 2$. After this step the expressions for F_1 and F_2 become

$$2x F_1(x, Q^2) = \sum_n \text{Im} \, g_n x^{1-j_n(0)} Q^{2j_n(0)} \bar{P}_{13}^{(1,n)}(Q^2) \,, \tag{2.36}$$

$$F_2(x, Q^2) = \sum_n \text{Im} \, g_n x^{1-j_n(0)} Q^{2j_n(0)} \bar{P}_{13}^{(2,n)}(Q^2) \,, \tag{2.37}$$

where

$$\bar{P}_{13}^{(1,n)} = \int dz \, f_Q^2 \, e^{(2-j_n)A+B-\Phi} \psi_n(j_n, z), \tag{2.38}$$

$$\bar{P}_{13}^{(2,n)} = \int dz \left[f_Q^2 + \frac{1}{Q^2}(\partial_z f_Q)^2 \right] e^{(2-j_n)A+B-\Phi} \psi_n(j_n, z), \tag{2.39}$$

with j_n evaluated at $t = 0$. The constants g_n, which involve the AdS local couplings and an integral over the proton wavefunction, will be used as fitting constants of the model. They are defined by

$$g_n = -\frac{\pi}{2}\left(i + \cot\frac{\pi j_n}{2}\right)\frac{\kappa_{j_n}\bar{\kappa}_{j_n}}{2^{j_n}}\frac{dj_n}{dt}\int d\bar{z}\, e^{-(j_n-7/2)A}v_m^2(\bar{z})\psi_n^*(\bar{z})\,. \tag{2.40}$$

To compute the minimal coupling contribution to F_L one just needs to use the identity $F_2 - 2xF_1$.

We shall now compute the contribution to F_2 of the nonminimal coupling (2.22) to the exchange of a spin J field, corresponding to the Witten diagram in Fig. 2.1. The contribution to F_L is obtained in an analogous way but without taking into account the transverse polarization of the off-shell photon. Since this constitutes original work from the author of this thesis, we will present more details than in the calculation of the minimal coupling contribution. Using the Regge kinematics (2.5) and taking as external states $F_i^{ab}(X)$ for $i = 1, 3$ and $\Upsilon_j(\bar{X})$ for $j = 2, 4$, we obtain for forward scattering the expression

$$\beta_J\bar{\kappa}_J\sum_{\lambda=1}^{3}\int d^5X d^5\bar{X}\sqrt{-g}\sqrt{-\bar{g}}\,e^{-\Phi}e^{-\bar{\Phi}}\Upsilon_2(\bar{\partial}^-)^J\Upsilon_4\times$$

$$\left[F_1^{+z}\left(\partial^+\right)^{J-2}F_{3\,z}^{+}\mathcal{D}_{\parallel}^J + F_1^{+\mu}\left(\partial^+\right)^{J-2}F_{3\,\mu}^{+}\mathcal{D}_{\perp}^J\right]\Pi_{+\cdots+,-\cdots-}(X,\bar{X})\,, \tag{2.41}$$

where bars denote quantities evaluated at $\bar{X}$. Notice that the couplings involving derivatives along the boundary in (2.22) vanish for forward scattering. Using (2.14) and (2.15) for the external states and performing the sum over polarizations we find

$$-\beta_J\bar{\kappa}_J s^J\int d^5X d^5\bar{X}\sqrt{-g}\sqrt{-\bar{g}}\,e^{-(\Phi+\bar{\Phi})-2J(A+\bar{A})}v_m^2(\bar{z})\times$$

$$e^{-2A}\left(f_Q^2(z)\mathcal{D}_{\perp}^J + \frac{\dot{f}_Q^2(z)}{Q^2}\mathcal{D}_{\parallel}^J\right)\Pi_{+\cdots+,-\cdots-}\,. \tag{2.42}$$

We remark that the terms with $\mathcal{D}_{\perp}^J$ and with $\mathcal{D}_{\parallel}^J$ defined in (2.23) are, respectively, the leading contribution arising from the transverse and longitudinal polarizations, therefore justifying our notation.

Performing the change of variable $w = x - \bar{x}$, setting $l_\perp = x_\perp - \bar{x}_\perp$, $t = -q_\perp^2$ and using the identity 2.34 we finally obtain

$$i\frac{\beta_J\bar{\kappa}_J s^J}{2^J}V\int dz d\bar{z}\,e^{-\Phi-\bar{\Phi}-2J(A+\bar{A})+3A+5\bar{A}}v_m^2(\bar{z})\times \tag{2.43}$$

$$\left(f_Q^2(z)\mathcal{D}_{\perp}^J + \frac{\dot{f}_Q^2(z)}{Q^2}\mathcal{D}_{\parallel}^J\right)\left[e^{(J-1)(A+\bar{A})}G_J(z,\bar{z},0)\right]\,.$$

In this equation the space-time volume V comes from the delta function momentum conservation that we imposed from the beginning on the external states and of course G_J has the spectral decomposition of equation (2.35).

In order to get the total amplitude we need to sum over even spin J fields with $J \geq 2$. Again, we assume analytic continuation of the amplitude for spin J exchange to the complex J-plane and apply a Sommerfeld-Watson transform, followed by a deformation of the contour from the poles at even J, to the poles to the poles $J = j_n(t)$ defined by $t_n(J) = t$.

$$
\mathcal{A}(s,0) = \sum_n h_n s^{j_n} \int dz \, e^{-\Phi} e^{A(-2j_n+3)} \times \tag{2.44}
$$
$$
\left(f_Q^2 \mathcal{D}_\perp^{j_n(0)} + \frac{\dot{f}_Q^2}{Q^2} \mathcal{D}_\parallel^{j_n(0)} \right) \left[e^{A(j_n(0)-1)} e^B \psi_n \big(j_n(0), z \big) \right],
$$

with h_n defined as

$$
h_n = -\frac{\pi}{2} \frac{\beta_{j_n} \bar{\kappa}_{j_n}}{2^{j_n}} \left(i + \cot \frac{\pi j_n}{2} \right) j_n' \int d\bar{z} \, e^{\bar{A}(4-j_n)} e^{-\bar{\Phi}} e^{\bar{B}} \upsilon_m^2(\bar{z}) \, \psi_n^* \big(j_n, \bar{z} \big). \tag{2.45}
$$

Finally, the action of the differential operators on the functions of z allows us to rewrite the forward scattering amplitude as

$$
\mathcal{A}(s,0) = \sum_n h_n s^{j_n} \int dz \, e^{-(j-2)A+B-\Phi} \left(f_Q^2 \tilde{\mathcal{D}}_\perp + \frac{\dot{f}_Q^2}{Q^2} \tilde{\mathcal{D}}_\parallel \right) \psi_n \big(j_n(0), z \big), \tag{2.46}
$$

with

$$
\tilde{\mathcal{D}}_\perp = e^{-2A} \left(\dot{A} \partial_z + \dot{A}^2 + \dot{A}\dot{B} \right), \tag{2.47}
$$
$$
\tilde{\mathcal{D}}_\parallel = e^{-2A} \left(\partial_z^2 - \big(\dot{A} - 2\dot{B} \big) \partial_z + \ddot{B} + \ddot{A} + \dot{B}^2 - \dot{A}\dot{B} \right).
$$

2.2.4 F_2 and F_L structure functions

The DIS structure function can be written in Regge theory in the following form

$$
F_2(x,Q^2) = \sum_n \left(f_n^{2,\,\mathrm{MC}}(Q^2) + f_n^{2,\,\mathrm{NMC}}(Q^2) \right) x^{1-j_n}, \tag{2.48}
$$

$$
F_L(x,Q^2) = \sum_n \left(f_n^{L,\,\mathrm{MC}}(Q^2) + f_n^{L,\,\mathrm{NMC}}(Q^2) \right) x^{1-j_n}, \tag{2.49}
$$

where we separated the contributions from the minimal and nonminimal couplings between the graviton trajectory and the $U(1)$ current that arise from the holographic

computation. From [1], for $B = \Phi - A/2$, and using the identity $F_L = F_2 - 2xF_1$ we have

$$f_n^{2,\,\mathrm{MC}}(Q^2) = g_n Q^{2j_n} \int dz \, e^{-\left(j_n - \frac{3}{2}\right)A} \left(f_Q^2 + \frac{\dot{f}_Q^2}{Q^2} \right) \psi_n \,, \qquad (2.50)$$

$$f_n^{L,\,\mathrm{MC}}(Q^2) = g_n Q^{2j_n} \int dz \, e^{-\left(j_n - \frac{3}{2}\right)A} \frac{\dot{f}_Q^2}{Q^2} \psi_n \,. \qquad (2.51)$$

Using the definitions (2.2) and (2.3), we may take the imaginary part of the forward scattering (2.46), to obtain the contribution from the nonminimal coupling

$$f_n^{2,\,\mathrm{NMC}}(Q^2) = \tilde{g}_n Q^{2j_n} \int dz \, e^{-\left(j_n - \frac{3}{2}\right)A} \left(f_Q^2 \tilde{\mathcal{D}}_\perp + \frac{\dot{f}_Q^2}{Q^2} \tilde{\mathcal{D}}_\parallel \right) \psi_n \,, \qquad (2.52)$$

$$f_n^{L,\,\mathrm{NMC}}(Q^2) = \tilde{g}_n Q^{2j_n} \int dz \, e^{-\left(j_n - \frac{3}{2}\right)A} \frac{\dot{f}_Q^2}{Q^2} \tilde{\mathcal{D}}_\parallel \psi_n \,, \qquad (2.53)$$

where $\tilde{g}_n = \mathrm{Im}(h_n)/(4\pi^2\alpha)$. Both constants g_n and $\tilde{g}_n$ are used as fitting parameters in our setup, thus the details of holographic wave function for the proton are not important in the fit. Notice that the g_n and $\tilde{g}_n$ do not have the same dimensions, indeed comparing both couplings we see that $[\tilde{g}_n/g_n] = L^2$. Formulas (2.52) and (2.53) are one of the main results of this chapter.

2.2.5 Improved Holographic QCD

To test the above ideas against experimental data we need to consider a concrete QCD holographic model. As pointed out before, we shall consider the improved holographic QCD model introduced in [91,92,96]. This fixes the background fields $A(z)$ and $\Phi(z)$, which give an approximate dual description of the QCD vacuum.

Next we need to consider the equation of motion for the spin J fields that are dual to the twist two operators, whose exchange gives the dominant contribution in DIS at low x. This equation is then analytically continue in J, in order to do the Sommerfeld-Watson transform in Regge theory. This procedure was described in detail in [1], so we will not repeat it here. In chapter 5 we will do a similar analysis for a model of holographic QCD that contains a dilaton and a tachyon coupled to gravity with backreaction effects included. The upshot is that the function B introduced in (2.35) to define the transverse propagator is given by $B = \Phi - A/2$ and the normalizable modes of the spin J field $\psi_n(z)$ solve a Schrödinger problem

$$\left(-\frac{d^2}{dz^2} + U_J(z) \right) \psi_n(z) = t_n \psi_n(z) \,, \qquad (2.54)$$

where

$$U_J(z) = \frac{3}{2}\left(\ddot{A} - \frac{2}{3}\dddot{\Phi}\right) + \frac{9}{4}\left(\dot{A} - \frac{2}{3}\dot{\Phi}\right)^2 + (J-2)e^{-2A}\left[\frac{2}{l_s^2}\left(1 + \frac{d}{\sqrt{\lambda}}\right) + \frac{J+2}{\lambda^{4/3}}\right.$$
$$\left. + e^{2A}\left(a\ddot{\Phi} + b\left(\ddot{A} - \dot{A}^2\right) + c\dot{\Phi}^2\right)\right],$$

where the first two terms represent the potential for the graviton and the remaining deform the graviton potential. This potential is analytically continued in J in such a way that the value of the intercept $J = j_n$ is obtained when the nth eigenvalue satisfies $t_n(J) = 0$.

The constants l_s, a, b, c and d are used as fitting parameters and will be adjusted such that the best match with $F_2(x, Q^2)$ and $F_L(x, Q^2)$ data is achieved. In particular, from the low energy effective string theory perspective, l_s is related to the string tension; d is related to the anomalous dimension curve of the twist 2 operators, or it can also be thought as encoding the information of how the masses of the closed strings excitations are corrected in a slightly curved background; the constants a, b and c encode the first order derivative expansion of a presumed string field theory lagrangian; $\lambda = e^\Phi$ is the 't Hooft coupling.

2.3 Data analysis
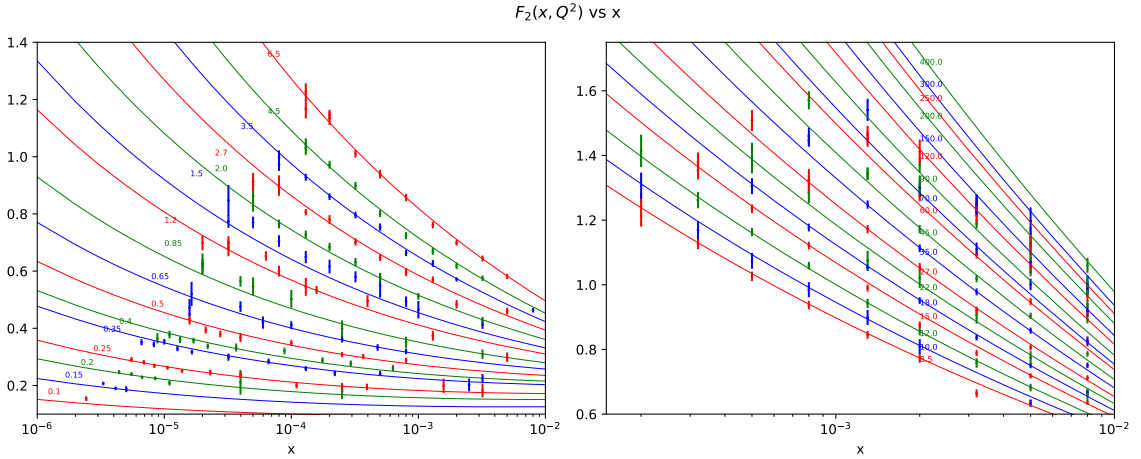
Figure 2.2: Structure function $F_2(Q^2, x)$. Experimental points vs prediction of this work with a $\chi^2_{dof} = 1.42$. Each line corresponds to a given Q^2 (GeV^2) as indicated.

With the previously described setup we proceed to find the best values for the potential parameters l_s, a, b, c and d, as well as for the coupling values β, g_n and $\tilde{g}_n$ that better fit
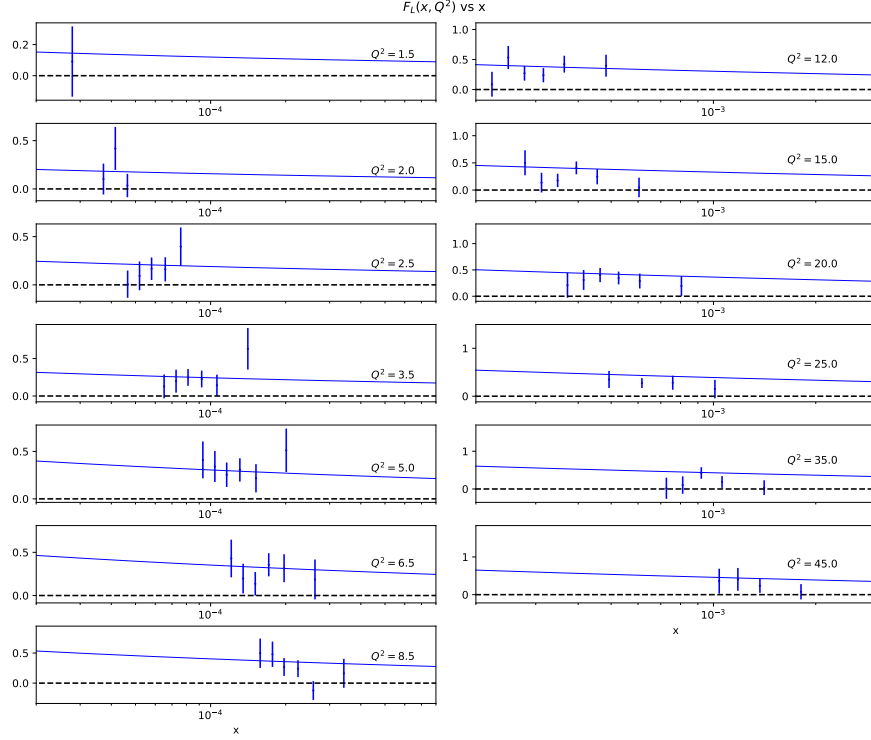
Figure 2.3: Structure function $F_L(Q^2, x)$. Experimental points vs prediction of this work with a $\chi^2_{dof} = 1.42$. Each line corresponds to a given Q^2 (GeV^2) as indicated.

the data. We look, as usual, for the best set of parameter values such that the sum of the weighted difference squared between experimental data and model predicted values is minimum, using as weight the inverse of the experimental uncertainty. Since this is a highly nontrivial numerical optimization problem in which we do not known explicitly the gradient of the function to be optimized, we use the Nelder-Mead algorithm, using C++ language, and try with different starting points in the parameter space. We have used a Chebyshev algorithm with 1000 Chebyshev points for solving the Schrodinger problem. We have found that the inclusion of the nonminimal coupling contribution considerable decreases the convergence ratio of the minimizing routine compared with the case where only the minimal coupling case is used, consistent with the fact that the new function to optimize has a much rougher landscape. Our best fit results with only the contribution of the minimal coupling for $F_2(x, Q^2)$ and $F_L(x, Q^2)$ are presented in figures 2.2 and 2.3. In this fit we considered values of x in the range $x < 10^{-2}$, and of the photon virtuality $Q^2 < 400$ GeV^2. This gives a total number of 249 data points for $F_2(x, Q^2)$ and 64 points for $F_L(x, Q^2)$. The χ^2_{dof} for this fit is 1.42. As in [1], aiming to make a consistent model for the soft Pomeron, we have forced the intercept of the second trajectory to be around $j_1 = 1.09$. This is achieved penalizing those set

65
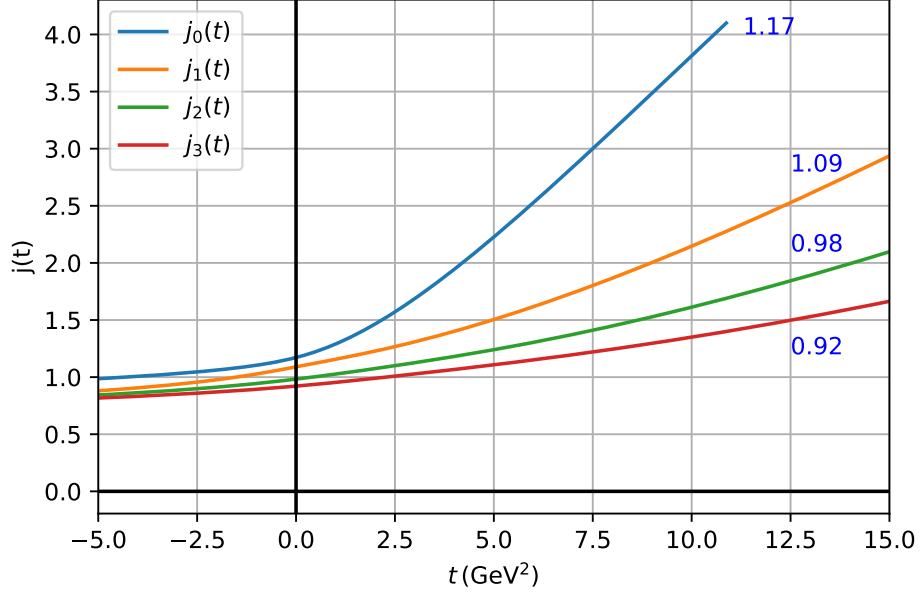
Figure 2.4: Regge trajectories obtained from our model and their intercepts. Configurations that give the soft Pomeron intercept $j_1 = 1.09$ were favoured in the fitting process.

of parameters which give a different second intercept by adding a term of the type $10^4(j_1 - 1.09)^2$ to the function to be optimized. The correspondent Regge trajectories can be seen in figure 2.4.

The values of the parameters that give the best fit are summarized in Table 2.1. We also evaluated the contribution of the nonminimal coupling to the description of the proton structure functions. Using the same data as mentioned above we have obtained a slightly better χ^2_{dof} around 1.40. The best fit parameters including the nonminimal coupling contribution are displayed in Table 2.2. We would like to understand the scale defined by the nonminimal coupling. The best fit fixes the value of this coupling in the equation of motion (2.9) for the $U(1)$ gauge field to be $\beta = -0.000593\,\text{GeV}^{-2}$. This numerical value correspond to an energy of 41 GeV and therefore the energy scale associated with this correction is in the range of $10 - 100$ GeV. We may also look at the ratio between the constants g_n and $\tilde{g}_n$, given by,

$$\frac{\tilde{g}_n}{g_n} = \frac{\beta_{j_n(0)}}{\kappa_{j_n(0)}}, \tag{2.55}$$

which has dimensions $length^2$. This follows from taking the imaginary part of (2.45) and from the fact that g_n has a similar expression [1]. Looking at Table 2.2 it is simple

to see that the ratio $\tilde{g}_n/g_n$, for each n, is also in the energy range of $10 - 100$ GeV.

2.4   Conclusion

In this chapter we extended the results of [1] by including the proton structure function $F_L(x, Q^2)$ and the contribution of a nonminimal coupling between the $U(1)$ gauge field and the higher spin fields in the graviton Regge trajectory. These nonminimal couplings are expected to be present and to play an important role in theories with higher spin fields.

With the inclusion of the $F_L(x, Q^2)$ data we have improved the χ^2_{dof} of 1.7 from [1] to 1.42, without changing much the values of the parameters found there. With the inclusion of the nonminimal coupling we improved this result slightly to a χ^2_{dof} of 1.40. The energy scale associated with its contribution is in the range of $10 - 100$GeV while

Table 2.1: Values of the parameters for the best fit found. All parameters are dimensionless except for $[l_s] = L$. Numerical values are expressed in GeV units.

parameter	value	couplings	value
l_s^{-1}	6.48	g_0	0.167
a	-4.56	g_1	0.108
b	1.41	g_2	0.112
c	0.661	g_3	-1.48
d	-0.110		

Table 2.2: Values of the parameters for the best fit found. All parameters are dimensionless except for $[l_s] = L$, $[\beta] = L^2$ and $[\tilde{g}_i] = L^2$. Numerical values are expressed in GeV units.

parameter	value	couplings	value	couplings	value
l_s^{-1}	6.47298	g_0	0.160194	$\tilde{g}_0$	0.000215132
a	-4.54429	g_1	0.0951361	$\tilde{g}_1$	-0.000162181
b	1.50201	g_2	0.25418	$\tilde{g}_2$	0.00205165
c	0.658871	g_3	-1.48431	$\tilde{g}_3$	-0.000487255
d	-0.112694				
β	-0.000593076				

the maximum value of Q considered in our data is $20\,\text{GeV}$. This could mean that this coupling contributions are more important at higher values of Q. However, for higher values of Q one also needs to take care of the contributions from the Z^0 boson to DIS. On the other hand, it is expected that non-minimal couplings terms are controlled by the gap between the graviton and the next higher spin field [101]. Our results are not consistent with this expectation since the scale we obtained for the non-minimal coupling has an order of magnitude larger than the mass difference between the spin 2 and spin 4 glueballs. This could mean that the effective field theory approach to the equation of motion of the spin J fields in the graviton's Regge trajectory favours the minimal coupling. Given that the non-minimal coupling does not improve much the results of the fits we will drop it in the upcoming chapters.

Nevertheless, it seems we are getting closer to a very satisfactory holographic description of low x data. There are two immediate questions that we believe deserve some further attention. As a working example we have been considering the improved holographic QCD model of [91, 92, 96]. We take this model as our QCD vacuum, and then introduce higher spins fields for which we do Regge theory. Clearly we should study to which extent other models can also be used to reproduce the data here analysed. Our expectation is that holography is very appropriate to study processes dominated by Pomeron exchange, so that other models that are close enough to QCD should give similar results. Another interesting point is to extend this analysis to other processes. Previous studies of deeply virtual Compton scattering and vector meson production could now be revisited. For example, in the case of DVCS the cross section depends on three kinematical quantities, namely x, Q^2 and momentum transfer t. Extending this model to nonvanishing t gives a very non-trivial dependence that deserves to be looked at. In the next chapters we will consider other processes with null momentum transfer t and the case of DVCS.

3
$\gamma^*\gamma$ and γ^*p scattering in improved holographic QCD

Chapter abstract: In this chapter we perform joint fits using measurements of the proton structure functions $F_2(x, Q^2)$ and $F_L(x, Q^2)$, of the photon structure function $F_2^\gamma(x, Q^2)$ and of the total cross-sections $\sigma(\gamma p \to X)$ and $\sigma(\gamma\gamma \to X)$. The data is gathered from several sources including HERA and LEP. The kinematical range considered is wide with a photon virtuality $Q^2 \leq 400\,\mathrm{GeV}^2$, Bjorken variable $x < 0.01$ and $\sqrt{s} > 4\,\mathrm{GeV}$. This is done by considering a $U(1)$ vector gauge field minimally coupled to the graviton Regge trajectory in improved holographic QCD. We find good agreement with the data for a joint fit of F_2^γ and $\sigma(\gamma\gamma \to X)$ with a $\chi^2_{dof} = 1.07$. For a joint fit of F_2, F_L and $\sigma(\gamma p \to X)$ we find $\chi^2_{dof} = 1.40$. A joint fit of all observables for both processes $\gamma^*\gamma$ and γ^*p gives a $\chi^2_{dof} = 1.38$. The gravitational couplings of the $U(1)$ vector gauge field and of the proton with the Reggeons of the graviton Regge trajectory are given as an output of the fitting procedure. An approximate relation between the structure functions, valid at NLO QCD, is used to estimate the parton distribution function (PDF) of the gluon inside the proton.

3.1 Introduction

As we have mentioned in the introduction of this thesis, holography has been quite successful in describing QCD processes dominated by Pomeron exchange. Usually these studies are related to a process that include the scattering of an off-shell photon produced by an incoming electron with a target proton (γ^*p scattering). One process that has been less explored is $\gamma^*\gamma^*$ scattering, which arises in high-energy e^+e^- interactions for which some electrons and positrons are scattered by emitting virtual photons whose virtualities can be computed by measuring the angles and energies

of the scattered electrons and positrons. The virtual photons can then fluctuate into quark-anti-quark pairs and hence generate a hadronic final state X. It is in this context that we refer to $\gamma^*\gamma^*$ scattering.

The goal of this chapter is to extend the results of the previous chapter by including another γ^*p observable in our fits, the total cross-section $\sigma(\gamma p \to X)$, as well a new class of $\gamma^*\gamma^*$ processes. The latter are a much cleaner application of holography because an off-shell photon generates a source for the quark bilinear operator $J^\mu = \bar{\psi}\gamma^\mu\psi$ which is dual to the non-normalizable mode of a bulk $U(1)$ gauge field. Describing a proton as an external on-shell state is notoriously more difficult in holography.

As in the previous chapter, we use the Improved holographic QCD model constructed in [91, 92, 96]. We start by fitting the product of the bulk couplings between the bulk fields dual to J^μ and the proton with the Reggeons of the graviton Regge trajectory as well as the parameters of the Pomeron kernel. This initial fit has nine parameters which are fixed by the HERA data of F_2 and F_L presented in [99, 100] as well $\sigma(\gamma p \to X)$ data from [102]. The fit uses 358 data points, covering the very large kinematical range of $x < 10^{-2}$ and $Q^2 \leq 400\,\mathrm{GeV}^2$ for $F_2(x, Q^2)$ and $Q^2 \leq 45\,\mathrm{GeV}^2$ for $F_L(x, Q^2)$ and $\sqrt{s} > 4.6\,\mathrm{GeV}$ for $\sigma(\gamma p \to X)$, where Q^2 is the photon virtuality. We have found a χ^2_{dof} of 1.40. We shall then use the fixed Pomeron kernel parameters and the data for $F_2^\gamma(x, Q^2)$ and $\sigma(\gamma\gamma \to X)$ to fit the local couplings of the bulk $U(1)$ gauge field with the Reggeons of the graviton Regge trajectory. For this fit we have found a χ^2_{dof} of 1.07.

We also consider global fits, including both γ^*p and $\gamma^*\gamma$ processes. As we shall see, allowing all the parameters of the model to vary does not move these parameters significantly from the values determined before, therefore further extending the range of Pomeron exchange processes described by holography in a consistent manner.

In this chapter we will also study the qualitative behaviour of the gluon PDF. This will be done by using our holographic expressions for the structure functions F_2 and F_L. This was done in the context of holographic QCD in [103] using the BPST kernel for pomeron exchange and a hard-wall in AdS_5 to add confinement effects. The results presented in [103] were obtained using a χ^2 fit with data for $Q^2 \leq 10\,\mathrm{GeV}^2$. Since we have a good description of both F_2 and F_L in a wider photon virtuality range, we use the same method to compute the holographic gluon PDF. We compare our results with the NLO results of the CTEQ and NNPDF PDF sets, finding good agreement throughout the larger kinematical region.

3.2   Holographic total cross-section $\gamma p \to X$

In the previous chapter we have mentioned that the proton structure functions are related to polarized cross-sections of γ^*p scattering through equations (2.2). In the limit that the off-shell photon virtuality $Q \to 0$ the longitudinal cross-section vanishes since an on-shell photon only has transverse polarization. Hence, the total cross-section of the process $\gamma p \to X$ is related to the proton structure function $F_2^p(x, Q^2)$ through

$$\sigma(\gamma p \to X) = 4\pi^2 \alpha \lim_{Q^2 \to 0} \frac{F_2^p(x, Q^2)}{Q^2}\,. \tag{3.1}$$

In this chapter the DIS structure functions F_2 and $F_L = F_2 - 2xF_1$ are given by

$$F_2^p(x, Q^2) = \sum_n \frac{\operatorname{Im} g_n}{4\pi^2 \alpha} x^{1-j_n} f_n^2(Q^2)\,, \tag{3.2}$$

$$F_L^p(x, Q^2) = \sum_n \frac{\operatorname{Im} g_n}{4\pi^2 \alpha} x^{1-j_n} f_n^L(Q^2)\,, \tag{3.3}$$

where f_n^2 and f_n^L have the same expressions as equations (2.50) and (2.51), respectively, except for the g_n factor

$$f_n^2(Q^2) = Q^{2j_n} \int dz\, e^{-\left(j_n - \frac{3}{2}\right)A} \left(f_Q^2 + \frac{\dot{f}_Q^2}{Q^2} \right) \psi_n(z)\,, \tag{3.4}$$

$$f_n^L(Q^2) = Q^{2j_n} \int dz\, e^{-\left(j_n - \frac{3}{2}\right)A} \frac{\dot{f}_Q^2}{Q^2} \psi_n(z)\,. \tag{3.5}$$

Previously the factor of $4\pi^2 \alpha$ in (3.1) was not relevant for the fits but here it is important to have it explicitly in order to have consistent holographic expressions for the proton structure functions and the total cross-section $\sigma(\gamma p \to X)$. The constant g_n is given by equation (2.40). In our holographic setup the non-normalizable modes of the bulk $U(1)$ gauge field satisfy

$$\lim_{Q \to 0} f_Q(z) = 1\,, \quad \lim_{Q \to 0} \frac{\dot{f}_Q}{Q} = 0\,, \tag{3.6}$$

and after taking the limit (3.1) we obtain the holographic expression for the total cross-section

$$\sigma(\gamma p \to X) = \sum_n \operatorname{Im} g_n\, s^{j_n - 1} \int dz\, e^{-\left(j_n - \frac{3}{2}\right)A} \psi_n(z)\,. \tag{3.7}$$

3.3 $\gamma^*\gamma^*$ observables

In this section we describe the observables in $\gamma^*\gamma^*$ scattering and how to compute them using holography. In this process photons can reveal either their point-like or hadron-like behaviour. In the point-like case one of the quarks takes part in the hard interaction while in the hadron-like case the photons fluctuate into hadrons with the same quantum numbers of the photon (i.e. vector mesons like ρ, ω, ϕ) and the interaction is the same as in hadron-hadron scattering. These pictures coexist together and are dominant in different kinematical regions. For high transverse momentum of the quarks or high virtuality of one of the photons the point-like nature is dominant. For lower values of the photon virtuality the interaction is spread over longer times, giving time for the quarks to form bound states through gluon exchange. This is the regime we are interested here.

The process $e^+e^- \to e^+e^- X$ is factorised into three terms: one for the radiation of the virtual photon from the electron, one for the radiation of the other virtual photon from the positron and the term that couples the $\gamma^*\gamma^*$ system to the final hadronic state X. Like in e^-p DIS we can define the following variables

$$y_1 = \frac{k_1 \cdot p_2}{p_1 \cdot p_2}, \quad y_2 = \frac{k_2 \cdot p_1}{p_1 \cdot p_2}, \quad x_1 = \frac{Q_1^2}{2k_1 \cdot p_2}, \quad x_2 = \frac{Q_2^2}{2k_2 \cdot p_1}, \tag{3.8}$$

where p_1 and p_2 are the incoming leptons momenta, and k_1 and k_2 the momenta of the two off-shell photons with virtualities $Q_1^2 = k_1^2$ and $Q_2^2 = k_2^2$. In terms of these variables we can write the differential cross-section for $e^+e^- \to e^+e^- X$ as [52]

$$\begin{aligned}
\frac{d^4\sigma}{dy_1 dy_2 dQ_1^2 dQ_2^2} &= \left(\frac{\alpha}{2\pi}\right)^2 \Big[P_{\gamma/e^-}^T\big(y_1, Q_1^2\big) P_{\gamma/e^+}^T\big(y_2, Q_2^2\big) \sigma^{TT}\big(Q_1^2, Q_2^2, W^2\big) + \\
&+ P_{\gamma/e^-}^T\big(y_1, Q_1^2\big) P_{\gamma/e^+}^L\big(y_2\big) \sigma^{TL}\big(Q_1^2, Q_2^2, W^2\big) + P_{\gamma/e^-}^L\big(y_1\big) P_{\gamma/e^+}^T\big(y_2, Q_2^2\big) \times \\
&\times \sigma^{LT}\big(Q_1^2, Q_2^2, W^2\big) + P_{\gamma/e^-}^L\big(y_1\big) P_{\gamma/e^+}^L\big(y_2\big) \sigma^{LL}\big(Q_1^2, Q_2^2, W^2\big) \Big] \frac{1}{Q_1^2 Q_2^2},
\end{aligned} \tag{3.9}$$

where $W = \sqrt{s}$ and the functions $P_{\gamma/e}^T$ and $P_{\gamma/e}^L$ are related to flux factors and are given by

$$P_{\gamma/e}^T\big(y, Q^2\big) = \frac{1 + (1-y)^2}{y} - \frac{2m_e^2 y}{Q^2}, \tag{3.10}$$

$$P_{\gamma/e}^L(y) = 2\frac{1-y}{y}. \tag{3.11}$$

The cross sections $\sigma^{ij}(Q_1^2, Q_2^2, W^2)$, with $i, j = T, L$, are the total cross sections for the process $\gamma^*(Q_1^2)\gamma^*(Q_2^2) \to$ X where the incoming photons have transverse (T) or

longitudinal (L) polarization in their centre-of-mass frame. The differential cross-section expression also results from integrating over the angle between the plane of the scattered leptons in the center-of-mass frame of the $\gamma^*\gamma^*$ system and does not include terms that are present for polarized lepton beams.

The observables we want to study can be expressed in terms of the cross-sections $\sigma^{ij}(Q_1^2, Q_2^2, W^2)$. Hence we will compute these cross-sections holographically starting from the general scattering amplitude of $\gamma^*(Q_1)\gamma^*(Q_2) \to \gamma^*(Q_3)\gamma^*(Q_4)$ for arbitrary polarisation of the incoming and outgoing virtual photons. Later, from this general amplitude, we specify for the case of the cross-section $\sigma(\gamma\gamma \to X)$ and of the structure function $F_2^\gamma(x, Q^2)$. The Witten diagram that is relevant for our calculations is the one in figure 3.1. The off-shell photons source the quark-bilinear operator current $\bar{\psi}\gamma^\mu\psi$ so the $\gamma^*\gamma^* \to \gamma^*\gamma^*$ amplitude can be computed form the $2 \to 2$ scattering of bulk photons described by a $U(1)$ gauge field.
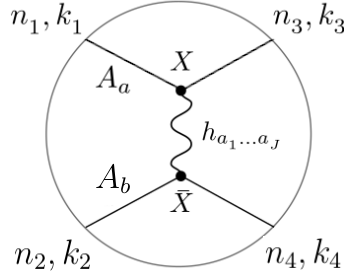
Figure 3.1: Tree level Witten diagram representing spin J exchange in a $2 \to 2$ scattering process between bulk photons. We will consider a kinematical regime dominated by the exchange of spin J fields in the graviton Regge trajectory.

Finally, we describe the kinematics we will be considering. Using the same light-cone coordinates as in the previous chapter, the incoming photons have the space-like momenta

$$k_1 = \left(\sqrt{s}, -\frac{Q_1^2}{\sqrt{s}}, 0\right), \qquad k_2 = \left(-\frac{Q_2^2}{\sqrt{s}}, \sqrt{s}, 0\right), \tag{3.12}$$

while for the outgoing photons,

$$k_3 = -\left(\sqrt{s}, \frac{q_\perp^2 - Q_3^2}{\sqrt{s}}, q_\perp\right), \quad k_4 = -\left(\frac{q_\perp^2 - Q_4^2}{\sqrt{s}}, \sqrt{s}, -q_\perp\right), \tag{3.13}$$

where $Q_i^2 = k_i^2 > 0$ ($i = 1, \ldots, 4$) is the off-shellness. We consider the Regge limit of large s and fixed $t = -q_\perp^2$. We can now define the photons polarization vectors n_i^λ that satisfy the condition $n_i^\lambda \cdot k_i = 0$. The incoming off-shell photons have the following

polarization vectors

$$
n_1 = \begin{cases} (0, 0, \epsilon_\lambda), & \lambda = 1, 2 \\ \frac{1}{Q_1}\left(\sqrt{s}, \frac{Q_1^2}{\sqrt{s}}, 0, 0\right), & \lambda = 3 \end{cases}, \tag{3.14}
$$

$$
n_2 = \begin{cases} (0, 0, \epsilon_\lambda), & \lambda = 1, 2 \\ \frac{1}{Q_2}\left(\frac{Q_2^2}{\sqrt{s}}, \sqrt{s}, 0, 0\right), & \lambda = 3 \end{cases}, \tag{3.15}
$$

where $\epsilon_1 = (1, 0)$ and $\epsilon_2 = (0, 1)$, while for the outgoing photons we have

$$
n_3 = \begin{cases} \left(0, \frac{2q_\perp \cdot \epsilon_\lambda}{\sqrt{s}}, \epsilon_\lambda\right), & \lambda = 1, 2 \\ \frac{1}{Q_3}\left(\sqrt{s}, \frac{Q_3^2 + q_\perp^2}{\sqrt{s}}, q_\perp\right), & \lambda = 3 \end{cases}, \tag{3.16}
$$

$$
n_4 = \begin{cases} \left(-\frac{2q_\perp \cdot \epsilon_\lambda}{\sqrt{s}}, 0, \epsilon_\lambda\right), & \lambda = 1, 2 \\ \frac{1}{Q_4}\left(\frac{Q_4^2 + q_\perp^2}{\sqrt{s}}, \sqrt{s}, -q_\perp\right), & \lambda = 3 \end{cases}. \tag{3.17}
$$

Notice that the transverse photons ($\lambda = 1, 2$) are normalized such that $n^2 = 1$, while the longitudinal photons ($\lambda = 3$) are normalized such that $n^2 = -1$.

3.3.1 Computation of Witten diagram

The amplitude associated to the exchange of a spin J field in the Witten diagram of figure 3.1 is given by

$$
A_J(k_i, \lambda_j) = -\kappa_J^2 \int d^5 X d^5 \bar{X} \sqrt{-g}\sqrt{-\bar{g}}\, e^{-\Phi} e^{-\bar{\Phi}} F_{-a}^{(1)}(k_1, z) \partial_-^{J-2} F_-^{a\,(3)}(k_3, z) \times
$$
$$
\times F_{+b}^{(2)}(k_2, \bar{z}) \bar{\partial}_+^{J-2} F_+^{b\,(4)}(k_4, \bar{z}) \, \Pi^{-\cdots-,+\cdots+}\left(X, \bar{X}\right). \tag{3.18}
$$

Using the kinematics introduced above we obtain

$$
A_J(k_i, \lambda_j) = -\kappa_J^2 \left(\frac{i}{2}\sqrt{s}\right)^{2J-4} \int d^5 X d^5 \bar{X} \frac{e^{5(A+\bar{A})}}{4} e^{-\Phi - \bar{\Phi}} \left(4e^{-2(A+\bar{A})}\right)^J \times
$$
$$
\times F_{-a}^{(1)} F_-^{a\,(3)} F_{+b}^{(2)} F_+^{b\,(4)} e^{-iq_\perp \cdot (x_\perp - \bar{x}_\perp)} \Pi_{+\cdots+,-\cdots-}\left(X, \bar{X}\right). \tag{3.19}
$$

By performing the change of variables $w = x - \bar{x}$ and using the propagator identity in equation (2.34) we arrive at the result

$$
A_J(k_i, \lambda_j) = \frac{iV\kappa_J^2}{2^J} s^J \int dz d\bar{z}\, e^{3(A+\bar{A})} e^{-\Phi - \bar{\Phi}} \times
$$
$$
\times e^{-(1+J)(A+\bar{A})} F(1, 3) F(2, 4) G_J(z, \bar{z}, t), \tag{3.20}
$$

where

$$F(i,j) = \begin{cases} f_{Q_i} f_{Q_j}, & \lambda_i = \lambda_j = 1,2 \\ \dot{f}_{Q_i} \dot{f}_{Q_j}/(Q_i Q_j), & \lambda_i = \lambda_j = 3 \end{cases}, \tag{3.21}$$

and $G_J(z, \bar{z}, t)$ is given by (2.35).

Next we need to sum the above amplitude over the even spin-J fields with $J > 2$, as we described in the previous chapter. Such sum can be computed through a Sommerfeld-Watson transform

$$\frac{1}{2} \sum_J s^J + (-s)^J \rightarrow -\frac{\pi}{2} \int \frac{dJ}{2\pi i} \frac{s^J + (-s)^J}{\sin \pi J} . \tag{3.22}$$

This assumes that an analytic continuation of the amplitude to the complex J-plane is possible. We now deform the integral from the poles at even J, to the poles $J = j_n(t)$ defined by $t_n(J) = t$. The scattering domain of negative t contains these poles along the real axis for $J < 2$. Thus the forward scattering amplitude ($t = 0$) of $\gamma^*(Q_1)\gamma^*(Q_2) \rightarrow \gamma^*(Q_3)\gamma^*(Q_4)$ is

$$\mathcal{A}^{\lambda_1,\lambda_2,\lambda_3,\lambda_4}_{Q_1,Q_2,Q_3,Q_4}(s, t=0) = -\frac{\pi}{2} \sum_n s^{j_n} \left[i + \cot\left(\frac{\pi j_n}{2}\right) \right] \frac{\kappa^2_{j_n}}{2^{j_n}} \frac{dj_n}{dt} \times$$

$$\times \int dz\, e^{-(j_n - 3/2)A} F(1,3) \psi_n(z) \int d\bar{z}\, e^{-(j_n - 3/2)\bar{A}} F(2,4) \psi_n^*(\bar{z}) . \tag{3.23}$$

Finally, we remark that the total cross-sections $\sigma^{ij}(Q_1^2, Q_2^2, W^2)$, with $i, j = T, L$, can now be computed using the optical theorem and appropriate photon polarisations, as well by setting $Q_3^2 = Q_1^2$ and $Q_4^2 = Q_2^2$.

3.3.2 Photon structure function F_2^γ

We consider first scattering between a virtual and an on-shell photon. In analogy with deep inelastic $e^\pm p$ scattering, we can think of this process as deep inelastic $e^\pm \gamma$ scattering. Just as for $e^\pm p$ scattering, we can define a hadronic tensor $W^{\mu\nu}$ and two structure functions related by

$$\frac{W^{\mu\nu}(x, Q^2)}{8\pi^2 \alpha} = -\left(g^{\mu\nu} + \frac{q_1^\mu q_1^\nu}{Q^2} \right) F_1^\gamma(x, Q^2) +$$

$$+ \frac{1}{q_1 \cdot q_2} \left(q_2^\mu + q_1^\mu \frac{q_1 \cdot q_2}{Q^2} \right) \left(q_2^\nu + q_1^\nu \frac{q_1 \cdot q_2}{Q^2} \right) F_2^\gamma(x, Q^2) , \tag{3.24}$$

such that the cross section for the process $e\gamma \rightarrow eX$ can be written as

$$\frac{d^2\sigma}{dxdy} = \frac{4\pi\alpha^2}{xyQ^2} \left[(1-y) F_2^\gamma(x, Q^2) + xy^2 F_1^\gamma(x, Q^2) \right] . \tag{3.25}$$

The structure functions are related to the total cross-sections of equation (3.9) through the relations

$$F_2^\gamma(x, Q^2) = \frac{Q^2}{4\pi^2\alpha}\left[\sigma_{TT}(s, Q^2, 0) + \sigma_{LT}(s, Q^2, 0)\right],\tag{3.26}$$

$$2xF_1^\gamma(x, Q^2) = \frac{Q^2}{4\pi^2\alpha}\,\sigma_{TT}(s, Q^2, 0)\,.\tag{3.27}$$

Before continuing with the holographic computation let us discuss in which kinematical region will it be applicable. The hadronic photon structure function F_2^γ differs from the proton structure function due to the point-like coupling of the photon to the quarks. This coupling makes the photon structure function to rise towards large values of Bjorken x, while in the case of the proton it decreases. Moreover, F_2^γ has positive scaling violations for all values of x, while F_2^p has positive scaling violations only at small values of x. Also, the point-like part can be evaluated at all orders in perturbative QCD and dominates for large values of Q^2 and for values of $x > 0.1$. On the other hand, the hadronic-like part can not be computed in perturbative QCD. Like its F_2^p counterpart, only its evolution with Q^2 can be determined. As in the case of the proton, an ansatz for the x dependence at some scale Q_0^2 is given as input to QCD evolution equations. This ansatz can be derived from the Vector Meson Dominance model, since the photon can fluctuate in a vector meson like the ρ meson. After that, one assumes that the F_2^ρ structure function is the same as the $F_2^{\pi^0}$ structure function which has been measured experimentally. Then this hadron-like component can be evolved using perturbative QCD and we can compare it with the F_2^γ structure function that contains both the point-like and hadron-like contributions. The result is that although the hadron-like component is not important for high values of Q^2 and $x > 0.1$, it clearly dominates for very small values of x, meaning that we can use the Pomeron exchange picture to study this process. Hence our holographic expression is only valid for $x < 0.01$. Thus we proceed to the holographic computation of F_2^γ in this kinematical region.

As mentioned, one photon in this process is quasi-real. Let us represent such photon by the lower part of the Witten diagram. Then the $\bar{z}$ integral simplifies to

$$\int d\bar{z}\, e^{-(j_n - 3/2)A}\psi_n^*(j_n, \bar{z})\,.\tag{3.28}$$

Defining

$$g_n = -\frac{\pi}{2}\left(i + \cot\frac{\pi j_n}{2}\right)\frac{\kappa_{j_n}^2}{2^{j_n}}j_n'\int d\bar{z}\, e^{-(j_n - 3/2)A}\psi_n^*(j_n, \bar{z})\,,\tag{3.29}$$

and using the optical theorem, we can write the total cross-sections σ_{TT} and σ_{LT} as

$$\sigma_{TT} = \sum_n \operatorname{Im} g_n s^{j_n-1} \int dz\, e^{-(j_n-3/2)A} f_Q^2\, \psi_n(z)\,, \tag{3.30}$$

$$\sigma_{LT} = \sum_n \operatorname{Im} g_n s^{j_n-1} \int dz\, e^{-(j_n-3/2)A} \frac{\dot{f}_Q^2}{Q^2}\, \psi_n(z)\,. \tag{3.31}$$

Using (3.26) and $s = Q^2/x$, the holographic expression for F_2^γ is then

$$F_2^\gamma\big(x, Q^2\big) = \sum_n \frac{\operatorname{Im} g_n}{4\pi^2\alpha}\, x^{1-j_n} f_n^\gamma(Q^2)\,, \tag{3.32}$$

where

$$f_n^\gamma(Q^2) = Q^{2j_n} \int dz\, e^{-(j_n-3/2)A} \left(f_Q^2 + \frac{\dot{f}_Q^2}{Q^2} \right) \psi_n(z)\,. \tag{3.33}$$

3.3.3   Total cross section $\gamma\gamma \to X$

In this process both photons are considered quasi-real, i.e. $Q_1^2 \approx 0$ and $Q_2^2 \approx 0$. Therefore, using (3.23), (3.6) and the optical theorem, the cross sections $\sigma^{LL}(0,0,W)$, $\sigma^{TL}(0,0,W)$ and $\sigma^{LT}(0,0,W)$ vanish. This is expected since real photons only have transverse polarisation and hence cross-sections that involve at least one longitudinal on-shell photon do not contribute to this process. Thus

$$\sigma(\gamma\gamma \to X) = \sigma^{TT}\big(0,0,s=W^2\big) = \sum_n \operatorname{Im} g_n s^{j_n-1} \int dz\, e^{-(j_n-3/2)A}\psi_n(z)\,. \tag{3.34}$$

Like in the case of γ^*p processes the numbers $\operatorname{Im} g_n$ have the same definition as the ones in our holographic expression F_2^γ and these observables are related by

$$\sigma(\gamma\gamma \to X) = 4\pi^2\alpha \lim_{Q^2\to 0} \frac{F_2^\gamma}{Q^2}\,. \tag{3.35}$$

3.4   Data analysis and results

With the previously described setup we proceed to find the best values for the Pomeron potential parameters l_s, a, b, c and d, as well as for the coupling values $\operatorname{Im} g_n$. The $\operatorname{Im} g_n$ constants have different definitions for $\gamma^*\gamma$ and γ^*p processes, so we will determine a set of values for each process class. We use the first four Reggeons, which are enough to reproduce the non-trivial x behaviour of the proton structure functions F_2^p, F_L^p and

the total cross-section $\sigma(\gamma p \to X)$. Adding several trajectories explains the so-called hard-pomeron behaviour for large Q and the soft-pomeron behaviour for smaller Q, as discussed in [1]. Each Im g_n is associated with a Reggeon.

We find the best set of parameter values α_i by minimising the χ^2 quantity

$$\chi^2 = \sum_{n=1}^{N} \left(\frac{O_k^{\text{pred.}}(\alpha_i) - O_k^{\text{exp.}}}{\sigma_k} \right)^2, \tag{3.36}$$

that is, the sum of the weighted difference squared between experimental data and model predicted values where the weight is the inverse of the experimental uncertainty. Usually a fit is deemed of good quality if the quantity $\chi^2_{\text{dof}} \equiv \chi^2/(N - N_{par})$, where $N_{\text{par.}}$ is the number of parameters to be fitted, is close to one. Throughout the rest of this chapter the parameter errors represent the 68 percent confidence interval for the parameter estimates.

In equation (5.96) O_k represents a generic data point of one or several observables mentioned in the previous sections. For the proton structure functions σ_k is simply the experimental error of each point. For total cross-section data we also need to take into account that some data points have uncertainties in the values of s (e.g. in $\gamma\gamma \to X$ that is always the case because it is a measured quantity). To account for this we compute the total cross-section for $s + \Delta s$ and $s - \Delta s$, and compute

$$\sigma_{\text{eff}} = \max \left(|\sigma^{\text{pred}}(s + \Delta s) - \sigma^{\text{pred}}(s)|, \right.$$
$$\left. |\sigma^{\text{pred}}(s - \Delta s) - \sigma^{\text{pred}}(s)| \right). \tag{3.37}$$

For these cases $\sigma_k = \sqrt{(\sigma_{\text{exp}})^2 + (\sigma_{\text{eff}})^2}$ where σ_{exp} is the experimental error.

For $\sigma(\gamma\gamma \to X)$ and $\sigma(\gamma p \to X)$ we use the hadronic cross-section data files from the Particle Data Group [102]. These data sets are a compilation of experimental results obtained in the last decades from several collaborations. The dataset of $\sigma(\gamma p \to X)$ has cross-section values as a function of the laboratory momentum of the incoming on-shell photon. Hence we computed the respective center of mass energy $\sqrt{s}$ before performing the fits. We also considered only subsets of data with $\sqrt{s} > 4\,\text{GeV}$ for $\sigma(\gamma\gamma \to X)$ and $\sigma(\gamma p \to X)$, yielding 39 and 45 experimental points respectively. The lower bound cuts result from the fact that our model does not realise the meson trajectory with an intercept around $0.35 - 0.55$. This trajectory dominates for smaller values of s and the best our model can do is to reproduce data in the intermediate range of s through the third and fourth trajectories. For the source of data for the proton structure functions $F_2(x, Q^2)$ and $F_L(x, Q^2)$ we use the HERA measurements of

Table 3.1: Values of the parameters for the best joint fit of the proton structure functions $F_2\left(x, Q^2\right)$ and $F_L\left(x, Q^2\right)$ and $\sigma\left(\gamma p \to X\right)$ data from PDG with $x \leq 0.01$, $Q^2 \leq 400\,\mathrm{GeV}^2$ and $\sqrt{s} > 4.6\,\mathrm{GeV}$. We obtained a χ^2_{dof} of 1.40 with 358 experimental points.

Kernel parameters	couplings	intercept
$a = -4.70 \pm 0.04$	$\mathrm{Im}\, g_0 = -0.051 \pm 0.001$	$j_0 = 1.165$
$b = 1.13 \pm 0.05$	$\mathrm{Im}\, g_1 = 0.017 \pm 0.007$	$j_1 = 1.082$
$c = 0.66 \pm 0.01$	$\mathrm{Im}\, g_2 = -0.07 \pm 0.01$	$j_2 = 0.977$
$d = -0.098 \pm 0.006$	$\mathrm{Im}\, g_3 = 0.358 \pm 0.007$	$j_3 = 0.918$
$l_s^{-1} = 6.47 \pm 0.08$		

Table 3.2: Parameters for the fit with the photon structure functions $F_2^\gamma\left(x, Q^2\right)$ and $\sigma\left(\gamma\gamma \to X\right)$ data from PDG with $\sqrt{s} > 4\,\mathrm{GeV}$. $\chi^2_{dof} = 1.07$ with 61 experimental points.

couplings	value $\times\, 10^{-4}$
$\mathrm{Im}\, g_0$	-1.789 ± 0.065
$\mathrm{Im}\, g_1$	1.94 ± 0.33
$\mathrm{Im}\, g_2$	-3.19 ± 1.11
$\mathrm{Im}\, g_3$	13.37 ± 1.21

these observables available in [99, 100]. There are 249 points in the kinematical region with $x < 10^{-2}$ and $Q^2 \leq 400\,\mathrm{GeV}^2$ for $F_2\left(x, Q^2\right)$, and 64 points with $x < 10^{-2}$ and $Q^2 \leq 45\,\mathrm{GeV}^2$ for $F_L\left(x, Q^2\right)$. For the photon structure function $F_2^\gamma\left(x, Q^2\right)$ we consider the measurements of ALEPH [104, 105], L3 [106] and OPAL [107–109] collaborations at LEP and of the TPC/Two Gamma collaboration [110] at SLAC e^+e^- storage ring PEP. These measurements contribute with 22 points with $x \leq 0.0235$ and $Q^2 \leq 17.8\,\mathrm{GeV}^2$.

We now present the results of three fits we have performed. First we included only the data from observables of γ^*p processes. Using data from the proton structure functions and of the total cross-section $\sigma(\gamma p \to X)$ the best fit values for the Pomeron kernel parameters and constants $\mathrm{Im}\, g_n$ defined in (2.40) are present in table 3.1. The corresponding intercepts of the Reggeons are also displayed in the same table. The total number of experimental points used in this fit is 358 and a χ^2_{dof} per degree of freedom of 1.40 was obtained. With those parameter values we compare the predictions of our model against the experimental data in figures 3.2, 3.3 and 3.4.

Figure 3.2: Predicted proton structure function $F_2\left(x, Q^2\right)$ vs experimental points. The curves were obtained using the values of table 3.1.

For the fit including the photon structure functions F_2 and the total cross section of $\gamma\gamma$ scattering, we obtained the values present in table 3.2. We emphasize that in this fit the Pomeron kernel parameters were kept fixed and equal to the values in table 3.1. The number of points used in this fit was 61 and a χ^2_{dof} per degree of freedom of 1.07 has been obtained. The predictions of our model for these parameters against the $\sigma\left(\gamma\gamma \to X\right)$ and F_2^γ data are displayed in figures 3.4 and 3.5, respectively.

The good quality of the fits obtained so far and the definitions of $\operatorname{Im} g_n$ for $\gamma^*\gamma$ and of $\operatorname{Im} g_n$ for γ^*p processes suggest that a joint fit using all experimental data is possible. The fitting parameters in this fit are the gravitational couplings κ_{j_n} between the bulk $U(1)$ gauge field with the n-th reggeon defined in (2.21), and the product of the gravitational couplings $\bar{\kappa}_{j_n}$ of the bulk field dual to the proton in (2.25) together with the corresponding $\bar{z}$ integral. We have done such a fit making use of the combined 419 experimental points of the different observables. A χ^2_{dof} per degree of freedom of 1.38

Figure 3.3: Predicted proton structure function $F_L\left(x, Q^2\right)$ vs experimental points. The curves were obtained using the values of table 3.1.

was obtained with the parameters of table 3.3. For completeness the corresponding values of $\operatorname{Im} g_n$ for the $\gamma^*\gamma$ and γ^*p processes are also given in table 3.4 and are very close to those found previously in tables 3.1 and 3.2.

Finally, we have also performed a global fit where the pomeron kernel parameters were also allowed to vary. We have found a χ^2_{dof} of 1.36 and parameter values close to the ones of tables 3.1, 3.2 and 3.3 therefore showing the consistency of our results.

(a)   (b)
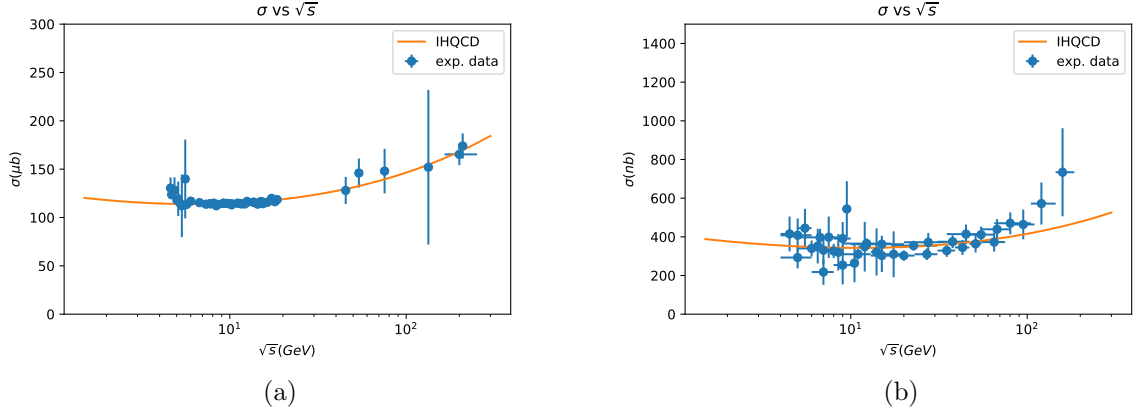
Figure 3.4: (a) Predicted $\sigma\left(\gamma p \to X\right)$ vs experimental points. The curve was obtained using the values from table 3.1. (b) Predicted $\sigma\left(\gamma\gamma \to X\right)$ vs experimental points. The curve was obtained using the parameter values in table 3.2.

Table 3.3: Values for the joint fit of $\gamma^*\gamma$ and γ^*p processes. There are 419 experimental points giving a $\chi^2_{dof} = 1.38$.

n	κ_{j_n}	$\bar{\kappa}_{j_n} \times \bar{z}\,\text{integral}$
1	0.05106 ± 0.00093	-18.040 ± 0.335
2	0.0631 ± 0.0055	-5.45269 ± 0.610
3	0.228 ± 0.040	10.0 ± 1.8
4	-0.261 ± 0.012	-56.1 ± 2.7

Table 3.4: Values of $\operatorname{Im} g_n^{\gamma^*\gamma}$ and $\operatorname{Im} g_n^{\gamma^*p}$ from the best fit parameters of table 3.3.

n	$\operatorname{Im} g_n^{\gamma^*\gamma}$	$\operatorname{Im} g_n^{\gamma^*p}$
1	-1.78883×10^{-4}	-0.0510176
2	1.93696×10^{-4}	0.017369
3	-3.19052×10^{-4}	-0.0744977
4	13.3664×10^{-4}	0.357739

3.5   Gluon Parton distribution functions

The structure functions F_2 and F_L of the proton can be written in terms of the proton's PDFs. Their physical meaning is the probability density for finding a parton with a certain longitudinal momentum fraction x at resolution scale Q^2. In the naive quark parton model $F_2 = \sum_i e_i^2 x q_i(x)$, where the phenomena of Bjorken scaling is predicted,
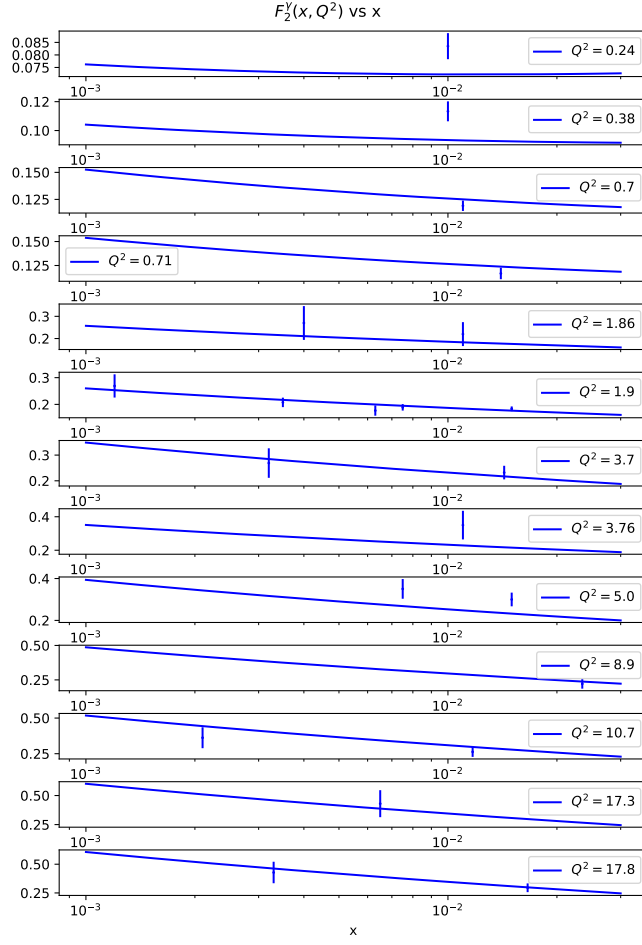
Figure 3.5: Predicted $F_2^{\gamma}\left(x, Q^2\right)$ vs experimental points. The curves were obtained using the values from table 3.2.

i.e. F_2 depends only on x and not Q^2. The parton model also predicts that

$$F_L\left(x, Q^2\right) = F_2\left(x, Q^2\right) - 2xF_1\left(x, Q^2\right) = 0\,, \tag{3.38}$$

which is known as the Callan-Gross relationship and is satisfied if the partons inside the proton have spin-$\frac{1}{2}$. These relations follow from considering only the QED diagram γ^*-parton and assuming that the partons have zero transverse momentum. At NLO QCD gluon radiation and $g \to q\bar{q}$ processes give rise to $\ln Q^2$ scaling violations and to partons with non-zero transverse momentum. Hence the Callan-Gross relation is no longer true, and F_L can be related to F_2 and the gluon PDF $g(x, Q^2)$ through [111]

$$F_L\left(x, Q^2\right) = \frac{\alpha_s(Q^2)}{4\pi}\left(\frac{16}{3}I_F + 8\bar{e}^2 I_G\right)\,, \tag{3.39}$$

83

where

$$I_F = \int_x^1 \frac{dy}{y} \left(\frac{x}{y}\right)^2 F_2(y, Q^2), \tag{3.40}$$

$$I_G = \int_x^1 \frac{dy}{y} \left(\frac{x}{y}\right)^2 \left(1 - \frac{x}{y}\right) \mathcal{G}(y, Q^2), \tag{3.41}$$

and where $\mathcal{G}(y, Q^2) = yg(y, Q^2)$, α_s is the QCD coupling and $\bar{e}^2$ is the sum of the squares of the electric charges of the active quark flavours. The number of active flavours n_f changes with the scale at which we want to evaluate the PDF. In this work we will assume that $n_f = 3$ for $Q^2 \leq m_c$, $n_f = 4$ for $m_c < Q^2 \leq m_b$ and $n_f = 5$ otherwise. m_c and m_b are the masses of the charm and bottom quarks, respectively. We wish to express the gluon PDF $g(x, Q^2)$ in terms of the structure functions F_2 and F_L. This can be done by computing the derivative with respect to x of (3.39) and using the definition of the integrals I_F and I_G. A straightforward computation yields

$$\bar{e}^2 \mathcal{G}(x, Q^2) = \left(-2 + \frac{2x}{3}\frac{\partial}{\partial x}\right) F_2(x, Q^2) +$$

$$\frac{\pi}{\alpha_s(Q^2)} \left(3 - 2x\frac{\partial}{\partial x} + \frac{x^2}{2}\frac{\partial^2}{\partial x^2}\right) F_L(x, Q^2). \tag{3.42}$$

We use the NLO result (3.42) to estimate the function $\mathcal{G}(x, Q^2)$ at small x from the holographic values for F_2 and F_L computed using the best fit parameters in table 3.1. We shall compare our gluon PDFs with the CT18 and NNPDF collaborations [112,113], also at NLO. For the coupling constant $\alpha_s(Q^2)$ in (3.42) we used the holographic value (see [32] for a plot of this function).

Since the functions F_2 and F_L do not reproduce the data in the range $10^{-2} < x < 1$, and in particular have the wrong asymptotics for $x \to 1$, we do not expect to be able to reproduce $\mathcal{G}(x, Q^2)$ in the transition region $x \sim 10^{-2}$ where there are other contributions to the structure functions from quarks. To match the correct asymptotic values in this transition region, we added a constant function $f(Q^2)$ to $\mathcal{G}(x, Q^2)$ such that we match the value of $\mathcal{G}(x, Q^2)$ given by the average of the other collaborations at the specific value $x = 10^{-2}$. Our main goal is to assess whether or not we can predict the correct low x evolution of the gluon PDFs starting from $x = 10^{-2}$ to lower values of x. Our results are presented in figure 3.6. It clear that we are able to reproduce the correct behaviour within the other collaborations allowed regions. Of course these results should be taken as a simple qualitative indication, since we are using a NLO expression for the gluon PDFs together with the holographic structure functions and coupling constant. Also, as mentioned above, the resulting PDF's do not have the

correct asymptotics for $x \to 1$ [114, 115], but this is expected since the whole analysis is only valid in the low x region.

3.6 Conclusion

In this chapter we extended the results of chapter 2 by including the total cross-section $\sigma(\gamma p \to X)$, the photon structure function F_2^γ and the total cross-section of $\gamma\gamma$ scattering. For γ^*p processes the χ^2 quality of our fit improved slightly from $\chi^2_{dof} = 1.42$ to $\chi^2_{dof} = 1.40$. This is due to the fact that, in addition to the 313 data points from the structure function F_2 and F_L, we have an extra of 45 data points from the cross-section $\sigma(\gamma p \to X)$, which can also be described holographically. These results are obtained in a very large kinematical window of $x < 10^{-2}$ and $Q^2 \leq 400\,\mathrm{GeV}^2$ for F_2, $Q^2 \leq 45\,\mathrm{GeV}^2$ for F_L and $\sqrt{s} > 4.6\,\mathrm{GeV}$ for $\sigma(\gamma p \to X)$.

Then we have shown that the Pomeron kernel found in the fit of the γ^*p processes
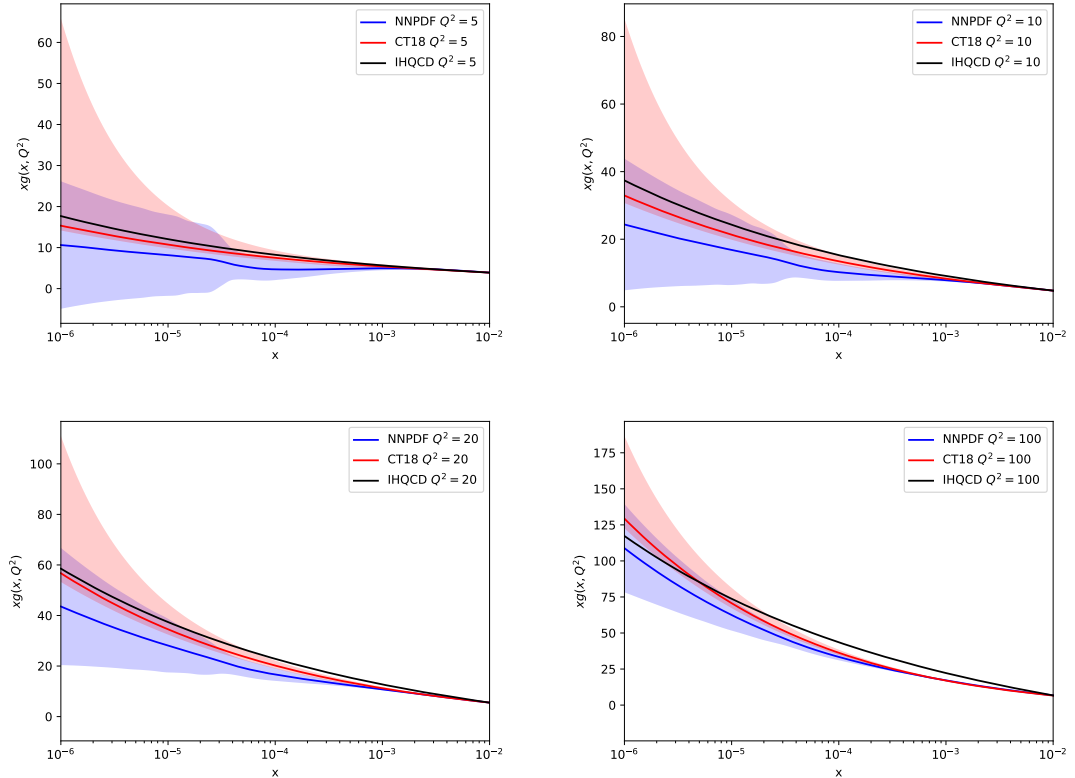
Figure 3.6: Comparison between the holographic gluon PDFs with the ones of CT18NNLO and NNPDF for $Q^2 = 5, 10, 20, 100\,\mathrm{GeV}^2$.

could be used to achieve excellent fits of the $\gamma^*\gamma$ processes discussed in section 3.3. We have also checked from a global fit, where we include all the processes and vary all the parameters, that the fitting parameters do not vary much, showing the consistency of the model. To our knowledge, this is the first text of the IHQCD pomeron model in such a vast class of processes in a wide kinematical range.

Using the NLO relation (3.42) we were able to reproduce the low x evolution of gluonic PDFs using as input the holographic functions F_2, F_L and $\alpha_s(Q^2)$. In the region of larger Q^2 there is more tension in matching to the PDFs of the other collaborations, as can be seen in the $Q^2 = 100 \text{ GeV}^2$ plot of figure 3.6. According to equation (3.42), in this region it is essential to have a good description of F_L because it is divided by α_s which is small for high values of Q^2 due to asymptotic freedom. Since we are performing a χ^2 fit to the data, the fitting process favours a good description of F_2 because the uncertainties are lower than those of F_L as compared with the value measured. The uncertainties of F_L are of the same size as the measured value. Thus, better measurements of F_L might help our model give a better description of the gluon PDFs. Moreover, for high values of Q^2 it is important to include heavy quarks in global QCD fits. Nowadays PDF groups use variable flavour schemes in order to produce high quality results. To holography this means that the holographic dual must contain quark flavour degrees of freedom if the model ought to be successful at computing them. The IHQCD model we used as our QCD vacuum exhibits the properties of large N_c Yang-Mills, including the running of the coupling constant. Following the ideas of [97], it would be very interesting to include flavour degrees of freedom in this holographic QCD model and to test if the quality of our fits generically improve, mainly for high Q^2. Including quarks is actually necessary because it is believed that the third and fourth dominant Regge trajectory actually come from the mesonic sector, instead of the glueball sector. We will start to build a holographic Regge theory with quarks in chapter 5.

Another problem would be to determine holographically the gluonic PDFs, without making reference to perturbative QCD definitions. Holography may actually be the right set up for a non-perturbative definition. In fact, gluonic PDFs can be defined using a Wilson loop operator (see for example [116]). Thus, it would be very interesting to use the duality between Wilson loops and strings in the dual geometry to explore this problem.

4

Deeply Virtual Compton Scattering and the holographic Pomeron

Chapter abstract: We present our current progress in the computation of scattering amplitudes as a function of Mandelstam t by considering the Deeply Virtual Compton Scattering (DVCS) processes. We show that at least it is possible to describe simultaneously the differential cross-section and total cross-section of DVCS data with a single holographic model for the Pomeron. We also discuss future work, namely how to include consistently the processes analysed in chapter 3. These results have not been published and in the present form are purely exploratory.

4.1 Holographic Deeply Virtual Compton Scattering

From the groundbreaking of BPST [8] till today, many research projects [1,9–33,35–48] have shown how the theoretical ideas of AdS/CFT can be used to model experimental data where Pomeron exchange dominates. However, these works are not consistent in the sense that each of them is tailored for a specified process and/or kinematic regimes. On the other hand, we have shown in chapter 3 that a holographic model with few free parameters that describes successfully several processes dominated by Pomeron exchange is indeed possible. The processes analysed were sensitive to the forward scattering amplitude, i.e. for Mandelstam $t = 0$. So it remains an open question if it is possible to extend previous results to processes where amplitudes with non-zero values of t are necessary. One such example is Deeply Virtual Compton Scattering (DVCS).

DVCS is an exclusive Compton scattering process where the incoming photon has high virtuality. It has been studied thoroughly by the H1 and ZEUS collaborations as well at JLAB. While DIS allows us to determine the PDFs of a nucleon (e.g. the proton PDFs), DVCS data helps us to study the Generalized parton distribution functions (GDP) [117, 118], which are related to the correlation between the transverse and longitudinal components of the momentum of quarks and gluons inside the nucleons.

Holographic techniques have been already employed to describe DVCS data. In [27] the conformal and hard wall Pomeron models have been used while in [119] a holographic description of dipole-dipole scattering has been studied. DIS is connected to the forward Compton scattering amplitude via the optical theorem. Hence, our analysis of DVCS in this chapter is close to the one presented in [1]. We will show that in order to include the description of DVCS data one needs to include extra parameters that are related to the holographic wave function of the proton and the coupling dependence with the spin.

4.2   Holographic computation of the amplitudes

We now derive our holographic expressions for the differential cross-section $d\sigma \left(\gamma^* p \to \gamma p \right) / dt$ and total cross-section $\sigma \left(\gamma^* p \to \gamma p \right)$ of the DVCS process. To compute the proton structure functions F_2^p and F_L^p and the total cross-section $\sigma \left(\gamma p \to X \right)$ we have determined first the forward scattering amplitude of the process $\gamma^* p \to \gamma^* p$. Then, the only difference between the DIS and the DVCS computation is that the outgoing photon is *on-shell*. The associated Witten diagram is show in figure 4.1. Hence we will consider the general case of $\gamma^* p \to \gamma^* p$ where the incoming photon has virtuality Q_1^2 while the outgoing photon has virtuality Q_3^2. At the end of the calculation we take $Q^3 \equiv k_3^2 \to 0$ and use equation (3.6).

We will use the same kinematical definitions as in [1] and chapter 2 so we omit them here. As usual, the minimal coupling between the spin 1 gauge field and the higher spin field $h_{a_1 \dots a_J}$ is

$$k_J \int d^5 X \sqrt{-g} e^{-\Phi} F_{b_1 a} D_{b_2} \dots D_{b_{J-1}} F_{b_J}^a h^{b_1 \dots b_J}, \qquad (4.1)$$

and the coupling of the scalar field is

$$\bar{k}_J \int d^5 X \sqrt{-\bar{g}} e^{-\bar{\Phi}} \bar{\Upsilon} \bar{D}_{b_1} \dots \bar{D}_{b_J} \bar{\Upsilon} \bar{h}^{b_1 \dots b_J}. \qquad (4.2)$$
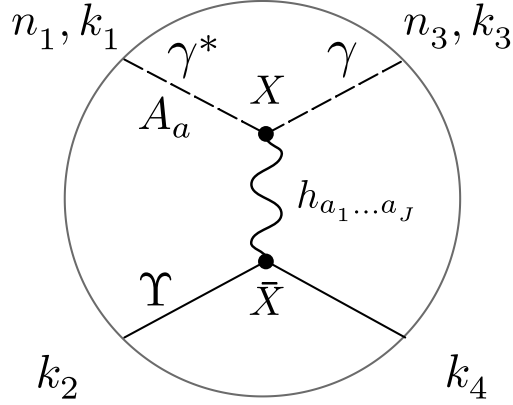
Figure 4.1: Tree level Witten diagram associated with the computation of the amplitude $\mathcal{A}_J^{\lambda_1\lambda_3}$ of the DVCS process $\gamma^* p \to \gamma p$. The bottom lines represent the proton modelled by a scalar Υ.

The computation of the scattering amplitude follows the same steps as the ones presented in the last chapters, so we will not repeat it here. The scattering amplitude for $\gamma^* p \to \gamma p$ is

$$\mathcal{A}^{\gamma^* p \to \gamma p}(s,t) = \sum_n g_n(t) s^{j_n(t)} \int dz e^{-(j_n(t) - \frac{3}{2})A} f_Q \psi_n(j_n(t)), \tag{4.3}$$

where, as in the $\gamma^* p$ case of chapter 3,

$$g_n(t) = H(j_n(t)) \left[i + \cot\left(\frac{\pi j_n(t)}{2}\right) \right] \frac{dj_n}{dt} \int d\bar{z} e^{(-j_n(t) + \frac{7}{2})\bar{A}} \bar{\upsilon}_2 \bar{\upsilon}_4 \bar{\psi}_n(j_n(t))^*, \tag{4.4}$$

with

$$H(J) = \frac{\pi}{2} \frac{k_J \bar{k}_J}{2^J}. \tag{4.5}$$

The last amplitude is the one where both photons have transverse polarizations, other combinations are subleading in s. To obtain this expression we have used equation (3.6).

To move forward we need to know the proton wavefunction in order to compute the $\bar{z}$ integral. In AdS/QCD, it is expected that baryons are dual to a configuration where three open strings are attached to a D-brane [120, 121]. So far it is not known how to get the baryon's spectrum from such a configuration. An acceptable holographic description of the proton would consist of a spectrum that matches the mass of the proton as well of the other hadrons in the same trajectory. Here we will follow the phenomenological approach by approximating the combination $e^{3A-\Phi}\upsilon_2\upsilon_4$ by the delta function $\delta(z - z^*)$. The z^* parameter is related, by dimensional analysis, to the inverse

of the mass of the proton and we will use it as a fitting parameter. By making this approximation we are assuming that $e^{3A-\Phi}\upsilon_2\upsilon_4$ is null in the UV and the IR, and that it has a global maximum. This is expected if the spectrum of the baryons is associated with a Schrodinger problem whose ground state is the proton. This approach, as an example, has successfully described DVCS data in [27].

Another issue is the unknown functional form of $H(J)$. In the next section we motivate a good ansatz for this expression, at least in the range $0.6 \lesssim J \lesssim 1.3$.

4.3   Ansatz for $H(J)$

To find a good ansatz for $H(J)$ let us first recall that, based on the forward scattering amplitude for the process $\gamma^*p \to \gamma^*p$, our holographic formula for the proton structure function F_2^p is given by

$$F_2^p(x,Q^2) = \sum_n \frac{\operatorname{Im} g_n}{4\pi^2\alpha}\, x^{1-j_n} Q^{2j_n} \int dz\, e^{-\left(j_n-\frac{3}{2}\right)A} \left(f_Q^2 + \frac{\dot{f}_Q^2}{Q^2} \right) \psi_n(z)\,, \qquad (4.6)$$

where

$$\operatorname{Im} g_n = H(j_n(0))j_n'(0) \int d\bar{z} e^{\left(-j_n(0)+\frac{7}{2}\right)\bar{A}}\bar{\upsilon}_2\bar{\upsilon}_4\bar{\psi}_n(j_n(0))^*\,. \qquad (4.7)$$

Using equation (4.4) and the approximation $e^{3A-\Phi}\upsilon_2\upsilon_4 \sim \delta(z-z^*)$ we can compute $H(J)$ for any value of $j_n(t)$

$$H(j_n(t)) = \frac{\operatorname{Im} g_n(t)}{e^{\left(-j_n(t)+\frac{1}{2}\right)A^*}\psi_n^*(j_n(t))\frac{dj_n(t)}{dt}}\,. \qquad (4.8)$$

We can now plot $H(J)$ as a function of J using the values of $\operatorname{Im} g_n$, j_n and ψ_n found in [1] and by choosing z^* to be around 1, since by dimensional analysis it should be proportional to the inverse mass of the proton (in GeV units). In a logarithmic plot, $\log H(J)$ can be well approximated by a quadratic curve in J, i.e. $\log H(J) = h_0 + h_1(J-1) + h_2(J-1)^2$. We can then choose z^* and the h_i to get the best quadratic fit. For the best fit value of $z^* = 0.565$ we obtain the result shown in figure 4.2, where the black dots represent the actual reconstructed values of $H(J)$ for each n.

We can check if the resulting curve has physical meaning by considering the shape of the $\kappa(J)$ and $\bar{\kappa}(J)$ functions with J in the range $0.6 \lesssim J \lesssim 1.3$. According to the gauge/gravity duality such coupling is related to the coefficient of a spin J operator in the OPE with two spin 1 operators. In the UV fixed point the coefficient can
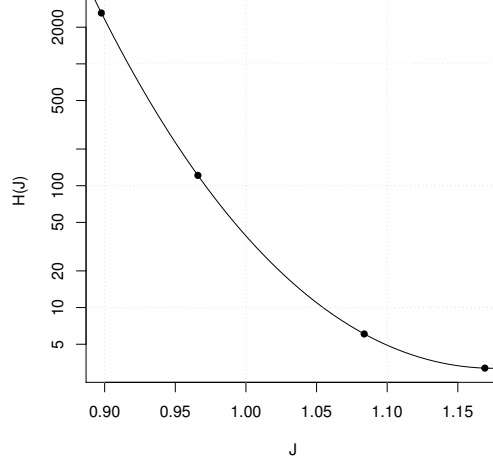
Figure 4.2: Reconstruction of the $H(J)$ function using the best parameters found in [1] and $z^* = 0.565$. The solid line represents the function $\exp\left(h_0 + h_1(J-1) + h_2(J-1)^2\right)$ with $h_0 = 3.70$, $h_1 = -30.3$ and $h_2 = 89.1$.

be computed exactly since we would be dealing with a free theory and hence only Wick contractions contribute. Of course, QCD is not a free theory and perturbative corrections should be taken into account. Instead of performing such computation we will consider the $O(N)$ vector model which is a similar theory in the UV fixed point and whose computation has been done in [122]. In this model we can retrieve a similar shape of $H(J)$ as the one in figure 4.2 from the three-point bulk vertex coupling between massless higher spins field of spin $s_1 = 1$, $s_2 = 1$ and $s_3 = J$ in type A minimal higher-spin theory in AdS_{d+1}. The coupling, as a function of s_1, s_2 and s_3 is given by

$$g_{s_1,s_2,s_3} = \frac{\pi^{\frac{d-3}{4}} 2^{\frac{3d-1+s_1+s_2+s_3}{2}}}{\sqrt{N}\Gamma(d+s_1+s_2+s_3-3)} \sqrt{\frac{\Gamma(s_1+\frac{d-1}{2})}{\Gamma(s_1+1)}\frac{\Gamma(s_2+\frac{d-1}{2})}{\Gamma(s_2+1)}\frac{\Gamma(s_3+\frac{d-1}{2})}{\Gamma(s_3+1)}} . \quad (4.9)$$

Moreover, after approximating the gamma functions in the resulting expression with the Stirling formula and expanding up to quadratic order around $J = 1$ we get a $H(J)$ consistent with our ansatz. Because we are comparing different theories caution should be taken. However, our point is that the overall function shapes does not change, and beyond the fixed point, corrections may be well captured in suitable redefinitions of the h_i parameters in our ansatz. In the next section we test our hypothesis agains the DVCS experimental data.

4.4   Data analysis and results

Now that we have a reasonable parameterisation of $H(J)$ we proceed to find the best values for the gluon kernel parameters l_s, a, b, c and d, and h_0, h_1 and h_2 in the $H(J)$ ansatz. The optimal set of parameters is found by minimising the χ^2 statistic

$$\chi_g^2 = \chi_\sigma^2 + \chi_{\frac{d\sigma}{dt}}^2 \,, \tag{4.10}$$

which is the sum of the χ^2 of $\sigma\left(\gamma^* p \to \gamma p\right)$ with the χ^2 of $\frac{\sigma(\gamma^* p \to \gamma p)}{dt}$. As in the last chapters, for a given observable $O \in \{\sigma\left(\gamma^* p \to \gamma p\right), \frac{\sigma(\gamma^* p \to \gamma p)}{dt}\}$, the respective χ^2 function is defined as

$$\chi_O^2 \equiv \sum_n \left(\frac{O_n^{\text{pred}} - O_n}{\delta O_n}\right)^2 \,, \tag{4.11}$$

with O^{pred} being the predicted theoretical value and δO the experimental uncertainty and the sum goes over the available experimental points. The total and differential cross-section data used is the combined one from H1-ZEUS available in [123, 124].

The DVCS differential cross-section is given by

$$\frac{d\sigma}{dt} = \frac{1}{16\pi s^2} \frac{1}{2} \sum_{\lambda_1, \lambda_3 = 1}^{2} \left|A^{\lambda_1, \lambda_3}\left(s, t\right)\right|^2 = \frac{1}{16\pi^2 s^2} |\mathcal{A}^{\gamma^* \gamma}(s, t)|^2, \tag{4.12}$$

where we average over the incoming photon polarization and the scattering amplitude is given by equation (4.3). The total cross-section is just the integral of the above

$$\sigma = \int_{-1}^{0} dt \, \frac{d\sigma(t)}{dt}. \tag{4.13}$$

The range $-1 \leq t \leq 0$ comes from the data.

The solve the χ^2 minimisation problem we developed the `HQCDP R` package. The Schrodinger problem associated to the gluon kernel is solved with $N = 400$ Chebyshev points. To compute the differential and total cross-sections efficiently we divided the interval $-1 \leq t \leq 0$ in 20 pieces of length 0.05 and computed the differential cross-section for each point. From these values we create a spline interpolation function that can be used to predict the differential cross-section values and the total cross-section through equation (4.13). We also make use of the `REDIS` *in memory* database to avoid redoing expensive computations. The code also makes use of multiple cores, if available, in order to compute in parallel the integrals that appear in (4.3) for different kinematical points. The present results were found using a node in a High Performance Computing (HPC) cluster with 16 cores.

The best fit to the data we have found has a $\chi^2_{dof} \sim 1.5$ with the parameter values of table 4.1. The individual values of χ^2_{dof} for the total and differential cross-section experimental data are 1.8 and 1.3 respectively, meaning that the model offers a good description of both processes. The comparison of the theoretical predictions against the experimental data can be seen in figures 4.3 and 4.4.

Kernel parameters	Extra parameters	Intercepts
$a = -4.55$	$h_0 = 4.74$	$j_0 = 1.24$
$b = 0.980$	$h_1 = -35.9$	$j_1 = 1.13$
$c = 0.809$	$h_2 = 142$	$j_2 = 1.08$
$d = -0.160$	$z^* = 0.296$	$j_3 = 1.05$
$l_s = 0.153$	–	–

Table 4.1: The 9 parameters for our best fit and the intercept of the first four pomeron trajectories. All parameters are dimensionless except z^* and l_s which are in GeV^{-1}.
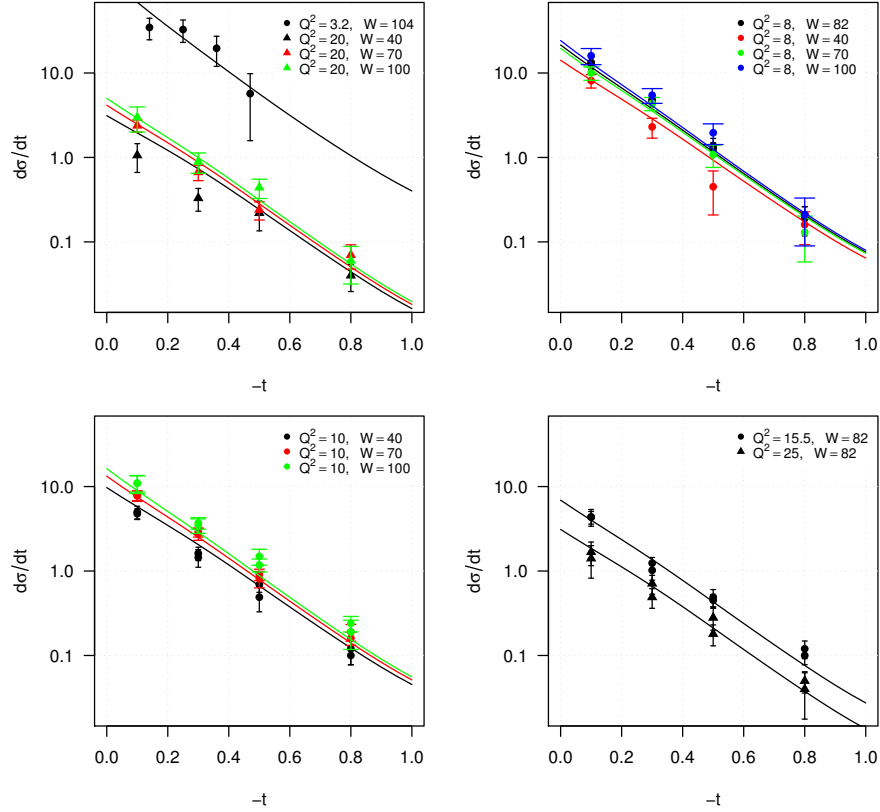
Figure 4.3: Predicted vs. experimental values of the differential cross-section $\frac{d\sigma(t)}{dt}$ for DVCS. Different gray levels correspond to different combinations of Q^2 and W as described in the legends. Here Q^2 and t are in GeV^2, W in GeV and $\frac{d\sigma}{dt}$ is in $\frac{\text{nb}}{\text{GeV}^2}$.
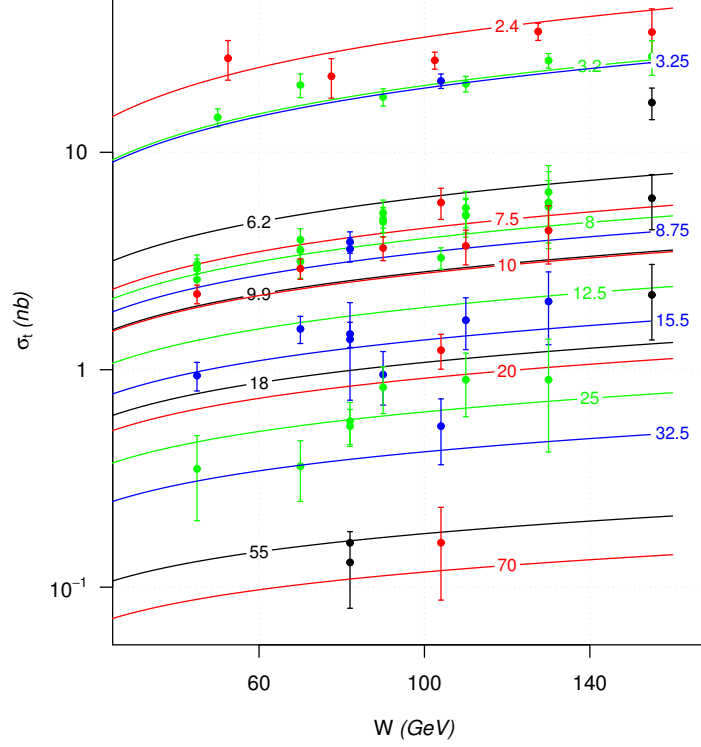
Figure 4.4: Predicted vs. experimental values of the total cross-section σ of DVCS. Small numbers attached to lines and points of the same grey level indicate the respective value of Q^2 in GeV.

4.5 Conclusions

We have shown that the holographic model presented in the last chapters can be extended to include a quantitative description of total and differential cross-sections of DVCS data from H1-ZEUS. If we use the parameter values of table 4.1 we get a large χ^2_{dof} for the proton structure function F_2^p. By looking at the intercept values of table 4.1 we can see that they are considerably different from the ones found in table 3.1. Since F_2^p is very sensitive to their values this is expected. The relative differences of kernel parameters a, b, c, d and l_s^{-1} are respectively 3.19 %, 13.3 %, 22.6 %, 63.3 % and 1 %. This means that a better ansatz for $H(J)$ or actually performing the $\bar{z}$ integral may lead to a successful joint fit of DVCS with other processes. One should also include the kernel of the twist 2 fermion operators, as suggested by Donnachie and Landshoff [125] and study its impact on the results above. A first step towards the inclusion of the twist 2 fermion operators is done in the next chapter.

5

Regge theory in a Holographic dual of QCD in the Veneziano Limit

Chapter abstract: We initiate the study of Regge theory in a bottom-up holographic model for QCD in the Veneziano limit, where the backreaction of the quarks to the gluon dynamics is included. We determine the parameters of the model by carrying out a precise fit to the meson spectrum in QCD. The spectrum for spin-one and pseudoscalar mesons is well reproduced. We then generalise the model to include higher spin fields in the bulk trajectories dual to the Pomeron and meson Regge trajectories at the boundary. With this setting, we fit the masses of the mesons with spins $J = 2$, 3, and 4, as well as the experimental data of the total cross-sections $\sigma(\gamma\gamma \to X)$, $\sigma(\gamma p \to X)$ and $\sigma(pp \to X)$. For the cross sections we obtain a χ^2_{dof} of 0.74 for a total of 199 experimental points.

5.1 Introduction

In the previous chapters we have presented a holographic model capable of describing several observables in a kinematical window where QCD is dominated by a gluon rich medium. In this regime the Bjorken variable x is small, or the Mandelstam variable s is large, corresponding to high center of mass energies. However, besides gluons QCD also has quarks. Thus their inclusion in a holographic model is important in order to achieve a complete model for holographic Regge theory. In this chapter we make a first attempt to include quark degrees of freedom in a holographic description of Regge theory.

In order to describe the total cross-section data of hadronic processes in QCD, one

also includes, besides the Pomeron trajectory, a meson trajectory (e.g. see [52]). This trajectory can be obtained by a linear fit of the meson spins against the meson squared masses. With the resulting straight line, one extrapolates from $t > 0$ to $t \leq 0$ in order to make predictions in the scattering region. In particular, for the total cross-section we are interested in the value of the trajectory for $t = 0$, also known as the meson intercept, and the above linear fit yields an intercept of 0.55. There is no theoretical justification to assume that the meson trajectory is linear aside from the fact that it has described successfully scattering data, provided t is not too negative. In this work we use holography to study this issue by first fitting the meson spectrum for $J = 0, 1, 2, 3, 4$ and check if the resulting holographic intercept is able to describe the experimental data of the total cross-sections of $\gamma\gamma$, γp and pp scattering. In the previous chapters and in [1] the dynamics of the higher spin J fields in the graviton Regge trajectory by generalising the bulk graviton equation of motion has been studied. This was done using effective field theory inspired by Regge theory of a $5D$ string theory. In this work we will not only follow the same procedure for the Pomeron trajectory, but also apply it to the meson trajectory by generalising to higher spin the equation of motion of the bulk field dual to the vector mesons.

Before we start such procedure, we need to guarantee that our model is describing with accuracy the spectrum of the vector mesons. This will be done by considering the extension of the Improved Holographic QCD model of [91, 92], with a backreacted quark sector [126, 127], as presented in [97]. This model (V-QCD) consists of five-dimensional dilaton gravity coupled to a tachyon described in terms of a generalised Sen-like tachyonic Dirac-Born-Infeld (DBI) action [128]. Our numerical solution includes the full backreaction of the tachyon in the dilaton and metric. The asymptotic behavior of the model at weak and strong coupling is chosen such that various generic features of QCD, such as asymptotic freedom and confinement, are reproduced [92, 97]. The remaining free parameters of the model will be determined through an extensive comparison of the spectrum of the quadratic fluctuations against the experimental meson masses.

This chapter is organized as follows. In section 5.2 we discuss in detail the holographic model, as well as how to compute the spectrum of the quadratic fluctuations. This section ends with a fit to the meson spectrum, fixing our background fields for the remaining of the chapter. In section 5.3 we derive holographic expressions for the total cross-sections that will be used later to fit data from the Particle Data Group [129]. In section 5.4 we focus on the holographic duals of the pomeron and meson trajectories, and in particular in constructing the analytic continuation of the spin J equations

that govern the dynamics of fields in these trajectories. These equations contain two parameters that will be fixed by the soft-pomeron intercept and the spin $J = 2, 3, 4$ meson masses in section 5.5. This fixes the pomeron and meson kernels that are used in the total cross-section fits. We discuss our results and suggest further work in section 5.6.

5.2 Holographic model for QCD in the Veneziano Limit

We consider a slight generalisation of Quantum Chromodynamics which consist of a gauge field in the adjoint representation of $SU(N_c)$ coupled to N_f fermions (quarks) in the fundamental representation of $SU(N_c)$. This generalisation has been studied in great depth in the 't Hooft large-N_c limit, where $N_c \to \infty$ and $\lambda = g_{YM}^2 N_c$ and N_f are kept fixed. This limit is also known as the *quenched* limit since nontrivial quark contributions to observables are suppressed in powers of $\frac{N_f}{N_c} \to 0$. Another interesting large-N_c limit is the Veneziano limit [130] where

$$N_c \to \infty\,, \quad N_f \to \infty\,, \quad \frac{N_f}{N_c} = x\,, \quad \lambda = g_{YM}^2 N_c\,. \tag{5.1}$$

with x and λ fixed. In this limit the quark contributions are not suppressed, and their backreaction to the gluon dynamics must be taken into account.

A holographic dual (V-QCD) that reproduces several expected features of QCD in the Veneziano limit was presented in [97]. It consists of a system of a dilaton and tachyon coupled to five-dimensional gravity. Let us first discuss the field content and the action of the model, and then present the precise structure of the various potentials appearing in the action.

5.2.1 The model

The action in the gravitational sector is the same as in the Improved Holographic QCD (IHQCD) model [91, 92]. We work at zero temperature so that Poincaré invariance is intact. The metric Ansatz is therefore

$$ds^2 = g_{ab}dx^a dx^b = e^{2A(z)} \left(\eta_{\mu\nu} dx^\mu dx^\nu + dz^2 \right)\,, \tag{5.2}$$

where the warp factor A is identified with the logarithm of the energy scale in the field theory at the boundary. The exponential of the dilaton field $\lambda = e^\Phi$ is dual to the $\mathrm{Tr}F^2$

operator with its background value equal to the 't Hooft coupling (near the boundary where the coupling can be unambiguously defined). The action for the metric and dilaton fields is given by five-dimensional Einstein gravity coupled to a scalar field,

$$S_g = M_p^3 N_c^2 \int d^5 x \sqrt{- \det g} \left[R - \frac{4}{3} \frac{(\partial \lambda)^2}{\lambda^2} + V_g(\lambda) \right] , \qquad (5.3)$$

where M_p is the five-dimensional Planck scale. The dilaton potential $V_g(\lambda)$ will be specified below. We choose the potential to be qualitatively similar to that studied in [131, 132] – see [133, 134] for an alternative approach focused on the fit to QCD thermodynamics.

To add matter we insert space-filling $D_4 - \bar{D}_4$ branes that give rise to a tachyon field T and the gauge fields A_L, A_R living on the branes [126, 127]. A similar approach has been considered in the probe limit in [135, 136], and also in the Witten-Sakai-Sugimoto model [137–140]. In the boundary theory the operators with lowest dimension involving fermions are $\bar{\psi}_R^i \psi_L^j$ with spin 0 and the two spin 1 conserved currents $\bar{\psi}_L^i \gamma^\mu \psi_L^j$ and $\bar{\psi}_R^i \gamma^\mu \psi_R^j$, where i, j are the flavour indices. The spin 0 and spin 1 operators are dual to bulk complex scalars T_{ij} and two bulk gauge fields $A_{L,ij}^\mu$ and $A_{R,ij}^\mu$, respectively. The tachyon transforms as $(N_f, \bar{N}_f)$ of the flavour symmetry $U(N_f)_R \times U(N_f)_L$, while the fields $A_{L,ij}^\mu$ and $A_{R,ij}^\mu$ transform in the adjoint representations of $U(N_f)_L$ and $U(N_f)_R$, respectively. In string theory the three bulk fields can be modelled by considering N_f flavour branes (R) and N_f flavour antibranes (L). In this configuration the complex scalar fields T_{ij} are the lowest modes of open strings with one end in a D-brane and another in the anti-D-brane, while the bulk gauge fields are the lowest open string modes with both ends on a D-brane or on an anti-D-brane. The system obeys a tachyonic Dirac-Born-Infeld (DBI) action [97, 98, 127]

$$S_{\text{DBI}} = - \frac{M_p^3 N_c}{2} \int d^5 x \, \mathbf{Str} \left[V_f \left(\lambda, T^\dagger T \right) \sqrt{- \det \left(g_{ab} + \kappa(\lambda) D_{(a} T^\dagger D_{b)} T + w(\lambda) F_{ab}^L \right)} \right.$$

$$\left. + V_f \left(\lambda, T T^\dagger \right) \sqrt{- \det \left(g_{ab} + \kappa(\lambda) D_{(a} T D_{b)} T^\dagger + w(\lambda) F_{ab}^R \right)} \right] , \qquad (5.4)$$

where $\mathbf{Str}$ is the symmetric trace over the (hidden) flavour indices and the determinant is taken with respect to the five dimensional space-time indices a, b (since we are going to work up to quadratic order we can actually replace the symmetric trace by the usual trace of matrices for the purposes of this work). The functions $V_f(\lambda)$, $\kappa(\lambda)$, and $w(\lambda)$ will be given explicitly below. The normalisation convention for the symmetrisation of indices is $F_{(a} G_{b)} = \frac{1}{2} (F_a G_b + F_b G_a)$. The covariant derivative terms are given by

$$D_a T = \partial_a T - i T A_a^L + i A_a^R T , \qquad D_a T^\dagger = \partial_a T^\dagger - i A_a^L T^\dagger + i T^\dagger A_a^R , \qquad (5.5)$$

and the field strengths by

$$F^{L,R} = dA^{L,R} - iA^{L,R} \wedge A^{L,R} \,. \tag{5.6}$$

In this work we are assuming that the light quark masses are equal and under this assumption the tachyon is just $T = \tau \, \mathbb{I}_{N_f}$. Furthermore, for the QCD vacuum we have $A_a^R = 0 = A_a^L$. Using these conditions in the action (5.4) we obtain the flavour action

$$S_f = -x M_p^3 N_c^2 \int d^5 x \, V_f(\lambda, \tau) \sqrt{-\det\left(g_{ab} + \kappa(\lambda)\partial_a \tau \partial_b \tau\right)}\,. \tag{5.7}$$

The brane action also contains a Wess-Zumino term [127] which we will not need as it does not contribute to the background solutions or mass spectra considered here.

There is also an additional pseudo-scalar axion field a, which is dual to the operator $\text{Tr} F \wedge F$ and therefore sources the θ angle in QCD [127]. Its action takes the form [91, 92, 98, 141]

$$S_a = -\frac{M_p^3 N_c^2}{2} \int d^5 x \sqrt{-\det g} \, Z(\lambda) \Big[\partial_b a - x\left(V^{(a)}(\lambda,\tau)(\hat{A}_b^L - \hat{A}_b^R) - \rho\,\partial_b V^{(a)}(\lambda,\tau)\right)\Big]^2 , \tag{5.8}$$

where $\hat{A}_b^{L,R}$ are the singlet fields, $\hat{A}_b^{L,R} = \text{Tr} A_b^{L,R}/N_f$, the potential $V^{(a)}(\lambda,\tau)$ will be specified below, and we allowed the tachyon to have an overall phase ρ, i.e. we took $T = \tau e^{i\rho} \mathbb{I}_{N_f}$.

5.2.2   Choice of potentials

Let us now discuss the choices for the various potentials (V_g, V_f, κ, w, $V^{(a)}$ and Z). The generic picture is that the leading IR asymptotics of the various functions is chosen to agree with known features of QCD (which will be soon specified). The UV asymptotics is set by rough agreement with perturbative QCD, in particular by the perturbative UV dimensions of the QCD operators. For intermediate scales the functions need to be determined by an extensive comparison to experimental and lattice QCD data; here the functions will be fitted to the meson spectrum in QCD. In this section we will present the Ansätze for these functions which will obey the asymptotics at small and large λ determined by qualitative comparison to QCD, and the fit to data will be carried out in section 5.2.4.

We start with the action for the gluon sector, i.e. the action of improved holographic QCD. In IHQCD the dynamics of the dilaton is set by its potential $V_g(\lambda)$, which is constrained [91, 92] in the UV to reproduce the YM β-function and in the IR to yield

confinement and a "good" singularity in the classification of [142]. In this work we will take [143, 144]

$$V_g(\lambda) = 12 + V_1\,\lambda + V_2\,\frac{\lambda^2}{1 + \frac{\alpha_\lambda\lambda}{\lambda_0}} + 3V_{\mathrm{IR}}\,e^{-\frac{\lambda_0}{\alpha_\lambda\lambda}}\frac{\lambda^{4/3}}{4\pi^{8/3}}\sqrt{\log\left(1 + \frac{\alpha_\lambda\lambda}{\lambda_0}\right)}\,, \qquad (5.9)$$

where

$$V_1 = \frac{44}{9\pi^2}\,, \qquad V_2 = \frac{4619}{3888\pi^4}\,, \qquad \lambda_0 = 8\pi^2\,. \qquad (5.10)$$

The values of V_1 and V_2 are fixed by the gluon sector contribution to the QCD β-function, while the parameters α_λ and V_{IR} will be fitted by the spectrum, in particular by computing meson mass ratios and comparing them to experimental results, following [145]. The spectrum of the theory can be found by analysing the action of the quadratic fluctuations around the background solution followed by the reduction to the four-dimensional dynamics. For example, in the case of pure Yang-Mills (i.e. $x = 0$), the quadratic fluctuations are dual to glueballs with quantum numbers $J^{PC} = 0^{++}, 2^{++}$ and with $J^{PC} = 0^{-+}$ by considering an axion term. For pure Yang-Mills we have found that $\alpha_\lambda \approx 2.504$ and $V_{\mathrm{IR}} \approx 3.478$ reproduce[1] the lattice ratios of 1.46 and 1.87 of $m_{2^{++}}/m_{0^{++}}$ and $m_{0^{*++}}/m_{0^{++}}$ respectively. In the IR, $V_g \sim \lambda^{\frac{4}{3}}(\log\lambda)^{\frac{1}{2}}$, which gives linear asymptotic trajectories for glueballs.

The DBI action that we described above is analogous to the flat space Sen action for the $D - \bar{D}$ system [128]. Since we are in the presence of a curved space-time and other non-trivial background fields which fully backreact to the metric, we correct it by including the general potentials $V_f(\lambda, \tau)$, $\kappa(\lambda)$ and $w(\lambda)$. However these potentials must satisfy some properties. The tachyon potential V_f is expected to have a regular series expansion in λ and τ near the boundary (i.e. $\lambda \to 0$, $\tau \to 0$) [97]

$$V_f(\lambda, \tau) = V_0(\lambda) + V_1(\lambda)\tau^2 + \mathcal{O}(\tau^4)\,, \qquad (5.11)$$

and to vanish exponentially in the IR when $\tau \to \infty$ [141]. In particular in the flat space string theory $V_s \sim \frac{1}{\lambda}e^{-\mu\tau^2}$. Our Ansatz for V_f is

$$V_f(\lambda, \tau) = V_{f0}(\lambda)\,V_\tau(\tau)\,, \qquad (5.12)$$

where

$$V_\tau(\tau) = \left(1 + a_1\tau^2\right)e^{-a_2\tau^2}\,, \qquad (5.13)$$

$$V_{f0}(\lambda) = W_0 + W_1\lambda + W_2\,\frac{\lambda^2}{1 + \frac{\alpha_\lambda\lambda}{\lambda_0}} + \frac{3W_{IR}}{16\pi^4}(\alpha_\lambda\,\lambda)^2 e^{-\frac{\lambda_0}{\alpha_\lambda\lambda}}\left(1 + \frac{\lambda_0 W_1}{\alpha_\lambda\,\lambda}\right)\,,$$

---

[1]We will instead determine these parameters by a global fit to the meson spectrum as we will explain in section 5.2.4.

with

$$W_1 = \frac{24 + (11 - 2x)\,W_0}{27\pi^2}, \quad W_2 = \frac{24(857 - 46x) + W_0(4619 - 1714x + 92x^2)}{46656\pi^4}.$$

(5.14)

This Ansatz is identical to that considered in [144] except for the introduction of the coefficients a_i in $V_\tau(\tau)$. These are motivated by the observation that the correct mass gap of the mesons at large quark mass can only be reproduced if the coefficient of τ^2 in the exponent determining the large-τ asymptotics of V_τ (i.e. a_2 above) differs from the second order series coefficient of V_τ at small τ (here $a_2 - a_1$) [146]. Notice that one of these coefficients can be eliminated by adjusting the normalisation of the τ field.

As both $\kappa(\lambda)$ and $w(\lambda)$ are coupling functions under the square root of the DBI action we expect them to have similar qualitative behaviour. On the other hand, in order to have the correct UV dimension of the $\bar{q}q$ operator we need to impose

$$\kappa(0) = 8\,\frac{a_2 - a_1}{12 - xW_0}.$$

(5.15)

The IR asymptotics of the potentials κ and w directly affect the meson spectrum. We are interested in the case where the mesons have an asymptotic linear spectrum and the meson towers have the same asymptotics. This can be achieved with the following IR asymptotics $\kappa(\lambda) \sim \lambda^{-4/3}(\log\lambda)^{1/2}$ and $w(\lambda) \sim \lambda^{-4/3}\log\lambda$ [98, 147] (see also [148]). Taking into account these considerations, we adopt the following Ansätze for κ and w,

$$\kappa(\lambda) = 8\,\frac{a_2 - a_1}{12 - xW_0}\left[1 + \frac{\alpha_\lambda\,\kappa_1\lambda}{\lambda_0} + \bar{\kappa}_0\,\frac{e^{-\frac{\lambda_0}{\alpha_\kappa\lambda}}\left(1 + \frac{\lambda_0\bar{\kappa}_1}{\alpha_\kappa\lambda}\right)\left(\frac{\alpha_\kappa\lambda}{\lambda_0}\right)^{4/3}}{\sqrt{\log\left(1 + \frac{\alpha_\kappa\lambda}{\lambda_0}\right)}}\right]^{-1},$$

(5.16)

$$w(\lambda) = w_0\left[1 + \frac{\alpha_\lambda w_1\lambda}{\lambda_0\left(1 + \frac{\alpha_\lambda\lambda}{\lambda_0}\right)} + \bar{w}_0\,\frac{e^{-\frac{\lambda_0}{\alpha_w\lambda}}\left(1 + \frac{\lambda_0\bar{w}_1}{\alpha_w\lambda}\right)\left(\frac{\alpha_w\lambda}{\lambda_0}\right)^{4/3}}{\log\left(1 + \frac{\alpha_w\lambda}{\lambda_0}\right)}\right]^{-1}.$$

(5.17)

In order to compute the profiles of the background fields we need to specify the values of the parameters that appear in the definition of the potentials presented above. These parameters will be fitted to the ratios between the low-spin meson masses and the ρ^0 meson mass as predicted by the model.

Finally, we need to specify the potentials in the CP-odd action S_a (5.8). In flat-space tachyon condensation $V^{(a)}(\lambda, \tau)$ is independent of λ and is the same as the tachyon potential that appears in the DBI action. However in principle it may be different, so we will take $V^{(a)}$ to be V_f defined above without the V_{0f} term. This form

guarantees that it becomes a field-independent constant at $\tau = 0$ and that it vanishes exponentially at $\tau = \infty$. The $Z(\lambda)$ function is defined by

$$Z(\lambda) = Z_a + c_a \left(\frac{\lambda}{\lambda_0} \right)^4 . \tag{5.18}$$

The definition is constrained by Yang-Mills theory [92, 141, 149]. In this work the parameters Z_a and c_a will be determined by fitting the spectrum of singlet axial vector mesons.

5.2.3 Evaluation of the meson spectrum

The quadratic fluctuations around the background fields can be mapped to the spectrum of mesons and glueballs. The normalisable fluctuations of dilaton Φ, QCD axion a, and the (traceless part of the) metric g_{ab}, correspond to glueballs with $J^{PC} = 0^{++}$, 0^{-+}, and 2^{++}, respectively[2]. Here J is the spin, P refers to parity, and C refers to charge conjugation. The meson sector comes from the normalisable fluctuations of the tachyon T and of the gauge fields $A_a^{L/R}$. They correspond to mesons with $J^{PC} = 0^{++}$, 0^{-+}, 1^{++}, and 1^{--}.

The fluctuations can be further classified according to how they transform under the vectorial $SU(N_f)$. They can be grouped in flavour singlet and flavour non-singlet modes, i.e. mesons transforming in the adjoint of $SU(N_f)$. The fluctuations that come from S_f and S_a are only flavour singlet, while the ones coming from S_g include singlet and non-singlet terms. The singlet terms from S_f will mix with with the singlet terms coming from S_g and S_a.

The masses of the different glueballs and mesons can be obtained after expanding the action $S = S_g + S_f + S_a$ to quadratic order of the fluctuations of the background fields. Due to flavour and rotational covariance the fluctuations decouple in separate sectors [98], apart from the mixing of the flavor singlet sectors mentioned above. In summary, there are flavour singlet rank-two tensor fluctuations ($J^{PC} = 2^{++}$), flavour singlet and non-singlet vector mesons ($J^{PC} = 1^{--}$), flavour singlet and non-singlet axial vector mesons ($J^{PC} = 1^{++}$), flavour singlet and non-singlet scalars ($J^{PC} = 0^{++}$) and flavour singlet and non-singlet pseudoscalars ($J^{PC} = 0^{-+}$). These fluctuations generate towers of 2^{++} glueballs, singlet and non-singlet vector mesons, singlet and non-singlet axial vector mesons, non-singlet scalar mesons and mixtures between 0^{++}

---

[2]To be precise, it is the diffeomorphism invariant combination of the fluctuations of the dilaton and the trace of the metric which is dual to the 0^{++} glueballs.

glueballs and σ mesons, and non-singlet pseudoscalar mesons and mixtures between 0^{-+} glueballs and η' mesons, respectively. These towers of mesons and glueballs come as solutions of a Schrödinger problem associated with the equation of motion of the associated fluctuation. The eigenvalues correspond to the square of the mass of the glueballs or mesons and their holographic wave functions are the associated eigenfunctions. In this work we will not consider the flavour singlet states of $J^{PC} = 0^{++}$, 0^{-+}, as they involve mixing of the 0^{++} glueball with the flavour singlet σ meson and mixing between the 0^{-+} glueball with the η' meson, respectively. Therefore their analysis is considerably more challenging than that of the flavor nonsinglet states (see [98, 141, 150]) and would slow down the computer code for the spectrum significantly. Notice that these states are not central for the Regge analysis which is the main application of this work.

A detailed derivation of the equations of motion and Schrödinger problems associated with each fluctuation has been done in [98] and hence we will just summarise the main results relevant for the present work (see Appendix 5.B for the analysis of the spin 1 fluctuations). The singlet and non-singlet vector mesons have the same equation of motion

$$\frac{1}{V_f(\lambda,\tau)w(\lambda)^2 e^A G}\,\partial_z\Big(V_f(\lambda,\tau)w(\lambda)^2 e^A G^{-1}\partial_z\psi_V\Big) + m_V^2\psi_V = 0\,, \tag{5.19}$$

where $\psi_V = \psi_V(z)$ is their wavefunction. By performing the change of variable defined by

$$\frac{du}{dz} = G(z) \equiv \sqrt{1 + e^{-2A}\kappa(\lambda)(\partial_z\tau)^2}\,, \tag{5.20}$$

and rescaling

$$\psi_V(z) = \alpha(z)/\Xi_V\,, \qquad \Xi_V = w(\lambda)\sqrt{V_f(\lambda,\tau)\,e^A}\,, \tag{5.21}$$

one can rewrite the equation of motion in the Schrödinger form

$$-\frac{d^2\alpha}{du^2} + V_V(u)\,\alpha = m_n^2\,\alpha\,, \tag{5.22}$$

with potential

$$V_V(u) = \frac{1}{\Xi_V(u)}\frac{d^2\Xi_V(u)}{du^2}\,. \tag{5.23}$$

The singlet and non-singlet axial vector mesons have Schrödinger potentials differing by a term coming from the action S_a. The potentials of the non-singlet axial vector

mesons and of the singlet axial vector mesons are, respectively,

$$V_{NSA}(u) = V_V(u) + 4\,\frac{\tau^2 e^{2A}}{w(\lambda)^2}\,\kappa(\lambda)\,, \tag{5.24}$$

$$V_{SA}(u) = V_{NSA}(u) + 4\,x\,\frac{e^{2A}Z(\lambda)V^{(a)}(\lambda,\tau)^2}{V_f(\lambda,\tau)Gw(\lambda)^2}\,. \tag{5.25}$$

The non-singlet scalar mesons have the potential

$$V_S(u) = \frac{1}{\Xi_S(u)}\frac{d^2\Xi_S(u)}{du^2} + H_S(u)\,, \tag{5.26}$$

with

$$\Xi_S(u) = \frac{1}{G}\sqrt{V_f(\lambda,\tau)\kappa(\lambda)e^{3A}}\,,\qquad H_S(u) = -\frac{e^{2A}}{\kappa(\lambda)}\left(\frac{(\partial_\tau V_\tau)^2}{V_\tau^2} - \frac{\partial_\tau^2 V_\tau}{V_\tau}\right)\,, \tag{5.27}$$

where the expression for H_S differs from that of [98] because our Ansatz for V_τ is different. Finally the equation of motion of the non-singlet pseudoscalar fluctuations is given by[3]

$$V_f(\lambda,\tau)\,\tau^2 e^{3A}G^{-1}\kappa(\lambda)\,\partial_z\left[\frac{1}{V_f(\lambda,\tau)\tau^2\kappa(\lambda)e^{3A}G}\,\partial_z\psi_P\right] -$$
$$-\,4\tau^2 e^{2A}\frac{\kappa(\lambda)}{w(\lambda)^2}\,\psi_P + m^2\psi_P = 0\,, \tag{5.28}$$

with associated Schrödinger potential

$$V_P(u) = \frac{1}{\Xi_P(u)}\frac{d^2\Xi_P(u)}{du^2} + H_P(u)\,, \tag{5.29}$$

where

$$\Xi_P(u) = \frac{1}{\tau\sqrt{V_f(\lambda,\tau)\kappa(\lambda)e^{3A}}}\,,\qquad H_P(u) = \frac{4\tau^2 e^{2A}\kappa(\lambda)}{w(\lambda)^2}\,. \tag{5.30}$$

The numerical determination of the spectrum proceeds by first finding the background solution (the metric and the scalar fields λ and τ) of the equations of motion defined by the action $S = S_g + S_f$. Details of the numerical procedure can be found in appendix 5.A. We then solve the fluctuation equations on top of the numerical background. For the cases of singlet and non-singlet vector and axial vector fluctuations,

---

[3]Notice that the UV boundary condition for the pseudoscalar fluctuations is nontrivial and also depends on whether the quark mass is finite or not [98]. A consistent way which leads to UV finiteness of the fluctuated action in all cases is to require that the factor in square brackets (rather than the wave function ψ_P) in (5.28) vanishes in the UV. For the pseudoscalars we actually solved the differential equation by using a different method than in the other sectors (i.e. by shooting) because of the complication with the boundary condition.

and for non-singlet scalar fluctuations, we compute the Schrödinger potential and use a pseudospectral method based on Chebyschev polynomials to compute the predicted masses of this model. The number of Chebyschev points used was 1000 and we checked the results were stable by computing the masses with a higher number of points. The reliability of the results was also studied by considering different IR and UV cutoffs on the background fields used to solve the Schrödinger problems. The masses of the pseudoscalars were computed using the shooting method. These methods were implemented in *C++* and all results were also cross-checked against the (significantly slower) Mathematica code used in [98].

5.2.4   Fitting the spectrum

We now proceed to fix the parameters that appear in the potentials by comparing the predictions of our model with the experimental values of the meson masses quoted by the Particle Data Group [129].

The overall energy units in the model is also a free parameter. Its effect on the background and spectrum is trivial due to a scaling symmetry of the holographic model [97] which reflects the scale independence of the QCD Lagrangian. The scaling symmetry implies, in particular, that the equations of motion are unchanged under the transformation

$$A \to A - \log \Lambda \,, \quad z \to \Lambda z \,. \tag{5.31}$$

By applying this transformation to the spectrum we see that all masses are scaled by the factor Λ. We will in effect choose Λ such that the numerical mass of the ρ meson matches the experimental result in GeV units. This is equivalent to fitting the parameters of the to the numerical values of ratios of masses (with respect to the ρ meson mass) instead of numerical values of masses.

We will only consider mesons made of light up and down quarks. This sets the x parameter coming from the flavour sector to be 2/3. In table 5.1 we show all the mesons listed in [129] under *light unflavoured mesons* with the values of J^{PC} mentioned before. The exceptions are the flavour singlet scalars and pseudoscalars and the $a_0(980)$. Whether the latter is a quark-antiquark state or a four-quark state is still debatable, although the literature favours more the four-quark state hypothesis. For this reason we did not include it in this work. In table 5.2 we have the mesons listed in [129] under *other light unflavoured mesons*, which are still not well established. We also included theses masses in our fit, therefore in case some of these states are

J^{PC}	I	Meson	Mass Measured (GeV)
1^{--}	1	ρ	0.7755
1^{--}	1	$\rho(1450)$	1.465
1^{--}	1	$\rho(1700)$	1.720
1^{--}	0	$\omega(782)$	0.78265
1^{--}	0	$\omega(1420)$	1.420
1^{--}	0	$\omega(1650)$	1.670
1^{++}	1	$a_1(1260)$	1.230
1^{++}	0	$f_1(1285)$	1.2819
1^{++}	0	$f_1(1420)$	1.4264
0^{++}	1	$a_0(1450)$	1.474
0^{-+}	1	π_0	0.134977
0^{-+}	1	$\pi_0(1300)$	1.300
0^{-+}	1	$\pi_0(1800)$	1.812

Table 5.1: Light unflavoured mesons from [129] used in the spectrum fit. The quantum number $I = 1$ means the meson is a flavour non-singlet state while $I = 0$ means the meson is a flavour singlet state.

not confirmed this work should be updated.

As our goal is to include the Regge behavior of vector and axial vector mesons, the most important criterion for the fit will be the deviation of the vector meson masses of the model from the experimental results. We have explored different fitting strategies. We tested fits where the parameters α_λ and $V_{\rm IR}$ are fitted either independently to Yang-Mills data or together with the other parameters to "final" meson mass data. We also tried including lattice data for glueball masses. The result of these tests was that the optimal method, which lead to a physically sound solution for the metric and a good fit of the spin 1 states, was to do a global simultaneous fit of all parameters, excluding the glueball masses, and also imposing specific constraints to the fit parameters. We will explain the details below.

The profile of the background fields and the mesons masses (excluding axial vector singlet states which will be discussed below) are determined by 17 parameters. 16 of these parameters (α_λ, α_κ, α_w, W_0, w_0, κ_1, w_1, $V_{\rm IR}$, $W_{\rm IR}$, $\bar{\kappa}_0$, $\bar{w}_0$, W_1, $\bar{\kappa}_1$, $\bar{w}_1$, a_1, and a_2) are parameters of the potentials appearing in the action and τ_0 is a parameter that characterises the IR asymptotics of the tachyon field. In our fits a_1 and a_2 are fixed by imposing the following constraints: we choose $a_2 - a_1 = 1$ by rescaling the τ field, and

J^{PC}	I	Meson	Mass Measured (GeV)
1^{--}	1	$\rho(2000)$	2.000
1^{--}	1	$\rho(2270)$	2.265
1^{--}	0	$\omega(1960)$	1.960
1^{--}	0	$\omega(2205)$	2.205
1^{--}	0	$\omega(2290)$	2.290
1^{--}	0	$\omega(2330)$	2.330
1^{++}	1	$a_1(1930)$	1.930
1^{++}	1	$a_1(2095)$	2.095
1^{++}	1	$a_1(2270)$	2.270
1^{++}	0	$f_1(1970)$	1.971
1^{++}	0	$f_1(2310$	2.310
0^{++}	1	$a_0(2020)$	2.025
0^{-+}	1	$\pi_0(2070)$	2.070
0^{-+}	1	$\pi_0(2360)$	2.360

Table 5.2: Other light mesons from [129] used in the spectrum fit. The quantum number $I = 1$ means the meson is a flavour non-singlet state while $I = 0$ means the meson is a flavour singlet state.

set $a_2 = 2\kappa(0)$ in order for the mass gap of the mesons to be correct at large quark mass [146]. This reduces the number of free parameters to 15.

It turns out that it is useful to set extra constraints for the behavior of the tachyon which guarantee that the fit parameters remain in the domain of physically reasonable solutions. The first is related to chiral symmetry breaking. The chirally symmetric vacuum solution of the model flows to an IR fixed point [97]. We require that there is an instability towards forming a tachyon condensate in the IR around this fixed point, which will imply chiral symmetry breaking on the field theory side. The presence of the instability, and therefore chiral symmetry breaking, is guaranteed if the Breitenlohner-Freedman (BF) bound [151] of the tachyon is violated at the fixed point. This means that $-m_\tau^2 \ell_*^2 > 4$, where

$$-m_\tau^2 \ell_*^2 = \frac{24(a_2 - a_1)}{\kappa(\lambda_*)V_{\text{eff}}(\lambda_*)}, \qquad V_{\text{eff}}(\lambda) = V_g(\lambda) - V_f(\lambda, \tau = 0). \qquad (5.32)$$

Here the location of the fixed point is the maximum of the effective potential, $V_{\text{eff}}'(\lambda_*) = 0$, and ℓ_* is the IR AdS radius. Actually, while violation of the BF bound guarantees tachyon condensation and chiral symmetry breaking, it turns out that, in practice, values close to the bound are enough to trigger condensation. Therefore we will in

fact require $-m_\tau^2 \ell_*^2 \gtrsim 3.5$.

The other condition is to require that the tachyon diverges fast enough in the IR to set all potential IR boundary terms arising from the flavour action to zero. This is required, among other things, for the correct implementation of the flavour anomalies [127, 141]. For our choice of potentials the asymptotics of the tachyon in the IR is

$$\tau \sim \tau_0 \, z^{\tau_c} \,, \qquad \tau_c = \frac{1}{8} \frac{(12 - xW_0) \, \bar{\kappa}_0 a_2}{V_{\text{IR}}(a_2 - a_1)} \,, \tag{5.33}$$

and the flavor action vanishes fast enough in the IR if $\tau_c > 1$, which is roughly what we require below.

We then fit these parameters to ratios between the meson masses in tables 5.1 and 5.2 and the ρ mass, by minimising the function

$$J = \sum_i \frac{|R_{\text{pred.}\,i} - R_{\text{obs.}\,i}|}{R_{\text{obs.}\,i}} + W_\tau \, e^{-(4\tau_c/3 - 1)} + W_\tau \, e^{-\left(-m_\tau^2 \ell_*^2 - 3.5\right)}, \tag{5.34}$$

excluding the singlet axial vector mesons. This gives a total of 22 data points. The sum term is the absolute relative difference between the predictions of our model and the ones obtained by using experimental data, while the other two terms are the constraints we want our background to satisfy. We repeated the fit with different values of the W_τ parameter in order to balance the ability of the model to reproduce the observed ratios and still be consistent and stable. We have found that $W_\tau = 0.1$ is a good choice and the results that we present below were obtained with such value. Having fixed the background, we fit the parameters Z_a and c_a of equation (5.18) against the four mass ratios between the singlet axial vector mesons and the ρ meson. With this procedure we have obtained the parameter values presented in table 5.3 and the corresponding mass ratios of table 5.4. This fit has $-m_\tau^2 \ell_*^2 \approx 6.200$ and $\tau_c \approx 1.956$ which ensure presence of chiral symmetry breaking and IR decoupling of the tachyon.

Several remarks are in order. Firstly, the fit is stiff: while the number of parameters is large, the dependence of the results on their values is relatively mild. This is because the fit parameters appear through only a few functions of λ, the asymptotics at large and small coupling of which have already been determined by qualitative arguments and comparison to perturbation theory. Therefore the fit parameters essentially only affect the functions in the middle, at $\lambda \sim 1$. Also there is limited parameter space where the functions are simple, monotonic functions, and one can check from the fit result that it indeed lies within this regime of the parameter space.

Given the stiffness of the fit, the results for the spin-one mesons are really good. There are a few isolated states for which the deviation is $\gtrsim 10\%$, but in general the deviations

Parameter	value	Parameter	value	Parameter	value
α_λ	2.8328	α_κ	3.1670	α_w	1.6926
W_0	2.4289	w_0	0.9400	κ_1	1.3254
w_1	-0.2898	V_{IR}	1.8042	W_{IR}	1.1345
$\bar\kappa_0$	1.7647	$\bar w_0$	2.9291	W_1	0.2342
$\bar\kappa_1$	-0.3076	$\bar w_1$	3.0358	a_1	0.5413
a_2	1.5413	τ_0	0.9232	Z_a	-0.0377
c_a	23.307				

Table 5.3: Best fit parameters of the background potentials to the mass ratios between the mesons listed on tables 5.1 and 5.2 and the ρ meson.

are in the ballpark of 1% or even less than that. The masses of the pseudoscalar mesons are also reproduced at a very good precision. There are, however, significant deviations in the scalar sector. While the scalar sector is challenging to explain in any model among other things due to the presence of significant four-quark contribution [129], the predicted nonsinglet scalar masses are still clearly too low, unlike in the probe limit study of [135, 136] which used similar flavor action as the current work with the fixed background of [152]. While exploring different fit procedures, we noticed that there are parameter values for which the scalar masses are reproduced to a much better precision, but such parameter values are not favored by the overall fit which stresses the masses of the spin 1 mesons. Understanding this shortcoming requires further study. Notice that the scalar states are not needed for the analysis of the Regge trajectories which is the topic of discussion in the remainder of this thesis.

The fitted value of $Z_a = Z(0)$ in Table 5.3 is negative. Due to the positive value of c_a, however, the function $Z(\lambda)$ is mostly positive so that $Z(\lambda)$ has a node at small λ. This behavior is unexpected and does not agree with phenomenology, i.e. the physics of the θ-angle in QCD and in particular the value of the topological susceptibility [92, 141]. Apparently this issue arises because the singlet axial meson masses are relatively insensitive to the shape of the function $Z(\lambda)$, and would be cured if additional observables (e.g. the topological susceptibility) would be included in the fit. The precise functional form of $Z(\lambda)$ is again irrelevant for the Regge analysis of the following sections.

It is also interesting to compare the fit results to those obtained in the same holographic model [144] by fitting the potentials independently to lattice data for QCD thermodynamics. Namely, most of the values are very close to those obtained in that study, deviations are typically in the ballpark of 10%. In particular, the scale

Ratio	$R_{pred.}$	$R_{obs.}$	$|R_{pred.} - R_{obs.}|/R_{obs.}$
$m_{\rho(1450)}/m_\rho$	1.662	1.890	0.121
$m_{\rho(1700)}/m_\rho$	2.141	2.219	0.035
$m_{\rho(2000)}/m_\rho$	2.559	2.580	0.008
$m_{\rho(2270)}/m_\rho$	2.940	2.922	0.006
$m_{\omega(782)}/m_\rho$	1	1.010	0.010
$m_{\omega(1420)}/m_\rho$	1.662	1.832	0.093
$m_{\omega(1650)}/m_\rho$	2.141	2.154	0.006
$m_{\omega(1960)}/m_\rho$	2.559	2.528	0.012
$m_{\omega(2205)}/m_\rho$	2.940	2.844	0.034
$m_{\omega(2290)}/m_\rho$	3.289	2.954	0.127
$m_{\omega(2330)}/m_\rho$	3.610	3.005	0.201
$m_{a_1(1260)}/m_\rho$	1.591	1.587	0.003
$m_{a_1(1930)}/m_\rho$	2.095	2.489	0.158
$m_{a_1(2095)}/m_\rho$	2.523	2.702	0.066
$m_{a_1(2270)}/m_\rho$	2.916	2.928	0.004
$m_{f_1(1285)}/m_\rho$	1.653	1.654	0.001
$m_{f_1(1420)}/m_\rho$	2.128	1.840	0.157
$m_{f_1(1970)}/m_\rho$	2.543	2.542	0.0004
$m_{f_1(2310)}/m_\rho$	2.930	2.980	0.017
m_π/m_ρ	0.1740	0.1741	0.0006
$m_{\pi(1300)}/m_\rho$	1.731	1.677	0.032
$m_{\pi(1800)}/m_\rho$	2.337	2.337	5×10^{-5}
$m_{\pi(2070)}/m_\rho$	2.785	2.670	0.043
$m_{\pi(2360)}/m_\rho$	3.173	3.044	0.042
$m_{a_0(1450)}/m_\rho$	0.685	1.901	0.640
$m_{a_0(2020)}/m_\rho$	1.492	2.612	0.429

Table 5.4: Mass ratios obtained with the parameter values of table 5.3 and their comparison to experimental values.

parameters α_λ and α_κ are close to the value 1 used in this reference, whereas α_w is a bit higher than what was obtained through the fit to thermodynamics (α_w equals to $3w_s$ of [144]) but still smaller than the other scale parameters, in agreement with the earlier fit. We also note that there is rough agreement with [153,154] where the model was compared to lattice results at finite magnetic field and temperature by using a slightly different Ansatz for the potentials of the model. The parameter c of these references, which controls the scale in the λ dependence of the $w(\lambda)$ function, maps roughly to the ratios α_w/α_λ or α_w/α_κ in this work. For the ratios we obtain numbers close to 0.5 whereas $c \approx 0.25$ was preferred by the thermodynamics at finite magnetic field. That is, the numerical values are different, but clearly smaller than one in both cases. Moreover the value of W_0 (which was a free parameter in [144]) is determined by the spectrum fit to be near 2.5. This results is therefore an important constraint with respect to the earlier fit. The most significant difference between the fits is the value of $\bar{w}_0$, which here is smaller by a factor of about 5 to 10 with respect to the various fits of [144]. This is apparently connected to the change in the value of α_w.

5.3 $\gamma\gamma$, γp and pp total cross-sections in holographic QCD

In this section we present the necessary ingredients to compute the total cross-sections of $\gamma\gamma$, γp and pp scattering in holographic models of QCD in the Veneziano limit. First we will discuss the kinematics of each process. Then we will present generic holographic expressions of the forward scattering amplitude, in the Regge limit, via the exchange of higher spin J fields. We conclude by deriving the holographic expression of the total cross-sections by taking the imaginary part of the amplitudes and using the optical theorem.

5.3.1 Kinematics

For all processes we will use light-cone coordinates $(+, -, \perp)$, with flat space metric $ds^2 = -dx^+ dx^- + dx_\perp^2$, where $x_\perp \in \mathbb{R}^2$. For the $\gamma^* p \to \gamma^* p$ process the incoming and outgoing off-shell photons are the following

$$k_1 = \left(\sqrt{s}, -\frac{Q_1^2}{\sqrt{s}}, 0 \right), \qquad -k_3 = \left(\sqrt{s}, \frac{q_\perp^2 - Q_3^2}{\sqrt{s}}, q_\perp \right), \tag{5.35}$$

while the incoming and outgoing protons with mass M have momenta

$$k_2 = \left(\frac{M^2}{\sqrt{s}}, \sqrt{s}, 0 \right), \qquad -k_4 = \left(\frac{q_\perp^2 + M^2}{\sqrt{s}}, \sqrt{s}, -q_\perp \right). \tag{5.36}$$

The momentum transfer $q_\perp$ is a $\mathbb{R}^2$ vector and is related to the Mandelstam variable t through $t = -q_\perp^2$. We work in the Regge limit of large Mandelstam variable s. For the forward scattering amplitude the momentum transfer $q_\perp = 0$ and the photon virtualities satisfy $Q_3 = Q_1 = Q$, since the outgoing off-shell photon has $k_3 = -k_1$ and the outgoing proton $k_4 = -k_2$. The incoming and outgoing photon polarizations are the same. The possible polarization vectors are

$$n(\lambda) = \begin{cases} (0, 0, \epsilon_\lambda), & \lambda = 1, 2 \\ (\sqrt{s}/Q, Q/\sqrt{s}, 0), & \lambda = 3 \end{cases}, \tag{5.37}$$

where ϵ_λ is just the usual transverse polarization vector.

For the $\gamma^* \gamma^* \to \gamma^* \gamma^*$ process the incoming photons have the four momenta

$$k_1 = \left(\sqrt{s}, -\frac{Q_1^2}{\sqrt{s}}, 0 \right), \qquad k_2 = \left(-\frac{Q_2^2}{\sqrt{s}}, \sqrt{s}, 0 \right), \tag{5.38}$$

while the outgoing photons have

$$k_3 = -\left(\sqrt{s}, \frac{q_\perp^2 - Q_3^2}{\sqrt{s}}, q_\perp \right) \qquad k_4 = -\left(\frac{q_\perp^2 - Q_4^2}{\sqrt{s}}, \sqrt{s}, -q_\perp \right), \tag{5.39}$$

where $Q_i^2 = k_i^2 > 0$ $(i = 1, \ldots, 4)$ are the corresponding virtualities. As in the case of $\gamma^* p$ scattering, for the forward scattering amplitude the momentum transfer is null. The possible polarization vectors are, respectively,

$$n_{1,3} = \begin{cases} (0, 0, \epsilon_\lambda), & \lambda = 1, 2 \\ \frac{1}{Q} \left(\sqrt{s}, \frac{Q^2}{\sqrt{s}}, 0, 0 \right), & \lambda = 3 \end{cases} \tag{5.40}$$

$$n_{2,4} = \begin{cases} (0, 0, \epsilon_\lambda), & \lambda = 1, 2 \\ \frac{1}{Q} \left(\frac{Q^2}{\sqrt{s}}, \sqrt{s}, 0, 0 \right), & \lambda = 3 \end{cases}, \tag{5.41}$$

since in the forward amplitude the incoming and outgoing off-shell photons have the same polarizations. Notice that the transverse photons ($\lambda = 1, 2$) are normalized such that $n^2 = 1$, while for the longitudinal photons ($\lambda = 3$) $n^2 = -1$.

Finally, the large s kinematics of pp scattering is given by

$$k_1 = \left(\sqrt{s}, \frac{M^2}{\sqrt{s}}, 0 \right), \quad k_3 = -\left(\sqrt{s}, \frac{q_\perp^2 + M^2}{\sqrt{s}}, q_\perp \right), \tag{5.42}$$

$$k_2 = \left(\frac{M^2}{\sqrt{s}}, \sqrt{s}, 0 \right), \quad k_4 = -\left(\frac{M^2 + q_\perp^2}{\sqrt{s}}, \sqrt{s}, -q_\perp \right),$$
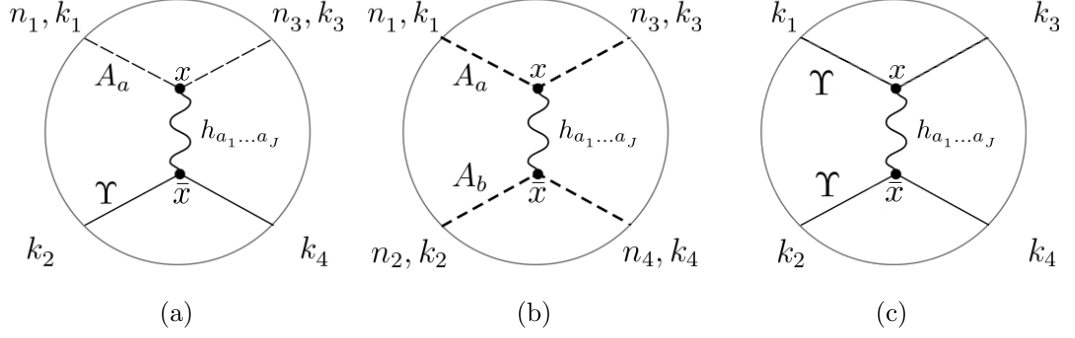
Figure 5.1: Tree level Witten diagram representing spin J exchange in (a) $\gamma^* p \to \gamma^* p$, (b) $\gamma\gamma \to \gamma\gamma$ and (c) $pp \to pp$ scattering. The n_1 and n_2 labels denote the incoming photon polarizations while n_3 and n_4 label the outgoing photon polarizations. For forward scattering $n_1 = n_3$ and $n_2 = n_4$. A_a represents the non-normalizable mode of a $U(1)$ gauge field dual to the source of the conserved current $\bar{\psi}\gamma^\mu\psi$ and Υ is a normalizable mode of a bulk scalar field that represents an unpolarised proton. x and $\bar{x}$ represent the bulk points where the external scattering states couple with the spin J fields.

where k_1 and k_2 are the incoming proton momenta and k_3 and k_4 are the outgoing proton momenta. As in the other processes we will only compute the forward scattering amplitude for which $q_\perp = 0$.

5.3.2 Holographic scattering amplitudes

Before we start the computation of the forward scattering amplitudes we need to define the external states as well as the interaction between them and the spin J fields that are exchanged in the Witten diagrams of figure 5.1.

An external photon is a source of the conserved current $\bar{\psi}\gamma^\mu\psi$, where the quark field ψ comes from the open string sector. According to the gauge/gravity duality this field is dual to the nonnormalizable mode of a vector field in the bulk. In the context of this model the natural candidate is the linear combination of the A^L and A^R gauge fields

$$V_a = \frac{A_a^L + A_a^R}{2} \, . \tag{5.43}$$

In the string frame the action of this field is

$$S = -\frac{1}{4} M^3 N_c N_f \int d^5 x \sqrt{-g_s} \, e^{-\frac{10}{3}\Phi} V_f \, w_s^2 \, G F_{ab} \tilde{g}^{ac} \tilde{g}^{bd} F_{cd} \, , \tag{5.44}$$

where g_s is the determinant of the metric in the string frame, $\tilde{g}^{ab}$ is the inverse of $\tilde{g}_{ab} = g_{sab} + \kappa_s(\lambda)\partial_a\tau\partial_b\tau$, $\kappa_s(\lambda) = \lambda^{4/3}\kappa(\lambda)$ and $w_s(\lambda) = \lambda^{4/3}w(\lambda)$ and G was defined in equation (5.20). Working in the gauge $V_z = 0$ and $\partial_\mu V^\mu = 0$, the vector field components describing a boundary plane wave solution with polarization n_μ take the form

$$V_\mu(x, z) = n_\mu f_Q(z) e^{ik\cdot x}, \qquad k^2 = Q^2, \tag{5.45}$$

where f_Q satisfies the differential equation

$$\frac{1}{V_f(\lambda, \tau)w(\lambda)^2 e^A G}\partial_z\left(V_f(\lambda, \tau)w(\lambda)^2 e^A G^{-1}\partial_z f_Q\right) - Q^2 f_Q = 0, \tag{5.46}$$

subject to the boundary conditions $f_Q(0) = 1$ and $\partial_z f_Q(z \to \infty) = 0$. For the computation of the Witten diagrams that have photons as external states, in particular to compute the bulk interaction vertex, it is convenient to know the field strength of a given mode

$$F_{\mu\nu} = 2ik_{[\mu}n_{\nu]}f_Q(z)e^{ik\cdot x}, \quad F_{z\mu} = n_\mu\dot{f}_Q(z)e^{ik\cdot x}, \tag{5.47}$$

where we use the notation $\dot{f}_Q = \partial_z f_Q$.

For the proton external state we consider that it is dual to the normalizable mode of a bulk scalar field $\Upsilon(x, z) = e^{iP\cdot x}\upsilon(z)$ that represents an unpolarised proton. We will see that the contribution of the proton wavefunction to the scattering amplitudes is inside an integral that will be absorbed in the coupling constants and hence the precise details will not be important.

The last ingredient of our model are the higher spin fields $h_{a_1\cdots a_J}$ that will mediate the interaction between the external states in the considered scattering states. In this work we will consider bulk spin J fields that are dual to the spin J twist two operators made of the gluon field, as well as bulk spin J fields dual to the spin J twist two operators made of the quark bilinears. This extends the previous works [1, 32, 33], where only bulk fields dual to the gluon operators were considered. As discussed in appendix 5.B, we will consider a coupling between the $U(1)$ gauge field and these spin J fields given by

$$k_J\int d^5x\sqrt{-g_s}Ge^{-\frac{10}{3}\Phi}V_f(\lambda, \tau)\,w_s(\lambda)^2\tilde{g}^{ab}F^V_{ac}\nabla_{a_1}\ldots\nabla_{a_{J-2}}F^V_{bd}\,h^{cda_1\ldots a_{J-2}}, \tag{5.48}$$

while for the scalar field Υ dual to the proton state the coupling is

$$\bar{k}_J\int d^5x\sqrt{-g_s}\,e^{-\Phi}\left(\Upsilon\nabla_{b_1}\ldots\nabla_{b_J}\Upsilon\right)h^{b_1\ldots b_J}. \tag{5.49}$$

In equations (5.48) and (5.49) ∇_a is the covariant derivative, while k_J and $\bar{k}_J$ are the couplings constants between the the $U(1)$ gauge field and the bulk scalar with the spin J field, respectively.

The higher spin J field $h_{a_1 \cdots a_J}$ is totally symmetric, traceless and satisfies the transversality property $\nabla^{a_1} h_{a_1 \cdots a_J} = 0$. This implies that, in the Regge limit, it is not important in which external fields the covariant derivatives in (5.48) and (5.49) act. Below we assume that the spin J field has a propagator, without specifying its form. In the next section we focus on the dynamics of this field in detail for the case of pomeron and meson trajectories.

Now we will show how to compute the forward scattering amplitude for the case of γp scattering. The calculations for $\gamma\gamma$ and pp follow the same pattern and bring no additional difficulty. For those cases we will simply present the results. In the Regge limit, the amplitude describing the spin J exchange between the incoming gauge field $V_a^{(1)} \sim e^{ik_1 \cdot x}$ and scalar field $\Upsilon^{(2)} \sim e^{ik_2 \cdot x}$, and outgoing gauge field $V_a^{(3)} \sim e^{ik_3 \cdot x}$ and scalar field $\Upsilon^{(4)} \sim e^{ik_4 \cdot x}$, can be written as

$$
\mathcal{A}_J = k_J \bar{k}_J \int d^5 x \int d^5 \bar{x} \sqrt{-g_s} \sqrt{-\bar{g}_s}\, G\, e^{-\frac{10}{3}\Phi} V_f\, w_s^2\, e^{-\bar{\Phi}} \times
$$
$$
\times\, \tilde{g}^{ab} F_{a-}^{(1)}(x) \partial_-^{J-2} F_{b-}^{(3)}(x)\, \Pi^{-\cdots-,+\cdots+}(x,\bar{x}) \Upsilon^{(2)}(\bar{x}) \partial_+^J \Upsilon^{(4)}(\bar{x})\,, \tag{5.50}
$$

where bars denote quantities evaluated at $\bar{x}$ in the Witten diagrams. The tensor $\Pi^{a_1 \cdots a_J, b_1 \cdots b_J}(x,\bar{x})$ is the propagator of the spin J field. Using the kinematics of equations (5.35), (5.36) and (5.37), the expressions (5.47) and summing over the photon polarisations, the amplitude takes the form

$$
\mathcal{A}_J = k_J \bar{k}_J s^J \int d^5 x\, d^5 \bar{x} \sqrt{-g_s} \sqrt{-\bar{g}_s}\, G\, e^{-\frac{10}{3}\Phi} V_f\, w_s^2\, e^{-\bar{\Phi}} e^{-2J(A+\bar{A})} e^{-2A} \times
$$
$$
\times \left(f_Q^2 + \frac{\dot{f}_Q^2}{Q^2 G^2} \right) \bar{v}^2 e^{-iq_\perp \cdot (x_\perp - \bar{x}_\perp)} \Pi_{+\cdots+,-\cdots-}(x,\bar{x})\,. \tag{5.51}
$$

To make progress we make the change of variable $x - \bar{x} = (w^+, w^-, l_\perp) \equiv w$ and define the transverse propagator in transverse space $G_J(z, \bar{z}, t)$ through

$$
\int d^2 l_\perp e^{-iq_\perp l_\perp} \int \frac{dw^+ dw^-}{2} \Pi_{+\cdots+,-\cdots-}(z, \bar{z}, w^+, w^-, l_\perp) = -\frac{i}{2^J} \left(e^{A+\bar{A}} \right)^{J-1} G_J(z, \bar{z}, t)\,, \tag{5.52}
$$

that is valid both for spin J fields of the graviton Regge and meson trajectories.

Defining $V = (2\pi)^4 \delta^4 \left(\sum k_i \right)$ we obtain

$$
\mathcal{A}_J = -iV \frac{k_J \bar{k}_J}{2^J} s^J \int dz d\bar{z} \, e^{2A} e^{4\bar{A}} \, G \, e^{-\frac{10}{3}\Phi} \, V_f \, w_s^2 \, e^{-\bar{\Phi}} e^{-J(A+\bar{A})} \times
$$
$$
\times \left(\dot{f}_Q^2 + \frac{\dot{f}_Q^2}{Q^2 G^2} \right) \bar{v}^2 G_J(z, \bar{z}, t) \,. \tag{5.53}
$$

In the next section we will propose phenomenological equations of motion for the higher spin fields $h_{a_1 \cdots a_J}$ of both trajectories. In particular, it will be shown that the function $G_J(z, \bar{z}, t)$ for the pomeron and meson trajectories admits a spectral decomposition associated to a Schrödinger potential that describes spin J glueballs or spin J mesons. This function can be written in terms of the eigenfunctions $\psi_n(J, z)$ and eigenvalues $t_n(J)$ of this Schrödinger potential in the following way

$$
G_J(z, \bar{z}, t) = e^{B + \bar{B}} \sum_n \frac{\psi_n(J, z) \, \psi_n^*(J, \bar{z})}{t_n(J) - t} \,. \tag{5.54}
$$

As already observed in chapter 2, the function $B(z)$ depends on the holographic QCD model as well on the trajectory that the higher spin field belongs to. We will determine it them in the next section.

Finally, in order to get the total amplitude we need to sum over the spin J fields with $J \geq J_{min}$, where J_{min} is the minimal spin in the corresponding Regge trajectory. As described in previous chapters we can apply a Sommerfeld-Watson transform

$$
\frac{1}{2} \sum_{J \geq J_{min}} \left(s^J + (-s)^J \right) \frac{\mathcal{A}_J}{s^J} = -\frac{\pi}{2} \int \frac{dJ}{2\pi i} \frac{s^J + (-s)^J}{\sin \pi J} \frac{\mathcal{A}_J}{s^J} \,, \tag{5.55}
$$

which requires analytic continuation of the amplitude for the spin J exchange to the complex J-plane. The contour on the complex plane consists of circles around simple poles at integer values of J. Then, we assume that the J-plane integral can be deformed from the poles at physical values of J to the poles $J = j_n(t)$ defined by $t_n(J) = t$. The scattering domain of negative t contains these poles along the real axis for $J < J_{min}$. The scattering amplitude for $t = 0$ is then

$$
\mathcal{A}(s, 0) = \sum_n g_n^{\gamma p} s^{j_n(0)} \int dz \, e^{A(2 - j_n(0))} \, G \, e^{-\frac{10}{3}\Phi} \, V_f \, w_s^2 \left(\dot{f}_Q^2 + \frac{\dot{f}_Q^2}{Q^2 G^2} \right) e^B \psi_n(j_n, z) \,, \tag{5.56}
$$

where

$$
g_n^{\gamma p} = \frac{\pi}{2} \frac{k_{j_n(0)} \bar{k}_{j_n(0)}}{2^{j_n(0)}} \left(i + \cot \frac{\pi j_n(0)}{2} \right) \frac{d j_n}{dt} \int d\bar{z} \, e^{\bar{A}(4 - j_n)} e^{-\bar{\Phi}} \bar{v}^2 e^{\bar{B}} \psi(j_n, \bar{z})^* \,. \tag{5.57}
$$

By analysing (the regular solution to) the equation (5.46) we see that

$$\lim_{Q \to 0} f_Q = 1, \qquad \lim_{Q \to 0} \frac{\dot{f}_Q}{Q} = 0. \tag{5.58}$$

It therefore follows from the optical theorem that

$$\sigma(\gamma p \to X) = \sum_n \operatorname{Im}\left(g_n^{\gamma p}\right) s^{j_n - 1} \int du\, e^{-(j_n - 2)A} e^{-\frac{10}{3}\Phi} V_f\, w_s^2\, e^B \psi_n(u), \tag{5.59}$$

where we have made the change of variable $du = Gdz$.

As mentioned before the procedure to compute the holographic total cross-sections for the other processes is similar to the one just presented. These calculations are done in appendices 5.C and 5.D. Hence, we finish this section by presenting the final results. For $\gamma\gamma \to X$ we have

$$\sigma(\gamma\gamma \to X) = \sum_n \operatorname{Im}\left(g_n^{\gamma\gamma}\right) s^{j_n - 1} \int du\, e^{-(j_n - 2)A} e^{-\frac{10}{3}\Phi} V_f\, w_s^2\, e^B \psi_n(u), \tag{5.60}$$

where

$$g_n^{\gamma\gamma} = \frac{\pi}{2} \frac{k_{j_n(0)}^2}{2^{j_n(0)}} \left(i + \cot \frac{\pi j_n(0)}{2}\right) \frac{dj_n}{dt} \int d\bar{u}\, e^{-(j_n - 2)\bar{A}} e^{-\frac{10}{3}\bar{\Phi}} \bar{V}_f\, \bar{w}_s^2\, e^{\bar{B}} \psi_n(u)^*. \tag{5.61}$$

For the $pp \to X$ process the total cross-section is

$$\sigma(pp \to X) = \sum_n \operatorname{Im}\left(g_n^{pp}\right) s^{j_n - 1}, \tag{5.62}$$

where

$$g_n^{pp} = \frac{\pi}{2} \frac{\bar{k}_{j_n(0)}^2}{2^{j_n(0)}} \left(i + \cot \frac{\pi j_n(0)}{2}\right) \frac{dj_n}{dt} \left| \int dz\, e^{A(4 - j_n)} e^{-\Phi} \bar{v}^2 e^B \psi(j_n, z) \right|^2. \tag{5.63}$$

5.4 Spin J Dynamics

The Witten diagrams of figure 5.1 allow to compute four-point functions dominated by exchange of twist 2 operators in the large s limit. We consider spin J operators $\mathcal{O}_J$ of the form

$$\mathcal{O}_J \sim \operatorname{tr}\left[F_{\beta\alpha_1} D_{\alpha_2} \cdots D_{\alpha_{J-1}} F^{\beta}_{\alpha_J}\right], \qquad \mathcal{O}_J \sim \bar{\psi}\gamma_{\alpha_1} D_{\alpha_2} \cdots D_{\alpha_J}\psi. \tag{5.64}$$

The first set of operators are gluonic while the second set are quark operators. These twist 2 operators are dual to bulk spin J fields whose dynamics will be specified below.

We shall then follow an effective field theory approach, by proposing a general form of the equations of motion with phenomenological parameters that can be fixed by data. We will propose two different equations of motion, one that describes the gluon sector, which includes the energy-momentum tensor $T_{\alpha\beta}$, and the other the quark sector, which includes the quark bilinear current J_α. These equations will satisfy two requirements: *i)* compatibility with the graviton's equation of motion for the case $J = 2$ for gluonic operators, and compatibility for $J = 1$ with the equation of motion of the $U(1)$ current dual to the operator J_α; *ii)* reduction to the conformal limit case (pure AdS space and constant dilation and tachyon).

In pure AdS the equation of motion of a spin J field is

$$\left(\nabla^2 - M^2\right) h_{a_1 \cdots a_J} = 0 \,, \qquad (LM)^2 = \Delta\left(\Delta - 4\right) - J \,, \qquad (5.65)$$

where L is the AdS length scale and Δ is the dimension of the dual operator $\mathcal{O}_J$. These fields are symmetric, traceless and transverse (TT). The independent components are the ones along the boundary direction (i.e. $h_{\alpha_1 \cdots \alpha_J}$) due to the transversality condition. Decomposing these into irreducible representations of the Lorentz group $SO(1,3)$, the TT components $h^{\text{TT}}_{\alpha_1 \cdots \alpha_J}$ decouple from the others and they describe the operator $\mathcal{O}_J$ in the dual theory. The UV asymptotics of these fields are

$$h_{\alpha_1 \cdots \alpha_J} \sim z^{4-\Delta-J} \mathcal{J} + \cdots + z^{\Delta-J} \langle \mathcal{O}_J \rangle + \cdots \,, \qquad (5.66)$$

with the free theory value $\Delta = J+2$, where $\mathcal{J}$ is the source of $\mathcal{O}_J$ and $\langle \mathcal{O}_J \rangle$ its vacuum expectation value.

We will now motivate two equations of motion for spin J, one for the fields in the Pomeron trajectory and another for the fields in the meson trajectory.

5.4.1 Pomeron in Holographic QCD in the Veneziano limit

The Pomeron is dual to the graviton Regge trajectory [8]. To derive the equation of motion of the spin J fields in the graviton's Regge trajectory we follow the same approach as in [1,32], that is we derive first the equation of motion of the graviton and then generalize it based on the two requirements mentioned above. Only the gluon part of the action S_g, contributes to the fluctuations in the spin-2 sector. Therefore the equation of motion of the TT components of the graviton in this class of models is, in the Einstein frame, the same as in IHQCD [92]

$$\nabla^2 h^{\text{TT}}_{\mu\nu} + 2\dot{A}^2 e^{-2A} h^{\text{TT}}_{\mu\nu} = 0 \,, \qquad (5.67)$$

which also equals equation (A.108) of [98] for the 2^{++} glueballs. This equation reduces to (5.65) for the AdS case since $\Delta = 4$ and $J = 2$ for the AdS graviton. The corresponding equation of motion in the string frame can be obtained by noting that the warp factor in the Einstein frame is related with the warp factor in the string frame A_S through $A = A_S - 2\Phi/3$, and that the expected relationship between the string frame TT perturbations $h_{\alpha\beta}^{\mathrm{TT}\,S}$ and Einstein frame TT perturbations $h_{\alpha\beta}^{\mathrm{TT}}$ is $h_{\alpha\beta} = e^{-4\Phi/3} h_{\alpha\beta}^{S}$. Then the equation of motion in the string frame is (dropping the superscript S in $h_{\alpha\beta}^{\mathrm{TT}\,S}$)

$$\left[\nabla^2 - 2e^{-2A_s} \dot{\Phi} \nabla_z + 2\dot{A}_s^2 e^{-2A_s} \right] h_{\alpha\beta}^{\mathrm{TT}} = 0 \,. \tag{5.68}$$

We propose that the equation of motion of the spin J fields in the graviton's Regge trajectory is

$$\left[\nabla^2 - 2e^{-2A_s} \dot{\Phi} \nabla_z - \frac{\Delta(\Delta - 4)}{L^2} + J\dot{A}_s^2 e^{-2A_s} + e_g \left(J - 2 \right) e^{-2A_s} \dot{\tau}^2 \right] h_{\alpha_1 \ldots \alpha_J}^{\mathrm{TT}} = 0 \,, \tag{5.69}$$

where e_g is a constant that will be fixed later by setting the soft pomeron intercept to 1.08. We note that: *i)* for $J = 2$ we get the the graviton's equation (5.68); *ii)* for the conformal case, i.e. $A = -\log(z/L)$ and Φ and τ constant, the equation reduces to (5.65); *iii)* the second term comes from the tree level coupling of a closed string, as appropriate for the graviton Regge trajectory in a large N approximation; *iv)* following an effective field theory rational we could have included other terms proportional to derivatives of A_s and Φ, that is terms proportional to

$$e^{-2A_s} \left(\ddot{A}_s - \dot{A}_s^2 \right) \,, \quad e^{-2A_s} \dot{\Phi}^2 \,, \quad e^{-2A_s} \ddot{\Phi} \,, \quad e^{-2A_s} \dot{A}_s \dot{\Phi} \,. \tag{5.70}$$

All these terms, of dimension inverse squared length, are compatible with the constraint *i)* and also with constraint *ii)* provided they multiply $J - 2$. Like the term proportional to $\dot{\tau}^2$, these terms are all subleading in the UV. However in the IR, where the wavefunctions of the associated Schrödinger problem are localised, the term $\dot{\tau}^2$ dominates and for this reason we will only consider this term. We have also not included the terms $\ddot{\tau}$, $\dot{\tau}\dot{A}_s$ and $\dot{\tau}\dot{\Phi}$ because the background is symmetric under $\tau \to -\tau$.

The third term in (5.69) is a mass term obtained by the analytic continuation of the dimension of the exchanged operators $\Delta = \Delta(J)$. We shall set

$$\frac{\Delta(\Delta - 4)}{L^2} = \frac{J^2 - 4}{\lambda^{4/3}} \,. \tag{5.71}$$

In the boundary theory the dimension of the operator $\mathcal{O}_J$ can be written as $\Delta = 2 + J + \gamma_J$, where γ_J is the anomalous dimension. In free theory $\gamma_J = 0$. The term we

added in the right-hand side of (5.71) ensures the correct UV asymptotic behaviour of (5.69) leading to the free theory result $h^{\mathrm{TT}}_{+\cdots+} \sim z^2$. Beyond perturbation theory, the curve must pass through the point $J = 2$ and $\Delta = 4$ as it represents the energy-momentum tensor which is protected. Equation (5.71) guarantees such properties.

The propagator for the spin J fields in the graviton's Regge trajectory is the solution of

$$(\mathcal{D}\Pi)_{a_1\cdots a_J, b_1\cdots b_J}(x, \bar{x}) = ie^{2\Phi}g_{a_1(b_1}\cdots g_{|a_J|b_J)}\delta_5(x, \bar{x}) - \mathrm{traces}, \tag{5.72}$$

where the notation $g_{a_1(b_1}\cdots g_{|a_J|b_J)}$ means that symmetrisation is applied only among the indices b_i, $i = 1, \cdots J$. As we have seen in the previous section, in the Regge limit we are only interested in the component $\Pi_{+\cdots+,-\cdots-}$. By using the identity (5.52) one can show that

$$\left[\Delta_3 - e^{-2A_s}\left(2\dot{\Phi}\partial_z + 2\dot{A_s}^2 + \ddot{A}_s - 2\dot{A}_2\dot{\Phi}\right) - m_J^2(z)\right]G_J(z, \bar{z}, l_\perp) = -e^{2\Phi}\delta_3(y, \bar{y}), \tag{5.73}$$

where $l_\perp = x_\perp - \bar{x}_\perp$ and $y = (z, x_\perp)$ and $\bar{y} = (\bar{z}, \bar{x}_\perp)$ are points in the scattering transverse space with metric $ds_3^2 = e^{2A_s}[dz^2 + dx_\perp^2]$. Δ_3 is the corresponding Laplacian and $m^2(z)$ is given by

$$m_J^2(z) = (J - 2)\left[\frac{J + 2}{\lambda^{\frac{4}{3}}} + e_g\, e^{-2A_s}\dot{\tau}^2\right]. \tag{5.74}$$

The homogeneous version of equation (5.73) can be transformed in a Schrödinger problem through the Ansatz

$$G_J(z, \bar{z}, t) = e^{\Phi - \frac{A_s}{2}}\psi(z), \tag{5.75}$$

where ψ satisfies the Schrödinger equation

$$\left[-\partial_z^2 - t + V_J(z)\right]\psi(z) = 0, \tag{5.76}$$

with $t = -q_\perp^2$ and

$$V_J(z) = \frac{3}{2}\left(\ddot{A}_s - \frac{2}{3}\ddot{\Phi}\right) + \frac{9}{4}\left(\dot{A}_s - \frac{2}{3}\dot{\Phi}\right)^2 + e^{2A_s}m_J^2(z). \tag{5.77}$$

The spectrum for each integer J discretises $t = t_n(J)$ and the corresponding eigenfunctions satisfy the identity $\sum_n \psi_n(z)\psi_n^*(\bar{z}) = \delta(z - \bar{z})$. Hence, the solution to equation (5.73) is given by

$$G_J(z, \bar{z}, t) = e^{\Phi + \bar{\Phi} - \frac{A_s}{2} - \frac{\bar{A}_s}{2}}\sum_n \frac{\psi_n(J, z)\,\psi_n^*(J, \bar{z})}{t_n(J) - t}. \tag{5.78}$$

and the B function in equations (5.59), (5.60), (5.62) is $\Phi - A_s/2$ when considering exchange of reggeons in the Pomeron trajectory.
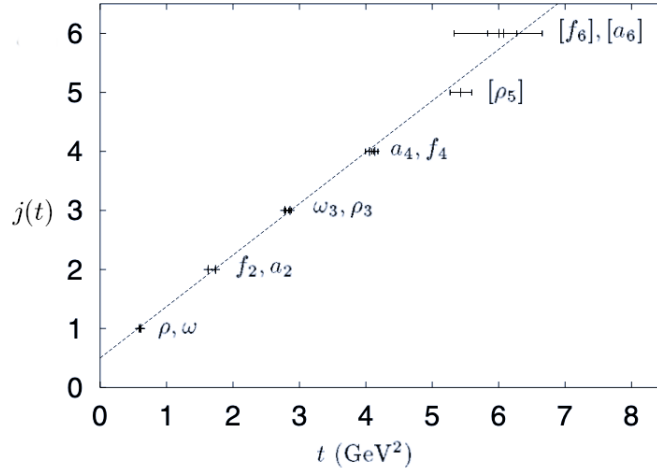
Figure 5.2: Chew-Frautschi plot of four degenerate meson Regge trajectories. All the mesons shown are well established experimentally, except ρ_5, f_6 and a_6. The particle spins are plotted agains their squared masses t. Figure adapted from [52].

5.4.2   Meson Trajectory

Next we discuss how to describe the dynamics of spin J fields in the mesons trajectory. The Chew-Frautschi plot of figure 5.2 shows two important properties of the mesons trajectories. The first is linearity which is usually used to extrapolate from the t-channel physical region to the s-channel scattering region where $t < 0$. That is, we find the best line to the points and use it to find $j(t)$ for $t < m_\rho^2$. In particular, for total cross-sections we are interested in the intercept value at $t = 0$. Another important property is the near degeneracy of the four trajectories $\{f_2(1270), f_4(2050), \cdots\}$, $\{a_2(1320), a_4(2040), \cdots\}$, $\{\omega(780), \omega_3(1670), \cdots\}$ and $\{\rho(770), \rho_3(1690), \cdots\}$.

Using the fact that the four trajectories are nearly degenerate and that we had a very good description of the spectrum for non-singlet and singlet vector mesons (ρ and ω) we will construct the holographic meson trajectory by generalizing the equation of motion of vector mesons to any spin J field in the same trajectory. We will follow the same procedure of last section. Later we will validate our approach by showing how, with just one single parameter, one can simultaneously have a good description of scattering data, the spectrum of the meson trajectory, and an approximately linear Regge trajectory for the mesons.

From the action (5.44) for the vector field in the string frame, one gets the equation of motion

$$\nabla_a \left(e^{-\frac{10}{3}\Phi} V_f \, w_s^2 \, G \, \tilde{g}^{ac} \tilde{g}^{bd} F_{cd} \right) = 0 \,. \tag{5.79}$$

121

In order to simplify the notation, from now on we assume all the warp factors and effective metrics are in the string frame. As a first step to generalize (5.79) we write it as

$$\tilde{g}^{ab}\nabla_a\nabla_b A_\alpha + \left(\frac{\partial_z \tilde{V}}{\tilde{V}G^2} + \left(3\dot{A}\left(\frac{1}{G^2}-1\right) - \frac{\dot{G}}{G^3}\right)\right)e^{-2A}\left(\nabla_z A_\alpha - \nabla_\alpha A_z\right) -$$

$$-\left(1-\frac{1}{G^2}\right)\nabla_\alpha\nabla_\lambda A^\lambda + \left(\frac{\ddot{A}}{G^2}+3\dot{A}^2\right)e^{-2A}A_\alpha = 0\,, \tag{5.80}$$

where $\tilde{V} = e^{-\frac{10}{3}\Phi}V_f w_s^2$. In the conformal limit (pure AdS with constant dilaton and tachyon) the above equation reduces to

$$\left(\nabla^2 - M^2\right)A_\alpha = 0\,, \tag{5.81}$$

with $(LM)^2 = -4$, as expected for a bulk field dual to the current operator $\bar{\psi}\gamma^\mu\psi$ with spin $J = 1$ and protected dimension $\Delta = 3$.

We now propose an equation of motion for the symmetric, traceless and transverse spin J field $h_{a_1\cdots a_J}$ in the meson Regge trajectory. As in the graviton case, we are interested in the TT part $h_{\alpha_1\cdots\alpha_J}^{\mathrm{TT}}$ which are the propagating degrees of freedom that decouple from the other components after decomposing the field in $SO(1,3)$ irreducible representations. We propose the equation

$$\left[\tilde{g}^{ab}\nabla_a\nabla_b + \left(\frac{\partial_z \tilde{V}}{\tilde{V}\,G^2} + 3\dot{A}\left(\frac{1}{G^2}-1\right) - \frac{\dot{G}}{G^3}\right)e^{-2A}\left(\partial_z - (J-1)\dot{A}\right) - \right. \tag{5.82}$$

$$\left. \left(1-\frac{1}{G^2}\right)\nabla_{\alpha_1}\nabla_\lambda - \left(\Delta(\Delta-4)\dot{A}^2 - J\frac{\ddot{A}}{G^2}\right)e^{-2A} + e_m(J-1)e^{-2A}\dot{\tau}^2\right]h_{\alpha_1\cdots\alpha_J}^{\mathrm{TT}} = 0\,.$$

We note that: *i)* this equation reduces to the vector meson equation of motion for $J = 1$; *ii)* in the AdS case the second, third and fifth terms vanish, reducing this equation to the equation of motion of the TT components of spin J fields in AdS; *iii)* Following the same logic as for the fields in the Pomeron trajectory we only included the two-derivative term in $\dot{\tau}^2$ that is compatible with *i)* and *ii)*. Also, as in the case of the Pomeron, the $\Delta(J)$ curve follows from the analytic continuation of the dimension of the exchanged operators and imposing the correct UV asymptotic behaviour of the spin J fields:

$$\Delta(\Delta-4) = -3 + \frac{e^{2A}}{\dot{A}^2}\frac{J^2-1}{\lambda^{\frac{4}{3}}}\,. \tag{5.83}$$

The last term guarantees the correct UV behaviour of the spin J fields given in (5.66), while the first one ensures that the curve passes through the protected point $\Delta = 3$, $J = 1$.

Equation (5.82) can be brought to Schrödinger form by first rewriting it in terms of the u variable defined previously. After that we can write the spin J field as

$$h^{\mathrm{TT}}_{\alpha_1\cdots\alpha_J} = \epsilon_{\alpha_1\cdots\alpha_J} e^{iq\cdot x} \frac{e^{(J-1)A}}{\sqrt{e^{-\frac{10}{3}\Phi} V_f\, w_s^2\, e^A}}\, \psi(u), \tag{5.84}$$

where ψ satisfies the Schrödinger equation

$$-\frac{d^2\psi}{du^2} + V_J(u)\, \psi = t\, \psi. \tag{5.85}$$

The Schrödinger potential is given by

$$V_J(u) = V_V(u) + \left(J^2 - 1\right) e^{2A - \frac{4}{3}\Phi} + (J-1)\left[G^2 \dot{A}^2 - \frac{\dot{A}\dot{G}G + G^2\ddot{A}}{G^2} - e_m G^2 \dot{\tau}^2\right], \tag{5.86}$$

where V_V is the Schrödinger potential of the vector mesons given in (5.23). Here the dots mean derivatives with respect to the u variable. We will denote the eigenvalues of this Schrödinger potential as $t_n(J)$ and the corresponding eigenfunctions as $\psi_n(J,u)$.

The propagator for this spin J field obeys an equation of the type

$$(\mathcal{D}\Pi)_{a_1\cdots a_J, b_1\cdots b_J} = i g_{a_1(b_1}\cdots g_{|a_J|b_J)}\delta_5(x,\bar{x})\, \frac{G}{e^{-\frac{10}{3}\Phi}V_f w_s^2}, \tag{5.87}$$

where $\mathcal{D}$ is a differential operator defined by (5.82). In the Regge limit we will be interested in the components $\Pi_{+\cdots+,-\cdots-}$ and for this particular case

$$\mathcal{D}\Pi_{+\cdots+,-\cdots-} = i\left(-\frac{e^{2A}}{2}\right)^J \delta_5(x,\bar{x})\, \frac{G}{e^{-\frac{10}{3}\Phi}V_f w_s^2}. \tag{5.88}$$

Consider now the integral

$$\int \frac{dw^+ dw^-}{2}\, \Pi_{+\cdots+,-\cdots-} = -i\left(-\frac{1}{2}\right)^J e^{(J-1)(A+\bar{A})} G_J(u,\bar{u},l_\perp), \tag{5.89}$$

that defines the transverse propagator G_J. Applying the operator $\mathcal{D}$ on both sides of this equation and noting that

$$\mathcal{D}\left[e^{(J-1)\left(A+\bar{A}\right)}G_J(u,\bar{u},l_\perp)\right] = e^{(J-1)\left(A+\bar{A}\right)}\mathcal{D}_3 G_J(u,\bar{u},l_\perp), \tag{5.90}$$

where $\mathcal{D}_3$ is the differential operator

$$\mathcal{D}_3 = e^{-2A}\partial_u^2 + e^{-2A}\left(\dot{A} - \frac{10}{3}\dot{\Phi} + 2\frac{w_s'\dot{\Phi}}{w_s} + \frac{\partial_u V_f}{V_f}\right)\partial_u + e^{-2A}\partial_{l_\perp}^2 + \tag{5.91}$$

$$+ (J-1)\,e_m e^{-2A} G^2 \dot{\tau}^2 - \frac{J^2-1}{\lambda^{4/3}} - (J-1)\,e^{-2A}\left[G^2\dot{A}^2 - \frac{\dot{A}\dot{G}G + G^2\ddot{A}}{G^2}\right] ,$$

we conclude that G_J satisfies

$$\mathcal{D}_3\, G_J(u,\bar{u},l_\perp) = -\delta_3(y,\bar{y})\,\frac{G}{e^{-\frac{10}{3}\Phi}V_f w_s^2} , \tag{5.92}$$

where y and $\bar{y}$ are coordinates in transverse space, as defined after (5.73).

To solve (5.92) we consider its homogeneous version and the following Ansatz

$$G_J(u,l_\perp) = \frac{e^{iq\cdot l_\perp}}{\sqrt{e^{-\frac{10}{3}\Phi}V_f w_s^2 e^A}}\,\psi(u) . \tag{5.93}$$

It follows that ψ is a solution of the Schrödinger problem (5.85). Since the eigenfunctions of the Schrödinger potential satisfy $\sum_n \psi_n(u)\psi_n(\bar{u})^* = \delta(u-\bar{u})$, the solution to (5.92) is

$$G_J(u,\bar{u},t) = \left(e^{-\frac{10}{3}\Phi}V_f w_s^2 e^A\right)^{-1/2}\bigg|_u \left(e^{-\frac{10}{3}\Phi}V_f w_s^2 e^A\right)^{-1/2}\bigg|_{\bar{u}} \sum_n \frac{\psi_n(u)\psi_n(\bar{u})}{t_n(J)-t} . \tag{5.94}$$

Thus, the implications of this result for (5.59), (5.60) and (5.62) is that

$$B = -\frac{1}{2}\log\left(e^{-\frac{10}{3}\Phi}V_f w_s^2 e^A\right) , \tag{5.95}$$

when considering exchange of reggeons in the meson trajectory.

5.5 Fit of $\gamma\gamma$, γp and pp total cross-sections in holographic model

In this section we will test the presented phenomenological model for $\gamma\gamma$, γp and pp total cross-sections against the hadronic cross-section data files from the Particle Data Group [129]. These data sets are formed from experimental results obtained by different groups over the last decades. The datasets of $\sigma(\gamma p \to X)$ and $\sigma(pp \to X)$ have cross-section values as a function of the laboratory momentum of an incoming

on-shell photon or proton, respectively. A calculation of the respective center of mass energy $\sqrt{s}$ was performed before starting the fits. We also considered only subsets of data with $\sqrt{s} > 4\,\text{GeV}$ for $\sigma(\gamma\gamma \to X)$, $\sigma(\gamma p \to X)$ and $\sigma(pp \to X)$, yielding 39, 45 and 115 experimental points, respectively.

We find the best set of parameter values α_i by minimising the χ^2 quantity

$$\chi^2 = \sum_{n=1}^{N} \left(\frac{O_k^{\text{pred}}(\alpha_i) - O_k^{\text{exp}}}{\sigma_k} \right)^2 , \tag{5.96}$$

that is, the sum of the weighted difference squared between experimental data and model predicted values where the weight is the inverse of the experimental uncertainty. In our fits the parameters α_i are the couplings $k_{j_n}^{g/m}$ and $\bar{k}_{j_n}^{g/m}$ defined in equations (5.57), (5.61) and (5.63), where the superscript refers the coupling to the pomeron or meson trajectory. Usually a fit is deemed of good quality if the quantity $\chi^2_{\text{d.o.f.}} \equiv \chi^2/(N - N_{\text{par}}) \sim 1$, where N_{par} is the number of parameters α_i to be fitted. In (5.96) O_k represents a generic data point of one or several observables mentioned previously and, usually, σ_k is the experimental uncertainty associated with the measurement. Some data points have uncertainties in the values of s (e.g. in $\gamma\gamma \to X$ that is always the case because it is measured experimentally). To account for this we calculate the total cross-section for $s + \Delta s$ and $s - \Delta s$, and evaluate

$$\sigma_{\text{eff.}} = \max\left(\left| \sigma^{\text{pred.}}(s + \Delta s) - \sigma^{\text{pred.}}(s) \right| , \left| \sigma^{\text{pred.}}(s - \Delta s) - \sigma^{\text{pred.}}(s) \right| \right). \tag{5.97}$$

For these cases $\sigma_k = \sqrt{(\sigma_{\text{exp.}})^2 + (\sigma_{\text{eff.}})^2}$ where $\sigma_{\text{exp.}}$ is the experimental error.

By minimising (5.96) with all the data mentioned above we can find the best values for the potentials parameters e_g and e_m, as well as for the coupling values k_{j_n} and $\bar{k}_{j_n}$ with $n = 1, 2, \cdots$ for each trajectory. We will follow another approach. As shown in [1], the first two trajectories of the gluon kernel can be identified to the hard and soft pomeron trajectories. Here we will fix e_g by demanding that the intercept of the soft pomeron trajectory is 1.08. We also identify the meson trajectory with the first trajectory of the meson kernel and we will fix e_m such that we have agreement with the meson masses of (f_2, a_2), (ρ_3, ω_3) and (f_4, a_4) for $J = 2, 3, 4$, respectively. The numerical values of these parameters were found to be 0.246 and 1.712 for e_g and e_m, respectively. The intercept values obtained from these parameter values can be found in table 5.5 and the leading trajectories are shown in figure 5.3. The corresponding masses of the mesons for $J = 2, 3, 4$ are present in table 5.6. The intercept of the hard pomeron is close to 1.17 which was the one found in the IHQCD model [1,33]. We also note that the intercept of the 4th Pomeron trajectory and of the meson trajectory are very close to 0.55 found in the hadronic cross-section fits of [52].
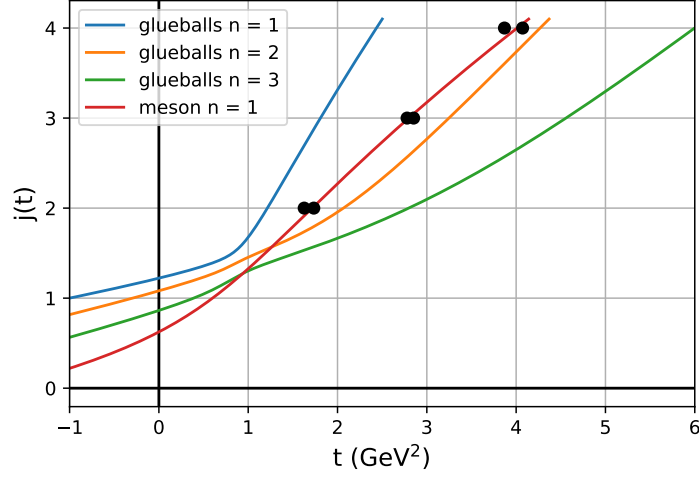
Figure 5.3: The first three Regge trajectories of the gluon kernel and the first meson trajectory of the meson kernel used in the cross section fits. They result from solving the Schrödinger problems (5.77) and (5.86) for several values of J. The black dots are the experimental values of the mesons f_2, a_2, ρ_3, ω_3, f_4 and a_4.

Table 5.5: Values of the intercepts of the first four trajectories of the Pomeron kernel and of the first two trajectories of the meson kernel. These values were obtained with $e_g = 0.246$ and $e_m = 1.712$.

Intercept	Intercept value
j_1^{g}	1.22
j_2^{g}	1.08
j_3^{g}	0.862
j_4^{g}	0.574
j_1^{m}	0.625
j_2^{m}	0.246

Table 5.6: Meson masses in GeV for $J = 2, 3, 4$ obtained for $e_m = 1.712$ and the corresponding experimental values.

meson	mass	predicted mass
$f_2(1270)$ / $a_2(1320)$	1.2755 / 1.3169	1.310
$\rho_3(1690)$ / $\omega_3(1670)$	1.6888 / 1.667	1.673
$f_4(2050)$ / $a_4(2040)$	2.018 / 1.967	2.003

Table 5.7: Values of the couplings for the joint fit of $\sigma\left(\gamma\gamma \to X\right)$, $\sigma\left(\gamma p \to X\right)$ and $\sigma\left(pp \to X\right)$ data. There are 199 experimental points giving a $\chi^2_{d.o.f.} = 0.74$.

γ coupling	value	proton coupling	value
$k^g_{j_1}$	0.0634496	$\bar{k}^g_{j_1}$	2.23798
$k^g_{j_2}$	-0.119512	$\bar{k}^g_{j_2}$	-15.485
$k^g_{j_3}$	0.0180875	$\bar{k}^g_{j_3}$	7.11293
$k^m_{j_1}$	0.043448	$\bar{k}^m_{j_1}$	12.8753

Figure 5.4: Fit of $\sigma(\gamma\gamma \to X)$ vs experimental points. The curve was obtained using the values from table 5.7.

After fixing the kernel parameters e_g and e_m, we fit the total cross-section data by minimising (5.96) with respect to the couplings $k^{g/m}_{j_n}$ and $\bar{k}^{g/m}_{j_n}$. Considering only the first three Pomeron trajectories and the first meson trajectory with the intercepts of table 5.5 we obtain a $\chi^2_{\text{d.o.f.}}$ of 0.74 for a total of 199 experimental points and 8 parameters. The best fit parameters are present in table 5.7 and the comparison of the experimental data with the predictions of the model for these parameters is present in figures 5.4, 5.5 and 5.6. These results show that one does not need to assume a linear meson trajectory after fixing it at $t > 0$ in order to describe total cross-section data, as it is often assumed in the literature, leading to an intercept value of 0.55. The Regge trajectory is convex line, which yields a slightly higher intercept.
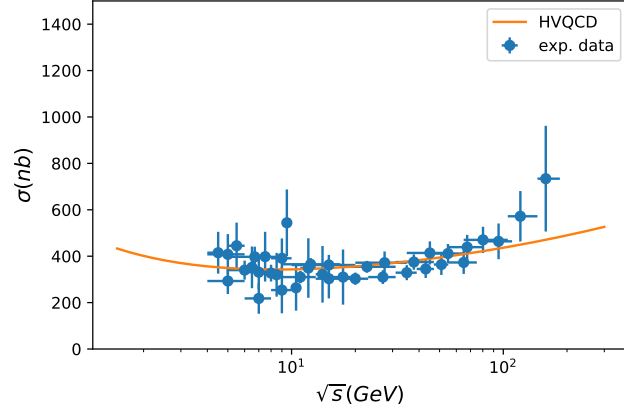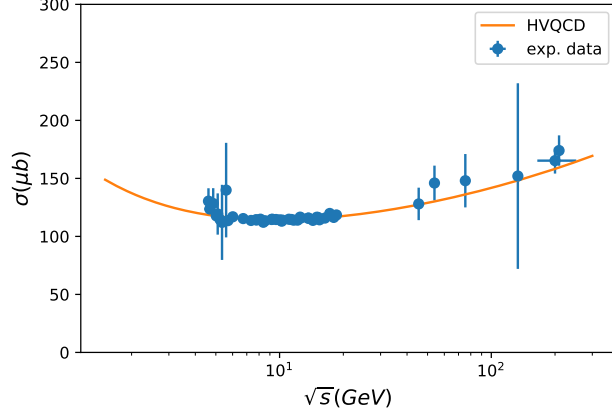
Figure 5.5: Fit of $\sigma(\gamma p \to X)$ vs experimental points. The curve was obtained using the values from table 5.7.
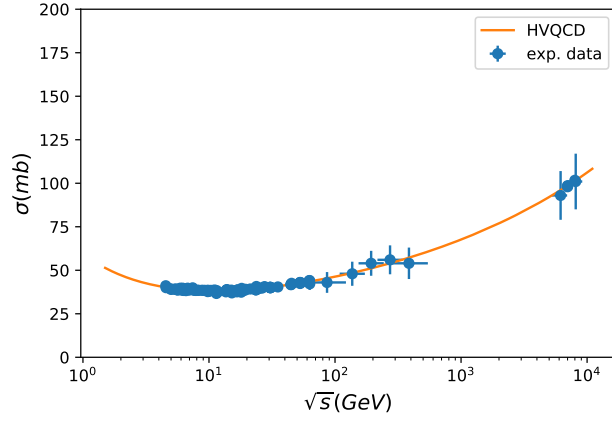
Figure 5.6: Fit of $\sigma(pp \to X)$ vs experimental points. The curve was obtained using the values from table 5.7.

5.6 Conclusions

In this chapter, we studied Regge theory in a full-fledged holographic model (V-QCD), which includes backreaction of quark degrees of freedom to the gluon dynamics in QCD. The main new results can be divided into two categories: Firstly, we made progress with the comparison of the model with QCD data by carrying out a detailed fit of the model parameters to the meson spectrum. Secondly, we developed a scheme to describe higher spin mesons and Regge trajectories in this model, and applied it to analyse the total QCD cross sections of scattering processes having protons and photons in the initial state.

As explained in section 5.2, the holographic model is strongly constrained by the requirement that it agrees with known features of QCD such as confinement, chiral symmetry breaking, asymptotic linearity of meson trajectories, qualitatively correct dependence of the spectrum on the quark mass, correct response to small chemical potential at small temperatures, and asymptotic freedom with correct dimensions (and anomalous dimensions) of the most important operators of QCD at weak coupling. Most of the remaining parameters, which are not determined by such qualitative considerations, amount to tuning of the various potentials of the V-QCD action at intermediate values of the coupling. In this work we have chosen to tune these parameters such that the meson spectrum of the model agrees well with experimental QCD data. The number of fitted parameters is large, because we want to make sure that our Ansatz for the potentials covers essentially all of the parameter space left free by the constraints listed above. However since the effect of all these parameters on the potentials is relatively small, the dependence of the result for the meson masses on the parameters is weak. In other words, one obtains a rather good description of the QCD spectrum for any reasonable values of the parameters, and the task carried out in this chapter is to tune the masses to agree as well with experimental values as possible.

Because here we were mostly interested in the Regge physics, we chose a strategy where we only fitted the meson masses with spins $J = 0$ and $J = 1$, but did not consider other data such as decay constants or thermodynamic potentials. Notice also that we included radial excitations with high masses and these state were fitted with the same weight as the "important" low-lying states such as the pions and the ρ-meson. That is, the fit was tailored for the purpose of studying the Regge physics where reproducing the correct asymptotics of the trajectories is important. It is anyhow interesting that the results of the fit are in good agreement with those obtained in [144] where essentially the same Ansatz was compared to the lattice data for the thermodynamics of Yang-Mills theory and QCD at finite temperature, and in rough agreement with the value of the parameter c of [153, 154] as we explained in section 5.2.4. We also remark that the fit carried out here appears to be more constraining than those carried out in the earlier references: our fit favors $W_0 \approx 2.5$ whereas this parameter was left unconstrained by the comparison to lattice thermodynamics. We obtained a very good fit for the spin 1 and pseudoscalar meson masses. This fit was more extensive than that carried out in the probe limit in the closely related model of [135, 136]. It also compares favourably to work in simpler holographic models and in models inspired by gauge/gravity duality, such as the hard [155, 156] and soft wall models [89], light front holography [157, 158], and the holography inspired stringy hadron model [159, 160].

There are several ways to further develop the holographic model and the fitting procedure in the future. A simple project would be to redo the fit to meson spectrum with the aim of producing a model for all purposes, which would mean to weight more the mesons having low masses and also consider other experimental data relevant for the zero temperature vacuum such as decay constants, the flavor singlet scalar and pseudoscalar states, topological susceptibility, the S-parameter and so on. The potentially challenging issue, which we noticed while doing the fit, is that the scalar meson masses agree poorly with the experimental values. This issue would need to be solved. A more ambitious project would be to carry out a simultaneous comparison of the zero temperature and finite temperature data, i.e. to also include the data for lattice thermodynamics at finite temperature and potentially also at finite magnetic field. Good agreement of the model parameters obtained by fitting the zero and finite temperature data independently suggests that such a project is feasible. As a part of the project, it might make sense to also generalise the model to include flavor dependent quark masses and flavor dependent coupling of the magnetic field to the quarks.

Having fixed the action for the geometry and the actions for scalar and vector mesons through the fit, we proposed the dynamics for the spin J fields dual to the gluon and quark twist two operators. This dynamics is controlled by two parameters that were fixed by making the second Pomeron trajectory intercept to be 1.08 (the known soft-pomeron intercept) and by reproducing quite accurately the masses of the mesons with $J = 2, 3, 4$. We have found that the hard pomeron intercept is close to 1.17 in IHQCD. We also note that the fourth Pomeron trajectory and the leading meson trajectory that we obtained have intercepts close to the meson intercept value of 0.55 commonly found in the literature. Using the first three pomeron trajectories and the first meson trajectory we had a very good fit of the total cross-sections of $\gamma\gamma$, γp and pp scattering. We note here that although our meson intercept is close to 0.55, the corresponding trajectory is non-linear in the $t > 0$ region (see figure 5.3), as it is often assumed. This suggests that the linearity of the trajectory might be at best a very good approximation to obtain an intercept that explains total cross-section data, and not its true shape in this region.

This work can now be extended to other processes like the proton structure functions F_2^{p} and F_L^{p} and the photon structure function F_2^{γ}, as done in [34]. In this model their holographic expressions are given respectively by equations (5.158), (5.159) and (5.155) from the appendix 5.E. From these expressions one can see that: i) the Bjorken x behaviour depends solely on the value of the intercept; and ii) the Q^2

dependence comes from an integral involving the non-normalizable mode of the $U(1)$ gauge field f_Q, functions of the background fields and the normalisable wave functions ψ_n of the pomeron and meson kernels. Having the background fixed, the first two classes of functions are uniquely determined while the ψ_n's might be controlled by phenomenological parameters (similar to e_g and e_f) of the equations of motion of the spin J fields. In this work, with the values of e_g and e_f fixed by the spectrum of higher spin mesons, we may have obtained the correct Bjorken x behaviour, but it is not guaranteed that the wave functions yield the observed dependence of the structure functions on Q^2. Hence, one needs to consider the neglected terms of equation (5.70) in order to get good agreement between our model and data. Of course this involves adding more parameters to these fits, making it harder to find a minimum for the χ^2 function that describes satisfactory all the data being considered. If successful, this would also extend [34] by including also pp total cross-section data in a consistent holographic Regge analysis.

Since this model reproduces well the masses of the towers of ρ and π mesons, one could also test this approach against the Vector Meson Production (VMP) data from HERA with a ρ meson in the final state and to include $\pi^0 p$ total cross-section data. This will introduce extra parameters in this holographic Regge model. In the $\pi^0 p$ total cross-section we could introduce couplings between the pions and the spin J fields of the different trajectories. On the other hand, the VMP data would promote the coupling constants k_J to functions of t since in differential cross-section data we work with more than one value of t. In order to control the amount of parameters to be introduced in this model, it would be interesting to fix the couplings, or the functional form of $k_{j_n(t)}$, to other observables where these couplings might be important. This could be done by first using a theoretical well motivated ansatz for $k_{j_n(t)}$ with some free parameters. These free parameters could then be fixed by the experimental values of decay rates. As an example of this, $k^m_{j_1(m^2_{f_2})}$ and $\Gamma(f_2 \to \gamma\gamma)$ are related through equation (5.48) for the $J = 2$ case.

To describe successfully VMP in this holographic setting we need a better approximation to the proton state than assuming it to be a scalar field. In this work this is sufficient, since the integrals that involve the proton wavefunction are absorbed in the fitting parameters. However, in the VMP case the proton state is in an integrand multiplying wavefunctions of the Pomeron and meson kernel that depend on t. Moreover, having a good model for the proton state could also allow to extend this work directly by including available data of pp differential cross-section data. In holography, baryons are dual to solitons in the bulk and hence the problem is

reduced to the calculations of these solutions [161]. Such solitons have been studied in the literature in the Witten-Sakai-Sugimoto model [162, 163] and in hard-wall models [164, 165]. In the V-QCD model, baryons have so far only been considered by employing an approximation scheme [148],the construction of these soliton solutions is an interesting problem. Such a solution could be a good starting point to model the proton state in holographic Regge theory.

5.A Solving the Equations of Motion

In this appendix we give details on how the equations of motion are solved. It turns out to be convenient to write the resulting equations in terms of A instead of the radial coordinate z. This change of coordinates stretches distances close to the boundary which eases the numerical UV analysis. To implement this one introduces the new variable

$$q(A) = \frac{dz}{dA}\, e^A \, , \tag{5.98}$$

so that the metric reads

$$ds^2 = q^2 dA^2 + e^{2A}\, \eta_{\mu\nu} dx^\mu dx^\nu \, . \tag{5.99}$$

From now on all the background fields will be functions of A and the differential equations we present are all with respect to A being the independent variable.

Yang-Mills Equations of Motion

If we set $x = 0$ we obtain the action of the IHQCD model and hence we are dealing with a pure Yang-Mills theory in the large N_c limit. The equations of motion are then

$$\frac{dq}{dA} = \frac{1}{3}\left(12q - q^3 V_g(\Phi)\right) \, , \tag{5.100}$$

$$\frac{d\Phi}{dA} = -\frac{\sqrt{3}}{2}\sqrt{12 - q^2 V_g(\Phi)} \, . \tag{5.101}$$

The solution of the pure Yang-Mills background is needed in our method for constructing the full V-QCD solution, as we explain below. We will therefore solve this coupled set of differential equations by shooting from the IR to the UV. The coordinate A runs from $-\infty$ to $+\infty$, but naturally we will need to intriduce cutoffs for the numerical solution. We set $A_{\text{IR}} = -150$ and $A_{\text{UVYM}} = 50$ as the lower and upper bound on A. In the IR the geometry ends in an IR singularity of the "good" kind according to the

classification of [142]. At the singularity the warp factor A and the dilaton Φ have the asymptotic forms [97]

$$A_{\mathrm{IR}}(z) = -z^2 + \frac{1}{4}\log(6z^2) - \frac{\log(V_{\mathrm{IR}})}{2} + \frac{23}{24} - \frac{173}{3456z^2} + \mathcal{O}\left(\frac{1}{z^4}\right), \qquad (5.102)$$

$$\Phi_{\mathrm{IR}}(z) = +\frac{3}{2}z^2 - \frac{23}{16} - \log\left(\frac{\alpha_\lambda}{\lambda_0}\right) - \frac{151}{2304z^2} + \mathcal{O}\left(\frac{1}{z^4}\right), \qquad (5.103)$$

as $z \to \infty$. This allows us to determine z_{IRYM} such that $A_{\mathrm{IR}}(z_{\mathrm{IRYM}}) = -150$ and use its numerical value to compute $\Phi(A_{\mathrm{IR}}) = \Phi_{\mathrm{IR}}(z_{\mathrm{IRYM}})$ and $q(A_{\mathrm{IR}}) = e^{A_{\mathrm{IR}}}/\frac{dA_{\mathrm{IR}}}{dz}$ and hence defining boundary conditions to solve equations (5.100) and (5.101). Note that α_λ and V_{IR} determine uniquely both the initial conditions as well as the evolution of the background fields in pure YM.

After we solve the YM equations we can determine $z(A)$ by using equation (5.98). We solve this numerically by taking $z(A_{\mathrm{IRYM}}) = z_{\mathrm{IRYM}}$ as initial condition and at the end we perform the shift $z(A) \to z(A) - z(A_{\mathrm{UVYM}})$ in order to have the UV singularity at $z = 0$.

We finish this section by specifying which algorithms we have used to find the numerical YM background. To compute z_{IRYM} we have used the root finding Van Wijngaarden-Dekker-Brent method described in [166]. The differential equations (5.100) and (5.101) were solved using integrate_const with a Runge-Kutta-Dormand-Prince stepper from the Boost *C++* library.

Solving the equations of motion in the holographic model

The solution of the equations of motion in V-QCD at zero temperature is done in four stages. This is because, as it turns out, the equations of motion are stiff in particular close to the IR singularity. Therefore for the numerical code to be stable, it is better to divide the range of A into region where different kind of approximations can be used that reduce the stiffness problem. In the first two regions we are deep in the IR and the tachyon is decoupled from the other background fields and $q(A)$ so that $\Phi(A)$ obey equations (5.100) and (5.101). In these stages we therefore use the YM background constructed as explained above for the metric and for the dilaton. In the third stage the tachyon will couple to the other background fields until it reaches the UV where it decouples again starting the fourth and last stage of the solution of the EOMs.

As in the YM case we start by first specifying the IR boundary conditions. We first

define $A_{\mathrm{IR}} = -150$, $A_{\mathrm{UVYM}} = 50$, $A_{\mathrm{UVc}} = 100$ and $A_{\mathrm{UVf}} = 1000$. Again we compute z_{IRYM} as in the YM case and we use it to compute $q(A_{\mathrm{IR}})$ and $\Phi(A_{\mathrm{IR}})$ as in YM and $\tau(A_{\mathrm{IR}})$ using the tachyon IR asymptotics

$$\tau \sim \tau_0 \, z^{\tau_c}, \quad \tau_c = \frac{(12 - xW_0) \, \bar{\kappa}_0 a_2}{8 V_{\mathrm{IR}}(a_2 - a_1)} \,, \tag{5.104}$$

where τ_0 is a parameter that is going to be fitted to the spectrum. The constants $\tau_{\mathrm{cut}} = 1000$ and $V_{\mathrm{f\,cut}} = 10^{-8}$ are defined and they mark the end of the first and second stages of the construction of the numerical background, respectively. The difference between the first and the second stage is that in the first stage, the tachyon is so large that nonlinear corrections $\sim 1/\tau^2$ can be ignored in the tachyon equation of motion. In the second stage we need to use the full tachyon equation of motion, while the tachyon remains decoupled (as signalled by the smallness of the tachyon potential, $V_f/V_g < V_{\mathrm{f\,cut}}$).

We start the construction of the background by computing the YM profile of $q(A)$ and $\Phi(A)$ from A_{IR} to A_{UVYM} as explained above. If $\tau_{\mathrm{IR}} > \tau_{\mathrm{cut}}$ the tachyon profile will be given by the solution of the differential equation (linearized at large τ)

$$\frac{d\tau}{dA} = \frac{2q^2 V_{f0} \frac{dV_\tau}{d\tau}}{V_\tau \left(8 V_{f0} \kappa + 2\kappa \frac{dV_{f0}}{d\Phi} \frac{d\Phi}{dA} + V_{f0} \frac{d\kappa}{d\Phi} \frac{d\Phi}{dA} \right)} \,, \tag{5.105}$$

until $\tau < \tau_{\mathrm{cut}}$, marking the end of the first stage. The value of A such that this condition is met is called A_{UV1} The values of q and Φ used are the ones given by YM.

In the second stage we solve the (full) tachyon differential equation

$$\frac{d^2\tau}{dA^2} = \frac{q^2 \frac{V_\tau}{d\tau}}{V_\tau \, \kappa} - 4 \frac{d\tau}{dA} + \frac{d\log q}{dA} \frac{d\tau}{dA} + \frac{\frac{V_\tau}{d\tau}}{V_\tau} \left(\frac{d\tau}{dA} \right)^2 - 4\kappa \frac{\left(\frac{d\tau}{dA} \right)^3}{q^2} - \tag{5.106}$$
$$- \frac{d\log V_{f0}}{d\Phi} \frac{d\tau}{dA} \frac{d\Phi}{dA} - \frac{d\log \kappa}{d\Phi} \frac{d\tau}{dA} \frac{d\Phi}{dA} - \kappa \frac{d\log V_{f0}}{d\Phi} \left(\frac{d\tau}{dA} \right)^3 \frac{\frac{d\Phi}{dA}}{q^2} - \frac{d\kappa}{d\Phi} \frac{d\Phi}{dA} \frac{\left(\frac{d\tau}{dA} \right)^3}{2q^2} \,,$$

from the value of A_{UV1} to A_{UVYM}. Using the profiles of q, Φ and τ we compute A_{UV2} such that $A_{\mathrm{UV1}} < A_{\mathrm{UV2}} < A_{\mathrm{UVYM}}$ and $V_f(\Phi, \tau) = V_{f0}(\Phi) V_\tau(\tau) = V_{\mathrm{f\,cut}} V_g(\Phi)$ are satisfied. This condition marks when the tachyon starts to couple with q and Φ from the IR to the UV.

In the stage where the tachyon is coupled the dynamics of the background fields obeys

$$\frac{dq}{dA} = \frac{4}{9} q \left(\frac{d\Phi}{dA} \right)^2 + x \, q V_f \kappa \frac{\left(\frac{d\tau}{dA} \right)^2}{6 \sqrt{1 + \kappa \left(\frac{d\tau}{q} \right)^2}} \,, \tag{5.107}$$

$$\frac{d^2\Phi}{d^2A} = -\frac{3}{8}q^2\frac{dV_g}{d\Phi} + \frac{9}{\frac{d\Phi}{dA}} + \frac{3}{4}\frac{q^2}{\frac{d\Phi}{dA}}\left(\frac{xV_f}{\sqrt{1+k\frac{\left(\frac{d\tau}{dA}\right)^2}{q^2}}} - V_g\right) - \tag{5.108}$$

$$-5\frac{d\Phi}{dA} + xV_f k\frac{\left(\frac{d\tau}{dA}\right)^2\frac{d\Phi}{dA}}{6\sqrt{1+\kappa\left(\frac{\frac{d\tau}{dA}}{q}\right)^2}} + \frac{4}{9}\left(\frac{d\Phi}{dA}\right)^3 +$$

$$+\frac{3}{8}xq^2\frac{\frac{dV_f}{d\Phi}}{\sqrt{1+\kappa\left(\frac{\frac{d\tau}{dA}}{q}\right)^2}} + \frac{3}{8}x\kappa\left(\frac{d\tau}{dA}\right)^2\frac{\frac{dV_f}{d\Phi}}{\sqrt{1+\kappa\left(\frac{\frac{d\tau}{dA}}{q}\right)^2}} +$$

$$+\frac{3}{16}xV_f\left(\frac{d\tau}{dA}\right)^2\frac{\frac{d\kappa}{d\Phi}}{\sqrt{1+\kappa\left(\frac{\frac{d\tau}{dA}}{q}\right)^2}} ,$$

$$\frac{d^2\tau}{dA^2} = \frac{q^2\frac{dV_\tau}{d\tau}}{V_\tau\kappa} - 4\frac{d\tau}{dA} + \frac{\frac{dV_\tau}{d\tau}}{V_\tau}\left(\frac{d\tau}{dA}\right)^2 - 4\frac{\kappa}{q^2}\left(\frac{d\tau}{dA}\right)^3 + x\kappa V_f(\Phi,\tau)\frac{\left(\frac{d\tau}{dA}\right)^3}{6\sqrt{1+\kappa\left(\frac{\frac{d\tau}{dA}}{q}\right)^2}} -$$

$$-\frac{d\log(V_{f0})}{dA}\frac{d\Phi}{dA}\frac{d\tau}{dA} - \kappa\frac{d\log V_{f0}}{dA}\frac{d\Phi}{dA}\frac{\left(\frac{d\tau}{dA}\right)^3}{q^2} + \frac{4}{9}\left(\frac{d\Phi}{dA}\right)^2\frac{d\tau}{dA} - \frac{d\log(\kappa)}{d\Phi}\frac{d\Phi}{dA}\frac{d\tau}{dA} - \tag{5.109}$$

$$-\frac{1}{2}\frac{d\kappa}{d\Phi}\frac{d\Phi}{dA}\frac{\left(\frac{d\tau}{dA}\right)^3}{q^2} .$$

This is a stiff system of differential equations and for this reason we had used the function integrate_adaptive with the rosenbrock4 stepper from the Boost *C++* library. This system is solved from A_{UV2} to A_{UVc}. The value $A_{\text{UVc}} = 50$ was chosen such that at this point we are in the UV and the tachyon decouples again from q and Φ: this is guaranteed as the tachyon is suppressed exponentially in the UV ($\tau \sim m_q e^{-A}$).

The UV equations of motion are

$$\frac{dq}{dA} = \frac{4}{9}q\left(\frac{\frac{d\lambda}{dA}}{\lambda}\right)^2 , \tag{5.110}$$

$$\frac{d^2\lambda}{dA^2} = -\frac{3}{8}(q\lambda)^2\frac{dV_g}{d\lambda} + 9\frac{\lambda^2}{\frac{d\lambda}{dA}} + \frac{3}{4}\frac{(q\lambda)^2}{\frac{d\lambda}{dA}}\left(xV_{f0}-V_g\right) - 5\frac{d\lambda}{dA} + \tag{5.111}$$

$$+\frac{d\log q}{dA}\frac{d\lambda}{dA} + \frac{\left(\frac{d\lambda}{dA}\right)^2}{\lambda} + \frac{3}{8}x(q\lambda)^2\frac{dV_{f0}}{d\lambda} , \tag{5.112}$$

$$\frac{d^2\tau_n}{dA^2} = 3\tau_n + \frac{e^A q^2\frac{V_\tau}{d\tau}}{V_\tau\kappa} + \tau_n\frac{d\log V_{f0}}{d\lambda}\frac{d\lambda}{dA} + \tau_n\frac{d\lambda}{dA}\frac{d\log\kappa}{d\lambda} - \frac{d\log q}{dA}\tau_n -$$

$$-2\frac{d\tau_n}{dA} - \frac{d\log V_{f0}}{d\lambda}\frac{d\lambda}{dA}\frac{d\tau_n}{dA} - \frac{d\lambda}{dA}\frac{d\tau_n}{dA}\frac{d\log\kappa}{d\lambda} + \frac{d\log q}{dA}\frac{d\tau_n}{dA} , \tag{5.113}$$

where $\tau_n = e^A \tau$. This system is solved from A_{UVc} to A_{UVf}. With the profile of τ_n and λ in this region we can compute an estimate the quark mass m_q through the UV asymptotic formula

$$m_{q\,\text{est}}(A) = \frac{1}{\ell_{\text{UV}}} \tau_n(A) e^{-\tau_{corr}(\lambda(A))}, \tag{5.114}$$

$$\tau_{\text{corr}}(\lambda) = \frac{(-88 + 16x + 27\alpha_\lambda \kappa_1) \log\left(\frac{24\pi^2}{(11-2x)\lambda}\right)}{12x - 66}, \tag{5.115}$$

where ℓ_{UV} is the UV AdS radius. We then obtain the final estimate for the quark mass by evaluating this estimate at two large values, i.e. at $A = A_{\text{UVf}}$ and at $A = A_{\text{UVf}} - 10$ and linearly extrapolating the result to the UV (i.e. $\lambda = 0$) on the $(\lambda, m_{q\,\text{est}})$ -plane. As in the YM case we can determine $z(A)$ by using equation (5.98) and perform the shift $z(A) \to z(A) - z(A_{\text{UVYM}})$ in order to have the UV singularity at $z = 0$.

5.B   EOM and couplings of the $U(1)$ gauge field

In this appendix we start deriving the action of the vector meson sector since the non-normalisable solution of the corresponding equations of motion is dual to the external photon in the boundary. Then, by linearising the action we find the coupling of the $U(1)$ gauge field to the graviton of the bulk theory. All of this is made in the Einstein frame. Since we will be dealing later with calculations on the string frame we will explain how to translate these results to the string frame. Finally we generalise the coupling to the graviton to any spin J field in the graviton's Regge trajectory.

The action of the vector $U(1)$ gauge field

As mentioned previously, for the QCD vacuum we set $A_a^R = 0 = A_a^L$. When we turn on the gauge fields, the flavour action becomes

$$S_f = -\frac{M^3 N_c}{2} \int d^5x \, V_f(\lambda, \tau) \mathbf{Tr}\left[\sqrt{-\det\left((g_{\text{eff}})_{ab} + T_{ab}^L\right)} + \sqrt{-\det\left((g_{\text{eff}})_{ab} + T_{ab}^R\right)}\right],$$

where

$$\begin{aligned}
(g_{\text{eff}})_{ab} &= g_{ab} + \kappa(\lambda)\, \partial_a \tau \partial_b \tau, \\
T_{ab}^L &= w(\lambda)\, F_{ab}^L + \kappa(\lambda)\, D_{(a}\tau D_{b)}\tau - \kappa(\lambda)\, \partial_a \tau \partial_b \tau, \\
T_{ab}^R &= w(\lambda)\, F_{ab}^R + \kappa(\lambda)\, D_{(a}\tau D_{b)}\tau - \kappa(\lambda)\, \partial_a \tau \partial_b \tau.
\end{aligned} \tag{5.116}$$

Here we remember that **Tr** is a trace over the flavour indices while the determinant is computed with respect to the space-time indices. Writing the determinants inside the square roots as

$$\det\left(g_{\text{eff}} + T^{L/R}\right) = \det\left(g_{\text{eff}}\right)\det\left(1 + g_{\text{eff}}^{-1}T^{L/R}\right), \tag{5.117}$$

defining $X^{L/R} = g_{\text{eff}}^{-1}T^{L/R}$ and using the identity

$$\ln\det\left(1 + X^{L/R}\right) = \text{tr}\ln\left(1 + X^{L/R}\right) = \text{tr}X^{L/R} - \frac{1}{2}\text{tr}\left(X^{L/R}\right)^2 + \cdots, \tag{5.118}$$

it follows that

$$\sqrt{\det\left(1 + X^{L/R}\right)} = 1 + \frac{1}{2}\text{tr}\,X^{L/R} - \frac{1}{4}\text{tr}\left(X^{L/R}\right)^2 + \cdots, \tag{5.119}$$

$$\text{tr}\,X^{L/R} = \sum_{a,b}\left(g_{\text{eff}}^{-1}\right)_{ab}T_{ab}^{L/R}, \tag{5.120}$$

$$\text{tr}\left(X^{L/R}\right)^2 = \sum_{a,b,c,d}\left(g_{\text{eff}}^{-1}\right)_{ac}T_{cb}^{L/R}\left(g_{\text{eff}}^{-1}\right)_{bd}T_{da}^{L/R}. \tag{5.121}$$

The expressions for the matrix elements of g_{eff}^{-1} and $T^{L/R}$ are

$$\left(g_{\text{eff}}^{-1}\right)_{zz} = \frac{e^{-2A}}{G^2} \quad, \quad \left(g_{\text{eff}}^{-1}\right)_{\mu\nu} = \eta^{\mu\nu}e^{-2A}, \tag{5.122}$$

$$\left(g_{\text{eff}}^{-1}\right)_{z\mu} = \left(g_{\text{eff}}^{-1}\right)_{\mu z} = 0, \tag{5.123}$$

$$T_{zz}^{L/R} = 0, \tag{5.124}$$

$$T_{z\mu}^{L/R} = -T_{\mu z}^{L/R} = w\left(\lambda\right)\left(\pm\partial_z A_\mu + \partial_z V_\mu\right), \tag{5.125}$$

$$T_{\mu\nu}^{L/R} = 4\kappa\left(\lambda\right)\tau^2 A_\mu A_\nu + w\left(\lambda\right)\left(\pm A_{\mu\nu} + V_{\mu\nu}\right), \tag{5.126}$$

where the vector and axial gauge fields V_a and A_a are linear combinations of the left and right gauge fields

$$V_a = \frac{A_a^L + A_a^R}{2}, \qquad A_a = \frac{A_a^L - A_a^R}{2}, \tag{5.127}$$

in the gauge $V_z = 0 = A_z$, $V_{\mu\nu} = \partial_\mu V_\nu - \partial_\nu V_\mu$ and $A_{\mu\nu} = \partial_\mu A_\nu - \partial_\nu A_\mu$.

From these identities and after some calculations one gets

$$S_f = -\frac{1}{2}M^3 N_c \int d^5x\, V_f(\lambda,\tau)\sqrt{-g_{\text{eff}}}\,\mathbf{Tr}\left[2 + 4e^{-2A}\kappa\left(\lambda\right)\tau^2 A_\mu A^\mu + \right. \tag{5.128}$$

$$\left. + \frac{w\left(\lambda\right)^2 e^{-4A}}{G^2}\left(\partial_z A_\mu \partial_z A^\mu + \partial_z V_\mu \partial_z V^\mu\right) + \frac{1}{2}e^{-4A}w\left(\lambda\right)^2\left(V_{\mu\nu}V^{\mu\nu} + A_{\mu\nu}A^{\mu\nu}\right)\right].$$

The first term is the background term, while the the two other terms can be packed into the actions

$$S_V = -\frac{1}{2} M^3 N_c \mathbf{Tr} \int d^5x \, V_f(\lambda, \tau) \, w(\lambda)^2 G^{-1} e^A \left(\partial_z V_\mu \partial_z V^\mu + \frac{1}{2} G^2 V_{\mu\nu} V^{\mu\nu} \right), \quad (5.129)$$

$$S_A = -\frac{1}{2} M^3 N_c \mathbf{Tr} \int d^5x \, V_f(\lambda, \tau) \, w(\lambda)^2 G^{-1} e^A \Big(\partial_z A_\mu \partial_z A^\mu +$$
$$+ \frac{1}{2} G^2 A_{\mu\nu} A^{\mu\nu} + 4 e^{2A} \frac{\kappa(\lambda) G^2 \tau^2}{w(\lambda)^2} A_\mu A^\mu \Big), \quad (5.130)$$

which are the actions for the Non-singlet Vector and Axial-Vector mesons presented in [98]. The equation (5.129) can still be rewritten as

$$S = -\frac{1}{4} M^3 N_c N_f \int d^5x \sqrt{-g} \, V_f \, w^2 G F_{ab} F^{ab}, \quad (5.131)$$

where here the notation $F_{ab} F^{ab}$ means

$$F_{ab} F^{ab} = \sum_{a,b,c,d} F_{ab} \left(g_{\text{eff}}^{-1} \right)_{ac} \left(g_{\text{eff}}^{-1} \right)_{bd} F_{cd}. \quad (5.132)$$

From Einstein frame to string frame

To compute the action of the $U(1)$ gauge field in the Einstein frame we approximated the square roots of the determinants present in S_f as

$$\sqrt{-\det\left(g_{\text{eff}} + T^{L/R}\right)} = \sqrt{-g_{\text{eff}}} \left[1 + \frac{1}{2} \text{tr} X - \frac{1}{4} \text{tr} X^2 + \frac{1}{8} (\text{tr} X)^2 + \dots \right], \quad (5.133)$$

with $X = g_{\text{eff}}^{-1} T^{L/R}$ for some tensor $T^{L/R}$. The string frame warp factor A_s is related to the Einstein frame warp factor A through $A_s = A + \frac{2}{3}\Phi$. From this it follows that $\sqrt{-g_{\text{eff}}} = e^{-10\Phi/3} \sqrt{-g_{\text{eff}\,s}}$ and the matrix X in the previous equation can be written as $X = g_s^{-1} T_s^{L/R}$ with $T_s^{L/R} = e^{4\Phi/3} T_E^{L/R}$. This implies that

$$\sqrt{-\det\left(g_{\text{eff}} + T^{L/R}\right)} = e^{-10\Phi/3} \sqrt{-\det\left(g_{\text{eff}\,s} + T_s^{L/R}\right)}, \quad (5.134)$$

i.e. S_f in the string frame is obtained by simply substituting the metric by the string frame metric g_s, substituting $\kappa(\lambda)$ and $w(\lambda)$ by $\kappa_s(\lambda) = e^{4\Phi/3}\kappa(\lambda)$ and $w_s(\lambda) = e^{4\Phi/3}w(\lambda)$ and multiplying V_f by the factor $e^{-10\Phi/3}$. The derivation of S_V in the string frame will be formally the same and hence the results equal to the Einstein frame ones but with w_s, κ_s and $e^{-10\Phi/3}V_f$ in place of w, κ and V_f respectively. The action (5.131) in the string frame takes the form

$$S = -\frac{1}{4} M^3 N_c N_f \int d^5x \sqrt{-g_s} e^{-\frac{10}{3}\Phi} V_f \, w_s^2 G F_{ab} F^{ab}. \quad (5.135)$$

Couplings with the spin J fields

We will now determine the gravitational coupling between the $U(1)$ gauge field and the spin J fields in the graviton's Regge trajectory. We first compute the coupling with the graviton and generalise to any even spin J field. All of this is done in the Einstein frame. To find the coupling in the string frame we just substitute the functions w, κ and V_f by w_s, κ_s and $e^{-10\Phi/3}V_f$ respectively, as discussed previously.

Again, we start by writing the square roots of the determinants as

$$\sqrt{-\det g_{\text{eff}}}\left[1 + \frac{1}{2}\text{tr}\left(g_{\text{eff}}^{-1}T^{L/R}\right) - \frac{1}{4}\text{tr}\left(g_{\text{eff}}^{-1}T^{L/R}g_{\text{eff}}^{-1}T^{L/R}\right) + \dots\right]. \tag{5.136}$$

The coupling with the graviton is found by linearising equation (5.136) around the background metric, i.e. $g_{ab} = \bar{g}_{ab} + h_{ab}$. To study the graviton Regge trajectory in our background we need to decompose the metric in $SO(1,3)$ irreducible representations. We will be only interested in the graviton TT components $h_{\alpha\beta}$, satisfying $\partial^\alpha h_{\alpha\beta} = 0$ and $h_\alpha^\alpha = 0$, and also set $h_{z\alpha} = h_{\alpha z} = h_{zz} = 0$.

For our purposes we can ignore the perturbation of $\sqrt{-\det g_{\text{eff}}}$ because it involves only a term proportional to $h = h_a^a = 0$. We will also neglect the terms involving the axial vector mesons A_μ since we are only interested in the coupling of V_μ with the graviton for now. We wish then to compute $\delta\text{tr}\left(g_{\text{eff}}^{-1}T^{L/R}\right)$ and $\delta\text{tr}\left(g_{\text{eff}}^{-1}T^{L/R}g_{\text{eff}}^{-1}T^{L/R}\right)$, where by δ we mean a perturbation relative to the background metric. Using the identity $\delta g_{\text{eff}}^{ab} = -g_{\text{eff}}^{am}g_{\text{eff}}^{bn}h_{mn}$ one can show that

$$\delta\text{tr}\left(g_{\text{eff}}^{-1}T^{L/R}\right) = -g_{\text{eff}}^{am}g_{\text{eff}}^{bn}h_{mn}T_{ab}^{L/R}, \tag{5.137}$$

$$\delta\text{tr}\left(g_{\text{eff}}^{-1}T^{L/R}g_{\text{eff}}^{-1}T^{L/R}\right) = -2g_{\text{eff}}^{am}g_{\text{eff}}^{bn}g_{\text{eff}}^{cd}T_{bc}^{L/R}T_{da}^{L/R}h_{mn}. \tag{5.138}$$

Using the expressions for the matrix elements of g_{eff}^{-1} and $T^{L/R}$ we get

$$\delta\text{tr}\left(g_{\text{eff}}^{-1}T^{L/R}\right) = 0, \tag{5.139}$$

$$\delta\text{tr}\left(g_{\text{eff}}^{-1}T^{L/R}g_{\text{eff}}^{-1}T^{L/R}\right) = 2e^{-6A}w(\lambda)^2 h^{\mu\nu}\left(V_{\mu\sigma}\eta^{\sigma\rho}V_{\nu\rho} + \frac{1}{G^2}\partial_z V_\mu \partial_z V_\nu\right). \tag{5.140}$$

Hence the coupling between the vector $U(1)$ gauge field and the graviton is given by

$$\frac{M^3 N_c N_f}{2}\int d^5x\sqrt{-\det g_{\text{eff}}}V_f(\lambda,\tau)e^{-6A}w(\lambda)^2 h^{\mu\nu}\left(V_{\mu\sigma}\eta^{\sigma\rho}V_{\nu\rho} + \frac{1}{G^2}\partial_z V_\mu \partial_z V_\nu\right), \tag{5.141}$$

or simply

$$\frac{M^3 N_c N_f}{2}\int d^5x\sqrt{-g}\,G\,V_f(\lambda,\tau)w(\lambda)^2 g^{cm}g^{dn}g_{\text{eff}}^{ab}F_{ac}^V F_{bd}^V h_{mn}. \tag{5.142}$$

In the string frame this coupling takes the form

$$\frac{M^3 N_c N_f}{2} \int d^5 x \sqrt{-g_s}\, G\, e^{-\frac{10}{3}\Phi} V_f(\lambda, \tau)\, w_s(\lambda)^2 g_s^{cm} g_s^{dn} g_{\text{eff}\,s}^{ab} F_{ac}^V F_{bd}^V h_{mn}^s\,. \tag{5.143}$$

We now generalise this coupling to the case of an interaction between the gauge field and a symmetric, transverse and traceless spin J field, $h_{a_1 \cdots a_J}$. The pomeron trajectory includes such higher spin fields of even J. Again there are several possibilities, but we shall focus on the simplest extension of the graviton coupling considered above. For a spin J field we take the coupling

$$k_J \int d^5 x \sqrt{-g_s}\, G\, e^{-\frac{10}{3}\Phi} V_f(\lambda, \tau)\, w_s(\lambda)^2 g_{\text{eff}\,s}^{ab} F_{ac}^V \nabla_{a_1} \ldots \nabla_{a_{J-2}} F_{bd}^V h^{cda_1 \ldots a_{J-2}}\,. \tag{5.144}$$

We note that the transverse condition of the spin J field $h_{a_1 \cdots a_J}$ guarantees that this term is unique up to dilaton and tachyon derivatives.

We now consider the coupling between the external photon states with the bulk spin J fields dual to the spin J twist two operators made of quark bilinears. To determine the coupling to any spin J in this trajectory we could proceed analogously with the case of the graviton's Regge trajectory. In the case of the coupling with the meson trajectory, one could first determine the coupling between the non-normalizable mode dual to the photon with the the ρ meson states and generalise the result to higher spin J fields. To do this we attempted to expand the DBI action to cubic order in the fluctuations and keep only the terms with three vector gauge fields $V_a V_b V_c$. We start by writing

$$\sqrt{\det(g_{\text{eff}} + T^{L/R})} = \sqrt{\det g_{\text{eff}}}\, \exp\left[\frac{1}{2} \text{Tr} \log\left(1 + X^{L/R}\right)\right]\,. \tag{5.145}$$

If we use the power series expansion of the exponential and of the logarithmic function we get

$$\sqrt{-\det g_{\text{eff}}}\left[1 - \frac{1}{4} \text{Tr}\left(X^{L/R}\right)^2 + \frac{1}{6} \text{Tr}\left(X^{L/R}\right)^3\right]\,, \tag{5.146}$$

where we have dropped terms involving products of $\text{Tr} X^{L/R}$ because they contribute only to axial gauge fields A_a. The quadratic term leads to the action of the quadratic fluctuations of the vector gauge field and hence the coupling $V_a V_b V_c$ if exists must be contained on $\text{Tr}\left(X^{L/R}\right)^3$. That is, we evaluated the expression

$$\text{Tr}\left(X^{L/R}\right)^3 = \sum_{i,k,j,l,m,n} \left(g_{\text{eff}}^{-1}\right)_{ik} \left(g_{\text{eff}}^{-1}\right)_{ln} \left(g_{\text{eff}}^{-1}\right)_{jm} T_{kj}^{L/R} T_{ml}^{L/R} T_{ni}^{L/R}\,, \tag{5.147}$$

which contains no coupling of the form $V_a V_b V_c$.

Another approach is to find the coupling between the vector gauge field with the bulk field dual to the f_2 meson and extrapolate to all the other spin J fields in the meson trajectory. In [167] the tensor meson f_2 state is the first Kaluza-Klein mode of a bulk spin-2 h_{ab} field that has the same equation of motion as the graviton in AdS_5. The coupling of f_2 to the photon is also the same as the one between a graviton and a bulk gauge field in AdS_5. The geometry is basically AdS_5 with a wall whose position is fixed by the mass of the ρ meson. After this they are able to predict not only the mass of f_2 but also the decay width $\Gamma(f_2 \to \gamma\gamma)$. f_2 also has the same quantum numbers of the tensor glueballs $J^{PC} = 2^{++}$ which are the normalisable modes associated with the graviton's equation of motion. For these reasons, in this work, we will assume that the coupling of the $U(1)$ gauge field with the f_2 meson is the same as the coupling with the graviton and hence, in general, the coupling of any bulk spin J field in the meson trajectory is also given by equation (5.144).

5.C pp scattering

In this appendix we will present the computation for the total cross-section of pp scattering. The steps of the computation are the same as in the case of γp show in the main text.

The scattering amplitude for spin J exchange between two incoming scalar fields $\Upsilon^{(1)} \sim e^{ik_1 \cdot x}$ and $\Upsilon^{(2)} \sim e^{ik_2 \cdot x}$ is

$$\mathcal{A}_J = \left(\bar{k}_J\right)^2 \int d^5x \, d^5\bar{x} \sqrt{-g}\sqrt{-\bar{g}} \, e^{-\Phi-\bar{\Phi}} \left(\Upsilon_1 \partial_-^J \Upsilon_3\right) \Pi^{-\cdots-,+\cdots+}(x,\bar{x}) \left(\bar{\Upsilon}_2 \bar{\partial}_+^J \bar{\Upsilon}_4\right),$$
(5.148)

where it was taken into account that the kinematics (5.42) implies that in the Regge limit the component $\Pi^{-,\cdots-,+\cdots+}$ dominates. Lowering the indices of the spin J propagator, making the change of variable $w = x - \bar{x}$ and using the identity

$$\int d^2 l_\perp e^{-iq_\perp \cdot l_\perp} \int \frac{dw^+ dw^-}{2} \Pi_{+\cdots+,-\cdots-}(x,\bar{x}) = -\frac{i}{(-2)^J} e^{(J-1)(A+\bar{A})} G_J(z,\bar{z},t), \quad (5.149)$$

after some algebra the scattering amplitude can be rewritten as

$$\mathcal{A}_J = -iV \frac{\bar{k}_J^2}{2^J} s^J \int dz \, d\bar{z} \, e^{4(A+\bar{A})} e^{-J(A+\bar{A})} e^{-\Phi-\bar{\Phi}} |v_1|^2 |v_2|^2 G_J(z,\bar{z},t). \quad (5.150)$$

As in the $\gamma^* p$ case, in order to get the total amplitude we need to sum over the spin J fields with $J \geq J_{min}$, where J_{min} is the minimal spin in the corresponding Regge

trajectory. Then we can apply a Sommerfeld-Watson transform

$$\frac{1}{2} \sum_{J \geq J_{min}} \left(s^J + (-s)^J \right) \frac{\mathcal{A}_J}{s^J} = -\frac{\pi}{2} \int \frac{dJ}{2\pi i} \frac{s^J + (-s)^J}{\sin \pi J} \frac{\mathcal{A}_J}{s^J}, \qquad (5.151)$$

where we are assuming the analytic continuation of the scattering amplitude $\mathcal{A}_J$ to the complex J-plane. Deforming the J-plane integral and catching all the poles $J = j_n(t)$ defined by $t_n(J) = t$ we get

$$\mathcal{A} = \frac{\pi}{2} \sum_n \frac{\bar{k}_{j_n}^2}{2^{j_n}} s^{j_n} \left[i + \cot\left(\frac{\pi j_n}{2}\right) \right] \frac{dj_n}{dt} \left| \int dz \, e^{-(j_n - 4)A} |v_1|^2 e^{-\Phi} e^B \psi_n(z) \right|^2. \qquad (5.152)$$

In the scattering domain of $t < 0$ these poles are in the real axis for $J < J_{min}$. This procedure yields equations (5.62) and (5.63).

5.D $\quad \gamma^* \gamma$ processes

In this section we derive the holographic expressions for F_2^γ and $\sigma(\gamma\gamma \to X)$ in the context of Holographic QCD in the Veneziano limit. We will consider the photon structure function F_2^γ and the total cross-section $\sigma(\gamma\gamma \to X)$. Like in the case of the proton structure function F_2^p the photon structure function F_2^γ is related to the transverse and longitudinal total cross-sections of $\gamma^* \gamma$ scattering by

$$F_2^\gamma = \frac{Q^2}{4\pi^2 \alpha} \left(\sigma_T^{\gamma^* \gamma} + \sigma_L^{\gamma^* \gamma} \right). \qquad (5.153)$$

The calculation of the forward scattering amplitude for $\gamma^* \gamma$ is the same as in $\gamma^* p$ scattering except that the external state in the Witten diagram of figure 5.1 is an on-shell photon. This means that the definition of $\text{Im}_n^{\gamma\gamma}$ should be proportional to $k_{j_n}^2$ instead of $k_{j_n} \bar{k}_{j_n}$ and the integral appearing in it should be

$$\int d\bar{u} \, e^{-(j_n - 2)\bar{A}} e^{-\frac{10}{3}\bar{\Phi}} \bar{V}_f \, \bar{w}_s^2 \, e^{\bar{B}} \psi_n(\bar{u}). \qquad (5.154)$$

Then, the holographic expressions for F_2^γ is

$$F_2^\gamma \left(x, Q^2 \right) = \sum_n \frac{\text{Im} g_n^{\gamma\gamma}}{4\pi^2 \alpha} Q^{2j_n} x^{1-j_n} \int du \, e^{-(j_n - 2)A} e^{-\frac{10}{3}\Phi} V_f \, w_s^2 \left(f_Q^2 + \frac{\partial_u f_Q^2}{Q^2} \right) e^B \psi_n(u),$$

$$(5.155)$$

while the holographic expression for $\sigma(\gamma\gamma \to X)$ is (5.60) and the definition of $g_n^{\gamma\gamma}$ is given by (5.61).

5.E Holographic structure functions

The forward scattering amplitude for $\gamma^* p$ scattering is given by equation (5.56). That equation was obtained summing the contributions of the transverse and longitudinal polarisations of the off-shell photon. In particular the term with f_Q^2 is the contribution from transverse polarisations while the term $\dot{f}_Q^2$ is the contribution for the longitudinal polarisation.

The proton structure functions F_2^p and F_L^p are related to the transverse and longitudinal total cross-sections of the process $\gamma^* p$ by

$$F_2\left(x, Q^2\right) = \frac{Q^2}{4\pi^2\alpha}\left(\sigma_T^{\gamma^* p} + \sigma_L^{\gamma^* p}\right),\tag{5.156}$$

$$F_L\left(x, Q^2\right) = \frac{Q^2}{4\pi^2\alpha}\sigma_L^{\gamma^* p}.\tag{5.157}$$

Using the optical theorem and the last relations one finds the contribution of the holographic expressions to the structure functions are

$$F_2\left(x, Q^2\right) = \sum_n \frac{\mathrm{Im}g_n^{\gamma p}}{4\pi^2\alpha}\, Q^{2j_n}x^{1-j_n}\int du\, e^{-(j_n-2)A}e^{-\frac{10}{3}\Phi}\, V_f\, w_s^2\left(f_Q^2 + \frac{\partial_u f_Q{}^2}{Q^2}\right)e^B\psi_n(u),\tag{5.158}$$

$$F_L\left(x, Q^2\right) = \sum_n \frac{\mathrm{Im}g_n^{\gamma p}}{4\pi^2\alpha}\, Q^{2j_n}x^{1-j_n}\int du\, e^{-(j_n-2)A}e^{-\frac{10}{3}\Phi}\, V_f\, w_s^2\partial_u f_Q{}^2 Q^2\, e^B\psi_n(u),\tag{5.159}$$

where the definition of $g_n^{\gamma p}$ is the one of equation (5.57). The function B will depend on whether the spin J fields belong to the pomeron or meson trajectory.

The structure function F_2^p is, as expected, related to the total cross-section $\sigma(\gamma p \to X)$ through

$$\sigma(\gamma p \to X) = 4\pi^2\alpha \lim_{Q^2 \to 0}\frac{F_2\left(x, Q^2\right)}{Q^2}.\tag{5.160}$$

6

Conclusions

We have reached the final chapter of this thesis. Here I would like to make a summary of its contents and future work directions.

In this thesis we have explored Pomeron physics in holographic bottom up models of QCD. In chapters 2, 3 and 4 we have used a model with only gluon degrees of freedom as our background, while in chapter 5 we considered its generalization with quark degrees of freedom. In both cases, the starting point is to fix the backgrounds by the spectrum of known QCD states. Then, we propose equations of motion for the bulk fields dual to the spin J fields of the Pomeron trajectory by deforming the well known spin J field equation in AdS. Of course, holographic expressions for the observables are also computed.

In [1], by studying the proton structure function $F_2(x, Q^2)$ data, such approach turned out to be a concrete realization of the idea that the Soft and Hard pomeron are part of the same object. In chapter 2 we extended those results by including the longitudinal proton structure function $F_L(x, Q^2)$ and a different coupling between the spin J fields of the graviton's Regge trajectory and the $U(1)$ gauge field dual to the hadronic current in the boundary. This study was motivated by the fact that in AdS there are only two possible couplings between such fields, but after conformal symmetry is broken more complex structures are allowed. We have considered a specific coupling in order to study the contribution of additional complex structures to DIS data. We showed that it does not lead to significant improvements in the joint description of F_2 and F_L data.

The proton observables F_2 and F_L are related to polarized cross-sections of $\gamma^* p$ scattering. In chapter 3 we extended the applicability of the model to $\gamma^* \gamma$ scattering and considered the $Q \to 0$ limit of $\gamma^* p$ scattering. One of the remarkable results

144

of this chapter is that once γ^*p processes fix the kernel of the Pomeron, we can achieve excellent joint fits of F_2^γ and $\sigma(\gamma\gamma \to X)$ data. The consistency of this result was checked by performing a global fit where all the processes are included and all the parameters vary. In the literature we find a large amount of effort to tune the parameters of a holographic model using data from a specific observable. But we never see the cross-validation of that model using data from processes that were not used to fit it. To the best of our knowledge, this chapter was the first work where this was first achieved. After fixing the boundary condition at $x = 10^{-2}$, we have also managed to reproduce the low x evolution of the gluonic PDFs $xg(x, Q^2)$ by using an approximate NLO QCD expression that relates F_2, F_L and $xg(x, Q^2)$. However, some tension was found for $Q^2 = 100 \text{ GeV}^2$, signalling that our model is incomplete.

The compute the observables analysed in chapters 2 and 3 we studied the holographic scattering amplitude for Mandelstam $t = 0$. We would like to explore the possibility of extending this model for the scattering region $t < 0$. With this in mind, in chapter 4 we have made a global fit with total cross-section and differential cross-section data from the DVCS process. An essential step towards it was an ansatz for the product of the relevant t-dependent gravitational couplings with an integral involving the holographic proton state. Although we reached an excellent fit for the DVCS data alone, we were not able to achieve a joint fit involving the proton structure function F_2 data included. This means that a better ansatz for the t-dependence of the couplings, or actually performing the integral involving the proton external state, may lead to the inclusion of DVCS data in a global fit with the processes considered in chapter 3.

In chapter 5 we studied Regge theory in a background with gluon and quarks degrees of freedom with backreaction included. The setup consists of a metric coupled to dilaton and tachyon fields whose dynamics is governed by the Einstein-Dilaton and DBI actions. These actions contain potentials that are constrained by perturbative QCD in UV and by known QCD features in the IR. For intermediate scales the functions the shape of the potentials is determined by a fit to the meson spectrum. This fit yielded very good results for the spin one and pseudoscalar mesons, with most deviations around or smaller 1% and some isolated states with $\gtrsim 10\%$. However, there is some tension with the scalar meson sector which generally is difficult to reproduce in holography and has contributions from four quark states. Another interesting result of this fit is that the parameter values are within 10% from the values one obtains when fitting the model to data from lattice QCD thermodynamics. This suggests that in the future it might be possible to do a fit with both the meson spectrum at zero temperature and the data for lattice thermodynamics at finite temperature and

potentially also at finite magnetic field. After fixing our background, we proposed the dynamics for the spin J fields dual to the gluon and quark twist two operators. The dynamics depends on two parameters that were fixed by the known value of the soft pomeron intercept and by reproducing very well the masses of the mesons with $J = 2, 3, 4$. We have found that the fourth Pomeron trajectory and the first meson trajectory have intercepts very close to the meson intercept value found in the literature. In particular, the meson trajectory derived from this holographic model is non-linear in the $t > 0$ region. Using the first three Regge trajectories and the leading meson trajectory we obtain an excellent fit of the total cross-sections of $\gamma\gamma$, γp and pp scattering. What we learn form this is that the assumed linearity of the meson trajectory is at best a very good approximation to compute an intercept that describes total cross-section data.

The results of this thesis would be impossible to obtain without computer programming. The code used to derive the results of this thesis is available at:

https://github.com/artur-amorim/gggpScatteringIHQCD
https://github.com/artur-amorim/PomeronHVQCD
https://github.com/rcarcasses/HQCD-P

By releasing our code publicly anyone can contribute to it or spot potential mistakes. This also makes it easy for anyone to reproduce the contents of this thesis in an age where reproducibility and testability of scientific results became a widespread problem.

We would like now to discuss a sequence of steps to achieve a more complete holographic Regge theory of QCD. In chapter 3 we mentioned that including quarks is important to have a better description of the gluon PDFs at higher values of Q^2. The starting point would be to extend the work in the previous chapter to fit the proton structure functions F_2, F_L. As discussed before, one would need to consider the neglected terms of equation (5.70) in order to have the correct low-x and Q^2 behaviour of these structure functions. Because of the additional parameters it gets harder to find a global minimum for the χ^2 statistic but we hope that with better search algorithms or code optimisation this might become a feasible task. Of course, the other possibility for the the gluon PDFs would be to use holography to compute the Wilson loops that appear in their non-perturbative definition. Another issue is the computation of the gluon PDF uncertainties. In this thesis we have performed χ^2 fits which mean that we are assuming that the experimental points follow a normal distribution and that they are uncorrelated. These experimental correlations change the computation of the χ^2 and should be addressed in the future, since neglecting

them leads to an underestimation of the gluon PDF uncertainties.

After achieving such milestone one can immediately also include the F_2^γ structure function reaching the stage of chapter 3 plus the total cross-section data of pp scattering. We have tried to include $\sigma(pp \to X)$, in the fits of that chapter but we could not find consistent results due to the fixed first four Pomeron intercepts values. However, in chapter 5 it was possible to include it with the total-cross sections of $\gamma\gamma$ and γp scattering due to "better" intercept values. After this step we have a successful holographic Regge theory for observables measured at Mandelstam $t = 0$.

The next step would be to extend the model to observables at $t < 0$. As discussed in chapter 4, this would need a better ansatz for the function $H(J)$ discussed there as well the knowledge of the holographic external state of the proton. With the answers to these problems one can consider to add DVCS data to the fit. Another processs that can be added is ρ meson production and $\sigma(\pi p \to X)$, since we have a good description of the towers of ρ and π mesons. The solution of these same issues would also allow to add the pp differential cross-section data. One could also consider other vector meson prodution processes (like J/ψ) after one underdstands how to identify them in the context of this model. All these steps are excinting on its own and having made each of them would result in far reaching holographic Regge theory of QCD. We hope this stage can be achieved one day. This thesis ends here.

References

[1] Alfonso Ballon-Bayona, Robert Carcassés Quevedo, and Miguel S. Costa. Unity of pomerons from gauge/string duality. *JHEP*, 08:085, 2017.

[2] A. Donnachie and P. V. Landshoff. Total cross-sections. *Phys. Lett. B*, 296:227–232, 1992.

[3] Victor S. Fadin, E. A. Kuraev, and L. N. Lipatov. On the Pomeranchuk Singularity in Asymptotically Free Theories. *Phys. Lett. B*, 60:50–52, 1975.

[4] E. A. Kuraev, L. N. Lipatov, and Victor S. Fadin. The Pomeranchuk Singularity in Nonabelian Gauge Theories. *Sov. Phys. JETP*, 45:199–204, 1977.

[5] I. I. Balitsky and L. N. Lipatov. The Pomeranchuk Singularity in Quantum Chromodynamics. *Sov. J. Nucl. Phys.*, 28:822–829, 1978.

[6] H. Kowalski, L. N. Lipatov, D. A. Ross, and G. Watt. Using HERA Data to Determine the Infrared Behaviour of the BFKL Amplitude. *Eur. Phys. J. C*, 70:983–998, 2010.

[7] Juan Martin Maldacena. The Large N limit of superconformal field theories and supergravity. *Int. J. Theor. Phys.*, 38:1113–1133, 1999.

[8] Richard C. Brower, Joseph Polchinski, Matthew J. Strassler, and Chung-I Tan. The Pomeron and gauge/string duality. *JHEP*, 12:005, 2007.

[9] C. A. Ballon Bayona, Henrique Boschi-Filho, and Nelson R. F. Braga. Deep inelastic scattering from gauge string duality in the soft wall model. *JHEP*, 03:064, 2008.

[10] Lorenzo Cornalba and Miguel S. Costa. Saturation in Deep Inelastic Scattering from AdS/CFT. *Phys. Rev. D*, 78:096010, 2008.

[11] B. Pire, C. Roiesnel, L. Szymanowski, and S. Wallon. On AdS/QCD correspondence and the partonic picture of deep inelastic scattering. *Phys. Lett. B*, 670:84–90, 2008.

[12] Javier L. Albacete, Yuri V. Kovchegov, and Anastasios Taliotis. DIS on a Large Nucleus in AdS/CFT. *JHEP*, 07:074, 2008.

[13] Richard C. Brower, Marko Djuric, and Chung-I Tan. Saturation and Confinement: Analyticity, Unitarity and AdS/CFT Correspondence. In *38th International Symposium on Multiparticle Dynamics*, pages 140–145, 2009.

[14] E. Levin, J. Miller, B. Z. Kopeliovich, and Ivan Schmidt. Glauber-Gribov approach for DIS on nuclei in N=4 SYM. *JHEP*, 02:048, 2009.

[15] Jian-Hua Gao and Bo-Wen Xiao. Polarized Deep Inelastic and Elastic Scattering From Gauge/String Duality. *Phys. Rev. D*, 80:015025, 2009.

[16] Yoshitaka Hatta, Takahiro Ueda, and Bo-Wen Xiao. Polarized DIS in N=4 SYM: Where is spin at strong coupling? *JHEP*, 08:007, 2009.

[17] Yuri V. Kovchegov, Zhun Lu, and Amir H. Rezaeian. Comparing AdS/CFT Calculations to HERA F(2) Data. *Phys. Rev. D*, 80:074023, 2009.

[18] E. Avsar, E. Iancu, L. McLerran, and D. N. Triantafyllopoulos. Shockwaves and deep inelastic scattering within the gauge/gravity duality. *JHEP*, 11:105, 2009.

[19] Lorenzo Cornalba, Miguel S. Costa, and Joao Penedones. Deep Inelastic Scattering in Conformal QCD. *JHEP*, 03:133, 2010.

[20] Fabio Dominguez. Particle production in DIS off a shockwave in AdS. *JHEP*, 09:007, 2010.

[21] Lorenzo Cornalba, Miguel S. Costa, and Joao Penedones. AdS black disk model for small-x DIS. *Phys. Rev. Lett.*, 105:072003, 2010.

[22] M. A. Betemps, V. P. Goncalves, and Joao Thiago de Santana Amaral. Diffractive deep inelastic scattering in an AdS/CFT inspired model: A phenomenological study. *Phys. Rev. D*, 81:094012, 2010.

[23] Jian-Hua Gao and Zong-Gang Mou. Polarized Deep Inelastic Scattering Off the Neutron From Gauge/String Duality. *Phys. Rev. D*, 81:096006, 2010.

[24] Yuri V. Kovchegov. R-Current DIS on a Shock Wave: Beyond the Eikonal Approximation. *Phys. Rev. D*, 82:054011, 2010.

[25] E. Levin and I. Potashnikova. Inelastic processes in DIS and N=4 SYM. *JHEP*, 08:112, 2010.

[26] Richard C. Brower, Marko Djuric, Ina Sarcevic, and Chung-I Tan. String-Gauge Dual Description of Deep Inelastic Scattering at Small-x. *JHEP*, 11:051, 2010.

[27] Miguel S. Costa and Marko Djuric. Deeply Virtual Compton Scattering from Gauge/Gravity Duality. *Phys. Rev. D*, 86:016009, 2012.

[28] Miguel S. Costa, Marko Djurić, and Nick Evans. Vector meson production at low x from gauge/gravity duality. *JHEP*, 09:084, 2013.

[29] Richard C. Brower, Marko Djuric, and Chung-I Tan. Diffractive Higgs Production by AdS Pomeron Fusion. *JHEP*, 09:097, 2012.

[30] Neil Anderson, Sophia K. Domokos, Jeffrey A. Harvey, and Nelia Mann. Central production of η and η? via double Pomeron exchange in the Sakai-Sugimoto model. *Phys. Rev. D*, 90(8):086010, 2014.

[31] Richard Nally, Timothy G. Raben, and Chung-I Tan. Inclusive Production Through AdS/CFT. *JHEP*, 11:075, 2017.

[32] Alfonso Ballon-Bayona, Robert Carcassés Quevedo, Miguel S. Costa, and Marko Djurić. Soft Pomeron in Holographic QCD. *Phys. Rev. D*, 93:035005, 2016.

[33] Artur Amorim, Robert Carcassés Quevedo, and Miguel S. Costa. Nonminimal coupling contribution to DIS at low x in Holographic QCD. *Phys. Rev. D*, 98(2):026016, 2018.

[34] Artur Amorim and Miguel S. Costa. $\gamma^*\gamma$ and γ^*p scattering in improved holographic QCD. *Phys. Rev. D*, 103(2):026007, 2021.

[35] Y. Hatta, E. Iancu, and A. H. Mueller. Deep inelastic scattering at strong coupling from gauge/string duality: The Saturation line. *JHEP*, 01:026, 2008.

[36] Yoshitaka Hatta. Relating e+ e- annihilation to high energy scattering at weak and strong coupling. *JHEP*, 11:057, 2008.

[37] Richard Brower, Marko Djuric, and Chung-I Tan. Elastic and Diffractive Scattering after AdS / CFT. In *13th International Conference on Elastic and*

Diffractive Scattering (Blois Workshop): Moving Forward into the LHC Era, pages 67–74, 11 2009.

[38] Sophia K. Domokos, Jeffrey A. Harvey, and Nelia Mann. The Pomeron contribution to p p and p anti-p scattering in AdS/QCD. *Phys. Rev. D*, 80:126015, 2009.

[39] Sophia K. Domokos, Jeffrey A. Harvey, and Nelia Mann. Setting the scale of the p p and p bar p total cross sections using AdS/QCD. *Phys. Rev. D*, 82:106007, 2010.

[40] Alexander Stoffers and Ismail Zahed. Holographic Pomeron: Saturation and DIS. *Phys. Rev. D*, 87:075023, 2013.

[41] Ezequiel Koile, Nicolas Kovensky, and Martin Schvellinger. Hadron structure functions at small x from string theory. *JHEP*, 05:001, 2015.

[42] Ezequiel Koile, Nicolas Kovensky, and Martin Schvellinger. Deep inelastic scattering cross sections from the gauge/string duality. *JHEP*, 12:009, 2015.

[43] David Jorrin, Martin Schvellinger, and Nicolas Kovensky. Deep inelastic scattering off scalar mesons in the 1/N expansion from the D3D7-brane system. *JHEP*, 12:003, 2016.

[44] Nicolas Kovensky, Gustavo Michalski, and Martin Schvellinger. Deep inelastic scattering from polarized spin-1/2 hadrons at low x from string theory. *JHEP*, 10:084, 2018.

[45] Chang Hwan Lee, Hui-Young Ryu, and Ismail Zahed. Diffractive Vector Photoproduction using Holographic QCD. *Phys. Rev. D*, 98(5):056006, 2018.

[46] Nicolas Kovensky, Gustavo Michalski, and Martin Schvellinger. $1/N$ corrections to F_1 and F_2 structure functions of vector mesons from holography. *Phys. Rev. D*, 99(4):046005, 2019.

[47] Kiminad A. Mamo and Ismail Zahed. Diffractive photoproduction of J/ψ and Υ using holographic QCD: gravitational form factors and GPD of gluons in the proton. *Phys. Rev. D*, 101(8):086003, 2020.

[48] Eduardo Folco Capossoli, Miguel Angel Martín Contreras, Danning Li, Alfredo Vega, and Henrique Boschi-Filho. Proton structure functions from an AdS/QCD model with a deformed background. *Phys. Rev. D*, 102(8):086004, 2020.

REFERENCES

[49] Artur Amorim, Miguel S. Costa, and Matti Järvinen. Regge theory in a Holographic dual of QCD in the Veneziano Limit. 2 2021.

[50] R. J. Eden, P. V. Landshoff, D. I. Olive, and J. C. Polkinghorne. The Analytic S-Matrix. *Cambridge University Press*, 1996.

[51] Jeffrey R. Forshaw and D. A. Ross. *Quantum chromodynamics and the pomeron*, volume 9. Cambridge University Press, 1 2011.

[52] S. Donnachie, Hans Gunter Dosch, O. Nachtmann, and P. Landshoff. *Pomeron physics and QCD*, volume 19. Cambridge University Press, 12 2004.

[53] A. V. Barnes, D. J. Mellema, A. V. Tollestrup, R. L. Walker, O. I. Dahl, R. A. Johnson, R. W. Kenney, and M. Pripstein. Pion Charge Exchange Scattering at High-Energies. *Phys. Rev. Lett.*, 37:76, 1976.

[54] S. Abatzis et al. Observation of a narrow scalar meson at 1450-MeV in the reaction $pp \to p(f)(\pi^+\pi^-\pi^+\pi-)p(s)$ at 450-GeV/c using the CERN Omega Spectrometer. *Phys. Lett.*, B324:509–514, 1994.

[55] Y. K. Hsiao and C. Q. Geng. Identifying Glueball at 3.02 GeV in Baryonic B Decays. *Phys. Lett.*, B727:168–171, 2013.

[56] Wolfgang Ochs. The Status of Glueballs. *J. Phys.*, G40:043001, 2013.

[57] David J. Gross and Frank Wilczek. Ultraviolet behavior of non-abelian gauge theories. *Phys. Rev. Lett.*, 30:1343–1346, Jun 1973.

[58] H. David Politzer. Reliable perturbative results for strong interactions? *Phys. Rev. Lett.*, 30:1346–1349, Jun 1973.

[59] H. Fritzsch, M. Gell-Mann, and H. Leutwyler. Advantages of the color octet gluon picture. *Physics Letters B*, 47(4):365–368, 1973.

[60] Walter Greiner, Stefan Schramm, and Eckart Stein. *Quantum chromodynamics.* 2007.

[61] R. Keith Ellis, W. James Stirling, and B. R. Webber. QCD and collider physics. *Camb. Monogr. Part. Phys. Nucl. Phys. Cosmol.*, 8:1–435, 1996.

[62] Michael E. Peskin and Daniel V. Schroeder. *An Introduction to quantum field theory.* 1995.

REFERENCES

[63] T. P. Cheng and L. F. Li. *GAUGE THEORY OF ELEMENTARY PARTICLE PHYSICS*. 1984.

[64] S. Chekanov et al. A ZEUS next-to-leading-order QCD analysis of data on deep inelastic scattering. *Phys. Rev. D*, 67:012007, 2003.

[65] Allan D. Martin. Proton structure, Partons, QCD, DGLAP and beyond.

[66] A. D. Martin, W. J. Stirling, R. S. Thorne, and G. Watt. Parton distributions for the LHC. *Eur. Phys. J.*, C63:189–285, 2009.

[67] R. Devenish and A. Cooper-Sarkar. *Deep inelastic scattering*. 3 2004.

[68] Joerg Gayler. Proton structure function measurements from HERA. In *32nd International Symposium on Multiparticle Dynamics*, pages 274–279, 11 2002.

[69] A. Donnachie and P. V. Landshoff. New data and the hard Pomeron. *Phys. Lett. B*, 518:63–71, 2001.

[70] A Donnachie and P V Landshoff. The Proton's gluon distribution. *Phys. Lett. B*, 550:160–165, 2002.

[71] Yuri V. Kovchegov and Eugene Levin. *Quantum chromodynamics at high energy*, volume 33. Cambridge University Press, 8 2012.

[72] L. V. Gribov, E. M. Levin, and M. G. Ryskin. Semihard Processes in QCD. *Phys. Rept.*, 100:1–150, 1983.

[73] Marcel Froissart. Asymptotic behavior and subtractions in the Mandelstam representation. *Phys. Rev.*, 123:1053–1057, 1961.

[74] A. Martin. Unitarity and high-energy behavior of scattering amplitudes. *Phys. Rev.*, 129:1432–1436, 1963.

[75] I. Balitsky. Operator expansion for high-energy scattering. *Nucl. Phys. B*, 463:99–160, 1996.

[76] Yuri V. Kovchegov. Small x F(2) structure function of a nucleus including multiple pomeron exchanges. *Phys. Rev. D*, 60:034008, 1999.

[77] Alfred H. Mueller and Bimal Patel. Single and double BFKL pomeron exchange and a dipole picture of high-energy hard processes. *Nucl. Phys. B*, 425:471–488, 1994.

[78] Nestor Armesto, Carlos A. Salgado, and Urs Achim Wiedemann. Relating high-energy lepton-hadron, proton-nucleus and nucleus-nucleus collisions through geometric scaling. *Phys. Rev. Lett.*, 94:022002, 2005.

[79] Francois Gelis, Edmond Iancu, Jamal Jalilian-Marian, and Raju Venugopalan. The Color Glass Condensate. *Ann. Rev. Nucl. Part. Sci.*, 60:463–489, 2010.

[80] I. R. Klebanov and A. M. Polyakov. AdS dual of the critical O(N) vector model. *Phys. Lett. B*, 550:213–219, 2002.

[81] S. S. Gubser, Igor R. Klebanov, and Alexander M. Polyakov. Gauge theory correlators from noncritical string theory. *Phys. Lett. B*, 428:105–114, 1998.

[82] Edward Witten. Anti-de Sitter space and holography. *Adv. Theor. Math. Phys.*, 2:253–291, 1998.

[83] Niklas Beisert et al. Review of AdS/CFT Integrability: An Overview. *Lett. Math. Phys.*, 99:3–32, 2012.

[84] Kostas Skenderis. Lecture notes on holographic renormalization. *Class. Quant. Grav.*, 19:5849–5876, 2002.

[85] Martin Ammon and Johanna Erdmenger. *Gauge/Gravity Duality: Foundations and Applications*. Cambridge University Press, 2015.

[86] Tadakatsu Sakai and Shigeki Sugimoto. Low energy hadron physics in holographic QCD. *Prog. Theor. Phys.*, 113:843–882, 2005.

[87] Tadakatsu Sakai and Shigeki Sugimoto. More on a holographic dual of QCD. *Prog. Theor. Phys.*, 114:1083–1118, 2005.

[88] Anton Rebhan. The Witten-Sakai-Sugimoto model: A brief review and some recent results. *EPJ Web Conf.*, 95:02005, 2015.

[89] Andreas Karch, Emanuel Katz, Dam T. Son, and Mikhail A. Stephanov. Linear confinement and AdS/QCD. *Phys. Rev. D*, 74:015005, 2006.

[90] Mei Huang and Danning Li. Dynamical holographic QCD model: resembling renormalization group from ultraviolet to infrared. *Springer Proc. Phys.*, 170:367–372, 2016.

[91] U. Gürsoy and E. Kiritsis. Exploring improved holographic theories for QCD: Part I. *JHEP*, 02:032, 2008.

[92] U. Gürsoy, E. Kiritsis, and F. Nitti. Exploring improved holographic theories for QCD: Part II. *JHEP*, 02:019, 2008.

[93] Colin J. Morningstar and Mike J. Peardon. The Glueball spectrum from an anisotropic lattice study. *Phys. Rev. D*, 60:034509, 1999.

[94] Y. Chen et al. Glueball spectrum and matrix elements on anisotropic lattices. *Phys. Rev. D*, 73:014516, 2006.

[95] Harvey B. Meyer. Glueball regge trajectories. Other thesis, 2004.

[96] Umut Gursoy, Elias Kiritsis, Liuba Mazzanti, Georgios Michalogiorgakis, and Francesco Nitti. Improved Holographic QCD. *Lect. Notes Phys.*, 828:79–146, 2011.

[97] Matti Järvinen and Elias Kiritsis. Holographic Models for QCD in the Veneziano Limit. *JHEP*, 03:002, 2012.

[98] Daniel Areán, Ioannis Iatrakis, Matti Järvinen, and Elias Kiritsis. The discontinuities of conformal transitions and mass spectra of V-QCD. *JHEP*, 11:068, 2013.

[99] F. D. Aaron et al. Combined Measurement and QCD Analysis of the Inclusive $e^{\pm}p$ Scattering Cross Sections at HERA. *JHEP*, 01:109, 2010.

[100] F. D. Aaron et al. Measurement of the Inclusive $e^{\pm}p$ Scattering Cross Section at High Inelasticity y and of the Structure Function F_L. *Eur. Phys. J. C*, 71:1579, 2011.

[101] Xián O. Camanho, José D. Edelstein, Juan Maldacena, and Alexander Zhiboedov. Causality constraints on corrections to the graviton three-point coupling. *Journal of High Energy Physics*, 2016(2):20, February 2016.

[102] M. Tanabashi et al. Review of Particle Physics - Data files and plots of cross-sections and related quantities. *Phys. Rev. D*, 98(3):030001, 2018.

[103] Akira Watanabe, Takahiro Sawada, and Mei Huang. Extraction of gluon distributions from structure functions at small x in holographic QCD. *Phys. Lett. B*, 805:135470, 2020.

[104] R. Barate et al. Measurement of the hadronic photon structure function at LEP-1 for (Q^2) values between $9.9\,\mathrm{GeV}^2$ and $284\,\mathrm{GeV}^2$. *Phys. Lett. B*, 458:152–166, 1999.

[105] A. Heister et al. Measurement of the hadronic photon structure function $F_2^\gamma(x, Q^2)$ in two-photon collisions at LEP. *Eur. Phys. J. C*, 30:145–158, 2003.

[106] M. Acciarri et al. Study of the hadronic photon structure function F_2^γ at LEP. *Phys. Lett. B*, 436:403–416, 1998.

[107] K. Ackerstaff et al. Measurement of the photon structure function F_2^γ at low x. *Phys. Lett. B*, 412:225–234, 1997.

[108] G. Abbiendi et al. Measurement of the low x behavior of the photon structure function F_2^γ. *Eur. Phys. J. C*, 18:15–39, 2000.

[109] G. Abbiendi et al. Measurement of the hadronic photon structure function F_2^γ at LEP-2. *Phys. Lett. B*, 533:207–222, 2002.

[110] H. Aihara et al. Measurement of the photon structure function $F_2^\gamma(x, Q^2)$ in the region $0.2 < Q^2 < 7$ GeV^2. *Z. Phys. C*, 34:1, 1987.

[111] Guido Altarelli and G. Martinelli. Transverse Momentum of Jets in Electroproduction from Quantum Chromodynamics. *Phys. Lett. B*, 76:89–94, 1978.

[112] Tie-Jiun Hou et al. New CTEQ global analysis of quantum chromodynamics with high-precision data from the LHC. *Phys. Rev. D*, 103(1):014013, 2021.

[113] Richard D. Ball et al. Parton distributions from high-precision collider data. *Eur. Phys. J. C*, 77(10):663, 2017.

[114] Stanley J. Brodsky and Ivan Schmidt. Polarized and unpolarized intrinsic gluon distributions. *Physics Letters B*, 234(1):144 – 150, 1990.

[115] Stanley J. Brodsky, Matthias Burkardt, and Ivan Schmidt. Perturbative QCD constraints on the shape of polarized quark and gluon distributions. *Nucl. Phys. B*, 441:197–214, 1995.

[116] John C. Collins and Davison E. Soper. Parton Distribution and Decay Functions. *Nucl. Phys. B*, 194:445–492, 1982.

[117] Xiangdong Ji. Deeply Virtual Compton Scattering. *Physical Review D*, 55(11):7114–7125, June 1997. arXiv: hep-ph/9609381.

[118] A. V. Radyushkin. Nonforward parton distributions. *Phys.Rev.*, D56:5524–5557, 1997.

[119] Alexander Stoffers and Ismail Zahed. Diffractive and deeply virtual Compton scattering in holographic QCD. 10 2012.

[120] Edward Witten. Baryons And Branes In Anti de Sitter Space. *Journal of High Energy Physics*, 1998(07):006–006, July 1998. arXiv: hep-th/9805112.

[121] Joseph Polchinski and Matthew J. Strassler. The String dual of a confining four-dimensional gauge theory. 3 2000.

[122] Charlotte Sleight and Massimo Taronna. Spinning Witten Diagrams. *JHEP*, 06:100, 2017.

[123] F. D. Aaron et al. Deeply Virtual Compton Scattering and its Beam Charge Asymmetry in e+- Collisions at HERA. *Phys.Lett.*, B681:391–399, 2009.

[124] S. Chekanov et al. A Measurement of the Q**2, W and t dependences of deeply virtual Compton scattering at HERA. *JHEP*, 0905:108, 2009.

[125] A. Donnachie and P. V. Landshoff. Small x: Two pomerons! *Phys. Lett. B*, 437:408–416, 1998.

[126] F. Bigazzi, Roberto Casero, A. L. Cotrone, E. Kiritsis, and Angel Paredes. Non-critical holography and four-dimensional CFT's with fundamentals. *JHEP*, 10:012, 2005.

[127] Roberto Casero, Elias Kiritsis, and Angel Paredes. Chiral symmetry breaking as open string tachyon condensation. *Nucl. Phys.*, B787:98–134, 2007.

[128] Ashoke Sen. Tachyon dynamics in open string theory. *Int. J. Mod. Phys. A*, 20:5513–5656, 2005.

[129] P.A. Zyla et al. Review of Particle Physics. *PTEP*, 2020(8):083C01, 2020.

[130] G. Veneziano. U(1) Without Instantons. *Nucl. Phys. B*, 159:213–224, 1979.

[131] Umut Gürsoy, Elias Kiritsis, Liuba Mazzanti, and Francesco Nitti. Deconfinement and Gluon Plasma Dynamics in Improved Holographic QCD. *Phys. Rev. Lett.*, 101:181601, 2008.

[132] U. Gürsoy, E. Kiritsis, L. Mazzanti, and F. Nitti. Holography and Thermodynamics of 5D Dilaton-gravity. *JHEP*, 05:033, 2009.

[133] Steven S. Gubser and Abhinav Nellore. Mimicking the QCD equation of state with a dual black hole. *Phys. Rev. D*, 78:086007, 2008.

[134] Oliver DeWolfe, Steven S. Gubser, and Christopher Rosen. A holographic critical point. *Phys. Rev. D*, 83:086005, 2011.

[135] Ioannis Iatrakis, Elias Kiritsis, and Angel Paredes. An AdS/QCD model from Sen's tachyon action. *Phys. Rev. D*, 81:115004, 2010.

[136] Ioannis Iatrakis, Elias Kiritsis, and Angel Paredes. An AdS/QCD model from tachyon condensation: II. *JHEP*, 11:123, 2010.

[137] Oren Bergman, Shigenori Seki, and Jacob Sonnenschein. Quark mass and condensate in HQCD. *JHEP*, 12:037, 2007.

[138] Avinash Dhar and Partha Nag. Sakai-Sugimoto model, Tachyon Condensation and Chiral symmetry Breaking. *JHEP*, 01:055, 2008.

[139] Avinash Dhar and Partha Nag. Tachyon condensation and quark mass in modified Sakai-Sugimoto model. *Phys. Rev. D*, 78:066021, 2008.

[140] Niko Jokela, Matti Järvinen, and Sean Nowling. Winding effects on brane/anti-brane pairs. *JHEP*, 07:085, 2009.

[141] Daniel Arean, Ioannis Iatrakis, Matti Järvinen, and Elias Kiritsis. CP-odd sector and θ dynamics in holographic QCD. *Phys. Rev.*, D96(2):026001, 2017.

[142] Steven S. Gubser. Curvature singularities: The Good, the bad, and the naked. *Adv. Theor. Math. Phys.*, 4:679–745, 2000.

[143] T. Alho, M. Järvinen, K. Kajantie, E. Kiritsis, and K. Tuominen. Quantum and stringy corrections to the equation of state of holographic QCD matter and the nature of the chiral transition. *Phys. Rev.*, D91(5):055017, 2015.

[144] Niko Jokela, Matti Järvinen, and Jere Remes. Holographic QCD in the Veneziano limit and neutron stars. 2018.

[145] U. Gürsoy, E. Kiritsis, L. Mazzanti, and F. Nitti. Improved Holographic Yang-Mills at Finite Temperature: Comparison with Data. *Nucl. Phys.*, B820:148–177, 2009.

[146] Matti Järvinen. Massive holographic QCD in the Veneziano limit. *JHEP*, 07:033, 2015.

[147] Daniel Areán, Ioannis Iatrakis, Matti Järvinen, and Elias Kiritsis. V-QCD: Spectra, the dilaton and the S-parameter. *Phys. Lett.*, B720:219–223, 2013.

[148] Takaaki Ishii, Matti Järvinen, and Govert Nijs. Cool baryon and quark matter in holographic QCD. *JHEP*, 07:003, 2019.

[149] U. Gürsoy, I. Iatrakis, E. Kiritsis, F. Nitti, and A. O'Bannon. The Chern-Simons Diffusion Rate in Improved Holographic QCD. *JHEP*, 02:119, 2013.

[150] Ioannis Iatrakis, Adith Ramamurti, and Edward Shuryak. Collective String Interactions in AdS/QCD and High-Multiplicity pA Collisions. *Phys. Rev. D*, 92(1):014011, 2015.

[151] Peter Breitenlohner and Daniel Z. Freedman. Positive Energy in anti-De Sitter Backgrounds and Gauged Extended Supergravity. *Phys. Lett. B*, 115:197–201, 1982.

[152] Stanislav Kuperstein and Jacob Sonnenschein. Non-critical, near extremal AdS(6) background as a holographic laboratory of four dimensional YM theory. *JHEP*, 11:026, 2004.

[153] Umut Gürsoy, Ioannis Iatrakis, Matti Järvinen, and Govert Nijs. Inverse Magnetic Catalysis from improved Holographic QCD in the Veneziano limit. *JHEP*, 03:053, 2017.

[154] Umut Gürsoy, Matti Järvinen, Govert Nijs, and Juan F. Pedraza. On the interplay between magnetic field and anisotropy in holographic QCD. 11 2020.

[155] Joshua Erlich, Emanuel Katz, Dam T. Son, and Mikhail A. Stephanov. QCD and a holographic model of hadrons. *Phys. Rev. Lett.*, 95:261602, 2005.

[156] Leandro Da Rold and Alex Pomarol. Chiral symmetry breaking from five dimensional spaces. *Nucl. Phys. B*, 721:79–97, 2005.

[157] Guy F. de Teramond and Stanley J. Brodsky. Hadronic spectrum of a holographic dual of QCD. *Phys. Rev. Lett.*, 94:201601, 2005.

[158] Stanley J. Brodsky, Guy F. de Teramond, Hans Gunter Dosch, and Joshua Erlich. Light-Front Holographic QCD and Emerging Confinement. *Phys. Rept.*, 584:1–105, 2015.

[159] Jacob Sonnenschein and Dorin Weissman. Rotating strings confronting PDG mesons. *JHEP*, 08:013, 2014.

[160] Jacob Sonnenschein and Dorin Weissman. Excited mesons, baryons, glueballs and tetraquarks: Predictions of the Holography Inspired Stringy Hadron model. *Eur. Phys. J. C*, 79(4):326, 2019.

[161] Edward Witten. Baryons and branes in anti-de Sitter space. *JHEP*, 07:006, 1998.

[162] Hiroyuki Hata, Tadakatsu Sakai, Shigeki Sugimoto, and Shinichiro Yamato. Baryons from instantons in holographic QCD. *Prog. Theor. Phys.*, 117:1157, 2007.

[163] Keun-Young Kim, Sang-Jin Sin, and Ismail Zahed. The Chiral Model of Sakai-Sugimoto at Finite Baryon Density. *JHEP*, 01:002, 2008.

[164] Alex Pomarol and Andrea Wulzer. Stable skyrmions from extra dimensions. *JHEP*, 03:051–051, 2008.

[165] Alex Pomarol and Andrea Wulzer. Baryon Physics in Holographic QCD. *Nucl. Phys. B*, 809:347–361, 2009.

[166] William H. Press, Saul A. Teukolsky, William T. Vetterling, and Brian P. Flannery. *Numerical Recipes 3rd Edition: The Art of Scientific Computing*. Cambridge University Press, USA, 3 edition, 2007.

[167] Emanuel Katz, Adam Lewandowski, and Matthew D. Schwartz. Tensor mesons in AdS/QCD. *Phys. Rev. D*, 74:086004, 2006.